Low-Dimensional Chiral Physics: Gross-Neveu Universality and Magnetic Catalysis

Dissertation

zur Erlangung des akademischen Grades
doctor rerum naturalium (Dr. rer. nat)

vorgelegt dem Rat der Physikalisch-Astronomischen Fakultät
der Friedrich-Schiller-Universität Jena

von Dipl.-Phys. Daniel David Scherer
geboren am 19. Dezember 1982 in Nürnberg

Gutachter:

1. Prof. Dr. Holger Gies, Friedrisch-Schiller-Universität Jena
2. Prof. Dr. Christian Fischer, Justus-Liebig-Universität Gießen
3. Jun. Prof. Dr. Lorenz Bartosch, Goethe-Universität Frankfurt

Tag der Disputation: 27. September 2012

Niedrigdimensionale Chirale Physik: Gross-Neveu-Universalität und magnetische Katalyse

Zusammenfassung

In der vorliegenden Dissertation wird das 3-dimensionale, chiral symmetrische Gross-Neveu Modell untersucht. Diese niedrigdimensionale Quantenfeldtheorie beschreibt den Kontinuumslimes des Niedrigenergiesektors bestimmter auf dem Gitter realisierter Modelle.

Die funktionale Renormierungsgruppe erlaubt es, auf nichtperturbative Art und Weise die physikalischen Eigenschaften quantenmechanischer Vielteilchensysteme und Quantenfeldtheorien zu studieren. Den Startpunkt hierfür stellt eine auf 1-Schleifen Niveau formal exakte Flussgleichung für das erzeugende Funktional der 1-Teilchen irreduziblen Vertexfunktionen dar. Im Rahmen einer Gradientenentwicklung - ideal für die Bestimmung der Infrarotasymptotik der impuls- und frequenzabhängigen Vertizes der Theorie – untersuchen wir das Regime starker Kopplung über den formalen Limes unendlicher Flavorzahlen hinaus. Dieses Regime wird durch einen entsprechenden Fixpunkt kontrolliert, der gleichzeitig eine kritische Mannigfaltigkeit definiert, welche wiederum eine Phase masseloser von einer Phase massiver Dirac-Fermionen trennt. Der zugehörige Quantenphasenübergang ist von 2. Ordnung. Nach einer ersten Analyse der Theorie in rein fermionischer Formulierung wird vermittels einer Hubbard-Stratonovich-Transformation zu einer partiell bosonisierten Beschreibung übergegangen. Innerhalb dieser bosonisierten Sprache werden universelle kritische Exponenten mit hoher Genauigkeit und exzellenter Übereinstimmung mit bekannten Resultaten aus $1/N_{\mathrm{f}}$-Entwicklungen und Monte Carlo Simulationen bestimmt, welche bezüglich ihrer Gültigkeit bereits exisitierende Ergebnisse übertreffen. über den Renormierungsgruppenfluss erhalten wir tiefere Einblicke in die globale und auch lokale Struktur der kritischen Mannigfaltigkeit und ebenso ein besseres Verständnis der relevanten Richtungen im Raum der Kopplungen, die hier von der Gaußschen Klassifikation abweichen. Für das sogenannte “asymptotic safety” Szenario – relevant für die Konstruktion einer echten Kontinuumstheorie – liefert das Gross-Neveu Modell ein einfaches und intuitives Beispiel einer nichtperturbativ renormierbaren Quantenfeldtheorie.

Weiterhin untersuchen wir die Gross-Neveu Betafunktionen unter dem Einfluss endlicher Temperatur. Wir bestimmen die kritische Temperatur für die Wiederherstellung der chiralen Symmetrie, also dem “Schmelzen” des chiralen Kondensats. Der Phasenübergang bei endlicher Temperatur fällt in die $2d$ Ising Universalitätsklasse. Darüber hinaus nutzen wir die Flussgleichungen um eine quantitative Aussage über die Unterdrückung der sogenannten Ginzburg-Region mit einer erhöhten Flavor-Zahl zu erhalten.

Im letzten Teil der Dissertation betrachten wir die niedrigdimensionalen fermionischen Freiheitsgrade unter Minimalkopplung an ein externes Hintergrundmagnetfeld, welches uns zum Phänomen der magnetischen Katalyse führt. Das äußere Magnetfeld verändert bereits die Modenstruktur der freien Dirac-Theorie zu relativistischen Landau-Niveaus. Hierdurch wird das System durch dimensionelle Reduktion im Wesentlichen empfindlicher auf fluktuationsinduzierte Quanteneffekte. Spontane Symmetriebrechung wird durch die Anwesenheit des externen Feldes für beliebige Kopplungsstärken induziert. Hier gewinnen wir die entsprechende Flussgleichung und können auf deren Basis den Renormierungsgruppenmechanismus hinter magnetischer Katalyse verstehen. Mittels der Flussgleichung bestimmen wir die Feldabhängigkeit der dynamisch erzeugten spektralen Lücke.

Low-Dimensional Chiral Physics: Gross-Neveu Universality and Magnetic Catalysis

Abstract

In this thesis, we investigate the 3-dimensional, chirally symmetric Gross-Neveu model with functional renormalization group methods. This low-dimensional quantum field theory describes the continuum limit of the low-energy sector in certain lattice systems.

The functional renormalization group allows to study in a nonperturbative way the physical properties of many-body systems and quantum field theories. The starting point is a formally exact flow equation with 1-loop structure for the generating functional of 1-particle irreducible vertices. Within a gradient expansion - tailor-made for extracting the infrared asymptotics of the momentum and frequency dependent vertices of the theory - we study the strong-coupling fixed point of the Gross-Neveu model even beyond the formal limit of infinite flavor number. This fixed point controls a 2nd order quantum phase transition from a massless phase to a phase with massive Dirac fermions. After a first analysis of the purely fermionic theory, a Hubbard-Stratonovich transformation is used to partially bosonize the theory. Within this bosonized description, we find universal critical exponents that are in excellent quantitative agreement with available results from $1/N_{\mathrm{f}}$-expansions and Monte Carlo simulations and are expected to improve upon earlier results. The renormalization group flow allows us to gain insights into the global and local structure of the critical manifold within given truncations and better understanding of the relevant directions in the space of couplings, which in general do not coincide with the Gaußian classification. Within the framework of the so-called "asymptotic safety"-scenario relevant for the construction of proper field theories, the fixed-point theory could be determined exactly in the limit of infinite flavor number. Here, the Gross-Neveu model yields a simple and intuitive example for how to define a nonperturbatively renormalizable quantum field theory.

Going beyond the determination of critical exponents, we analyze the Gross-Neveu beta functions at finite temperature. The critical temperature for the 2nd order phase transition within the $2d$-Ising universality class is determined as a function of the number of fermion species and we try to quantitatively describe the suppression of the so-called Ginzburg region with the number of fermion flavors.

Finally we analyze the minimal coupling of the fermionic degrees of freedom to a background magnetic field that leads to the phenomenon of magnetic catalysis. The external magnetic field modifies the mode structure of the free theory to relativistic Landau levels, enhancing the efficiency of quantum fluctuations by dimensional reduction, thus leading to spontaneous symmetry breaking even for subcritical values of the coupling. We identify the corresponding renormalization group mechanism and quantitatively study the magnetic field dependence of the dynamically generated spectral gap.

Table of Contents

Chapter 1

Why 3-dimensional Chiral Quantum Field Theories?

Chiral theories of fermionic fields have a long history in the realm of quantum field theory. In particle physics the quantum field theory called the standard model aims at a description of physical phenomena in 4-dimensional Minkowski spacetime in the energy range of[1] 10^{-9} eV to several TeV [1, 2]. There chirality was implicitly introduced by the discovery of Dirac fermions as the correct relativistic generalization of Pauli fermions. While the dynamics of the latter is governed by a nonrelativistic Schrödinger equation with Zeeman coupling, Dirac postulated a matrix-valued differential operator describing the spacetime propagation of relativistic fermions [3]. The necessity of a relativistic generalization from 2-component objects to 4-component Dirac spinors is closely tied to the representations of the Lorentz group. The elementary building blocks for a relativistic theory of fermions respecting discrete spacetime and proper orthochronous Lorentz transformations are two types of fields, the so-called *left-handed* and *right-handed* Weyl fermions, each yielding a 2-dimensional representation space of the Lorentz group. This "handedness" defines the notion of chirality. A Dirac spinor is built as the direct sum of these two Weyl spinors. If we were to describe noninteracting massless particles within such a relativistic theory, the two chiral species would be oblivious of each other. In other words, in the massless case, chirality is a constant of motion. As we move to the case of massive particles, however, the chiral species necessarily get coupled and chirality is no longer preserved during the time evolution of the quantum system. In the spirit of Noether's theorem [4], there is indeed a continuous symmetry behind this conserved quantity. Conventionally, this symmetry is referred to as *chiral symmetry*. It reflects the freedom to rotate to a different basis in spinor space, without changing the handedness of the fields. In this sense, we will call a theory invariant under such transformations *chirally symmetric* or simply *chiral*. Intriguingly, in many physical models, this chiral symmetry can be broken dynamically by fluctuations of fermionic quantum fields.

[1] Here we are referring to physical phenomena such as the Lamb-shift and particle collisions at LHC.

The phenomenon of symmetry breaking is encountered in practically all branches of physics [5]. In statistical mechanics and quantum statistical mechanics spontaneous symmetry breaking is the manifestation of a phase transition in the thermodynamic sense. The ground state of the system, i.e., the state with the lowest energy, breaks a symmetry of the underlying Hamiltonian (classical statistical mechanics) or Lagrangian (quantum statistical mechanics)[2]. This lack of ergodicity in phase space is strictly achieved only in the thermodynamic limit. Phase transitions can occur both at zero and finite temperature, albeit the mechanisms driving the transitions can be quite different in the two cases: thermodynamic fluctuations in one, and quantum fluctuations in the other case. In principle, if the partition function and thus the free energy of a given system is known, a phase transition will reveal itself as a nonanalyticity in the free energy as a function of its microscopic or macroscopic parameters (such as temperature) as the limit of an infinite number of degrees of freedom is approached. In the modern classification, a phase transition of nth order corresponds to a singular nth derivative of the free energy or an equivalent thermodynamic potential. The broken symmetry of the ground state is in general accompanied by a finite expectation value of a so-called order parameter. The order parameter can be used to distinguish the phase with broken symmetry, often referred to as the *ordered* phase, from the symmetric phase, accordingly referred to as the *disordered* phase, in the parameter space of the physical system. The precise nature of the order parameter of course entails a lot of the physical properties of the system.

Of special interest are (quantum) phase transitions of 2nd order. Here, the nonanalyticity arises in the 2nd derivatives of a thermodynamic potential. As the phase transition is approached by varying a certain control parameter, the fluctuations of the order parameter become increasingly long-ranged. The typical scales of correlations are quantified by the correlation length. Directly at the phase transition, the correlation length diverges[3]. We can actually identify the inverse correlation length with a mass for the order parameter fluctuations. The divergence of the correlation length at the phase transition is thus equivalent to the appearance of massless excitations. Whether massless excitations remain away from the phase transition within the ordered phase is a question of the broken symmetry. Only in the case of a broken continuous symmetry, the existence of massless Nambu-Goldstone modes is guaranteed. If a discrete symmetry is broken, no massless modes persist away from the transition within the broken phase. Naturally, an ordered state without the presence of Nambu-Goldstone modes is more robust with respect to changes in parameter space. A phase transition of 2nd order is also characterized by a smoothly vanishing order parameter, as the transition is approached from within the broken phase. A remarkable property of this type of phase transition essentially defines the arena of so-called *critical phenomena* or in the case of quantum many-body systems *quantum critical phenomena*. In the respective terminology, a 2nd order phase transition is called a *critical point*. These critical points exhibit an astonishing scaling

[2]The prime difference in the description of classical and quantum statistical mechanics in a functional representation being, that while the classical partition function is evaluated for static configurations, the quantum partition function is intrinsically taken over (imaginary) time-dependent configurations.

[3]At least in an infinitely extended system.

behavior, that can be captured by generalized homogeneity relations of thermodynamic potentials and correlation functions. These have direct impact on observable thermodynamic quantities and susceptibilities. These relations reflect a kind of fractal structure of the critical state: the critical fluctuations pervade the system on all length scales. Asymptotically close to such a thermodynamic singularity, they obey power-laws as a function of the distance to the critical parameters of the transition and are completely characterized by amplitudes and so-called *critical exponents*. It turns out, that different sets of critical exponents define *universality classes*. This means that different microscopic Hamiltonians/Lagrangians can be grouped together, if they feature a phase transition which is characterized by the same set of critical exponents. The behavior of a particular system close to its critical point is thus said to be universal, i.e., independent of its microscopic realization. In the context of quantum field theories, universality is a key point in showing that it is possible to define the field theory on all length scales. This is described in Weinberg's so-called *asymptotic safety* scenario [6–8].

It is an important and recurrent theme, that the degrees of freedom describing the low-energy properties of a macroscopic statistical or quantum system can be drastically different from the building blocks of a microscopic Hamiltonian/Lagrangian. In view of the above mentioned phenomenon of phase transitions, it is clear that the order parameter and its fluctuations dominate the system beyond length scales set by the value of the correlation length. Often a description in terms of so-called Landau-Ginzburg-Wilson functionals containing the relevant operator content in the renormalization group sense suffice for capturing the universal properties of the underlying system. For instabilities in itinerant fermion systems, an analogous Hertz-Millis approach was devised [9, 10]. However, in the case of low-dimensional gapless fermionic systems, the typical situation is that by the mediation of interactions, fermionic quantum fluctuations drive the system critical. It is also customary to speak of dynamical symmetry breaking. Often, the derivation of an effective action with only bosonic operator content by integrating out the fermions from the problem in one step is hindered by infrared singularities in induced interaction vertices [11] of the fluctuating order parameter field. This can be traced back to the gapless nature of the fermionic degrees of freedom. In these cases, the relevant operator content cannot be reduced to the subspace of bosonic fields describing collective excitations, but the simultaneous renormalization group treatment of both bosonic and fermionic degrees of freedom is compulsory. The appearing order parameter can be viewed as a bound state of the fermionic constituents. The generation of order is then typically accompanied by the generation of a gap in the fermionic single-particle spectrum. Even when the fermionic degrees of freedom have become massive and their fluctuations decouple from the theory, the low-energy long-distance properties can be captured by a reduction to a purely bosonic theory only in special cases, as close to a finite temperature phase boundary.

The chiral Gross-Neveu model [12] with an arbitrary number of fermion flavors – the central subject of investigation of this thesis – with its relatively simple field and operator content nevertheless

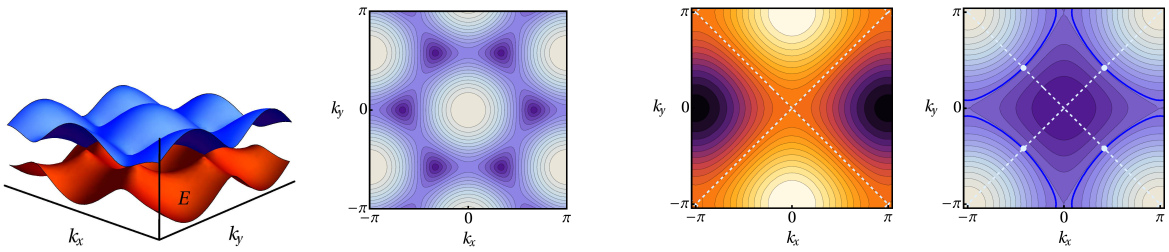

Figure 1.1: The left panel shows (a) the dispersion relation $\epsilon(k_x, k_y)$ of Bloch electrons as a function of crystal momenta k_x, k_y as obtained from a tight-binding model defined on a honeycomb lattice. The blue surface corresponds to the conduction, the red surface to the valence band. Also shown is (b) a contour plot of the tight-binding dispersion in the Brillouin zone, clearly illustrating the linear touching points (dark color) of the two bands. The right panel shows the (c) contour plots of the gap function of a planar d-wave superconductor, where the gap vanishes along the dashed white lines, leading to linearly dispersing states around the nodal points (white blobs) on the Fermi surface (blue line) shown in the rightmost part (d).

features many intriguing properties of an interacting low-dimensional theory of Dirac fermions. It is an ideal laboratory to study nonperturbative phenomena and the interplay of massless Dirac fermions with dynamically generated collective fluctuations. In its ground state, it features a chiral quantum phase transition to a phase with massive fermions and broken chiral symmetry tuned by the strength of the fermionic self-interaction. We will show, that the model provides an instance for the breakdown of a purely bosonic description akin to the Hertz-Millis philosophy. As a field theory, it provides a clear example of how nonperturbative renormalizability and the asymptotic safety scenario can be realized. This is closely tied to universality entailed by its chiral quantum phase transition. Due to its clear structure, it can be studied under a variety of conditions, like finite temperature and external electromagnetic fields. This further leads us to different patterns of the important concept of dimensional reduction. With the advent of monolayer graphene as a real laboratory material [13] and the as yet unclear origin of the unconventional behavior of high-temperature superconductors in their normal state [14, 15] as well as the rapidly developing field of topological band [16–18] and Mott insulators [19], the study of field theories of low-dimensional Dirac fermions is far from being a purely academic exercise.

In the past 20 years it has become evident that in many planar condensed matter model systems microscopically defined on a particular lattice, the low-energy physics can efficiently be described in terms of Dirac fermions. The appearance of these "relativistic" degrees of freedom can be understood by linearizing a given dispersion relation around a special set of points in the Brillouin zone, where either a linear band-crossing is realized (Fig. 1.1, (a), (b)) or the single-particle gap function vanishes at isolated points across a given Fermi surface (Fig. 1.1, (c), (d)).

The most prominent and well investigated example is probably the Hubbard model on the honeycomb lattice [20, 21]. This model describing the hopping of fermions on a hexagonal lattice with possible strong on-site and next-neighbor interactions serves as a minimal model for the electronic correlations in monolayer graphene and similar systems. Once the naive continuum limit has been

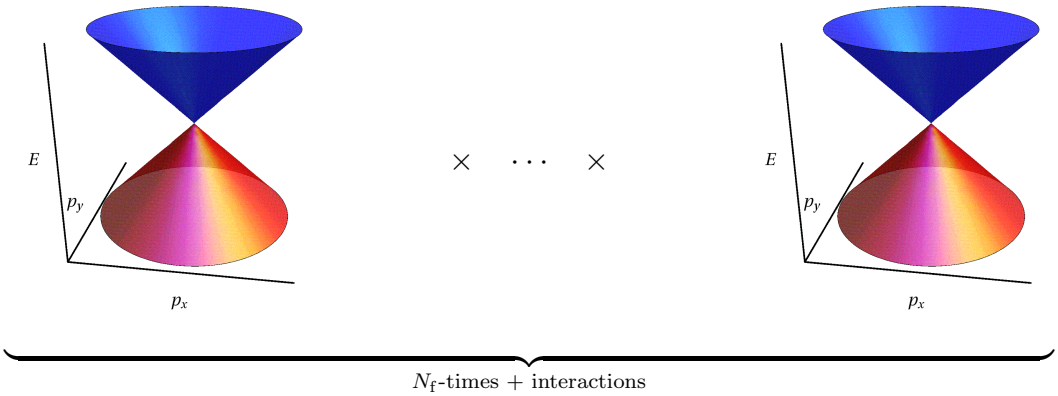

Figure 1.2: Schematic representation of the building blocks for effective Dirac-like models with chiral symmetry and linear dispersion. Here we consider the generalized many-flavor case of N_f Dirac cones, coupled by short-ranged interactions.

taken, one can expect a faithful representation of the low-energy sector by a quantum field theory for Dirac fermions moving in three-dimensional spacetime (see Fig. 1.2 for illustration) in the proximity to a second order quantum phase transition. The lattice symmetries of the Hubbard model get replaced by an "emergent" Lorentz symmetry and the free part of the Dirac action is invariant under continuous chiral transformations, reflecting a symmetry in the so-called valley and sublattice quantum numbers. Spin takes the role of flavor with the two spin polarizations yielding $N_f = 2$. The physical meaning of chiral symmetry in a low-energy field theory depends on the microscopic realization of the model. Note that for the chiral symmetry to be realized, a reducible 4-component representation of the Dirac algebra is necessary, which can be formed from the direct sum of two inequivalent 2-component representations. This asymptotic chiral symmetry is also realized for example in d-wave superconductors [22, 23] or quantum spin-liquid phases [24, 25]. In both cases, however, the underlying parent state is already assumed to break a specific symmetry, in contrast to the case of the Hubbard model on the honeycomb lattice. Other instances where no symmetry breaking is necessary are topological insulators, which support Dirac fermions as surface states [16–18]. These systems can be shown to be lattice realizations of quantum anomalies known from field theory, see e.g. [26] for the quantum anomalous Hall state and its relation to the three-dimensional parity anomaly. Another fruitful arena for Dirac fermions are ultracold quantum gases in optical lattices, where the band structure can be engineered by tuning the optical lattice [27] to a honeycomb structure. The inclusion of artificial gauge flux by keeping the gas in a rotating cylinder leads to Dirac fermions in the low-energy limit in the case of π flux per unit cell for an optical square lattice [28].

Once interactions are included in such a low-energy effective quantum field theory, we expect that the chiral symmetry is spontaneously broken as soon as the associated coupling exceeds a critical value. The fluctuation-driven interactions compatible with the symmetries determine the channel

of the formation of a condensate, i.e., in which a finite expectation value of an order-parameter field can take place. Quantum phase transitions falling into the Gross-Neveu universality class for two fermion flavors $N_\mathrm{f} = 2$ are for example the excitonic [29] and antiferromagnetic instabilities [30] in graphite and graphene, respectively. The universal properties of secondary d- to $d + \mathrm{i}s$-wave pairing transitions in nodal d-wave superconductors are also expected to be described by the Gross-Neveu model [22, 23]. Chiral symmetry breaking is known to occur for all flavor numbers N_f [31], whereas in models with continuous chiral symmetry and interactions in a vector-vector channel such as the Thirring model [34], a chiral condensate is stable only up to a critical flavor number.

From such simple and minimalistic models of Gross-Neveu type, many insights can be gained. To unravel the nonperturbative features of this interacting theory, in this thesis we employ functional renormalization group methods as an alternative to lattice Monte Carlo simulations and functional Dyson-Schwinger equations, which allow to treat the functional integral in a scale-resolved way, properly handling potential singularities. To this end, in Chap. 2 we briefly review functional integral quantization and the corresponding representations of quantum partition functions and introduce the flow equation for the one-particle irreducible (1PI) renormalization group scheme. In Chap. 3, we define the chiral Gross-Neveu model in three spacetime dimensions and present a symmetry analysis, gearing us for an analysis of the full quantum model. Chap. 4 is devoted to an in-depth study of the chiral quantum phase transition and the nonperturbative renormalizability featured by the Gross-Neveu field theory. There we will compute universal critical exponents characterizing the Gross-Neveu universality class in a flavor dependent way. It is natural to compare our results with those obtained from mean-field theory and the $1/N_\mathrm{f}$-expansion. Bringing the Gross-Neveu model in contact with a heat bath, in Chap. 5 we study the restoration of chiral symmetry by finite temperature and quantify various regimes such as the Ginzburg region, where nontrivial scaling can be observed. We address the suppression of the Ginzburg region with flavor number, which created confusion on the nature of the critical theory of the finite temperature phase transition over several years. The preceding symmetry analysis also included operators induced by the presence of external electromagnetic fields. The phenomenon of magnetic catalysis will then be discussed in Chap. 6, where we present our results for interacting Dirac fermions in the presence of a gauge background.

The compilation of this work is solely due to the author. However, parts of this work have been done in collaboration with colleagues from the research group on quantum field theory in Jena. The analysis of Gross-Neveu symmetries in Chap. 3 has been included in the publication [32] done together with Holger Gies. We have greatly profited from the experience and comments of Lukas Janssen. The results on the Gross-Neveu universality class and its quantum phase transition (cf. Sects. 4.2, 4.3 and 4.5) have been published in [31] in collaboration with Jens Braun and Holger Gies. In cross-checking the validity of the analytic expressions of threshold functions (cf. Appendix A.6) and the many-flavor phase diagram (cf. Sect. 5.2) I have been kindly supported by Jens Braun. The results of Chap. 5 will appear in a forthcoming publication [33]. The results presented in Chap. 6 have been obtained in collaboration with Holger Gies and have been published in [32]. Numerical evaluations have been performed with Mathematica 7.0 [35].

Chapter 2

Quantum Field Theory and the Functional Renormalization Group

To formulate quantum field theories, quantum many-body systems and classical statistical models, functional integrals have proved to be an extremely powerful and versatile tool. They allow both for a perturbative definition and the investigation of nonperturbative effects. In this chapter, we will collect the basics of the functional quantization of (Euclidean[1]) quantum field theories in their ground-state and in thermal equilibrium (Sect. 2.1). With these prerequisites, we are in a position to formulate a derivation of the renormalization group equation we will employ in this thesis (Sect. 2.2). In Sect. 2.3, we shall briefly recall the notion of a renormalization group fixed point and the infrared classification of directions in coupling space.

2.1 Functional Integral Quantization and Partition Functions

The functional quantization of field theories and many-body systems relies on the construction of suitable coherent states in (bosonic and fermionic) Fock space, where a coherent state is an eigenstate of a field operator. In the case of fermions, these coherent states are parameterized by variables taking values in a Grassmann algebra, while in the bosonic case, real or complex variables come into play. By time-slicing procedures and insertions of (overcomplete) resolutions of the identity in terms of coherent states, we obtain a functional integral representation for the vacuum-to-vacuum amplitude and more generally the generating functional for vacuum correlation functions. The appearance of products of fields at the same spacetime point necessitates ultraviolet (UV) regularization. The functional renormalization group introduced below offers a nonperturbative alternative to the definition of a field theory as the extrapolation to the continuum limit of lattice regularization.

[1]For a short exposition of Wick rotation, cf. Appendix A.1.

Generating Functionals for Correlators

Denoting the generating functional for vacuum correlators of a given theory by $\langle 0|0\rangle_J$, where J is an external source, we obtain[2] (with UV regularization indicated by the subscript Λ)

$$\mathcal{Z}[J] \equiv \langle 0|0\rangle_J = \int_\Lambda \mathcal{D}\Phi \, \mathrm{e}^{-S[\Phi]+(J,\Phi)} \tag{2.1}$$

with the "superfield" variable Φ and corresponding source fields J defined in Appendix A.3. The field variable Φ encodes both bosonic and fermionic degrees of freedom, and allows to treat both sectors of a theory equally in a condensed and convenient notation. The brackets $(\,\cdot\,,\,\cdot\,)$ are shorthand for suitable contractions of generalized indices. The classical (Euclidean) action $S[\Phi]$ governs by the variational principle the equations of motion of the classical theory to be quantized.

The time-ordered 2-point vacuum correlator (Green's function) for field operators $\hat{\Phi}(x)$ and $\hat{\Phi}(x')$ at spacetime points $x = (\tau, \boldsymbol{x})$ and $x' = (\tau', \boldsymbol{x}')$ is defined as

$$\langle 0|\mathcal{T}\hat{\Phi}_a(x)\hat{\Phi}^T_{a'}(x')|0\rangle \equiv \langle \Phi_a(x)\Phi^T_{a'}(x')\rangle = \frac{1}{\mathcal{Z}[J]}\frac{\overrightarrow{\delta}}{\delta J^T_a(x)}\mathcal{Z}[J]\left(\zeta_{a'}\frac{\overleftarrow{\delta}}{\delta J_{a'}(x')}\right)|_{J=0} \tag{2.2}$$

and $\mathcal{T}\hat{\Phi}_a(x)\hat{\Phi}^T_{a'}(x') = \Theta(\tau-\tau')\Phi_a(x)\Phi^T_{a'}(x') \pm \Theta(\tau'-\tau)\Phi_{a'}(x')\Phi^T_a(x)$ denotes the time ordering operator for bosonic $(+)$ and fermionic $(-)$ components. We introduced the symbol ζ_a which equals $+1$ for a labeling a bosonic field and -1 for a labeling a fermionic field. We collect this statistical factor in a matrix ζ as $\zeta_{a,a'} = \zeta_a\delta_{a,a'}$. Higher n-point functions are defined analogously. The knowledge of all n-point functions amounts to a solution of the quantum field theory (in its ground-state). They encode physical information about the propagation of quantum fluctuations in spacetime, the excitation spectrum of the quantum theory under consideration, scattering cross sections and lifetimes of quantum states and the dynamical or spontaneous breaking of symmetries. All the n-point functions can be obtained by functional differentiation of the functional $\mathcal{Z}[J]$. Since diagrammatically, the perturbative coefficients of $\mathcal{Z}[J]$ still contain disconnected contributions, we define the generating functional for connected correlators:

$$W[J] \equiv \ln \int_\Lambda \mathcal{D}\Phi \, \mathrm{e}^{-S[\Phi]+(J,\Phi)}. \tag{2.3}$$

Obviously, the 1-point function or field expectation value is the first functional derivative (see Appendix A.3 for the definition of left and right derivatives), i.e.,

$$\langle \Phi_a(x)\rangle = \frac{\overrightarrow{\delta}}{\delta J^T_a(x)}W[J]. \tag{2.4}$$

[2]Throughout this thesis, we set $\hbar = k_B = c = 1$.

The second functional derivative yields the connected 2-point function

$$\langle \Phi_a(x)\Phi^T_{a'}(x')\rangle - \langle \Phi_a(x)\rangle\langle \Phi^T_{a'}(x')\rangle = \zeta_{a'}\frac{\overrightarrow{\delta}}{\delta J^T_a(x)}W[J]\frac{\overleftarrow{\delta}}{\delta J_{a'}(x')}. \tag{2.5}$$

Quantum Effective Action

By a Legendre transform of $W[J]$ with respect to the source J, we arrive at yet another functional, the so-called quantum effective action $\Gamma[\Phi]$, where

$$\Gamma[\Phi] = (J,\Phi) - W[J], \qquad \Phi = \frac{\overrightarrow{\delta}}{\delta J^T}W[J]. \tag{2.6}$$

Diagrammatically, it is the generating functional for all 1PI vertex functions. For notational convenience, we here denoted the expectation value of the field with the same symbol as the field variable in the functional integral. Evaluated at constant field configurations[3], we obtain the effective potential $U(\Phi)$,

$$\Gamma[\Phi]|_{\Phi=\text{const.}} = (2\pi)^d\delta(0)U(\Phi). \tag{2.7}$$

Since in the presence of sources the expectation value is governed by the equation

$$\frac{\overrightarrow{\delta}}{\delta\Phi^T}\Gamma[\Phi] = \zeta J, \tag{2.8}$$

for constant field configurations and vanishing sources, this reduces to a condition yielding the extrema of the effective potential as a function of the variable Φ. Having a ground-state with a finite expectation value in the bosonic sector signals symmetry breaking. By considering a resolution of the identity in field space, we obtain the useful relation

$$\mathbb{1} = \Phi\frac{\overleftarrow{\delta}}{\delta\Phi} = \frac{\overrightarrow{\delta}}{\delta J^T}W[J]\frac{\overleftarrow{\delta}}{\delta J}\zeta\frac{\overrightarrow{\delta}}{\delta\Phi^T}\Gamma[\Phi]\frac{\overleftarrow{\delta}}{\delta\Phi}. \tag{2.9}$$

The quantum effective action can be shown to obey an integro-differential equation in functional form,

$$\Gamma[\Phi] = -\ln\int_\Lambda \mathcal{D}\chi \mathrm{e}^{-S[\chi+\Phi]+\left(\zeta\frac{\overrightarrow{\delta}}{\delta\Phi^T}\Gamma[\Phi],\chi\right)}. \tag{2.10}$$

By taking appropriate functional derivatives, one can derive so-called Dyson-Schwinger equations [36, 37] from Eq. (2.10). These provide another route into the nonperturbative realm of field theory and many-body systems.

[3]Expectation values of spinor fields vanish due to their anticommuting Grassmann property.

Finite Temperature Partition Functions

The formalism we have described up to now treats a field theory at zero temperature in its ground-state. It is known, that by compactification of the time direction to a circle with circumference $\beta = 1/T$, i.e, $\mathbb{R} \times \mathbb{R}^{d-1} \to \mathbb{S}^1 \times \mathbb{R}^{d-1}$ (with T denoting absolute temperature), one can obtain a functional integral representation of the grand-canonical partition function of a given quantum system specified by a Hamiltonian $\hat{H}$ [38]:

$$\mathcal{Z}(\beta, \mu) = \operatorname{tr} \mathrm{e}^{-\beta(\hat{H}-\mu\hat{Q})} \equiv \int \mathcal{D}\Phi \, \mathrm{e}^{-S[\Phi]}, \tag{2.11}$$

where now $S[\Phi] = \int_0^\beta \mathrm{d}\tau L(\Phi, \partial\Phi)$ and $\mu Q[\Phi]$ was absorbed into the action, with the Lagrange function $L(\Phi, \partial\Phi)$. The chemical potential μ for the operator $\hat{Q}$ (corresponding to a conserved charge) is included here for simplicity, since otherwise the trace has to be performed in a subset of Fock space. Of course, the case $\mu = 0$ can then be investigated with the functional representation Eq. (2.11). This provides us with the Matsubara formalism to compute observables of the field theory in thermal equilibrium. Due to the trace operation, the field configurations entering Eq. (2.11) have to be periodic in the time direction in the bosonic case, but antiperiodic in the fermionic case,

$$\Phi_a(\tau + \beta, \boldsymbol{x}) = \zeta_a \Phi_a(\tau, \boldsymbol{x}). \tag{2.12}$$

By Fourier transforming to frequency space (see App. A.2), this yields Matsubara modes with frequencies

$$p_0 = \begin{cases} \omega_n = 2\pi n/\beta, & \text{bosonic} \\ \nu_n = (2n+1)\pi/\beta, & \text{fermionic} \end{cases} \quad \text{for } n \in \mathbb{Z}. \tag{2.13}$$

The considerations above made for $T = 0$ carry over completely to the case of finite temperature.

2.2 Flow-Equation for the Effective Average Action

As the full content of a quantum theory can be specified in terms of generating functionals for correlation functions or vertices, we can more generally study the renormalization group behavior of a generating functional. In this thesis, we will exclusively employ the one-particle irreducible (1PI) renormalization group approach introduced by Wetterich [39]. In this section we briefly summarize a derivation of the Wetterich equation and remind of the essentials of the functional renormalization group in the 1PI scheme.

One-Parameter Family of Quantum Field Theories

We deform the definition $\mathcal{Z}[J]$ of the generating functional for vacuum correlators by inserting a parameter dependent regulator R_k into the Gaußian measure of the functional integral:

$$\int \mathcal{D}\Phi \, \mathrm{e}^{-\frac{1}{2}\left(\Phi, G^{-1}\Phi\right)} \quad \rightarrow \quad \int \mathcal{D}\Phi \, \mathrm{e}^{-\frac{1}{2}\left(\Phi, \left[G^{-1}+R_k\right]\Phi\right)} \tag{2.14}$$

We thus arrive at a one-paramter family of generating functionals $\mathcal{Z}_k[J]$ with

$$\mathcal{Z}[J] \quad \rightarrow \quad \mathcal{Z}_k[J] \equiv \int_\Lambda \mathcal{D}\Phi \, \mathrm{e}^{-S[\Phi]-\frac{1}{2}(\Phi,\mathcal{R}_k\Phi)+(J,\Phi)}. \tag{2.15}$$

The notation $\int_\Lambda \mathcal{D}\Phi$ for the functional integration indicates ultraviolet (UV) regularization, and Λ is the corresponding UV cutoff scale. In a componentwise momentum space representation[4] we define the regulator

$$R_{k,a,a'}(p,p') \equiv (2\pi)^d \delta(p-p')\delta_{a,a'} R_{k,a}(p) \tag{2.16}$$

to be diagonal in all indices[5]. For a meaningful deformation that will momentarily allow for an operational interpretation as a scale-dependent renormalization group transformation, the components $R_{k,a}(p)$ are required to fulfill the conditions

$$\text{i.} \qquad \lim_{\frac{p^2}{k^2}\to 0} R_{k,a}(p) > 0, \tag{2.17}$$

$$\text{ii.} \qquad \lim_{\frac{k^2}{p^2}\to 0} R_{k,a}(p) = 0, \tag{2.18}$$

$$\text{iii.} \quad \lim_{\Lambda\to\infty} \lim_{k\to\Lambda} R_{k,a}(p) \to \infty. \tag{2.19}$$

Each theory is specified by the infrared (IR) cutoff scale k. The regularization procedure should be compatible with the symmetries of the underlying classical theory. This guarantees, that all symmetries of the classical theory are preserved. Besides this point, the precise form of the regulator does not matter at this stage and will be specified eventually. The regulator matrix R_k essentially damps out field modes with momenta p below the IR cutoff scale k. It thus can be understood as a scale-dependent mass term, cf. Eq. (2.17), i.. The second condition Eq. (2.17), ii. ensures, that in the limit $k \to 0$, the generating functional approaches its undeformed definition. The third condition Eq. (2.17), iii. will eventually allow to formulate an initial value problem, where the initial condition is given by the classical action. Put differently, as k approaches the UV cutoff scale Λ, the regulator renders the classical action to be the leading contribution to the functional integral.

[4] Actually, a representation which diagonalizes the bilinear part in the action is advisable. Here for simplicity of the discussion we assume that this is achieved in a plane-wave basis.

[5] For each fermionic component, $R_{k,a}(p)$ is thus a 2×2 matrix in Nambu space.

We now further define the scale-dependent generating functional for connected correlators,

$$W_k[J] \equiv \ln \int_\Lambda \mathcal{D}\Phi \, \mathrm{e}^{-S[\Phi]-\frac{1}{2}(\Phi,R_k\Phi)+(J,\Phi)}. \tag{2.20}$$

Field expectation values in the presence of sources are simply obtained from $W_k[J]$ by functional differentiation with respect to the sources:

$$\langle\Phi\rangle_{k,J} = \frac{\overrightarrow{\delta}}{\delta J^T} W_k[J], \tag{2.21}$$

where averaging is carried out according to

$$\langle\,\cdot\,\rangle_{k,J} \equiv \frac{1}{\mathcal{Z}_k[J]} \int_\Lambda \mathcal{D}\Phi \,(\,\cdot\,)\mathrm{e}^{-S[\Phi]-\frac{1}{2}(\Phi,R_k\Phi)+(J,\Phi)}. \tag{2.22}$$

Flowing Effective Average Action

The scale dependent effective action is now defined as a modified Legendre transform with respect to the source field J:

$$\Gamma_k[\Phi] = (J,\Phi) - W_k[J] - \frac{1}{2}(\Phi, R_k\Phi). \tag{2.23}$$

The field expectation value Φ appears as the natural variable of the functional $\Gamma_k[\Phi]$ and for notational convenience we denote field averages with the same symbol as the integration variable in the functional integral. We will stick to this convention if not stated otherwise. The source fields are to be understood so as to cancel the k-dependence of the expectation value and thus acquire scale dependence themselves, $J \to J_k$. Taking derivatives on both sides with respect to the scale k in Eq. (2.23), we arrive at the functional differential equation for the scale dependent effective action $\Gamma_k[\Phi]$. We start with

$$\partial_k W_k[J_k] = \partial_k W_k[J_k]|_{J_k \text{ fixed}} + \left(\frac{\overrightarrow{\delta}}{\delta J^T} W_k[J]|_{J=J_k}, \partial_k J_k\right). \tag{2.24}$$

We now perform a chain of manipulations for the scale derivative evaluated at some fixed source field J (temporarily, let us explicitly distinguish between Φ as an integration variable and its expectation value $\langle\Phi\rangle_{k,J}$):

$$\begin{aligned}
\partial_k W_k[J] &= -\frac{1}{2}\left\langle(\Phi, \partial_k R_k \Phi)\right\rangle_{k,J} \\
&= -\frac{1}{2}\left\langle \sum_{a,a'} \Phi_a^T \partial_k R_{k,a,a'} \Phi_{a'} \right\rangle_{k,J} \\
&= -\frac{1}{2}\sum_{a,a'} \zeta_a \, \partial_k R_{k,a,a'} \left\langle \Phi_{a'} \Phi_a^T \right\rangle_{k,J} \\
&= -\frac{1}{2}\mathrm{Tr}\left\{ \partial_k R_k \frac{\overrightarrow{\delta}}{\delta J^T} W_k[J] \frac{\overleftarrow{\delta}}{\delta J} \right\} - \frac{1}{2}\left(\langle\Phi\rangle_{k,J}, \partial_k R_k \langle\Phi\rangle_{k,J}\right). \qquad (2.25)
\end{aligned}$$

In going from the third to the fourth line the arising minus sign in the fermionic sector is again absorbed into the right derivative acting on the k-dependent functional $W_k[J]$. The last term in Eq. (2.25) compensates for the disconnected subtraction yielding the connected 2-point correlation function generated by the second functional derivative. Using Eq. (2.25), Eq. (2.24) and the easily obtained relation

$$\mathbb{1} = \frac{\overrightarrow{\delta}}{\delta J^T} W_k[J] \frac{\overleftarrow{\delta}}{\delta J} \zeta \left(\frac{\overrightarrow{\delta}}{\delta \Phi^T} \Gamma_k[\Phi] \frac{\overleftarrow{\delta}}{\delta \Phi} + R_k \right) \qquad (2.26)$$

in the scale derivative of Eq. (2.23), we finally arrive at the flow equation for $\Gamma_k[\Phi]$ [39]:

$$\partial_t \Gamma_k[\Phi] = \frac{1}{2}\mathrm{STr}\left\{ \left(\frac{\overrightarrow{\delta}}{\delta \Phi^T} \Gamma_k[\Phi] \frac{\overleftarrow{\delta}}{\delta \Phi} + R_k \right)^{-1} \partial_t R_k \right\}. \qquad (2.27)$$

The Wetterich equation is a formally exact flow equation with 1-loop structure, which is technically very convenient. For field theories, everything can be formulated directly in a continuum language. The so-called "supertrace" $\mathrm{STr}\{\,\cdot\,\} \equiv \mathrm{Tr}\{\zeta\,\cdot\,\}$ traces over all indices of the appearing expression and is defined with a minus sign for the contributions from the fermionic sector of the theory. We also moved from the linear scale derivative ∂_k to the logarithmic renormalization group scale $t \equiv \ln\frac{k}{\Lambda}$. Upon approaching the infrared, i.e., $k \to 0$, the regulator insertion needs to vanish Eq. (2.17), ii., to make sure all fluctuating modes have been integrated out and $\Gamma_k[\Phi]$ approaches the full effective action $\Gamma[\Phi]$, which governs the equations of motion of the field expectation value Φ.

The differential kernel $\Gamma_k^{(2)}[\Phi] \equiv \frac{\overrightarrow{\delta}}{\delta\Phi^T}\Gamma_k[\Phi]\frac{\overleftarrow{\delta}}{\delta\Phi}$ and the choice for the regulator R_k determine how modes are "integrated out". In this thesis, we will assume R_k to be *spectrally adjusted* [40], meaning it is a function of $\Gamma_k^{(2)}[\Phi_0]$, with Φ_0 a given background configuration. From Eq. (2.27) it is obvious that R_k provides infrared regularization. The logarithmic scale derivative $\partial_t R_k$ regularizes

the ultraviolet behavior[6] and together with the IR damping of R_k leads to "localization" of the supertrace argument in momentum space. An infinitesimal renormalization group transformation can thus be understood as a regularized momentum shell integration. By varying k, we can "scan" for structures appearing at typical energy/momentum scales, determining the physical behavior encoded in the full quantum effective action.

Moreover, at the initial high-energy scale Λ where the flow will be initiated, the flowing effective action $\Gamma_k[\Phi]$ is supposed to match – at least approximately – the classical action $S[\Phi]$, realized by requiring Eq. (2.17), iii.. This ensures that our rather arbitrary deformation in the Gaußian integration measure is turned into a well defined initial value problem. A solution to Eq. (2.27) thus provides a trajectory in the space of action functionals. In short, it interpolates between the bare action S to be quantized, i.e., $\Gamma_{k\to\Lambda} \to S$ and the full quantum effective action $\Gamma = \Gamma_{k\to 0}$, being the generating functional of 1PI vertex functions. For reviews of the functional renormalization group approach to quantum field theories and quantum many-body systems with emphasis on fermionic problems, see [41–45] and particularly [46].

To proceed, we split $\Gamma_k^{(2)}[\Phi]$ into a field-independent part $\bar{\Gamma}_k^{(2)}$ and a field-dependent part $\tilde{\Gamma}_k^{(2)}[\Phi]$, containing interaction vertices. We thus define the scale-dependent regularized inverse propagator

$$G_k^{-1} \equiv \bar{\Gamma}_k^{(2)} + R_k. \tag{2.28}$$

We thus obtain the decomposition

$$\Gamma_k^{(2)}[\Phi] + R_k \equiv G_k^{-1} + \tilde{\Gamma}_k^{(2)}[\Phi]. \tag{2.29}$$

Note that the regulator R_k is contained in G_k^{-1}. Also, G_k^{-1} may still depend on some background field configuration. If we now introduce the so-called "tilde" derivative $\tilde{\partial}_t$, defined to act only on the regulator dependence of a given expression, we obtain from Eq. (2.27)

$$\begin{aligned} \partial_t \Gamma_k[\Phi] &= \frac{1}{2}\mathrm{STr}\left\{\tilde{\partial}_t \ln\left(G_k^{-1}\left(\mathbb{1} + G_k\tilde{\Gamma}_k^{(2)}[\Phi]\right)\right)\right\} \\ &= \frac{1}{2}\mathrm{STr}\,\tilde{\partial}_t \ln G_k^{-1} + \frac{1}{2}\mathrm{STr}\,\tilde{\partial}_t \sum_{l=1}^{\infty}\frac{(-1)^{l+1}}{l}(G_k\tilde{\Gamma}_k^{(2)}[\Phi])^l. \end{aligned} \tag{2.30}$$

In going from the first to the second line, we expanded the ln in powers of $G_k\tilde{\Gamma}_k^{(2)}[\Phi]$. Since this equation for the functional $\Gamma_k[\Phi]$ cannot be solved in general, we need to find a suitable as well as tractable parameterization, i.e., an ansatz for $\Gamma_k[\Phi]$ subject to initial and in general also to boundary conditions, from which we can extract physical information about the quantum field theory under consideration. Such an ansatz is referred to as a *truncation*.

[6] More generally, it provides a weighting function on the spectrum of $\Gamma_k^{(2)}[\Phi]$ with dominant support around and below the scale k.

Two notable ways to set up truncations in a systematic manner are the vertex and the gradient expansion. In a vertex expansion, the flowing functional $\Gamma_k[\Phi]$ is expanded in all possible monomials of the field Φ yielding flowing n-point functions (1PI vertices) as coefficients. However, only a finite number of vertices is kept. This leads to a coupled hierarchy of flow equations for the vertex functions. Typically, the interest lies in resolving frequency and/or momentum dependences. In a gradient expansion – which we will employ below –, we order the operators kept in the truncation according to the number of field derivatives. This type of truncation is tailor-made for extracting universal properties from a field theory or many-body system. First of all, however, we have to choose a parameterization of $\Gamma_k[\Phi]$. In general, we can write

$$\Gamma_k[\Phi] = \sum_i g_{i,k}\mathcal{O}_i[\Phi, \partial\Phi] \quad \Leftrightarrow \quad \partial_t\Gamma_k[\Phi] = \sum_i (\boldsymbol{\beta})_i \mathcal{O}_i[\Phi, \partial\Phi], \tag{2.31}$$

where $g_{i,k}$ is a (dimensionless) scale-dependent coupling parameterizing the given action, and $\mathcal{O}_i[\Phi, \partial\Phi]$ denotes an operator (where the index i follows some ordering principle) built from the field Φ and its derivatives $\partial\Phi$. In the space of couplings $g_{i,k}$, the renormalization group now provides us with a vector field $\boldsymbol{\beta}$, summarizing the renormalization group beta functions for these couplings $(\boldsymbol{\beta})_i = \beta_{g_{i,k}}(g_{1,k}, g_{2,k}, \dots) \equiv \partial_t g_{i,k}$. In general, this map of a quantum field theory to a flow in coupling space allows to extract universal physical information from the fixed points and from the associated manifolds controlling the flow toward the infrared.

Optimized Regulators

As to the choice of regulators, which are up to now only constrained by the conditions Eq. (2.17), i. – iii., in Chap. 4 and Chap. 5 we will make use of so-called *optimized* regulators [47–49]. This class of regulators fulfills an additional criterion, namely the maximization of the mass-gap

$$\min\left[\Gamma_k^{(2)}[\Phi] + R_k\right], \tag{2.32}$$

where the minimization is carried out over the spectrum of $\Gamma_k^{(2)}[\Phi]$ for some fixed reference configuration Φ. Thus, by maximizing the gap over the set of regulators, the flow is turned as regular as possible, and convergence properties with respect to expansions in parameters entering $\Gamma_k^{(2)}[\Phi]$ are improved. However, in certain situations (cf. Chap. 6), the evaluation of 1-loop integrals is easier to perform for nonoptimized regulators, such as the Callan-Symanzik regulator.

2.3 Fixed Points and Linearized Flows

Directly at a fixed point under renormalization group transformations as defined by Eq. (2.27), a theory remains invariant with respect to variation of k, it is thus scale-invariant. Parameterizing the effective average action $\Gamma_k[\Phi]$ as indicated above by a possibly infinite set of dimensionless couplings $g_{i,k}$, the Wetterich equation provides us with the flow of these couplings. A fixed point $g_{i,*}$ in coupling space is then defined by

$$\beta_i(g_{1,*}, g_{2,*}, ...) = 0, \forall\, i. \tag{2.33}$$

At a Gaußian fixed point, we have $g_{j,*} = 0$, $\forall\, i$. The fixed point is non-Gaußian, if at least one fixed-point coupling is nonzero $g_{j,*} \neq 0$. Considering the linearized flow in the fixed-point regime,

$$\partial_t g_{i,k} = \sum_j B_i{}^j (g_{j,k} - g_{j,*}) + \mathcal{O}\left((g_{j,k} - g_{j,*})^2\right), \quad B_i{}^j = \frac{\partial \beta_{g_i}}{\partial g_j}\Big|_{g=g_*}, \tag{2.34}$$

we encounter the stability matrix $B_i{}^j$, which we diagonalize

$$B_i{}^j\, V_j^I = -\Theta^I V_i^I, \tag{2.35}$$

in terms of right-eigenvectors V_i^I, enumerated by the index I. The eigenvalues yield the (negative) *critical exponents* Θ^I, providing us with a classification of physical parameters and more generally, directions in coupling space. The solution of the coupling flow in the linearized fixed-point regime is given by

$$g_{i,k} = g_{i,*} + \sum_I C^I\, V_i^I \left(\frac{k_0}{k}\right)^{\Theta^I}, \tag{2.36}$$

where the integration constants C^I define the initial conditions at a reference scale k_0. The existence of the fixed-point thus guarantees scaling behavior, i.e., power-laws of physical observables described by critical exponents. Critical exponents allow for the definition of *universality classes*. All theories in theory space, whose behavior is controlled by a given fixed point, share the same critical exponents, irrespective of their different microscopic definitions. This entails, of course, that all theories in the same universality class feature the same scaling laws. In principle, different physical mechanisms can provide us with this kind of universality, which can elegantly be formulated with renormalization group methods. In this thesis, we will encounter universality generated by 2nd order phase transitions, both of quantum and thermal type.

All eigendirections with $\Theta^I < 0$ are suppressed toward the IR and thus are *irrelevant*. All *relevant* directions with $\Theta^I > 0$ increase toward the IR and thus determine the macroscopic physics. For the *marginal* directions $\Theta^I = 0$, a linear stability analysis is not sufficient, and higher-order terms in

the expansion about the fixed point have to be regarded, yielding logarithmic corrections to scaling laws.

For the flow toward the IR, the linearized fixed-point flow Eq. (2.34) is generally not sufficient and the full nonlinear beta functions have to be taken into account. Even the parameterization of the effective action in terms of the same degrees of freedom in the UV and IR might be inappropriate, for instance, if bound states or condensates appear in the IR. This is precisely the case in fermionic models beyond criticality. Furthermore, the number of relevant and marginally-relevant directions determines the total number of physical parameters a theory has to be equipped with, to detect the universal features associated with a given fixed point. The theory is predictive if this number is finite.

From the asymptotic safety point of view, which we will discuss in more detail in Chap. 4, we desire a way to render a theory UV finite. This can be achieved, if the renormalization group trajectory hits a fixed point in the UV. Then, the UV cutoff used for intermediate regularization can safely be taken to infinity and the system approaches a scale-invariant state for $k \to \Lambda \to \infty$. Again, for the theory to be predictive, the number of physical parameters required for specifying the renormalization group trajectory needs to be finite.

Chapter 3

The 3-dimensional Gross-Neveu Model

In this chapter, we define the three-dimensional, chiral Gross-Neveu action and analyze its spacetime and chiral symmetries. This corresponds to a "classical analysis", i.e., quantum fluctuations are not yet included. However, the investigation of symmetries prepares the study of the quantum model.

3.1 Definition of the Model

We consider the Gross-Neveu model [12] within functional integral quantization. The microscopic degrees of freedom are represented by Grassmann-valued fields defined over three-dimensional Euclidean spacetime[1]. The model depends on a single parameter which is the coupling constant $\bar{g}$ with mass dimension $2-d$. That this statement is true beyond the inclusion of quantum fluctuations is nontrivial! We will show this by analyzing the fixed-point structure of the model in Chap. 4. We restrict our attention to $2 < d < 4$. In $d = 2$, the model is asymptotically free and perturbatively renormalizable, as the Gaußian fixed point is UV attractive. $d = 4$ will turn out to be a marginal case, where the theory becomes "trivial", i.e., noninteracting in the continuum limit, see Chap. 4 and [50]. The chiral symmetry of the model can be associated with a $\mathbb{Z}_2$ symmetry for the order parameter. As we shall discuss below, the infrared regime of the theory is governed by dynamical chiral symmetry breaking, provided the only parameter of the model, namely $\bar{g}$, is adjusted accordingly. To prepare our study of magnetic catalysis in Chap. 6, we also minimally couple the Dirac fermions to a background gauge-potential that realizes the external magnetic field. The defining local action to be quantized is given by

$$S[\bar{\psi}_j, \psi_j, \mathcal{A}] = \int_x \mathcal{L}(\bar{\psi}_j, \psi_j, \partial_\mu \bar{\psi}_j, \partial_\mu \psi_j, \mathcal{A}) \tag{3.1}$$

[1]For a brief review of Wick rotation in the functional integral for Grassmann-valued Dirac spinors, see Appendix A.1

with the Lagrangian density

$$\mathcal{L} = \sum_{j=1}^{N_\mathrm{f}} \bar{\psi}_j \mathrm{i}\not{D}[\mathcal{A}]\, \psi_j + \sum_{i,j=1}^{N_\mathrm{f}} \bar{\psi}_i \psi_i \frac{\bar{g}}{2N_\mathrm{f}} \bar{\psi}_j \psi_j, \tag{3.2}$$

where $\int_x = \int d^d x$ is a shorthand for the integral over the d-dimensional Euclidean spacetime. Here,

$$\not{D}[\mathcal{A}] = \gamma_\mu \left(\partial_\mu - \mathrm{i}q\mathcal{A}_\mu(x)\right), \quad \mu = 0, 1, 2, \tag{3.3}$$

denotes the covariant derivative acting on the spinor fields with q the respective charge under the Abelian U(1) gauge group. The fermionic fields $\bar{\psi}$ and ψ are independent integration variables. For a discussion of the "real" building blocks of a fermionic theory in Euclidean spacetime, see [51]. We consider N_f different flavor species indexed by $j = 1, \ldots, N_\mathrm{f}$, but keep the flavor number arbitrary. This model enjoys a global U(N_f) flavor symmetry. The canonical mass dimensions of the fields are given by $[\psi] = \frac{d-1}{2}$ and $[\mathcal{A}] = \frac{d-2}{2}$. This renders the gauge charge a dimensionful quantity with $[q] = \frac{4-d}{2}$. As mentioned in Chap. 1 we use a reducible four-component representation for the gamma matrices in this work, i.e., $d_\gamma = 4$ where $d_\gamma = \mathrm{tr}\mathbb{1}_4$ denotes the dimension of the representation space of the Dirac algebra and tr is the trace over spinor indices. In continuous dimensions $2 < d < 4$, we assume that a suitable analytic continuation for the Dirac structure exists, such that traces over the algebraic structure yield analytic functions in d and d_γ. Our choice for the 4×4 representation of the Dirac algebra is the so-called chiral one. This of course fixes the chiral basis in spinor space, where a four-component spinor can be decomposed into the *left-handed* and *right-handed* Weyl spinors $\psi_\mathrm{L} = \frac{1}{2}(1 + \gamma_5)$ and $\psi_\mathrm{R} = \frac{1}{2}(1 - \gamma_5)$, respectively. Here, the γ_5 matrix is in block-diagonal form.

The matrices are explicitly given by

$$\gamma_0 = \tau_2 \otimes \tau_3\,, \quad \gamma_1 = \tau_2 \otimes \tau_1\,, \quad \gamma_2 = \tau_2 \otimes \tau_2 \tag{3.4}$$

and

$$\gamma_3 = \tau_1 \otimes \tau_0\,, \quad \gamma_5 = \tau_3 \otimes \tau_0\,, \quad \gamma_{35} \equiv \mathrm{i}\gamma_3\gamma_5 \tag{3.5}$$

Here, the $\{\tau_i\}$'s denote the Pauli matrices which satisfy $\tau_i\tau_j = \delta_{ij}\tau_0 + \mathrm{i}\epsilon_{ijk}\tau_k$, with $i, j, k = 1, 2, 3$ and $\tau_0 = \mathbb{1}_2$ is a 2×2 unit matrix. The gamma matrices satisfy the anti-commutation relations

$$\{\gamma_\mu, \gamma_\nu\} = 2\delta_{\mu\nu}\mathbb{1}_4\,, \tag{3.6}$$

where $\mu, \nu = 0, 1, 2$. The matrices γ_3 and γ_5 anti-commute with all γ_μ, $\mu = 0, 1, 2$. In this representation γ_2, γ_3, γ_5 are symmetric and real, while γ_0, γ_1, γ_{35} are antisymmetric and purely imaginary 4×4 matrices. One easily verifies the following identities

$$\gamma_{35}\gamma_\mu\gamma_\nu = \delta_{\mu\nu}\gamma_{35} + \mathrm{i}\epsilon_{\mu\nu\sigma}\gamma_\sigma, \tag{3.7}$$

$$\mathrm{i}\gamma_5\gamma_\mu\gamma_\nu = \mathrm{i}\delta_{\mu\nu}\gamma_5 + \mathrm{i}\epsilon_{\mu\nu\sigma}\gamma_3\gamma_\sigma, \tag{3.8}$$

$$\mathrm{i}\gamma_3\gamma_\mu\gamma_\nu = \mathrm{i}\delta_{\mu\nu}\gamma_3 - \mathrm{i}\epsilon_{\mu\nu\sigma}\gamma_5\gamma_\sigma, \tag{3.9}$$

where the second and third line follow from the first one by left or right multiplication with an appropriate gamma matrix and making use of the Dirac algebra, and $\epsilon_{\mu\nu\sigma}$ is the completely antisymmetric tensor.

At zero magnetic field, $B \equiv 0$, the model depends on a single parameter [31], namely the dimensionful coupling constant $\bar{g}$ with mass dimension $2 - d$ describing the self-interaction of the fermionic degrees of freedom. In the following we consider the interesting case $\bar{g} > 0$. In the sense of statistical physics the coupling appears to correspond to an irrelevant operator within the perturbative Gaußian classification. However, this naive scaling analysis does not yield the correct picture for the infrared behavior of this model, as we will explain in detail in Chap. 4. From the point of view of quantum field theory, the Gross-Neveu model provides an example of a nonperturbatively renormalizable field theory [52], and the $(\bar{\psi}\psi)^2$ coupling becomes relevant near a non-Gaußian fixed point [31] in the renormalization group sense.

3.2 Spacetime and Chiral Gross-Neveu Symmetries

While the construction of local operators that conform to Lorentz[2] symmetry can be ensured by taking products of operators and performing suitable contractions over tensor indices, the transformation properties under discrete spacetime symmetries require more work. In [34] explicit representations for discrete spacetime transformations as realized on four-component spinor fields over three dimensional Euclidean space were given as follows:

$$\mathcal{C} : C_\xi = \frac{1}{2}\left[(1+\xi)\gamma_2\gamma_3 + \mathrm{i}(1-\xi)\gamma_2\gamma_5\right], \tag{3.10}$$

$$\mathcal{P} : P_\zeta = \frac{1}{2}\left[(1+\zeta)\gamma_1\gamma_3 + \mathrm{i}(1-\zeta)\gamma_1\gamma_5\right], \tag{3.11}$$

$$\mathcal{T} : T_\eta = \frac{1}{2}\left[(1+\eta)\gamma_1 + \mathrm{i}(1-\eta)\gamma_2\gamma_0\right], \tag{3.12}$$

where $\mathcal{C}$, $\mathcal{P}$, $\mathcal{T}$ denote charge conjugation, parity inversion and time reversal. To each transformation, there exists an associated unitary 4×4 matrix, which we denote by C_ξ, P_ζ and T_η, respectively.

[2] In this thesis we use the terms "Lorentzian" and "Euclidean" interchangeably. In any case, we build SO(3) or SO(2, 1) invariant operators by forming contractions of their respective irreducible representations. For a discussion of Wick rotation, see Appendix A.1. A proper discussion can be found in [51].

Other possible conventions were given for example in [53]. However, we will stick to the definition as displayed in Eqs. (3.10), (3.11) and (3.12). Concerning parity, it is worthwhile to mention that in three spacetime dimensions, parity inversion is properly defined by $(x_0, x_1, x_2) \mapsto (x_0, -x_1, x_2)$, i.e., only one of the spatial components is reversed. This is due to the fact, that in our case only a single generator for rotations exists. The above definition ensures that parity inversion is not an element of the connected component of rotations containing the identity. As can be seen in Eqs. (3.10)-(3.12), there exists an entire family of realizations of discrete transformations depending on pure phase variables ξ, ζ and η with unit modulus. We will simply set $\xi = \zeta = \eta = 1$ in the following and omit the subscripts on the transformation matrices. The realization of spacetime transformations on spinor fields reads for charge conjugation

$$\mathcal{C}\psi(x)\mathcal{C}^{-1} = (\bar{\psi}C)^T,\ \mathcal{C}\bar{\psi}(x)\mathcal{C}^{-1} = -(C^\dagger\psi(x))^T, \tag{3.13}$$

parity

$$\mathcal{P}\psi(x)\mathcal{P}^{-1} = P\psi(\tilde{x}),\ \mathcal{P}\bar{\psi}(\tilde{x})\mathcal{P}^{-1} = \bar{\psi}(\tilde{x})P^\dagger, \tag{3.14}$$

and time-reversal

$$\mathcal{T}\psi(x)\mathcal{T}^{-1} = T\psi(\hat{x}),\ \mathcal{T}\bar{\psi}(x)\mathcal{T}^{-1} = \bar{\psi}(\hat{x})T^\dagger. \tag{3.15}$$

Here we follow the notation as given in [53], and define

$$\tilde{x} = (x_0, -x_1, x_2)^T, \quad \hat{x} = (-x_0, x_1, x_2)^T. \tag{3.16}$$

Note that by virtue of $\mathcal{T}\,\mathrm{i}\,\mathcal{T}^{-1} = -\mathrm{i}$, time-reversal is an anti-unitary transformation. We will consider a theory to be symmetric under $\mathcal{C}$-, $\mathcal{P}$- and $\mathcal{T}$-transformations, if its Lagrangian density obeys

$$\mathcal{C}\mathcal{L}(x)\mathcal{C}^{-1} = \mathcal{L}(x), \tag{3.17}$$
$$\mathcal{P}\mathcal{L}(x)\mathcal{P}^{-1} = \mathcal{L}(\tilde{x}), \tag{3.18}$$
$$\mathcal{T}\mathcal{L}(x)\mathcal{T}^{-1} = \mathcal{L}(\hat{x}), \tag{3.19}$$

such that a simultaneous transformation acting on fields *and* coordinates leaves $\mathcal{L}$ invariant as a function of spacetime coordinates.

The Gross-Neveu model as defined in Eq. (3.2) is symmetric under the *discrete* chiral transformation

$$\psi \mapsto \gamma_5\psi, \quad \bar{\psi} \mapsto -\bar{\psi}\gamma_5. \tag{3.20}$$

Since the composite operator $\bar{\psi}\psi$ transforms into $-\bar{\psi}\psi$ under this discrete chiral transformation, a finite expectation value $\langle\bar{\psi}\psi\rangle \neq 0$ in a given quantum state signals the breakdown of chiral symmetry. In the following, we denote the discrete symmetry group by $\mathbb{Z}_2^5 = \{\mathbb{1}_4, \gamma_5\}$. However, there exists also a continuous Abelian chiral symmetry, generated by γ_{35}:

$$\psi \mapsto \mathrm{e}^{\mathrm{i}\varphi\gamma_{35}}\psi, \quad \bar{\psi} \mapsto \bar{\psi}\mathrm{e}^{-\mathrm{i}\varphi\gamma_{35}}. \tag{3.21}$$

It is easy to see that the element $\mathrm{e}^{\mathrm{i}\frac{\pi}{2}\gamma_{35}} \in \mathrm{U}^{35}(1)$ combined with the nontrivial $\mathbb{Z}_2^3$ transformation

$$\psi \mapsto \gamma_3\psi, \quad \bar{\psi} \mapsto -\bar{\psi}\gamma_3 \tag{3.22}$$

leads us back to the transformation Eq. (3.20). In this respect, the discrete $\mathbb{Z}_2^3$ does not yield a new symmetry of the theory and we will henceforth choose $\mathbb{Z}_2^5$ and $\mathrm{U}^{35}(1)$ to define the chiral symmetries of the three-dimensional Gross-Neveu model. In fact, taking tensor products of $\mathbb{1}$ and γ_{35} with the generators of $\mathrm{U}(N_\mathrm{f})$, the flavor symmetry is enhanced to $\mathrm{U}(N_\mathrm{f}) \times \mathrm{U}(N_\mathrm{f})$. The symmetry breaking by $\langle\bar{\psi}\psi\rangle \neq 0$ does not affect the flavor symmetry. It is perhaps worth mentioning that for the free theory, i.e., $\bar{g} = 0$, the symmetry transformations act independently on all flavor species j, $j = 1, \ldots, N_\mathrm{f}$. For finite couplings, however, all flavors are subject to a simultaneous chiral $\mathbb{Z}_2^5$ transformation, as we expect from the symmetry-breaking pattern induced by the interaction term. In the free case, i.e., for $\bar{g} = 0$, the model enjoys the usual *continuous* chiral symmetry of a chiral Dirac theory. Due to the flavor structure, this can be shown to yield a $\mathrm{U}(2N_\mathrm{f})$ symmetry[3], which is broken down to $\mathrm{U}(N_\mathrm{f}) \times \mathrm{U}(N_\mathrm{f})$ by $\sum_{j=1}^{N_\mathrm{f}}\langle\bar{\psi}_j\psi_j\rangle \neq 0$ (which can in fact be realized in a magnetically induced "quantum anomaly", even for a free system, cf. Chap. 6).

To conclude this section, we summarize the properties of electromagnetic quantities under discrete spacetime transformations. The gauge potential $\mathcal{A}$ transforms as

$$\mathcal{C}\mathcal{A}_\mu(x)\mathcal{C}^{-1} = -\mathcal{A}_\mu(x), \tag{3.23}$$

$$\mathcal{P}\mathcal{A}_\mu(x)\mathcal{P}^{-1} = \tilde{\mathcal{A}}_\mu(\tilde{x}), \tag{3.24}$$

$$\mathcal{T}\mathcal{A}_\mu(x)\mathcal{T}^{-1} = -\hat{\mathcal{A}}_\mu(\hat{x}), \tag{3.25}$$

[3]This comes about by forming tensor products of the N_f^2 generators of $\mathrm{U}(N_\mathrm{f})$ with the four generators $\mathbb{1}_4$, γ_3, γ_5 and γ_{35} of U(2), which yields an enlarged symmetry since flavor and chiral structure are independent. From another point of view, the chiral structure appears as a part of the enlarged flavor structure. If a mass term $\bar{\psi}\psi$ is included, γ_3 and γ_5 are "broken", and the remaining symmetries are generated by the elements of the Lie algebras $\mathrm{u}(N_\mathrm{f}) \otimes \mathbb{1}_4$ and $\mathrm{u}(N_\mathrm{f}) \otimes \gamma_{35}$. The resulting symmetry is compactly written as $\mathrm{U}(N_\mathrm{f}) \times \mathrm{U}(N_\mathrm{f})$.

where $\tilde{\mathcal{A}} = (\mathcal{A}_0, -\mathcal{A}_1, \mathcal{A}_2)^T$ and $\hat{\mathcal{A}} = (-\mathcal{A}_0, \mathcal{A}_1, \mathcal{A}_2)^T$. The field-strength tensor $\mathcal{F}_{\mu\nu} = \partial_\mu \mathcal{A}_\nu - \partial_\nu \mathcal{A}_\mu$ accordingly obeys

$$\mathcal{C}\mathcal{F}_{\mu\nu}(x)\mathcal{C}^{-1} = -\mathcal{F}_{\mu\nu}(x), \tag{3.26}$$
$$\mathcal{P}\mathcal{F}_{\mu\nu}(x)\mathcal{P}^{-1} = \tilde{\mathcal{F}}_{\mu\nu}(\tilde{x}), \tag{3.27}$$
$$\mathcal{T}\mathcal{F}_{\mu\nu}(x)\mathcal{T}^{-1} = -\hat{\mathcal{F}}_{\mu\nu}(\hat{x}). \tag{3.28}$$

Here, by $\tilde{\mathcal{F}}_{\mu\nu}$ and $\hat{\mathcal{F}}_{\mu\nu}$ we denote matrices which result from plugging Eqs. (3.24) and (3.25) into the definition of the field-strength tensor. The so-called dual "field-strength" $F_\mu \equiv \frac{1}{2}\epsilon_{\mu\nu\sigma}\mathcal{F}_{\nu\sigma}$ becomes a pseudo-vector quantity in three dimensions. Thus, it behaves as

$$\mathcal{C}F_\mu(x)\mathcal{C}^{-1} = -F_\mu(x), \tag{3.29}$$
$$\mathcal{P}F_\mu(x)\mathcal{P}^{-1} = -\tilde{F}_\mu(\tilde{x}), \tag{3.30}$$
$$\mathcal{T}F_\mu(x)\mathcal{T}^{-1} = \hat{F}_\mu(\hat{x}). \tag{3.31}$$

The simplest Lorentz, gauge and $\mathcal{C}$-, $\mathcal{P}$-, $\mathcal{T}$-invariants that can be built from the field strength and its dual are

$$\mathcal{F}_{\mu\nu}^2 \quad \text{and} \quad F_\mu^2. \tag{3.32}$$

Since $F_\mu^2 = \frac{1}{2}\mathcal{F}_{\mu\nu}^2$ there is only one linearly independent invariant.

3.3 Classification of Compatible Operators

Having collected the prerequisites to study all operators that are in principle compatible symmetry-wise with the Lagrangian density Eq. (3.2), we will give an exhaustive classification on the level of fermionic bilinears in Sect. 3.3.1 and then proceed to quartic fermionic terms including purely magnetically induced operators in Sect. 3.3.2.

3.3.1 Bilinear Operators

Fermionic bilinears are the building blocks of an action for fermionic degrees of freedom. Terms entering the quadratic part of the action define the inverse bare propagator of the theory. In our case we need to contract both spinor and Lorentz indices to form an appropriate scalar quantity. But due to the presence of the gauge background, we can as well use the gauge-invariant field strength tensor and its dual to build Lorentz invariant fermion bilinears. We consider only those bilinears which are Lorentz symmetric as a building block of the effective action. By use of Eqs. (3.13)-(3.15) and Eqs. (3.20), (3.21) we obtain the behavior of a given bilinear under discrete spacetime and chiral transformations. The results are collected in Tables 3.1, 3.2 and 3.3. For turning operators with

vector or tensor structure into Lorentz invariant scalars, we contract as indicated above with F_μ or $\mathcal{F}_{\mu\nu}$. By virtue of the canonical mass dimension of the fermion fields $[\psi] = \frac{d-1}{2}$ the mass dimension of a (nonderivative) fermion bilinear is $[\bar\psi\Gamma_O\psi] = d-1$ with $\Gamma_S \in \{\mathbb{1}, \gamma_3, \gamma_5, \gamma_{35}\}$ (scalar/pseudo-scalar), $\Gamma_V \in \{\gamma_\mu, \gamma_3\gamma_\mu, \gamma_5\gamma_\mu, \gamma_{35}\gamma_\mu$ (vector/axial-vector) or $\Gamma_T \in \{\sigma_{\mu\nu}, \gamma_3\sigma_{\mu\nu}, \gamma_5\sigma_{\mu\nu}, \gamma_{35}\sigma_{\mu\nu}\}$ (tensor/pseudo-tensor). Here

$$\sigma_{\mu\nu} = \frac{\mathrm{i}}{2}[\gamma_\mu, \gamma_\nu], \quad \mu, \nu = 0, 1, 2, \tag{3.33}$$

is the set of generators for (Euclidean) Lorentz transformations. For the contracted terms we obtain $[qF_\mu(\bar\psi\Gamma_\mu\psi)] = d+1$ and $[q\mathcal{F}_{\mu\nu}(\bar\psi\Gamma_{\mu\nu}\psi)] = d+1$, since $[F_\mu] = [\mathcal{F}_{\mu\nu}] = \frac{d}{2}$ and $[q] = \frac{4-d}{2}$. Taking into account that the spacetime integral in a local action contributes $[\int_x] = -d$ to the total mass dimension of a given local operator, these operators naively correspond to irrelevant directions in theory space. The charge q needs to be included in this consideration, since we are interested in magnetically *induced* phenomena. We could also perform two contractions of qF_μ with an appropriate tensor structure. This would inevitably increase the mass dimension by 2 and render this term even more power-counting irrelevant compared to mass terms (with mass dimension -1) and kinetic operators with mass dimension 0. However, from Tables 3.1-3.3, we see that none of these bilinear operators containing the magnetic field is compatible with the symmetries of the Gross-Neveu model. They cannot be generated during the RG flow in a continuous fashion. Combinations like $\mathcal{F}_{\mu\nu}(\bar\psi\sigma_{\mu\nu}\psi)$ and $F_\mu(\bar\psi\gamma_{35}\gamma_\mu\psi)$ conform to spacetime symmetries, but violate the chiral symmetries of the Gross-Neveu action. Chirally invariant combinations containing two F_μ fields are not even symmetric with respect to $\mathcal{C}$, $\mathcal{P}$ and $\mathcal{T}$.

To conclude, we would like to comment that each F_μ contraction with an appropriate vector bilinear can be rewritten as a contraction of $\mathcal{F}_{\mu\nu}$ with a tensor bilinear by means of Eqs. (3.7)-(3.9):

$$F_\mu(\bar\psi\gamma_\mu\psi) = -\frac{1}{2}\mathcal{F}_{\mu\nu}(\bar\psi\gamma_{35}\sigma_{\mu\nu}\psi), \tag{3.34}$$

$$F_\mu(\bar\psi\gamma_3\gamma_\mu\psi) = -\frac{\mathrm{i}}{2}\mathcal{F}_{\mu\nu}(\bar\psi\gamma_5\sigma_{\mu\nu}\psi), \tag{3.35}$$

$$F_\mu(\bar\psi\gamma_5\gamma_\mu\psi) = +\frac{\mathrm{i}}{2}\mathcal{F}_{\mu\nu}(\bar\psi\gamma_3\sigma_{\mu\nu}\psi), \tag{3.36}$$

$$F_\mu(\bar\psi\gamma_{35}\gamma_\mu\psi) = -\frac{1}{2}\mathcal{F}_{\mu\nu}(\bar\psi\sigma_{\mu\nu}\psi). \tag{3.37}$$

	$\mathcal{C}$	$\mathcal{P}$	$\mathcal{T}$	$\mathbb{Z}_2^5$	$\mathrm{U}^{35}(1)$
$(\bar\psi\psi)(x)$	$(\bar\psi\psi)(x)$	$(\bar\psi\psi)(\tilde x)$	$(\bar\psi\psi)(\hat x)$	$-(\bar\psi\psi)(x)$	$(\bar\psi\psi)(x)$
$(\bar\psi\gamma_3\psi)(x)$	$-(\bar\psi\gamma_3\psi)(x)$	$-(\bar\psi\gamma_3\psi)(\tilde x)$	$-(\bar\psi\gamma_3\psi)(\hat x)$	$(\bar\psi\gamma_3\psi)(x)$	$(\bar\psi\gamma_3\mathrm{e}^{2\mathrm{i}\varphi\gamma_{35}}\psi)(x)$
$(\bar\psi\gamma_5\psi)(x)$	$(\bar\psi\gamma_5\psi)(x)$	$(\bar\psi\gamma_5\psi)(\tilde x)$	$-(\bar\psi\gamma_5\psi)(\hat x)$	$-(\bar\psi\gamma_5\psi)(x)$	$(\bar\psi\gamma_5\mathrm{e}^{2\mathrm{i}\varphi\gamma_{35}}\psi)(x)$
$(\bar\psi\gamma_{35}\psi)(x)$	$(\bar\psi\gamma_{35}\psi)(x)$	$-(\bar\psi\gamma_{35}\psi)(\tilde x)$	$-(\bar\psi\gamma_{35}\psi)(\hat x)$	$(\bar\psi\gamma_{35}\psi)(x)$	$(\bar\psi\gamma_{35}\psi)(x)$

Table 3.1: Classification of scalar/pseudo-scalar fermion bilinears $(\bar\psi\Gamma_S\psi)(x)$ according to their behavior under discrete spacetime and chiral transformations.

	$\mathcal{C}$	$\mathcal{P}$	$\mathcal{T}$	$\mathbb{Z}_2^5$	$\mathrm{U}^{35}(1)$
$(\bar{\psi}\gamma_\mu\psi)(x)$	$-(\bar{\psi}\gamma_\mu\psi)(x)$	$(\bar{\psi}\tilde{\gamma}_\mu\psi)(\tilde{x})$	$-(\bar{\psi}\hat{\gamma}_\mu\psi)(\hat{x})$	$(\bar{\psi}\gamma_\mu\psi)(x)$	$(\bar{\psi}\gamma_\mu\psi)(x)$
$(\bar{\psi}\gamma_3\gamma_\mu\psi)(x)$	$-(\bar{\psi}\gamma_3\gamma_\mu\psi)(x)$	$-(\bar{\psi}\gamma_3\tilde{\gamma}_\mu\psi)(\tilde{x})$	$(\bar{\psi}\gamma_3\hat{\gamma}_\mu\psi)(\hat{x})$	$-(\bar{\psi}\gamma_3\gamma_\mu\psi)(x)$	$(\bar{\psi}\gamma_3\gamma_\mu \mathrm{e}^{2\mathrm{i}\varphi\gamma_{35}}\psi)(x)$
$(\bar{\psi}\gamma_5\gamma_\mu\psi)(x)$	$(\bar{\psi}\gamma_5\gamma_\mu\psi)(x)$	$(\bar{\psi}\gamma_5\tilde{\gamma}_\mu\psi)(\tilde{x})$	$(\bar{\psi}\gamma_5\hat{\gamma}_\mu\psi)(\hat{x})$	$(\bar{\psi}\gamma_5\gamma_\mu\psi)(x)$	$(\bar{\psi}\gamma_5\gamma_\mu \mathrm{e}^{2\mathrm{i}\varphi\gamma_{35}}\psi)(x)$
$(\bar{\psi}\gamma_{35}\gamma_\mu\psi)(x)$	$-(\bar{\psi}\gamma_{35}\gamma_\mu\psi)(x)$	$-(\bar{\psi}\gamma_{35}\tilde{\gamma}_\mu\psi)(\tilde{x})$	$(\bar{\psi}\gamma_{35}\hat{\gamma}_\mu\psi)(\hat{x})$	$-(\bar{\psi}\gamma_{35}\gamma_\mu\psi)(x)$	$(\bar{\psi}\gamma_{35}\gamma_\mu\psi)(x)$

Table 3.2: Classification of vector/axial-vector fermion bilinears $(\bar{\psi}\Gamma_V\psi)(x)$ according to their behavior under discrete spacetime and chiral transformations. Here, we have defined $\tilde{\gamma} = (\gamma_0, -\gamma_1, \gamma_2)^T$ and $\hat{\gamma} = (-\gamma_0, \gamma_1, \gamma_2)^T$. The bilinear $\bar{\psi}\gamma_{35}\gamma_\mu\psi$ can be shown to be related to $\bar{\psi}\sigma_{\mu\nu}\psi$, cf. Eq. (3.7).

	$\mathcal{C}$	$\mathcal{P}$	$\mathcal{T}$	$\mathbb{Z}_2^5$	$\mathrm{U}^{35}(1)$
$(\bar{\psi}\sigma_{\mu\nu}\psi)(x)$	$-(\bar{\psi}\sigma_{\mu\nu}\psi)(x)$	$(\bar{\psi}\tilde{\sigma}_{\mu\nu}\psi)(\tilde{x})$	$(\bar{\psi}\hat{\sigma}_{\mu\nu}\psi)(\hat{x})$	$-(\bar{\psi}\sigma_{\mu\nu}\psi)(x)$	$(\bar{\psi}\sigma_{\mu\nu}\psi)(x)$
$(\bar{\psi}\gamma_3\sigma_{\mu\nu}\psi)(x)$	$(\bar{\psi}\gamma_3\sigma_{\mu\nu}\psi)(x)$	$-(\bar{\psi}\gamma_3\tilde{\sigma}_{\mu\nu}\psi)(\tilde{x})$	$(\bar{\psi}\gamma_3\hat{\sigma}_{\mu\nu}\psi)(\hat{x})$	$(\bar{\psi}\gamma_3\sigma_{\mu\nu}\psi)(x)$	$(\bar{\psi}\gamma_3\sigma_{\mu\nu}\mathrm{e}^{2\mathrm{i}\varphi\gamma_{35}}\psi)(x)$
$(\bar{\psi}\gamma_5\sigma_{\mu\nu}\psi)(x)$	$-(\bar{\psi}\gamma_5\sigma_{\mu\nu}\psi)(x)$	$(\bar{\psi}\gamma_5\tilde{\sigma}_{\mu\nu}\psi)(\tilde{x})$	$(\bar{\psi}\gamma_5\hat{\sigma}_{\mu\nu}\psi)(x)$	$-(\bar{\psi}\gamma_5\sigma_{\mu\nu}\psi)(x)$	$(\bar{\psi}\gamma_5\sigma_{\mu\nu}\mathrm{e}^{2\mathrm{i}\varphi\gamma_{35}}\psi)(x)$
$(\bar{\psi}\gamma_{35}\sigma_{\mu\nu}\psi)(x)$	$-(\bar{\psi}\gamma_{35}\sigma_{\mu\nu}\psi)(x)$	$-(\bar{\psi}\gamma_{35}\tilde{\sigma}_{\mu\nu}\psi)(\tilde{x})$	$(\bar{\psi}\gamma_{35}\hat{\sigma}_{\mu\nu}\psi)(\hat{x})$	$(\bar{\psi}\gamma_{35}\sigma_{\mu\nu}\psi)(x)$	$(\bar{\psi}\gamma_{35}\sigma_{\mu\nu}\psi)(x)$

Table 3.3: Classification of tensor/pseudo-tensor fermion bilinears $(\bar{\psi}\Gamma_T\psi)(x)$ according to their behavior under discrete spacetime and chiral transformations. The matrices $\tilde{\sigma}_{\mu\nu}$ and $\hat{\sigma}_{\mu\nu}$ carry the same sign structure as $\tilde{\mathcal{F}}_{\mu\nu}$ and $\hat{\mathcal{F}}_{\mu\nu}$ in Eq. (3.27) and (3.28), respectively. The bilinear $\bar{\psi}\gamma_{35}\sigma_{\mu\nu}\psi$ can be shown to be equivalent to $\bar{\psi}\gamma_\mu\psi$, cf. Eq. (3.9). It also holds that $\bar{\psi}\gamma_{3/5}\sigma_{\mu\nu}\psi \sim \bar{\psi}\gamma_{5/3}\gamma_\mu\psi$.

3.3.2 Quartic Operators

Quartic fermionic terms describe the two-body interaction processes in our theory. We first ask for terms

$$\sum_{i,j=1}^{N_\mathrm{f}} (\bar{\psi}_i\Gamma_X\psi_i)(\bar{\psi}_j\Gamma_Y\psi_j) \tag{3.38}$$

which obey the symmetries of the original Gross-Neveu action and have canonical mass dimension $[(\bar{\psi}_i\Gamma_X\psi_i)(\bar{\psi}_j\Gamma_Y\psi_j)] = 2d-2$. In a next step, we analyze contributions with mass dimension $2d$, i.e., quartic terms that include a contraction with a mass dimension 2 object. In principle, one could also move to operators with higher mass dimension. But with increasing mass dimension our naive expectation is that these operators become increasingly irrelevant for the IR behavior of the theory, even near a non-Gaußian fixed point. Note that terms as captured by Eq. (3.38) are composed of flavor singlets. Invariant sums of bilinears with off-diagonal flavor structure can be brought into this singlet-singlet form by an appropriate Fierz transformation. The result is in general a sum over several singlet-singlet contributions with different Lorentz structure. Since a discrete chiral symmetry is less restrictive than continuous chiral symmetry, the number of allowed quartic terms appears to be quite large. However, the requirement for invariance under the *continuous* $\mathrm{U}^{35}(1)$ symmetry remedies the situation somewhat. The allowed terms in the absence of a magnetic field are exhausted by $(\bar{\psi}\psi)^2$, $(\bar{\psi}\gamma_\mu\psi)^2$, $(\bar{\psi}\sigma_{\mu\nu}\psi)^2$ and $(\bar{\psi}\gamma_{35}\psi)^2$, $(\bar{\psi}\gamma_{35}\gamma_\mu\psi)^2$, $(\bar{\psi}\gamma_{35}\sigma_{\mu\nu}\psi)^2$ as well as the

invariant combinations $(\bar{\psi}\gamma_3\psi)^2+(\bar{\psi}\gamma_5\psi)^2$, $(\bar{\psi}\gamma_3\gamma_\mu\psi)^2+(\bar{\psi}\gamma_5\gamma_\mu\psi)^2$ where we have omitted all flavor indices. Actually $(\bar{\psi}\gamma_{35}\gamma_\mu\psi)^2$ and $(\bar{\psi}\gamma_{35}\sigma_{\mu\nu}\psi)^2$ can be written as

$$(\bar{\psi}\gamma_{35}\sigma_{\mu\nu}\psi)^2 = \frac{1}{2}(\bar{\psi}\gamma_\mu\psi)^2, \tag{3.39}$$

$$(\bar{\psi}\gamma_{35}\gamma_\mu\psi)^2 = \frac{1}{2}(\bar{\psi}\sigma_{\mu\nu}\psi)^2, \tag{3.40}$$

since they are simply linear combinations of the Dirac algebra basis elements. The remaining six quartic terms are mutually independent. They parameterize the "Gross-Neveu theory space" without an external magnetic field in the pointlike limit. It is interesting to note that a renormalization group flow calculation in the pointlike limit does actually not make use of this full theory space, but only reproduces the Gross-Neveu coupling in the derivative expansion. This might be accidental or could point to a further hidden symmetry.

We now consider quartic fermionic terms that can be built by contracting once with $q\mathcal{F}_{\mu\nu}$ or qF_μ. Due to the identities Eqs. (3.34)-(3.37), it is sufficient to consider contractions with qF_μ only. From Tables 3.1-3.3 we conclude, that the following terms are allowed

$$(\bar{\psi}\psi)(\bar{\psi}\gamma_{35}\gamma_\mu F_\mu\psi) = -\frac{1}{2}(\bar{\psi}\psi)(\bar{\psi}\sigma_{\mu\nu}\mathcal{F}_{\mu\nu}\psi), \tag{3.41}$$

$$(\bar{\psi}\gamma_{35}\psi)(\bar{\psi}\gamma_\mu F_\mu\psi), \tag{3.42}$$

and

$$(\bar{\psi}\gamma_3\psi)(\bar{\psi}\gamma_5\gamma_\mu F_\mu\psi)+(\bar{\psi}\gamma_5\psi)(\bar{\psi}\gamma_3\gamma_\mu F_\mu\psi). \tag{3.43}$$

Of course, a $\mathrm{U}^{35}(1)$ invariant operator with fully contracted Lorentz indices squared is also compatible with the Gross-Neveu symmetries, but has mass dimension larger or equal to $2d+2$. One could also consider functions of the invariant $(qF_\mu)^2$ times a bilinear squared. This, however, corresponds to operators with arbitrarily high mass dimension. In Chap. 6 we show that starting from the naive Gross-Neveu action Eq. (3.1), a term of the type Eq. (3.41) is indeed generated in an infinitesimal renormalization group step.

Chapter 4

Gross-Neveu Universality and Chiral Quantum Phase Transition

Our analysis of the three dimensional Gross-Neveu model is performed within the modern formulation of the functional renormalization group. Employing a gradient expansion, we can immediately access the fixed-point structure of the model and directly compute universal properties, such as critical exponents. Fully analytic results for the fixed-point potential and all universal critical exponents (within a given truncation) can be obtained in the so-called large-N_f limit, formally defined by sending the number of fermion flavors to infinity.

As we mentioned at the end of Chap. 3, the Gross-Neveu Lagrangian includes a short-ranged interaction vertex, which from the viewpoint of field theory renders the theory perturbatively non-renormalizable. In seeking well defined continuum limits, i.e., true field theories, the requirement of renormalizability can formally be verified and realized in perturbatively renormalizable theories in a weak coupling expansion. Here, all free parameters of a model can be fixed to physical values and the renormalized trajectory can be constructed order-by-order in a perturbative expansion. This strategy can successfully be applied to theories that exist at least over a wide range of scales, but still suffer from a maximum scale of UV extension, such as QED [54–57] or the standard model Higgs sector [58–60]. If a theory is asymptotically free, i.e., if the point of vanishing coupling (Gaußian fixed point) is a UV attractive fixed point, the perturbative construction can even be applied on all scales, as in QCD. However, it has long been known that the conclusion about the perturbative non-renormalizability in the case of the Gross-Neveu model in $d = 3$ is only an artifact of perturbative quantization. By means of a Hubbard-Stratonovich transformation, the fermionic theory can be partially bosonized[1] such that an alternative expansion in terms of the inverse fermion flavor number N_f can conveniently be formulated. The large-N_f expansion is thus built around the well understood large-N_f limit. This expansion scheme turns out to be renormalizable to all orders, rather similar to a small coupling expansion in a perturbatively renormalizable model [61–63]. This suggests the

[1] Here we speak of partial bosonization to emphasize the difference to fermionic models in 2-dimensional spacetime, where bosonization refers to an equivalence of (local) fermionic and (nonlocal) bosonic operators.

existence of an interacting Gross-Neveu model in $d = 3$, i.e., a model with an interacting continuum limit. In the following we will reproduce these results with the functional renormalization group and establish the Gross-Neveu model as a benchmark system for simple truncations. Indeed, one may wonder whether this conclusion about the nonperturbative renormalizability of the model is actually nontrivial after all: at a first glance the partially bosonized version of the Gross-Neveu model appears to be identical to a Yukawa model. This in turn seems to suggest that the renormalizability in the large-N_f expansion may simply reflect the super-renormalizability of the $d = 3$ Yukawa model. In fact, four-fermi models in $d = 4$ are known to be related to Yukawa models near the Gaußian fixed point [64, 65]. In the following, we will elucidate that this is, in fact, not the case in $2 < d < 4$. As we show below, also the renormalization group flow of the partially bosonized formulation is controlled by a non-Gaußian fixed point. Similar observations have been made by studying the scaling properties of corresponding lattice models toward the continuum limit [66, 67].

Renormalizability is often described as a seemingly technical cornerstone for the construction of admissible models in particle physics. Renormalization fixes physical parameters of a model to measured values of observable quantities. A prime physical meaning of renormalizability is the capability of a model to provide an accurate description of a physical system over a wide range of scales at which measurements can be performed. The set of physical parameters, say, couplings or mass parameters etc., measured at different scales then define the renormalized trajectory in theory space. If one demands for a specific model to provide a *fundamental* description of nature, the model must be valid on all scales, in particular down to arbitrarily short-distance scales. The renormalized trajectory then must exist on all scales without developing singularities. As already hinted to above, renormalizability is by no means bound to a perturbative construction. Even though reliable nonperturbative information might be difficult to obtain, the concept of renormalizability and the existence of a renormalized trajectory on all scales can be formulated rather generally within Weinberg's *asymptotic safety scenario* [6]. Loosely speaking, asymptotic safety is the generalization of asymptotic freedom at the Gaußian fixed point to the case of a non-Gaußian fixed point. As a fixed point of the renormalization group by construction defines a point in parameter space where the system becomes scale invariant, renormalization group trajectories that hit the fixed point toward the ultraviolet (UV) can be extended to arbitrarily high energy/momentum scales, thereby defining a fundamental theory, for reviews see [7, 8, 68–70]. All renormalization group trajectories that would evolve into the fixed point as the renormalization scale is increased toward the UV span the so-called *critical surface*[2]. The dimension of the critical surface is simply given by the number[3] of IR relevant directions in theory space. If a theory lives on this hypersurface of fundamental theories (that is, with a well defined continuum limit), the values of all couplings describing IR irrelevant directions in theory space are fixed by the trajectory.

[2]Not to be confused with the critical manifold, which will appear shortly.

[3]In the case of quantum gravity, obtained by functionally quantizing an Einstein-Hilbert action, the dimension of the critical surface was found to be 2 and increases only slightly in larger truncations.

As fermionic models occur in many circumstances, for example as effective models for the many-body physics of strongly correlated electron systems and low-energy descriptions of QCD, our analysis of the microscopic completeness of the Gross-Neveu model also provides a lesson for the functional renormalization group treatment of such systems. Of course, model studies of fermionic systems conventionally aim at long-range IR phenomena instead of short-distance UV behavior. As will be detailed below, the non-Gaußian fixed-point facilitating microscopic completeness in the Gross-Neveu model at the same time serves as a quantum critical point associated with a 2nd order quantum phase transition toward a phase with broken discrete chiral symmetry. This phase transition has been studied already with a variety of techniques [66, 67, 74–81].

This point of view is strongly motivated by the explicit construction of a nontrivial continuum limit of a given quantum field theory and thus focuses on a special set of renormalization group trajectories. Yet, from a statistical physics/condensed matter point of view, which we alluded to in the introduction Chap. 1, it is perhaps more natural to argue in reverse. The continuum limit exists due to a 2nd order quantum phase transition in a microscopic model. The microscopic system and the quantum field theory differ in IR irrelevant directions. However, when the microscopic lattice model is tuned exactly to criticality, it will approach the non-Gaußian fixed point as the flow evolves toward the IR. A trajectory traced out by the model now lives on the *critical manifold*, i.e., the basin of IR attraction. In this sense, all *universal* properties of the lattice model can be extracted from the quantum field theory. Coming from a lattice model, there is, of course, no such thing as a fundamental theory extending beyond the scales set by the lattice spacing. From a more pragmatic, field theoretic perspective, any continuum model that shares the same universality class as defined by a fixed point of an underlying (possibly, *more fundamental*) theory, will yield a good description of the universal long-distance behavior of the deeper theory.

Our investigation of Gross-Neveu universality will start with the large-N_f limit in Sect. 4.1 after partial bosonization. There we will obtain a first glance at the chiral quantum phase transition, manifesting itself as a finite chiral condensate in the ground-state of the theory. It will also allow us to shed some light on the relation to three-dimensional Yukawa theories through the composite character of the bosonic field. In Sect. 4.2 we will analyze the beta function of the four-fermion vertex in the pointlike limit. Moving to Sect. 4.3 we incorporate an effective momentum dependence of the four-fermion vertex in the flow equations and show how corrections beyond the mean-field approximation can be systematically taken into account. Equipped with this improved truncation, we briefly investigate IR properties of both the broken and the symmetric ground-state in Sect. 4.4. Finally, in Sect. 4.5 we analyze the fixed-point structure obtained from the bosonized truncation and make contact with mean-field and $1/N_\mathrm{f}$ results.

4.1 Mean-Field Theory and $1/N_\mathrm{f}$-Expansion

To begin our analysis of the Gross-Neveu model, we will first study its large-N_f limit, where many results become analytically available. For the Gross-Neveu model, chiral symmetry breaking is known to occur in this limit. The dynamical symmetry breaking induced by fermionic quantum fluctuations corresponds to a quantum phase transition, i.e., a phase transition occuring at zero temperature. In such a transition, the ground-state of the system is restructured. The fermionic single-particle spectrum obtains a gap, as illustrated schematically in Fig. 4.2. To observe the transition, the Gross-Neveu model needs to be tuned to criticality. In fact, the breaking of chiral symmetry requires a finite critical coupling. We quantize the Gross-Neveu action considered in Chap. 3:

$$\mathcal{Z} = \int \prod_{j=1}^{N_\mathrm{f}} \mathcal{D}\bar{\psi}_j \mathcal{D}\psi_j \, \mathrm{e}^{-S[\{\bar{\psi}_j\},\{\psi_j\}]}, \tag{4.1}$$

where $\mathcal{Z}$ is the generating functional for ground state correlation functions evaluated at vanishing source. The action for the N_f species of Grassmann-valued spinor fields as given by Eqs. (3.1) and (3.2) reads

$$S[\{\bar{\psi}_j\},\{\psi_j\}] = \int_x \left\{ \sum_{j=1}^{N_\mathrm{f}} \bar{\psi}_j \mathrm{i}\partial\!\!\!/ \psi_j + \sum_{i,j=1}^{N_\mathrm{f}} \bar{\psi}_i \psi_i \frac{\bar{g}}{2N_\mathrm{f}} \bar{\psi}_j \psi_j \right\}. \tag{4.2}$$

Partial Bosonization

Dynamical symmetry breaking and the formation of a fermion condensate in the Gross-Neveu model can conveniently be studied by introducing an auxiliary bosonic field σ into the functional integral Eq. (4.1). Formulations of the Gross-Neveu model using partial bosonization can be employed to study various aspects such as its ground-state phase structure and its phase diagram at finite temperature and chemical potential [85–93]. Formally, we introduce this auxiliary field by multiplying the functional integral by a suitable resolution of the identity,

$$1 \propto \int \mathcal{D}\sigma \, \mathrm{e}^{-N_\mathrm{f} \frac{\bar{h}^2}{2\bar{g}} \int_x \sigma^2} = \int \mathcal{D}\sigma \, \mathrm{e}^{-\frac{\bar{g}}{2N_\mathrm{f}} \int_x \left\{ \left(\frac{\bar{g}}{N_\mathrm{f}}\right)^{-1} \bar{h}\sigma + \mathrm{i} \sum_{j=1}^{N_\mathrm{f}} \bar{\psi}_j \psi_j \right\}^2}, \tag{4.3}$$

which is known as a Hubbard-Stratonovich transformation [94, 95]. The judiciously chosen shift in the integration variable precisely cancels the four-fermion term in the original fermionic action. The functional integral representation of the generating functional $\mathcal{Z}$ then becomes

$$\mathcal{Z} = \int \prod_{j=1}^{N_\mathrm{f}} \mathcal{D}\bar{\psi}_j \mathcal{D}\psi_j \mathcal{D}\sigma \, \mathrm{e}^{-S[\{\bar{\psi}_j\},\{\psi_j\},\sigma]}, \tag{4.4}$$

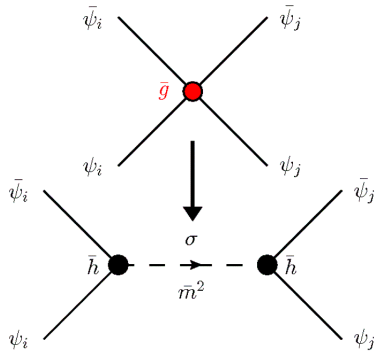

Figure 4.1: Diagrammatic representation of the Hubbard-Stratonovich decoupling, Eq. (4.3). The interaction between fermions is replaced by a boson exchange process.

where the partially bosonized action of the Gross-Neveu model reads as

$$S[\{\bar{\psi}_j\},\{\psi_j\},\sigma] = N_\mathrm{f}\int_x \frac{\bar{h}^2}{2\bar{g}}\sigma^2 + \int_x \sum_{j=1}^{N_\mathrm{f}} \bar{\psi}_j\left(\mathrm{i}\partial\!\!\!/ + \mathrm{i}\bar{h}\sigma\right)\psi_j. \tag{4.5}$$

The functional integral now includes integration measures for both fermionic and bosonic fields. As the auxiliary bosonic field only occurs quadratically in the action, it can be integrated out again. On the level of the action, this corresponds to replacing the bosonic field by its equation of motion, $N_\mathrm{f}\bar{m}^2\sigma = -\mathrm{i}\bar{h}\sum_{j=1}^{N_\mathrm{f}}\bar{\psi}_j\psi_j$. The action then reduces to the original Gross-Neveu action. The prefactor $\bar{m}^2 = \frac{\bar{h}^2}{\bar{g}}$ is understood as the bosonic mass. From the viewpoint of the Hubbard-Stratonovich transformation, the Yukawa coupling $\bar{h}$ is redundant as it can be scaled into the σ field. Only the ratio $\bar{h}^2/\bar{m}^2$ has a physical meaning. In our formulation, the Yukawa coupling $\bar{h}$ is implicitly understood to carry mass dimension $[\bar{h}] = \frac{4-d}{2}$ in order to deal with an auxiliary field with mass dimension $[\sigma] = \frac{d-2}{2}$. The mixed action Eq. (4.5) now contains only terms of order N_f. Under a discrete chiral transformation Eq. (3.20) the σ field transforms as $\sigma \mapsto -\sigma$. From a phenomenological point of view σ can be considered as a bound state of fermions, $\sigma \sim \bar{\psi}\psi$. Thus, the ground-state expectation value of σ is a proper order parameter for chiral symmetry breaking. Due to the Hubbard-Stratonovich transformation, the N_f fermion flavors enter only bilinearly and can be integrated out from the corresponding functional integral. The fermion determinant is equivalent to a trace-log contribution to the exponential. This yields a purely bosonic effective theory for the Gross-Neveu model:

$$S[\sigma] = N_\mathrm{f}\int_x \frac{1}{2}\bar{m}^2\sigma^2 - N_\mathrm{f}\,\mathrm{Tr}\ln\left[\mathrm{i}\partial\!\!\!/ + \mathrm{i}\bar{h}\sigma\right], \tag{4.6}$$

where $\mathrm{Tr}(\,\cdot\,)$ denotes a functional trace.

Derivation of the Mean-Field Phase Diagram

Since all the different flavors couple to the flavor-singlet σ in the same way, each flavor sector produces the same contribution to the bosonic action. With σ being a proper quantum field depending on spacetime coordinates, the fermionic trace-log is a highly nonlocal object and practically impossible to study analytically for arbitrary field configurations. Classical solutions of the action Eq. (4.6) obtained from the variational principle

$$\frac{\delta}{\delta\sigma(x)} S[\sigma] \stackrel{!}{=} 0 \tag{4.7}$$

correspond to the mean-field approximation. This neglects quantum fluctuations of the bosonic field completely. To solve Eq. (4.7) for a general $\sigma(x)$ still poses a formidable task. If we restrict ourselves to homogeneous mean-field configurations $\sigma = \langle\sigma\rangle \equiv$ const., where within the mean-field approach it is allowed to identify σ with its expectation value, we obtain the condition

$$\frac{\partial U(\sigma)}{\partial\sigma} \stackrel{!}{=} 0. \tag{4.8}$$

Here, $U(\sigma)$ is the effective potential. In fact, in $d = 2$ inhomogeneous condensates have been identified in some parts of the phase diagram at finite temperature and large values of the chemical potential [89]. The status of inhomogeneous mean-field solutions for higher-dimensional fermionic models is subject to ongoing work, see e. g. [96, 97]. A homogeneous ground state $\sigma_0 =$ const. is then implicitly given by the solution of:

$$\sigma_0 = 4\frac{\bar{h}^2}{\bar{m}^2} \int_p \frac{\sigma_0}{p^2 + \bar{h}^2\sigma_0^2}\,, \tag{4.9}$$

with $\int_p = \int \frac{d^dp}{(2\pi)^d}$. Apparently this equation has a trivial solution, $\sigma_0 = 0$. Moreover, nontrivial solutions for σ_0 can be found for suitably adjusted values of the four-fermion coupling $\bar{g} = \bar{h}^2/\bar{m}^2$. Since in $d = 3$ ($d = 4$) the right-hand side of Eq. (4.9) is linearly (quadratically) divergent, we impose a sharp UV cutoff $\Lambda \gg \bar{m}_{\mathrm{f}} = \bar{h}^2\sigma_0^2$. For $d = 3$, we find

$$\bar{m}_{\mathrm{f}} \simeq \frac{2}{\pi}\left(\Lambda - \frac{\pi^2}{2}\frac{\bar{m}^2}{\bar{h}^2}\right). \tag{4.10}$$

Thus, the fermions acquire a nonzero mass due to the spontaneous breakdown of chiral symmetry, provided we choose $\bar{m}^2/\bar{h}^2 < 2\Lambda/\pi^2$. In terms of the four-fermion coupling, we can read off a critical value for the dimensionless coupling $g = \Lambda\bar{g} = \Lambda\bar{h}^2/\bar{m}^2$ above which the IR physics is governed by dynamical symmetry breaking:

$$g_{\mathrm{c}} = \frac{\pi^2}{2}. \tag{4.11}$$

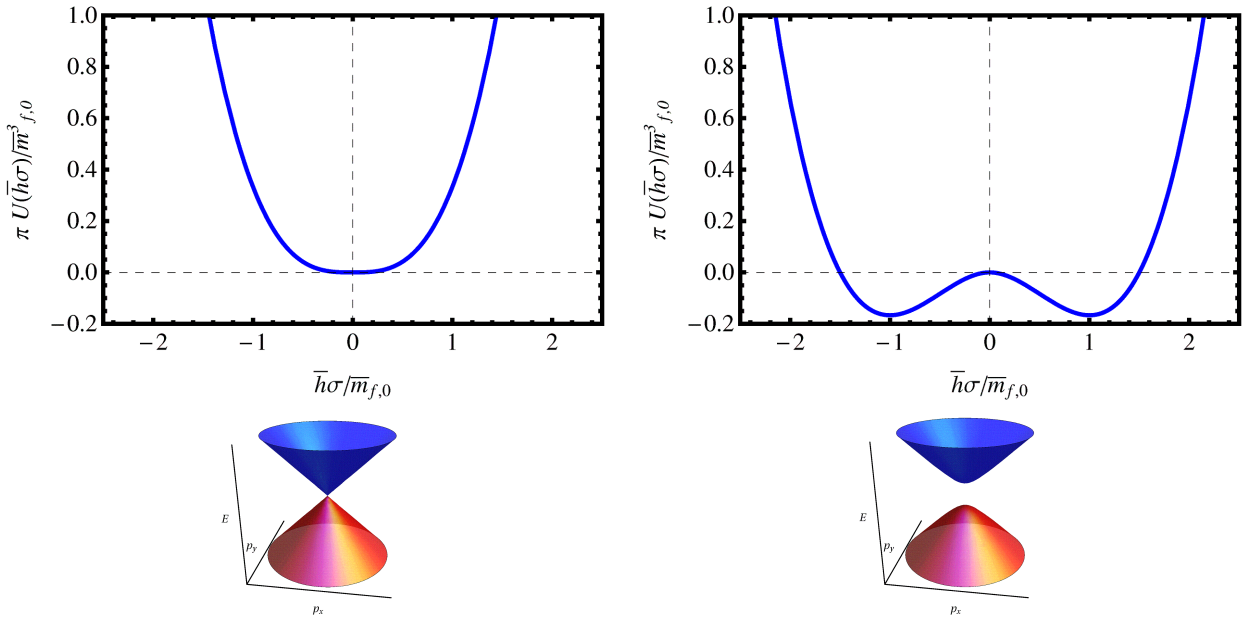

Figure 4.2: Plots of the bosonic effective potential Eq. (4.12) (as a function of $\bar{h}\sigma$) and schematic representation of the quantum phase transition on the level the fermionic single-particle spectrum. For subcritical values, the system resides in the chirally symmetric phase and only trivial minima in the effective potential occur associated with massless fermions (left). As the coupling exceeds its critical value, the chiral symmetry is broken dynamically and the fermions become massive with $\bar{m}_\mathrm{f}$ (right). The spectrum is changed from linear dispersion $E = \pm|\boldsymbol{p}|$ (left) defining a Dirac cone to $E = \pm\sqrt{\boldsymbol{p}^2 + \bar{m}_\mathrm{f}^2}$, defining a hyperboloid (right).

From the viewpoint of the partially bosonized theory, we find that the Yukawa coupling and the boson mass are not independent parameters. For a fixed ratio $\bar{h}^2/\bar{m}^2 > \bar{g}_\mathrm{c}$ the IR physics remains unchanged. Thus, the purely bosonic description of the theory in this approximation depends only on a single parameter.

We can integrate Eq. (4.9) to yield $U(\sigma)$. Assuming $\bar{m}_\mathrm{f} \neq 0$, we get in a scheme independent way [98]

$$U(\sigma) = \int_0^\sigma \frac{\partial}{\partial\sigma'} U(\sigma') = \frac{1}{\pi}\int_0^\sigma \left(\bar{h}^3|\sigma'|\sigma' - \bar{m}_\mathrm{f}\bar{h}^2\sigma'\right) = \frac{1}{\pi}\left(\frac{1}{3}\bar{h}^3|\sigma|^3 - \frac{\bar{m}_\mathrm{f}}{2}\bar{h}^2\sigma^2\right), \tag{4.12}$$

see Fig. 4.2 for a plot in both the symmetric and the broken phase. The scheme dependence is actually "hidden" in $\bar{m}_\mathrm{f}$. Keeping $\bar{m}_\mathrm{f}$ fixed (since it is a physical observable), our particular regularization scheme employed to arrive at Eq. (4.10) defines a pair $(\Lambda, \bar{g}(\Lambda))$ (remember $\bar{g} = \frac{\bar{h}^2}{\bar{m}^2}$), such that for different choices of Λ, we need to tune the bare parameter $g(\Lambda)$ in order to keep the dynamically generated fermion mass $\bar{m}_\mathrm{f}$ unaffected. Of course, using a regulator for only the spatial momentum integrations, these results remain unchanged [98].

Induced Bosonic Propagator

The fermionic loop, constituting the leading order contribution to the bosonic effective action in the $1/N_\mathrm{f}$-expansion, yields the inverse bosonic propagator [66, 99]

$$G_\sigma^{-1}(p) = \frac{d_\gamma \pi \bar{h}^2}{2(4\pi)^{3/2}\Gamma(3/2)} \left(p^2 + 4\bar{m}_\mathrm{f}^2\right) \frac{\arctan(\sqrt{p^2}/2\bar{m}_\mathrm{f})}{\sqrt{p^2}}, \tag{4.13}$$

where we assumed a symmetry broken ground state, i.e., $\bar{m}_\mathrm{f} \neq 0$ and $p^2 = p_0^2 + \cdots + p_{d-1}^2 \equiv p_0^2 + \boldsymbol{p}^2$, with $\boldsymbol{p} = (p_x, p_y)$ denoting spatial momenta. Obviously, in the broken phase, the bosonic mass is related to the dynamically generated fermion mass as $\bar{m} = 2\bar{m}_\mathrm{f}$.

In the limit $\frac{\sqrt{p^2}}{\bar{m}_\mathrm{f}} \to 0$, we obtain the asymptotic behavior

$$G_\sigma^{-1}(p) \propto p^2, \tag{4.14}$$

while in the chiral limit $\bar{m}_\mathrm{f} \to 0$

$$G_\sigma^{-1}(p) = \underbrace{\frac{d_\gamma \pi \bar{h}^2}{2(4\pi)^{3/2}\Gamma(3/2)} \frac{\pi}{2}}_{=\frac{\bar{h}^2}{4}} \sqrt{p^2}. \tag{4.15}$$

Thus Eq. (4.14) yields for the bosonic anomalous dimensions the large-N_f value $\eta_\sigma = 0$ in the broken phase. The result Eq. (4.15) as it stands is only valid at the critical point, since $\bar{m}_\mathrm{f} \neq 0$ is essential for the derivation of Eq. (4.13). Nevertheless, $\eta_\sigma = 1$ is valid in the entire symmetric phase, as can be inferred purely from dimensional analysis of the fermion loop for vanishing mass.

Here, the anomalous dimension η_σ is defined by

$$G_\sigma(p) \overset{\sqrt{p^2}\to 0}{\propto} \frac{1}{\sqrt{p^2}^{2-\eta_\sigma}}. \tag{4.16}$$

As a side remark, we would like to mention that the bosonic mass as extracted from the pole of the propagator Eq. (4.13) and the definition of the mass in a derivative expansion, i.e., $Z_\sigma^{-1} U''(\sigma)$ (discussed in detail in Sect. 4.3 and Sect. 4.4), do *not* coincide, even at the level of the large-N_f limit. This can easily be shown by obtaining $Z_\sigma = \lim_{\sqrt{p^2}\to 0} \frac{1}{2d} \Delta_p G_\sigma^{-1}(p)$ (cf. Appendix A.4) from Eq. (4.13) and taking the appropriate derivatives in Eq. (4.12) evaluated at the respective minimum. We find $\bar{m} \equiv Z_\sigma^{-1} U''(\sigma) = \sqrt{3}\bar{m}_\mathrm{f}$.

Corrections to Critical Exponents in $1/N_{\rm f}$-Expansion

The critical exponents characterizing the quantum phase transition of the model (in $d = 3$), have been computed to order $1/N_{\rm f}$ in e.g. [66]

$$\nu = 1 + \frac{8}{3N_{\rm f}\pi^2},\ \delta = 2 + \frac{8}{N_{\rm f}\pi},\ \beta = 1,\ \gamma = 1 + \frac{8}{N_{\rm f}\pi},\ \eta_\sigma = 1 - \frac{16}{3N_{\rm f}\pi^2},\ \eta_\psi = \frac{2}{3N_{\rm f}\pi^2}. \tag{4.17}$$

Notation follows standard convention, where ν describes the divergence of the correlation length as the critical point is approached, δ the response of the order parameter to an external source, β describes the scaling of the order parameter with the detuning from the critical point, γ gives the divergence of the order parameter susceptibility and η_σ is the bosonic, while η_ψ is the fermionic anomalous dimension. These exponents indeed satisfy the following *hyperscaling relations* [66, 100]

$$2\beta + \gamma = d\nu, \quad 2\beta\delta - \gamma = d\nu, \quad \beta = \frac{1}{2}\nu(d - 2 + \eta_\sigma), \quad \gamma = \nu(2 - \eta_\sigma). \tag{4.18}$$

One can infer from these equations, that only two of these exponents are independent. From [101–103] we get the values of ν, η_σ and η_ψ to order $1/N_{\rm f}^2$

$$\nu = 1 + \frac{8}{3N_{\rm f}\pi^2} - \frac{54\pi^2 + 752}{27N_{\rm f}\pi^4}, \tag{4.19}$$

$$\eta_\sigma = 1 - \frac{16}{3N_{\rm f}\pi^2} + \frac{1}{N_{\rm f}^2}\left(\frac{1216}{27\pi^4} - \frac{4}{\pi^2}\right), \tag{4.20}$$

$$\eta_\psi = \frac{2}{3N_{\rm f}\pi^2} + \frac{112}{27N_{\rm f}^2\pi^4}. \tag{4.21}$$

In [75], η_ψ was even given to order $1/N_{\rm f}^3$.

Some comments are in order on the chiral quantum phase transition discussed here in terms of a $1/N_{\rm f}$-expansion. Obviously, the critical exponents depend on the number of fermion flavors. So for each different flavor realization, we expect a different universality class. Even in the large-$N_{\rm f}$ limit, the critical exponents do not yield O(1) (mean-field) exponents, as one might have expected from a naive guess for the effective action controlling the order parameter field σ. These findings indicate, that a Hertz-Millis approach [9–11] fails due to the presence of massless fermionic degrees of freedom. The fermions are a relevant part of the critical theory. The failure of Hertz-Millis can also be inferred from expanding the fermionic $\mathrm{Tr}\ln(\,\cdot\,)$ in Eq. (4.6) – for massless fermions a highly nonlocal object – which yields IR singularities in the induced bosonic vertices.

4.2 Local Fermionic Truncation

We begin with a discussion of the fixed-point structure of the Gross-Neveu model as it becomes apparent already in a very elementary approximation within a purely fermionic description. Let us consider only a pointlike four-fermion interaction, such that our ansatz for the effective action reads

$$\Gamma_k[\{\bar{\psi}_j\},\{\psi_j\}] = \int_x \left\{ \sum_{j=1}^{N_\mathrm{f}} Z_{\psi,k} \bar{\psi}_j \mathrm{i}\partial\!\!\!/ \psi_j + \sum_{i,j=1}^{N_\mathrm{f}} \bar{\psi}_i \psi_i \frac{\bar{g}_k}{2N_\mathrm{f}} \bar{\psi}_j \psi_j \right\}, \tag{4.22}$$

where we allowed for a wave-function renormalization $Z_{\psi,k}$ in the standard kinetic term for Dirac fermions, and both $Z_{\psi,k}$ and $\bar{g}_k$ depend on the renormalization group scale k, as indicated by the respective subscripts. The regularized fermionic propagator is thus given in momentum space representation by

$$G_k^+(p,p') = (2\pi)^d \delta^d(p-p') \underbrace{\left[-p\!\!\!/ \left(1 + r_F\left(\frac{p^2}{k^2} \right) \right) \right]^{-1}}_{\equiv G_k^+(p)}. \tag{4.23}$$

The argument of the regulator shape function $r_F(y)$ indicates we are employing so-called spectrally adjusted regulators [40]. The simple ansatz Eq. (4.22) can be viewed as a derivative expansion of the effective action, with the leading order defined by $Z_{\psi,k} = \text{const}$. This expansion can, in fact, be associated with a potentially small expansion parameter in terms of the anomalous dimension $\eta_{\psi,k} = -\partial_t \ln Z_{\psi,k}$. Consequently, a running wave-function renormalization corresponds to a next-to-leading order derivative expansion. Put differently, the wave-function renormalization or its associated anomalous dimension captures the IR asymptotics of the momentum-dependent vertices. In the limit $k \to 0$, we can for example identify the dependence on the renormalization group scale k in the flowing propagator with its momentum dependence, i.e., $k \simeq \sqrt{p^2}$. Writing the wave-function renormalization as

$$\begin{aligned} \lim_{k\to 0} Z_{\psi,k} &= \lim_{k\to 0} Z_{\psi,\Lambda} \mathrm{e}^{-\int_\Lambda^k \frac{\mathrm{d}k'}{k'} \eta_{\psi,k'}} \\ &\propto \lim_{k\to 0} \mathrm{e}^{-\eta_{\psi,k} \ln k} \\ &\propto \lim_{k\to 0} k^{-\eta_{\psi,k}}, \end{aligned} \tag{4.24}$$

where in the second line we assumed the anomalous dimension $\eta_{\psi,k}$ to be approximately constant[4] during the flow. The initial condition for the wave-function renormalization is $Z_{\psi,\Lambda} = 1$, such that

[4] Typically, $\eta_{\psi,k}$ will not be constant for $k \in [0,\Lambda]$, but in a smaller interval $k \in [0,\Lambda']$, $\Lambda' < \Lambda$. Splitting the integration over the two intervals yields an additional prefactor in Eq. (4.24).

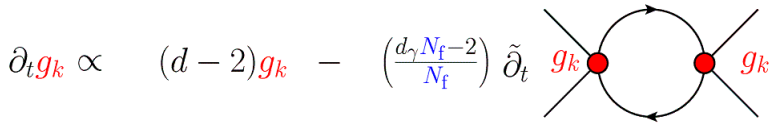

Figure 4.3: Diagrammatic representation of the beta function Eqs. (4.27), (4.32). The $\tilde{\partial}_t$ derivative generates regulator insertions in the diagrams, see Appendix A.5.

the kinetic term is normalized at the ultraviolet scale Λ. With these identifications, the fermionic propagator is then expected to behave as

$$\lim_{k\to 0} G_k^+(p) \overset{k\simeq\sqrt{p^2}}{\propto} \frac{1}{\sqrt{p^2}^{(1-\eta_{\psi,k\to 0})}}. \tag{4.25}$$

Aside from higher derivative operators, further interaction channels on the four-fermi level and higher-order interactions compatible with the symmetries discussed in Chap. 3 can be taken into account. The role of such interactions will be discussed below.

Large-N_f Fixed-Point Structure

Let us start with an analysis of the fixed-point structure in the large-N_f limit. Inserting the ansatz Eq. (4.22) into the flow equation Eq. (2.27) (with an empty bosonic sector), the flow of the dimensionless renormalized four-fermion coupling g_k,

$$g_k = Z_{\psi,k}^{-2} k^{d-2} \bar{g}_k \tag{4.26}$$

is given by

$$\lim_{N_\mathrm{f}\to\infty} \beta_{g_k} \equiv \lim_{N_\mathrm{f}\to\infty} \partial_t g_k = (d-2+2\eta_{\psi,k}) g_k - 4 d_\gamma v_d \, l_1^F(0) \, g_k^2, \tag{4.27}$$

where $v_d^{-1} = 2^{d+1}\pi^{d/2}\Gamma(d/2)$. Here, we projected the full flow equation straightforwardly onto the pointlike limit of the Gross-Neveu coupling. Interestingly, in the pointlike approximation, the flow equation is closed and no further four-fermi couplings are generated (while in principle being allowed by symmetry following our analysis in Chap. 3). See Fig. 4.3 for a diagrammatic representation of the beta function. Contributions from further – possibly fluctuation-induced – interaction channels as well as dependences on the Fierz basis [82–84] have been ignored for the sake of simplicity. The constant $l_1^F(0)$ (see Appendix A.5) depends on the choice of the regulator and parameterizes the regulator scheme dependence of the renormalization group flow. For instance, for a Litim regulator of the form [47–49]

$$R_{F,k}^+ = -Z_{\psi,k} \not{p} \, r_F\left(\frac{p^2}{k^2}\right), \quad r_F(y) = \left(\sqrt{\frac{1}{y}} - 1\right)\Theta(1-y), \tag{4.28}$$

we have $l_1^F(0) = 2/d$. Alternatively, for a sharp cutoff, we find $l_1^F(0) = 1$.

Apart from the Gaußian fixed point we find a second, albeit nontrivial fixed point for the coupling g_k, which is implicitly given by

$$g_* = \frac{d - 2 + 2\,\eta_{\psi,*}}{4 d_\gamma v_d\, l_1^F(0)}, \tag{4.29}$$

and the fermionic anomalous dimension $\eta_{\psi,*}$ in principle depends on g_*. By virtue of chiral symmetry in the massless case and in the pointlike approximation, it can be shown that $\eta_{\psi,k} \equiv 0$. At next-to-leading order of our derivative expansion we thus have

$$g_* = \frac{d(d-2)}{8 d_\gamma v_d} \overset{(d=3)}{=} \frac{3\pi^2}{4} \tag{4.30}$$

for the linear regulator and

$$g_* = \frac{d-2}{4 d_\gamma v_d} \overset{(d=3)}{=} \frac{\pi^2}{2} \tag{4.31}$$

for the sharp cutoff. We find, that within the same cutoff scheme, the large-N_f beta function reproduces the same value for the critical coupling as in the mean-field approach, cf. Eq. (4.11). The regulator dependence of the fixed-point value exemplifies the nonuniversality of this quantity. Nevertheless, the existence of the fixed point is a universal statement, as the regulator-dependent constant $l_1^F(0)$ is a positive number for any regulator. In Fig. 4.4, we show a sketch of $\beta_{g_k} = \partial_t g_k$. The arrows indicate the direction of the flow toward the infrared. The theory becomes trivial (noninteracting) in the infrared regime for initial values $g_\Lambda < g_*$. Choosing $g_\Lambda > g_*$, the four-fermion coupling increases rapidly toward the infrared and diverges eventually. The divergence of g_k at a finite renormalization group scale actually can be associated with the onset of chiral symmetry breaking and the formation of a chiral condensate, reflecting the quantum phase transition. This becomes more obvious in the bosonic formulation, which is discussed below in greater detail.

Fixed-Point Structure for Finite N_f

For finite N_f, the beta function of the scalar-scalar Gross-Neveu interaction is modified to

$$\beta_{g_k} \equiv \partial_t g_k = (d - 2 + 2\eta_{\psi,k}) g_k - 4 v_d \left(\frac{N_\mathrm{f} d_\gamma - 2}{N_\mathrm{f}}\right) l_1^F(0)\, g_k^2. \tag{4.32}$$

The non-Gaußian fixed point acquires flavor dependence and accordingly changes into

$$g_* = \left(\frac{N_\mathrm{f} d_\gamma - 2}{N_\mathrm{f}}\right)^{-1} \frac{d - 2 + 2\,\eta_{\psi,*}}{4 v_d\, l_1^F(0)}. \tag{4.33}$$

Statements about the existence of the fixed point remain valid for $N_\mathrm{f} \geq 1$. As N_f assumes smaller values, the position of the fixed point shifts to the right on the g_k-axis. Eq. (4.33) suggests something interesting could happen for $N_\mathrm{f} = \frac{1}{2}$. Since we are working with the direct sum of two two-component Weyl fermions, we can formally translate $(N_\mathrm{f} = \frac{1}{2}, d_\gamma = 4)$ to a single Weyl fermion, specified by $(N_\mathrm{f} = 1, d_\gamma = 2)$. Chiral symmetry breaking is replaced by a parity breaking mechanism. Such a Weyl Gross-Neveu model was discussed in [80]. There, the non-Gaußian fixed point can no longer be found in the symmetric regime of the flow. Instead, it is shifted into the broken regime, reminiscent of a bosonic Wilson-Fisher fixed point. A partially bosonized description is then compulsory.

In fact, the scale for a given IR observable $\mathcal{O}$ is set by the scale k_c at which $1/g_k \to 0$:

$$\mathcal{O} \sim k_\mathrm{c}^{[\mathcal{O}]}, \tag{4.34}$$

where $[\mathcal{O}]$ is the mass dimension of the observable $\mathcal{O}$. For $g_\Lambda < g_*$, the coupling never diverges but approaches zero. For $g_\Lambda > g_*$, we find

$$k_\mathrm{c} \propto \Lambda \left| \frac{1}{g_\Lambda} - \frac{1}{g_*} \right|^{\frac{1}{|\Theta|}}, \tag{4.35}$$

by integrating the beta function from $k = \Lambda$ to $k = k_\mathrm{c}$ and linearizing around g_*. The critical exponent Θ is given by

$$\Theta = -\left.\frac{\partial \beta_g}{\partial g}\right|_{g=g_*} = d - 2 + 2\eta_{\psi,*} - 2g_* \left.\frac{\partial \eta_\psi}{\partial g}\right|_{g=g_*}. \tag{4.36}$$

Relation (4.35) roughly determines how a given IR observable scales when the initial coupling g_Λ is varied.

As the initial condition g_Λ being larger or smaller than g_* distinguishes between two different phases in the long-distance limit, the fixed point g_* can be viewed as a quantum critical point which divides the model into two physically different regimes. In our simple fermionic truncation with only one coupling, the stability matrix boils down to a number, already represented by the critical exponent of the coupling direction in this one-dimensional theory space, see Eq. (4.36). At leading and next-to-leading order derivative expansion, where $\eta_{\psi,k} \equiv 0$, the critical exponent is positive for all $d > 2$, such that the Gross-Neveu coupling corresponds to a relevant coupling in the renormalization group sense, being attracted by the non-Gaußian fixed point toward the UV.

Looking through Asymptotic Safety Goggles

In this simple truncation, this suggests that the Gross-Neveu model can be renormalized and extended as a fundamental theory over all scales on renormalization group trajectories that emanate from the non-Gaußian fixed point. As there is only one relevant direction, only one physical parameter has to be fixed, say the value of the coupling at a UV scale, g_Λ, in order to predict all physical

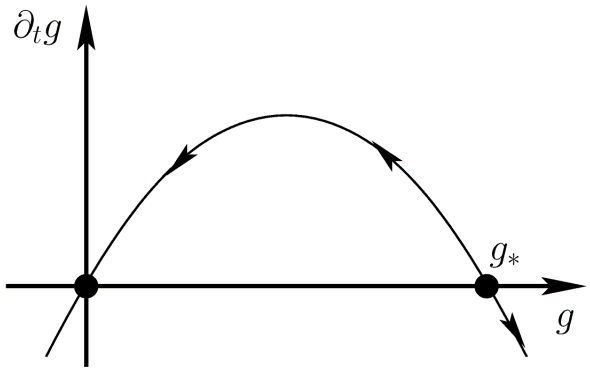

Figure 4.4: Sketch of the beta function of the four-fermion coupling. For $g_k \geq g_*$ the infrared regime of the Gross-Neveu model is governed by chiral symmetry breaking (diverging fermionic interaction $g_k \to \infty$). For $g_k < g_*$ the model becomes a trivial (noninteracting) theory $g_k \to 0$ in the infrared.

quantities in the long-distance limit, assuming that we follow a trajectory on the critical surface. In this simple truncation, the picture of a critical surface is a bit obscured, since no further irrelevant directions appear. The interplay of critical surface and critical manifold will become apparent once we move to a partially bosonized truncation.

It is instructive to compare these conclusions within the asymptotic safety language with standard perturbation theory near the Gaußian fixed point $g_{*,\text{Gauß}} = 0$. The corresponding critical exponent is

$$\Theta_{\text{Gauß}} = -\frac{\partial \beta_g}{\partial g}\bigg|_{g=g_{*,\text{Gauß}}} = 2 - d, \tag{4.37}$$

in agreement with (minus) the naive power-counting dimension of the coupling. At leading-order derivative expansion $\eta_{\psi,k} = 0$ and for $d > 2$, the critical exponent is negative and the fixed point thus infrared attractive[5]. A UV limit $\Lambda \to \infty$ can only be taken if the renormalization group trajectory emanates from the fixed point, but then the theory would be noninteracting on all scales and therefore "trivial". Within perturbation theory, the conclusion is that the Gross-Neveu model is perturbatively nonrenormalizable. Note that this conclusion remains unchanged also if the anomalous dimension is taken into account: within perturbation theory, $\eta_{\psi,k} = \mathcal{O}(g^2)$, such that $\eta_{\psi,*} = 0$ at the Gaußian fixed point, implying that standard power-counting can only be modified logarithmically. Let us conclude with a word of caution on the derivative expansion in the purely fermionic truncation: in this simple approximation, the fixed-point seems to exist with similar properties in any dimension $d > 2$, in particular also in $d = 4$ and beyond. This conclusion will change, once composite bosonic degrees of freedom are taken into account. Fluctuations of the latter which are formed by fermionic interactions will remove the fixed point in the Gross-Neveu model for $d \geq 4$ such that no asymptotic safety scenario appears to exist for $d \geq 4$ in this model. In

[5]For $d = 2 - \varepsilon$ with $\varepsilon \ll 1$, the Gaußian fixed point turns UV attractive and the model is rendered asymptotically free [12].

the fermionic language, the bosonic degrees of freedom correspond to specific nonlocal interactions or momentum structures in the fermionic vertices. These are not properly resolved in a derivative expansion. As $d = 4$ is a marginal case, the conclusions for fermionic theories in $d = 4$ may depend on the details of the interaction and the algebraic structure of a given model; for instance, an asymptotic safety scenario in a standard-model-inspired field theory has been discussed in [71].

4.3 Local Boson-Fermion Truncation

Let us now discuss the fixed-point structure of the partially bosonized theory. A partially bosonized description of the theory is appealing from a field-theoretical point of view, as it also forms the basis for the expansion in $1/N_\mathrm{f}$ for a large number of flavors. In addition, it allows us to systematically resolve parts of the momentum dependence of the vertices by means of a derivative expansion. As we shall see below, these two expansion schemes are not identical and should therefore not be confused with each other. For our study we employ the following ansatz for the effective action:

$$\Gamma_k[\{\bar{\psi}_j\},\{\psi_j\},\sigma] = N_\mathrm{f}\int_x\left\{U_k(\sigma)+\frac{1}{2}Z_{\sigma,k}(\partial_\mu\sigma)^2\right\}+\int_x\sum_{j=1}^{N_\mathrm{f}}\left\{Z_{\psi,k}\bar{\psi}_j\mathrm{i}\partial\!\!\!/\psi_j+\mathrm{i}\bar{h}_k\bar{\psi}_j\sigma\psi_j\right\}, \quad (4.38)$$

where we allow all couplings and wave-function renormalizations $Z_{\sigma,\psi}$, $Z_{\psi,k}$ to be scale dependent. The contribution $U_k(\sigma)$ is a flowing effective potential. In the following, we refer to an ansatz of the form Eq. (4.38) as an LPA$'$ truncation. Pure LPA truncations neglect wave-function renormalizations, and typically also discard the nontrivial running of the Yukawa vertex. The effective potential $U_k(\sigma)$ contains the scale dependent bosonic mass $\bar{m}_k$, as well as self-interaction vertices of the bosonic sector. Conventionally, the effective potential is expressed as a function of the invariant $\bar{\rho} = \frac{1}{2}\sigma^2$, which here reflects the discrete $\mathbb{Z}_2$ symmetry of the microscopic model. The effective action Eq. (4.38) can be regarded as the action of a three-dimensional chiral Yukawa system. Analogous to the considerations of the previous section, we obtain for the IR behavior of both bosonic and fermionic propagators

$$\lim_{k\to 0}G_{\sigma,k}(p)\overset{k\simeq\sqrt{p^2}}{\propto}\frac{1}{\sqrt{p^2}^{(2-\eta_{\sigma,k\to 0})}}\quad\text{and}\quad\lim_{k\to 0}G^+_k(p)\overset{k\simeq\sqrt{p^2}}{\propto}\frac{1}{\sqrt{p^2}^{(1-\eta_{\psi,k\to 0})}}, \quad (4.39)$$

respectively. The kinetic term of the boson field adds a new aspect: it corresponds to a specific momentum dependence in the scalar channel of the four-fermion coupling. As we shall see below, this term and the associated wave-function renormalization receive contributions to leading order in the large-N_f approximation. The large-N_f flow corresponds to the choice

$$\begin{aligned} Z_{\sigma,k\to\Lambda}&\to 0\,, \qquad \partial_t Z_{\sigma,k}\neq 0\,,\\ Z_{\psi,k\to\Lambda}&\equiv 1\,, \qquad \partial_t Z_{\psi,k}\equiv 0\,. \end{aligned} \quad (4.40)$$

This exemplifies the difference between large-N_f and derivative expansion, as with this choice we include next-to-leading order corrections in terms of a derivative expansion in the bosonic sector but treat the fermionic sector in the leading-order approximation. The vanishing bosonic wave-function renormalization at the UV scale Λ incorporates the compositeness of the σ field. At high energy/momentum scales, the bosonic field is purely auxiliary and does not propagate. As we saw in Sect. 4.1, fermionic fluctuations will induce a kinetic term. From our ansatz Eq. (4.38) we see that a nonzero homogeneous expectation value for $\mathrm{i}\bar{h}\sigma$ plays the role of a mass term for the fermions. By expanding the effective action about the homogeneous background σ we anticipate that condensation occurs only in the homogeneous channel. The quantum Yukawa model is matched to the fermionic Gross-Neveu model by a suitable choice of initial conditions for $\Gamma_k[\{\bar{\psi}_j\},\{\psi_j\},\sigma]$ at the UV scale $k=\Lambda$. This correspondence is established by the choice

$$Z_{\sigma,k\to\Lambda}\ll 1\,,\quad Z_{\psi,k\to\Lambda}\to 1\,,\quad U_{k\to\Lambda}(\rho)=\bar{m}^2_{k\to\Lambda}\rho. \tag{4.41}$$

Thus, the renormalized boson mass $Z_{\sigma,k}^{-\frac{1}{2}}\bar{m}_k$ at the UV cutoff Λ becomes much larger than Λ and renders the boson propagator essentially momentum independent. We thus require $\frac{\bar{m}_k}{Z_{\sigma,k}^{\frac{1}{2}}\Lambda}\gg 1$. This compositeness condition for the bosonic formulation can be considered as a locality condition at the UV scale for the four-fermion coupling g_k in the purely fermionic formulation of the model. We will see later in Sect. 4.3, especially Fig. 4.7, that this condition can equivalently be realized with a sufficiently large initial value of the Yukawa vertex. The flow equations for the effective potential as well as the Yukawa vertex and the anomalous dimensions are obtained from the ansatz Eq. (4.38) by the projection rules summarized in Appendix A.4. It is conventional and convenient to formulate the flow equations in terms of renormalized dimensionless quantities. Therefore, we define

$$u_k(\rho)=k^{-d}U_k(\sigma),\quad \rho=\frac{1}{2}Z_{\sigma,k}k^{2-d}\sigma^2, \tag{4.42}$$

and the dimensionless renormalized Yukawa coupling is given by

$$h_k^2=Z_\sigma^{-1}Z_{\psi,k}k^{d-4}\bar{h}_k^2. \tag{4.43}$$

We then obtain the flow equations for the effective potential expressed as a function of the dimensionless renormalized invariant ρ

$$\begin{aligned}\partial_t u_k(\rho) &= -du_k(\rho)+(d-2+\eta_{\sigma,k})u_k'(\rho)\rho\\ &\quad -2d_\gamma v_d\, l_0^{(F)d}(2h_k^2\rho;\eta_{\psi,k})+\frac{1}{N_\mathrm{f}}2v_d\, l_0^d(u_k'(\rho)+2\rho u_k''(\rho);\eta_{\sigma,k}),\end{aligned} \tag{4.44}$$

and the flow equation describing the running of the Yukawa vertex in the pointlike limit

$$\begin{aligned}\partial_t h_k^2 &= (d-4+2\eta_{\psi,k}+\eta_{\sigma,k})h_k^2 + \\ &\frac{1}{N_\mathrm{f}} 8 v_d\, h_k^4\, l_{1,1}^{(FB)d}(2h_k^2\kappa_k, [u_k'(\rho)+2\rho u_k''(\rho)]\,|_{\rho=\kappa_k}; \eta_{\psi,k}, \eta_{\sigma,k}) - \\ &\frac{1}{N_\mathrm{f}} \left(48\rho u''(\rho) + 32\rho^2 u'''(\rho)\right)|_{\rho=\kappa_k} v_d\, h_k^4\, l_{1,2}^{(FB)d}(2h_k^2\kappa_k, [u_k'(\rho)+2\rho u_k''(\rho)]\,|_{\rho=\kappa_k}; \eta_{\psi,k}, \eta_{\sigma,k}) - \\ &\frac{1}{N_\mathrm{f}} 32 v_d\, h_k^6\, \kappa_k\, l_{2,1}^{(FB)d}(2h_k^2\kappa_k, [u_k'(\rho)+2\rho u_k''(\rho)]\,|_{\rho=\kappa_k}; \eta_{\psi,k}, \eta_{\sigma,k}). \end{aligned} \tag{4.45}$$

The anomalous dimensions are given by

$$\begin{aligned}\eta_{\sigma,k} &= 8\frac{d_\gamma v_d}{d} h_k^2 \left[m_4^{(F)d}(2h_k^2\kappa_k;\eta_{\psi,k}) - 2h_k^2\kappa_k m_2^{(F)d}(2h_k^2\kappa_k;\eta_{\psi,k})\right] + \\ &\frac{1}{N_\mathrm{f}} 8\frac{v_d}{d}\kappa_k \left(3u''(\rho)+2\rho u'''(\rho)\right)|_{\rho=\kappa_k} m_{4,0}^d([u_k'(\rho)+2\rho u_k''(\rho)]\,|_{\rho=\kappa_k}, 0; \eta_{\sigma,k}), \end{aligned} \tag{4.46}$$

$$\eta_{\psi,k} = \frac{1}{N_\mathrm{f}} 8\frac{v_d}{d} h_k^2\, m_{1,2}^{(FB)d}(2h_k^2\kappa_k, [u_k'(\rho)+2\rho u_k''(\rho)]\,|_{\rho=\kappa_k}; \eta_{\psi,k}, \eta_{\sigma,k}). \tag{4.47}$$

The threshold functions in Eqs. (4.44) and (4.45)-(4.48) depend on the details of the regulator and are given in Appendix A.5. These functions essentially describe the threshold behavior of regularized 1PI diagrams. This set of flow equations was obtained already in [80, 81]. There, however, the contributions proportional to the Yukawa coupling arising in the broken regime were not included. These contributions were, however, already considered in [72]. The terms $2h_k^2\rho$ and $u_k'(\rho)+2\rho u_k''(\rho)$ entering the threshold functions renormalizeing the effective potential can be considered as "off-shell" mass terms for fermions and bosons, respectively. The remaining equations are evaluated "on-shell", at the minimum of the effective potential, denoted by κ_k.

The flow of κ_k is easily extracted from the flowing effective potential by requiring the scale-dependent stationarity condition $\partial_t \frac{\partial}{\partial_\rho} u_k|_{\rho=\kappa_k} \stackrel{!}{=} 0$. One obtains

$$\partial_t \kappa_k = -(d-2+\eta_\sigma)\kappa_k - \frac{\partial_t \hat{u}'(\rho)}{u''(\rho)}|_{\rho=\kappa_k}, \tag{4.48}$$

and we defined

$$\partial_t \hat{u}(\rho) = -2 d_\gamma v_d\, l_0^{(F)d}(2h_k^2\rho;\eta_{\psi,k}) + \frac{1}{N_\mathrm{f}} 2 v_d\, l_0^d(u_k'(\rho)+2\rho u_k''(\rho);\eta_{\sigma,k}). \tag{4.49}$$

Our computations are performed with an optimized regulator [47–49], for the fermionic fields see Eq. (4.28) and for the bosonic fields we have

$$R_k = Z_{\sigma,k} p^2 r_B\left(\frac{p^2}{k^2}\right), \quad r_B(y) = \left(\frac{1}{y}-1\right)\Theta(1-y). \tag{4.50}$$

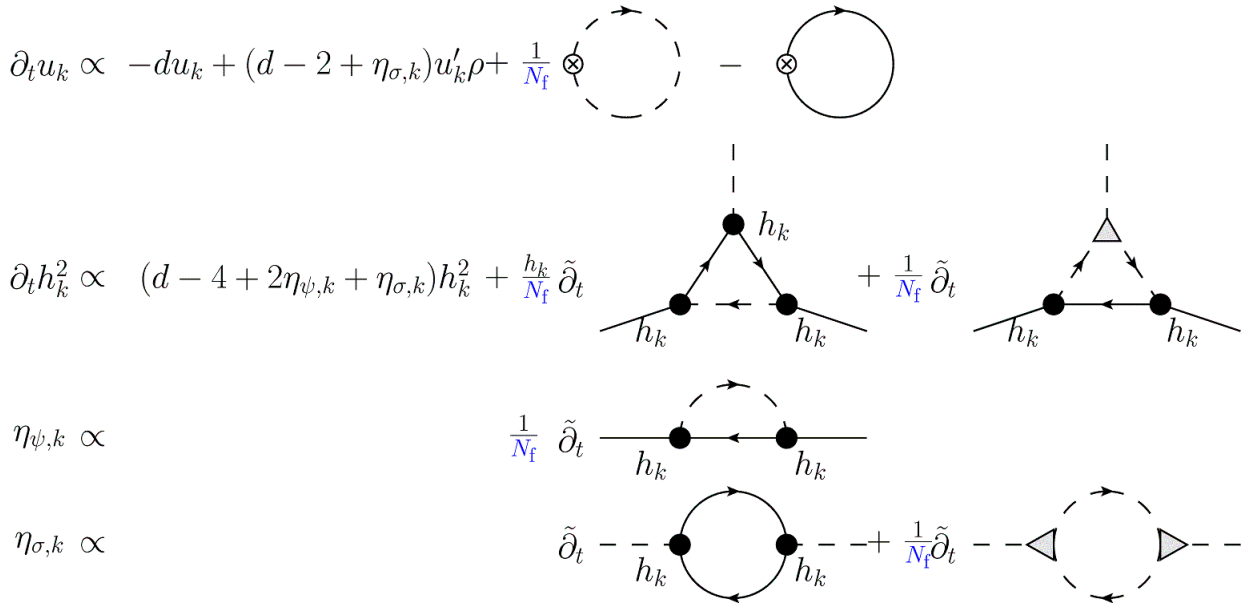

Figure 4.5: Diagrammatic representation of the beta functions contained in the truncation Eq. (4.38). Black blobs denote the Yukawa vertex, solid and dashed lines regularized fermionic and bosonic propagators, respectively. Gray triangles denote bosonic self-interactions $\propto U_k'''(\sigma)|_{\sigma=\sigma_{0,k}}$ (cf. Appendix A.4), which contribute only in the broken regime of the flow. The $\tilde{\partial}_t$ derivative generates regulator insertions in the diagrams, see Appendix A.5.

Actually, Eq. (4.42) is to be understood as a partial differential equation (PDE) for the function $u_k(\rho)$ in the variables t (or alternatively k) and ρ. We comment on the full solution of this PDE in the Gross-Neveu case (at finite temperature) in Chap. 5. In [80], the full PDE coupled to the "on-shell" differential equations Eqs. (4.45)-(4.48) was used to obtain critical exponents directly from flows in the fixed-point regime. In the Sect. 4.5, the critical exponents will be obtained directly from the linearized flow in the vicinity of the zeroes of the beta functions given above.

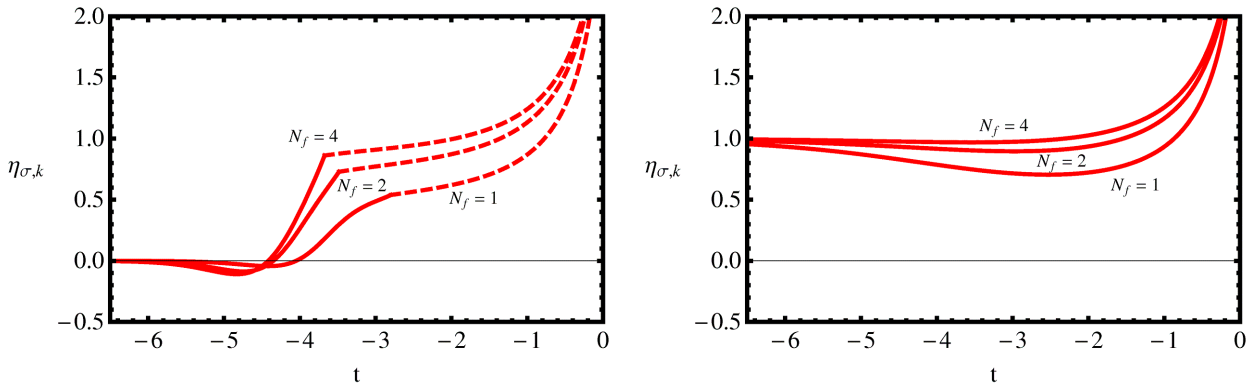

Figure 4.6: Left panel: bosonic anomalous dimension $\eta_{\sigma,k}$ as a function of the logarithmic renormalization group scale t for flavor numbers $N_\mathrm{f} = 1,\ 2,\ 4$ in the broken phase. To evaluate the flow, we used the parameters $t_\mathrm{IR} = -10$, $\Lambda = 100\,\mathrm{a.u.}$, $h_\Lambda = 18.0$ and $m_\Lambda \equiv \lambda_{2,\Lambda} = 1.025,\ 1.294,\ 1.423$. Here and throughout this thesis, a.u. refers to "arbitrary unit" of mass dimension 1. The large value of the initial Yukawa coupling helps realizing the compositeness condition Eq. (4.41), which is equivalent to $\lambda_{2,\Lambda} \ll 1$. This immediately leads to the large initial values $\eta_{\sigma,\Lambda} \gtrsim 2$. The dashed red curves describe the flow in the symmetric regime, while the solid red curves fall into the broken regime. Right panel: bosonic anomalous dimension in the symmetric phase. We tuned the initial conditions from the flows in the broken phase to $m_\Lambda = 1.125,\ 1.394,\ 1.523$.

4.4 Vacuum Infrared Properties

Before we turn to an in-depth analysis of the fixed-point structure and the flavor dependence of the Gross-Neveu critical exponents probing the UV region of the model, we shall evaluate the flows Eqs. (4.44)-(4.48) for specific initial conditions fulfilling Eq. (4.41) and investigate the IR properties as obtained from the renormalization-group evolution. From the mean-field picture Sect. 4.1 and the behavior of the beta function of the Gross-Neveu coupling g_k, we infer the existence of at least two regions in the space of all couplings captured by our truncation. For suitable initial conditions, symmetry breaking will occur and the flowing minimum κ_k will evolve to a nonzero value and we observe a phase with massive Dirac fermions. Choosing initial conditions such that no symmetry breaking is induced by quantum fluctuations will leave us with a gas of massless Dirac fermions.

IR Parameterization and Symmetry Breaking: Integrating the Flow toward the IR

In the symmetric regime, the effective potential will be parametrized by a polynomial expansion as

$$u_k(\rho) = \sum_{n=1}^{n_\mathrm{max}} \frac{1}{n!} \lambda_{2n,k} \rho^n, \tag{4.51}$$

where at $n = n_{\max}$ the polynomial expansion is truncated. From $[u_k'(\rho) + 2\rho u_k''(\rho)]\,|_{\rho=\kappa_k}$ being the dimensionless renormalized "on-shell" mass of the σ field, we find for $\kappa_k = 0$

$$\frac{\bar{m}_k^2}{Z_{\sigma,k}k^2} = [u_k'(\rho) + 2\rho u_k''(\rho)]\,|_{\rho=\kappa_k=0} = \lambda_{2,k}. \tag{4.52}$$

Higher coefficients for $n > 2$ describe the couplings of bosonic self-interaction operators in the pointlike approximation. The dimensionless renormalized couplings are related to the dimensionful effective potential as

$$\lambda_{2n,k} = Z_{\sigma,k}^{-n} k^{(n-1)d-2n} U_k^{(n)}\big|_{\rho=0}. \tag{4.53}$$

In the broken regime of the flow, the potential will be parametrized in a manner so as to incorporate $\kappa_k \neq 0$, corresponding to a shifted expansion point in field space. We use

$$u_k(\rho) = \sum_{n=2}^{n_{\max}} \frac{1}{n!}\lambda_{2n,k}(\rho - \kappa_k)^n. \tag{4.54}$$

The dimensionless renormalized bosonic mass then becomes

$$[u_k'(\rho) + 2\rho u_k''(\rho)]\,|_{\rho=\kappa_k\neq 0} = 2\kappa_k\lambda_{4,k}. \tag{4.55}$$

Since in any case the flow is initialized for high momentum scales in the symmetric regime, the dimensionless renormalized fermion mass $2h_k^2\kappa_k$ vanishes for $k \simeq \Lambda$.

The scale dependence of the anomalous dimension $\eta_{\sigma,k}$ is shown in Fig. 4.6 for different flavor realizations of the Gross-Neveu theory. While the fermionic anomalous dimension always evolves to zero, corresponding to a canonical kinetic term for the fermion fields, the bosonic anomalous dimension obeys $\eta_{\sigma,k} \to 1$ as $k \to 0$ in the symmetric phase. In the large-$N_{\rm f}$ limit, this result was anticipated by the IR asymptotic form of the induced bosonic propagator, cf. Eq. (4.15). In the broken phase, $\eta_{\sigma,k} \to 0$ as $k \to 0$, see Fig 4.6, as expected from Eq. (4.14). The dips $\eta_{\sigma,k} < 0$ shortly after the symmetry-breaking scale in the broken phase occurred for all initial values considered, but did not seem to affect the flow in any pathological manner. This proves our ansatz Eq. (4.38) is capable of properly describing the low-energy sector of the Gross-Neveu model. Furthermore, we observe that for small momenta, the momentum structure of the propagator is impervious to the specific choice of $N_{\rm f}$.

Boson vs. Fermion Mass

For initial conditions that induce symmetry breaking at a critical scale $k_{\rm c}$, the renormalization group evolution is computed first with the flow equations for $\kappa_k = 0$. At the critical scale, which in the bosonized scheme is identified by $\lambda_{2,k=k_{\rm c}} = 0$, the parameterization of the potential has to be

$n_{\max}$	2	3	4	5	6	7	8	9	10
$\frac{\bar{m}}{\bar{m}_\mathrm{f}}$	2.17096	2.38508	1.95631	1.94366	1.94291	1.94291	1.94307	1.94307	1.94304
$\frac{\bar{m}}{\bar{m}_\mathrm{f}}$	2.09115	1.77326	1.86327	1.84337	1.84802	1.84697	1.84721	1.84716	1.84717

Table 4.1: Truncation dependence of the mass ratio $\lim_{N_\mathrm{f}\to\infty}\frac{\bar{m}}{\bar{m}_\mathrm{f}}$ in the large-N_f limit for two different initial conditions. For $n_{\max} > 7$, the result of the numerical integration has pretty much converged. The relative deviation from the large-N_f result ($\lim_{N_\mathrm{f}\to\infty}\frac{\bar{m}}{\bar{m}_\mathrm{f}} = \sqrt{3}$) within a derivative expansion is about 10% for $h_\Lambda = 18.0$, $m_\Lambda \equiv \lambda_{2,\Lambda} = 1.54$ (first row) and 6% for $h_\Lambda = 6.0$, $m_\Lambda \equiv \lambda_{2,\Lambda} = 0.80$ (second row). In both cases we used $t_\mathrm{IR} = -10$ and $\Lambda = 100\,\mathrm{a.u.}$ for the UV cutoff. The first set of initial conditions ensures $\bar{m}_\mathrm{f} \simeq 1\,\mathrm{a.u.}$, while the second is tuned to $\bar{m}_\mathrm{f} \simeq 5\,\mathrm{a.u.}$.

changed from Eq. (4.51) to Eq. (4.54). Accordingly, upon entering the broken phase with $\kappa_k \neq 0$, the flows for h_k and $\eta_{\sigma,k}$ receive additional contributions due to the coupling of the bosonic fluctuations to the homogeneous background formed by the chiral condensate. Off criticality, fermionic and bosonic mass are interrelated, as we have seen from the pole structure of the large-N_f propagator. For $N_\mathrm{f} \to \infty$, within a derivative expansion we should obtain $\frac{\bar{m}}{\bar{m}_\mathrm{f}} = \sqrt{3}$, see Sect. 4.1. Here, the renormalized (dimensionful) fermion mass

$$\bar{m}_\mathrm{f} \equiv \lim_{k\to k_\mathrm{IR}} \left(k\sqrt{2h_k\kappa_k}\right), \tag{4.56}$$

and analogously the renormalized (dimensionful) boson mass

$$\bar{m} \equiv \lim_{k\to k_\mathrm{IR}} \left(k\sqrt{2\lambda_{4,k}\kappa_k}\right), \tag{4.57}$$

where the prefactor k restores the proper mass dimension. The IR scale k_IR is typically chosen as $k_\mathrm{IR} = \Lambda \mathrm{e}^{t_\mathrm{IR}}$, $t_\mathrm{IR} = -10$. This suffices to ensure for the given initial conditions a "freeze-out" of the renormalization group flow in all dimensionful quantities. In Table 4.1, we show the convergence properties of the mass ratio with increasing order of the polynomial truncation in the large-N_f limit for two different initial conditions. Table 4.1 also demonstrates the sensitivity of the ratio to initial conditions. The deviation from the result as obtained from large-N_f results within a derivative expansion is 10% and 6%, respectively. The mass ratio is obviously equivalent to a relation between the IR limit of the four-boson vertex and the Yukawa coupling:

$$\frac{\bar{m}}{\bar{m}_\mathrm{f}} = \lim_{k\to k_\mathrm{IR}} \sqrt{\frac{\lambda_{4,k}}{h_k^2}}. \tag{4.58}$$

The dependence of the mass ratio $\frac{\bar{m}}{\bar{m}_\mathrm{f}}$ on flavor number is given in Table 4.2 for $n_{\max} = 10$. Clearly, including fluctuations beyond infinite flavor number reduces the bosonic mass relative to the dynamically generated fermion mass. The decrease of the mass ratio with smaller N_f can be read as an increasingly stable bound state. We would like to stress that the mass definition in a derivative expansion leads to a different value of the pole mass ratio as extracted from the full

N_f	1	2	4	6	8	10	20	30	40
$\frac{\bar{m}}{\bar{m}_\mathrm{f}}$	1.16146	1.50483	1.70918	1.7762	1.81725	1.84816	1.92522	1.93985	1.93732
$\frac{\bar{m}}{\bar{m}_\mathrm{f}}$	1.12136	1.45273	1.6327	1.69795	1.7395	1.7709	1.83239	1.83538	1.82954

Table 4.2: Flavor dependence of the mass ratio $\frac{\bar{m}}{\bar{m}_\mathrm{f}}$ in a $\sigma^{20} \propto \rho^{10}$ truncation ($n_\mathrm{max} = 10$). The mass ratio roughly saturates for $N_\mathrm{f} \gtrsim 20$ and slowly approaches its $N_\mathrm{f} \to \infty$ value. We took the data for two different sets of initial conditions, such that $\bar{m}_\mathrm{f} \simeq 1\,\mathrm{a.u.}$ (first row) and $\bar{m}_\mathrm{f} \simeq 5\,\mathrm{a.u.}$ (second row). In both cases we used $t_\mathrm{IR} = -10$ and $\Lambda = 100\,\mathrm{a.u.}$ for the UV cutoff. The mass ratio turns out to be rather sensitive to the choice of initial conditions.

propagator Eq. (4.13). The sensitivity of the mass ratio to initial conditions might be related to the polynomial approximation of the effective potential, which at the mean-field level behaves as $\rho^{3/2}$.

4.5 Fixed Point Structure and GN_3 Universality Classes

Finally, we are going to investigate the flavor dependent Gross-Neveu universality classes in the partially bosonized language. Drawing on our results from Sect. 4.2, we anticipate that a possible non-Gaußian fixed point occurs in the symmetric regime. Therefore, we only need to study the renormalization group flow in the symmetric regime with vanishing vacuum expectation value for the σ field, i.e., $\kappa_k \equiv 0$. The flow equation for the dimensionless effective potential is given by Eq. (4.44). As before, we directly project onto the (dimensionless) bosonic mass parameter $\lambda_{2,k}$ and the higher-order bosonic couplings $\lambda_{2n,k}$.

The flow equations for the Yukawa coupling h_k as well as the anomalous dimensions $\eta_{\sigma,k}$ and $\eta_{\psi,k}$ read

$$\partial_t h_k^2 = (d - 4 + 2\eta_{\psi,k} + \eta_{\sigma,k}) h_k^2 + \frac{1}{N_\mathrm{f}} 8 v_d\, h_k^4\, l_{1,1}^{(FB)d}(0, \lambda_2; \eta_{\psi,k}, \eta_{\sigma,k})\,, \tag{4.59}$$

$$\eta_{\sigma,k} = 8 \frac{d_\gamma v_d}{d} h_k^2\, m_4^{(F)d}(0; \eta_{\psi,k})\,, \tag{4.60}$$

$$\eta_{\psi,k} = \frac{1}{N_\mathrm{f}} 8 \frac{v_d}{d} h_k^2 m_{1,2}^{(FB)d}(0, \lambda_{2,k}; \eta_{\psi,k}, \eta_{\sigma,k})\,,. \tag{4.61}$$

Large-N_f Fixed-Point Structure, Analytic Results

As we found a chiral quantum phase transition in the limit of infinite flavor number, it is worthwhile to study the fixed-point structure on the basis of the renormalization group flow in the same limit. This will at the same time provide a connection to the nonperturbative renormalizability of the

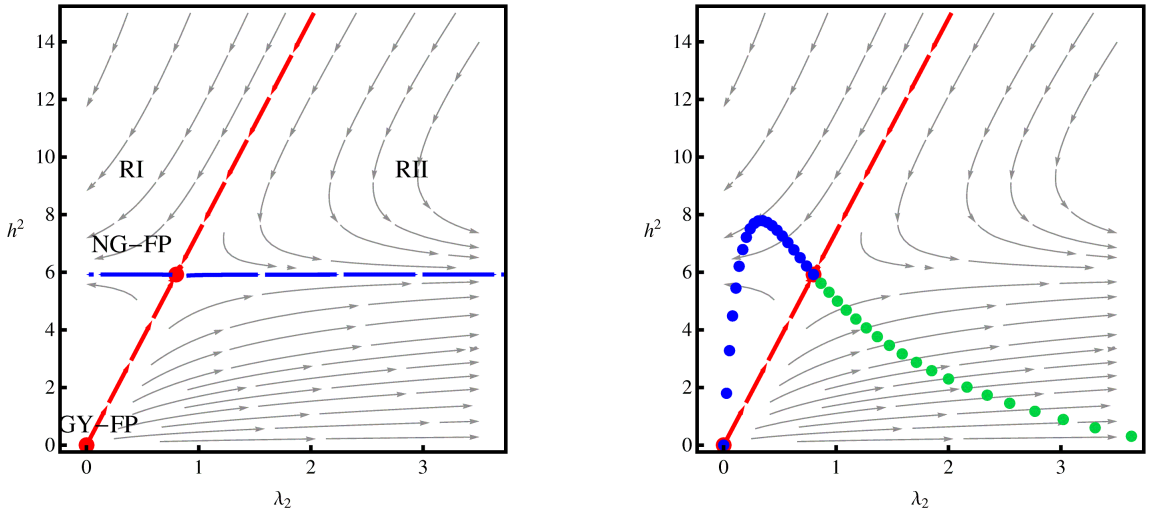

Figure 4.7: Left panel: leading-order RG flow in the $1/N_{\rm f}$ expansion for the partially bosonized Gross-Neveu model in the $(h_k^2, \lambda_{2,k})$ plane. The red line denotes the critical manifold of points drawn into the fixed point toward the infrared, at the same time acting as a separatrix for symmetry-breaking (RI) and symmetric initial conditions (RII). The blue line depicts the critical surface attracting the flow toward the IR. The critical surface contains all trajectories that emanate from the non-Gaußian fixed point (NG-FP) in the UV; its dimensionality equals the number of relevant directions and thus the number of physical parameters to be fixed. The red dots denote the Gaußian Yukawa fixed point (GY-FP) and the non-Gaußian fixed point, respectively. The arrows indicate the direction of flow toward the infrared. Right panel: leading-order RG flow in the $1/N_{\rm f}$ expansion for the partially bosonized Gross-Neveu model in the $(h_k^2, \lambda_{2,k})$ plane, additionally showing the analytic continuation in spacetime dimension d. Blue blobs show the limit $d \to 4$, while green blobs indicate $d \to 2 + \epsilon$. Approaching $d = 4$ from below yields a critical manifold with finite slope in the $(h_k^2, \lambda_{2,k})$ plane. Approaching $d = 2$ from above still yields a non-Gaußian fixed point. For $d \to 2 - \epsilon$, one would arrive at an asymptotically free theory [12].

Gross-Neveu model beyond $d = 2$, which has been proved to all orders in the $1/N_{\rm f}$ expansion. Our set of flow equations for the partially bosonized Gross-Neveu model reduces to

$$\partial_t u_k(\rho) = -d u_k + (d - 2 + \eta_{\sigma,k}) u_k'(\rho)\rho - 2 d_\gamma v_d \, l_0^{(F)d}(2h_k^2\rho; \eta_\psi), \tag{4.62}$$

$$\partial_t h_k^2 = (d - 4 + 2\eta_{\psi,k} + \eta_{\sigma,k}) h_k^2, \tag{4.63}$$

$$\eta_{\sigma,k} = 8 \frac{d_\gamma v_d}{d} h_k^2 \, m_4^{(F)d}(0; \eta_{\psi,k}) \,, \tag{4.64}$$

$$\eta_{\psi,k} = 0. \tag{4.65}$$

As the bosonic fluctuations carry no flavor number, we observe that 1PI diagrams with at least one inner bosonic line decouple completely from the large-$N_{\rm f}$ renormalization group flow. As a consequence, $\eta_{\sigma,k}$ is nonvanishing in leading order in the $1/N_{\rm f}$ expansion, whereas the fermionic anomalous dimension is zero.[6]

[6]It is worthwhile to emphasize, that the large-$N_{\rm f}$ counting is very different from scalar O(N) models, where the the anomalous dimensions are zero to leading order at large $N_{\rm f}$ [99]. Also the structure of the potential equation is very different, such that also the search for an exact solution requires a different strategy from that of O(N) models [104], see below.

The flow equations for the bosonic couplings are essentially driven by the fermion loop,

$$\partial_t \lambda_{2n,k} = \big(n(d-2+\eta_{\sigma,k})-d\big)\lambda_{2n,k} - (-1)^n n!\, 2^{n+2}\left(\frac{d_\gamma v_d}{d}\right)\big(h_k^2\big)^n . \tag{4.66}$$

Fixed-point values h_*^2, $\eta_{\sigma,*}$, $\lambda_{2,*}$, $\lambda_{4,*}$, $\lambda_{6,*}$, ... can be identified as the zeroes of the corresponding beta functions, $\partial_t h_k^2 \stackrel{!}{=} 0$, $\partial_t \lambda_{2,k} \stackrel{!}{=} 0, \ldots$ Of course, the Gaußian fixed point with all couplings vanishing solves these fixed-point equations. As the renormalization group flows for the bosonic couplings decouple in the large-N_f limit, a nontrivial fixed point requires $h_* \neq 0$. This immediately leads to

$$\eta_{\sigma,*} = 4 - d. \tag{4.67}$$

Here, this tight relation between the dimensionality and the bosonic anomalous dimension here is an artifact of the large-N_f expansion.

Similar sum rules are known for Yukawa theories with chiral symmetries [84]. Such a sum rule for a corresponding fixed point is also responsible for the universality of the BCS-BEC crossover in the broad resonance limit of ultracold fermi gases [105, 106]. In the present case, this fixes the value of the Yukawa fixed-point coupling,

$$h_*^2 = \left(\frac{d}{d_\gamma v_d}\right)\frac{(d-4)(d-2)}{(8-6d)}. \tag{4.68}$$

The fixed point is interacting for $2 < d < 4$ and merges with the Gaußian fixed point in $d = 4$. The fixed-point structure in the $(h_k^2, \lambda_{2,k})$-plane is depicted in Fig. 4.7, where we also include the fixed points for analytic continuation to arbitrary d (keeping the chiral structure constant for simplicity, i.e., $d_\gamma \equiv 4$). From Fig. 4.7, we can readily see that the non-Gaußian fixed point forms the basin of attraction (toward the IR) for all initial conditions falling onto the critical manifold. The critical manifold at the same time acts as the separatrix for symmetry breaking and symmetric flows. The critical surface, defined by the trajectories emanating from the fixed-point (again, toward the IR), is indeed one-dimensional. A fact we will prove momentarily by a stability analysis of the non-Gaußian fixed point. In asymptotic safety terms, the asymptotically safe trajectory can either fall into the symmetric or the broken phase. Toward the UV, both hit the same non-Gaußian fixed point, but of course cannot cross the barrier formed by the critical manifold.

The fixed-point values for the bosonic mass parameter and couplings can also be given analytically

$$\lambda_{2n,*} = \frac{(-1)^n n!\, 2^{n+2}}{(2n-d)}\left(\frac{d}{d_\gamma v_d}\right)^{n-1}\left(\frac{(d-4)(d-2)}{(8-6d)}\right)^n. \tag{4.69}$$

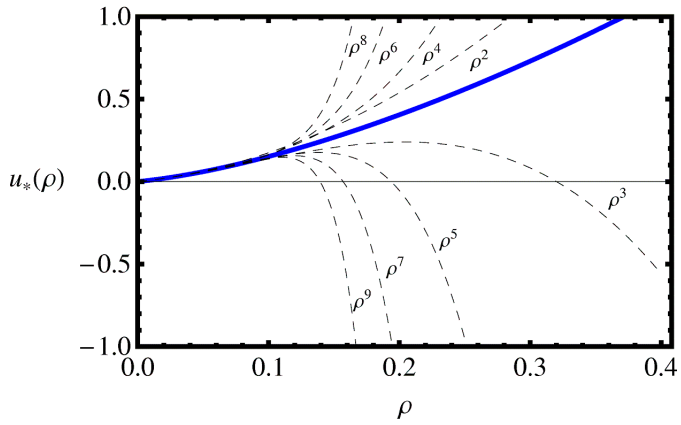

Figure 4.8: (Resummed) Fixed-point potential $u_*(\rho)$ for $d = 3$ in the large-N_f limit (blue/solid), see Eq. (4.70), and low-order polynomial approximations thereof ranging from ρ^2 to ρ^9 for small values of ρ (dashed lines).

Thus, the fixed-point values for all bosonic vertices $\lambda_{2n,k}$ are nonvanishing. In a purely fermionic formulation of the model, these higher bosonic self-interactions correspond to higher (nonlocal) fermionic self-interactions. In any case, we find that the UV fixed-point theory in $2 < d < 4$ for $N_\mathrm{f} \to \infty$ is not identical to the action $S[\{\bar{\psi}_j\}, \{\psi_j\}, \sigma]$, cf. Eq. (4.5), but involves infinitely many operators.

It turns out that the alternating series for the full renormalized effective potential can be resummed and yields the Gaußian Hypergeometric function ${}_2F_1(a, b; c; z)$ (see e.g. [107]). In terms of renormalized fields, the scale invariant fixed-point action then describes massless fermions coupled to a scalar boson with a potential

$$u_*(\rho) = -\tfrac{4d-16}{3d-4}\rho\, {}_2F_1\left(1-\tfrac{d}{2}, 1; 2-\tfrac{d}{2}; \tfrac{(d-4)(d-2)}{3d-4}\tfrac{d}{d_\gamma v_d}\rho\right). \tag{4.70}$$

This potential has a large-field asymptotic behavior $\propto \rho^{\frac{3}{2}}$, which agrees with our mean-field result for the full effective potential Eq. (4.12) formulated in terms of the $\mathbb{Z}_2$-invariant ρ. The small-field region is depicted in Fig. 4.8. The theory has predictive power, as the number of physical parameters is determined by the number of renormalization group relevant directions corresponding to the number of positive critical exponents. At the non-Gaußian fixed point in the large-N_f limit, the stability matrix assumes a particularly simple form where only a single column and the main diagonal are nonvanishing,

$$B = \begin{pmatrix} b_{h^2,h^2} & 0 & \cdots & & \\ b_{h^2,\lambda_2} & b_{\lambda_2,\lambda_2} & 0 & \cdots & \\ b_{h^2,\lambda_4} & 0 & b_{\lambda_4,\lambda_4} & 0 & \cdots \\ \vdots & \vdots & 0 & \ddots & \end{pmatrix}. \tag{4.71}$$

Therefore only the main diagonal of B enters into the stability analysis around the non-Gaußian fixed point. The important nonvanishing entries b_{h^2,h^2} and $b_{\lambda_{2n},\lambda_{2n}}$ turn out to be completely universal and are given by

$$b_{h^2,h^2} \equiv \frac{\partial \beta_{h^2}}{\partial h^2}\Big|_{g=g_*} = \eta_{\sigma,*} = 4 - d, \tag{4.72}$$

$$b_{\lambda_{2n},\lambda_{2n}} \equiv \frac{\partial \beta_{\lambda_{2n}}}{\partial \lambda_{2n}}\Big|_{g=g_*} = (n-1)d - 2n + n\eta_{\sigma,*} = 2n - d, \tag{4.73}$$

with $2n$ the number of external legs of the bosonic vertex $\lambda_{2n,k}$. The characteristic polynomial $\det(B + \Theta\mathbb{1})$ of the stability matrix B yielding the eigenvalues $-\Theta^I$ via its zeroes is then easily found to be

$$(-\Theta - (4-d)) \prod_{n=1}^{\infty} (-\Theta - (2n-d)) \,. \tag{4.74}$$

All large-N_f critical exponents are thus given by $d-4$ and $d-2n$. In $d=3$ this boils down to one positive critical exponent with value 1, i.e., one relevant direction, and infinitely many negative critical exponents $-1, -1, -3, -5, -7, \ldots$, corresponding to irrelevant directions. For the case of the Gaußian Yukawa fixed point, the characteristic polynomial of the stability matrix B is changed to

$$(-\Theta - (d-4)) \prod_{n=1}^{\infty} (-\Theta - (n(d-2) - d)) \,. \tag{4.75}$$

As expected, the critical exponents coincide with the mass dimension of the Yukawa coupling and the bosonic couplings, reproducing simple perturbative power counting. In total, this yields three relevant directions and one marginal direction. Note that the Gaußian fixed point found in the purely fermionic flow in Sect. 4.2 translates into a diverging dimensionless renormalized boson mass $\lambda_{2,k}^{1/2} \sim g_k^{-1/2}$, corresponding to the region RII in Fig. 4.7.

Returning to the non-Gaußian fixed point, we can, of course, make contact with the purely fermionic description and deduce the fixed point of the four-fermion coupling from the fixed point values of the Yukawa coupling and the bosonic mass parameter. We find

$$g_* = \frac{h_*^2}{\lambda_{2,*}} = \left(\frac{d}{d_\gamma v_d}\right) \frac{d-2}{8} \overset{(d=3)}{=} \frac{3\pi^2}{4}, \tag{4.76}$$

for the linear regulator which agrees with our findings in Sect. 4.2 (using the same regulator). In fact, the flow equation of the four-fermion interaction g_k can be reconstructed from the flow of the ratio $h_k^2/\lambda_{2,k}$,

$$\partial_t \left(\frac{h_k^2}{\lambda_{2,k}}\right) = (d-2)\left(\frac{h_k^2}{\lambda_{2,k}}\right) - \frac{8 d_\gamma v_d}{d}\left(\frac{h_k^2}{\lambda_{2,k}}\right)^2 + \mathcal{O}\left(\frac{1}{N_\mathrm{f}}\right). \tag{4.77}$$

Using the linear regulator in Eq. (4.32), we observe that the flow equation for g_k and $h_k^2/\lambda_{2,k}$ are identical in the large-N_f limit. Recall that $\eta_{\psi,k} \equiv 0$ in this limit.

Due to the equivalence of g_k and $h_k^2/\lambda_{2,k}$, the quantum critical point found in the purely fermionic formulation is also present in our study of the partially bosonized theory for $N_\mathrm{f} \to \infty$, as it should be the case. As it can be seen from the scaling law Eq. (4.35), this quantum critical point is associated with a vanishing boson mass, i.e., a diverging correlation length, in the long-distance limit.

Let us conclude our large-N_f analysis with a word of caution on the widely used so-called local potential approximation (LPA) in which wave-function renormalizations are neglected. Typically, also the nontrivial running of the Yukawa vertex is not included in such a truncation. If we had ignored the running of the wave-function renormalization of the bosonic field in the present case, the model would artificially depend on more than one physical parameter. To be more specific, let us consider the mass spectrum of the theory in the regime with broken chiral symmetry and assume that we have already fixed the mass of the fermions. Using the definition of the masses and the flow equations of the couplings, we find that the (dimensionless) renormalized boson mass in the broken regime can be written in terms of the (dimensionless) renormalized fermion mass m_f:

$$m_k^2 = 2\lambda_{4,k}\kappa_k \sim Z_{\sigma,k}^{-1} h_k^2 (h_k^2 \kappa_k) \sim Z_{\sigma,k}^{-1} h_k^2 m_{\mathrm{f,k}}^2. \tag{4.78}$$

Neglecting the running of $Z_{\sigma,k}$, i.e., $Z_{\sigma,k} \equiv$ const. as is done in the LPA, we observe that the boson mass does not depend on a single physical parameter, as it should be, but on two parameters independently, namely the fermion mass and the (only dimensionally running) Yukawa coupling. By contrast, taking the running of $Z_{\sigma,k} \sim h_k^2$ into account, the value of the boson mass is fixed solely in terms of the fermion mass, in agreement with both our fixed-point analysis and the explicit integration of the flows in Sect. 4.4. While this argument might be altered in $d = 4$ spacetime dimensions where the Yukawa coupling is marginal, it is true for the Gross-Neveu model in any dimension d in which the flow equation for $Z_{\sigma,k}$ is nonvanishing even at leading order in an expansion in $1/N_\mathrm{f}$. Therefore the flow of $Z_{\sigma,k}$ has to be taken into account in a systematic and consistent expansion of the flow equations in powers of $1/N_\mathrm{f}$. To be specific, for finite N_f the flow of the order parameter potential (4.44) incorporates already fluctuations at next-to-leading order in $1/N_\mathrm{f}$ due to the presence of the bosonic loop. However, for a systematic and consistent study of the effects of corrections beyond the large-N_f expansion the flow of $Z_{\sigma,k}$, $Z_{\psi,k}$ as well as of the Yukawa coupling is crucial.

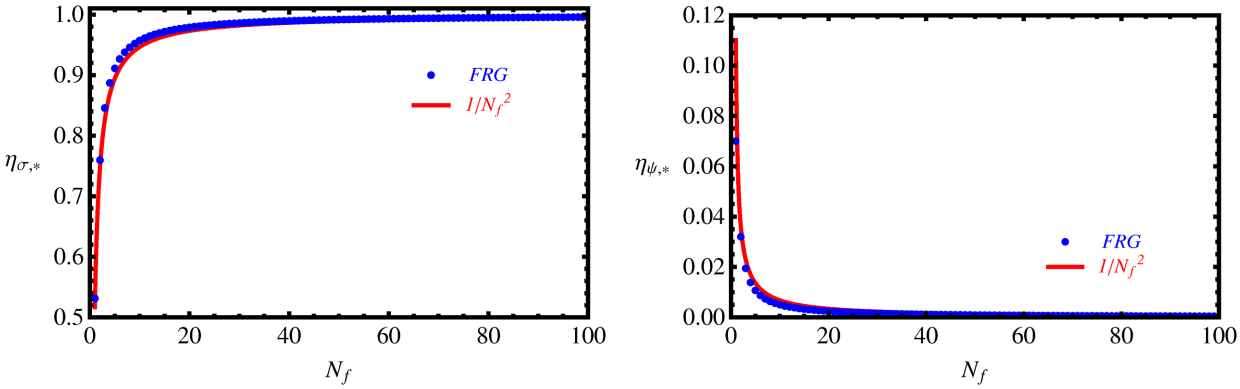

Figure 4.9: Fixed-point values of bosonic and fermionic anomalous dimensions $\eta_{\sigma,*}$ and $\eta_{\psi,*}$ for $N_\mathrm{f} = 1, 2, 3, \ldots, 100$ in $d = 3$ (blue blobs) from a 22nd-order approximation. The red curves are the anomalous dimensions to order $1/N_\mathrm{f}^2$, cf. Eq. (4.19).

Finite N_f Fixed-Point Structure, Numerical Results

Beyond the limit of large N_f, bosonic fluctuations begin to play a role. An immediate consequence is that a new fixed point for $h_* = 0$ arises for the flow of the effective potential for $2 < d < 4$. This fixed point of the purely bosonic theory is nothing but the Wilson-Fisher fixed point which describes critical phenomena in the three-dimensional Ising universality class. The non-Gaußian fixed point of the full Gross-Neveu system can now be understood as being sourced from the leading large-N_f terms discussed above and the bosonic fluctuations inducing a Wilson-Fisher fixed point. Depending on the value of N_f the non-Gaußian Gross-Neveu fixed point interpolates between the large-N_f fixed point for $N_\mathrm{f} \to \infty$ and the Wilson-Fisher fixed point in the formal limit of $N_\mathrm{f} \to 0$. For the latter, the functional renormalization group has already proved to be a useful quantitative tool for describing nonperturbative critical phenomena, see e. g. Refs. [41, 109–114].

Let us repeat the preceding analysis, now using the full flow equations at next-to-leading order derivative expansion, i.e., Eqs. (4.44), (4.45), (4.47), and (4.46). For all quantities of interest, such as critical exponents and fixed-point values of couplings, a solution of the potential flow in a polynomial expansion is sufficient, as suggested by our results obtained in the previous section. Confining our numerical studies to $d = 3$, all figures are produced within a truncated expansion up to 22nd order in σ (except for ν at $N_\mathrm{f} = 1$, which is taken from a 18th order truncation); quantitative results are derived from an expansion to the same order in σ. In the symmetric regime, a nontrivial fixed point in the Yukawa coupling requires the following inequality to be satisfied,

$$d - 4 + 2\eta_{\psi,*} + \eta_{\sigma,*} < 0, \quad \text{for } N_\mathrm{f} < \infty. \tag{4.79}$$

This is because the second term of the Yukawa flow Eq. (4.45) is strictly positive for admissible values of the anomalous dimensions $\eta_{\sigma,k}$, $\eta_{\psi,k} \lesssim \mathcal{O}(1)$. For instance, in $d = 3$, the sum of the anomalous-dimension terms is always slightly smaller than 1, see Figs. 4.9. The inequality becomes an equality in the large-N_f limit, see Eq. (4.67). The resulting fixed-point values for the Yukawa

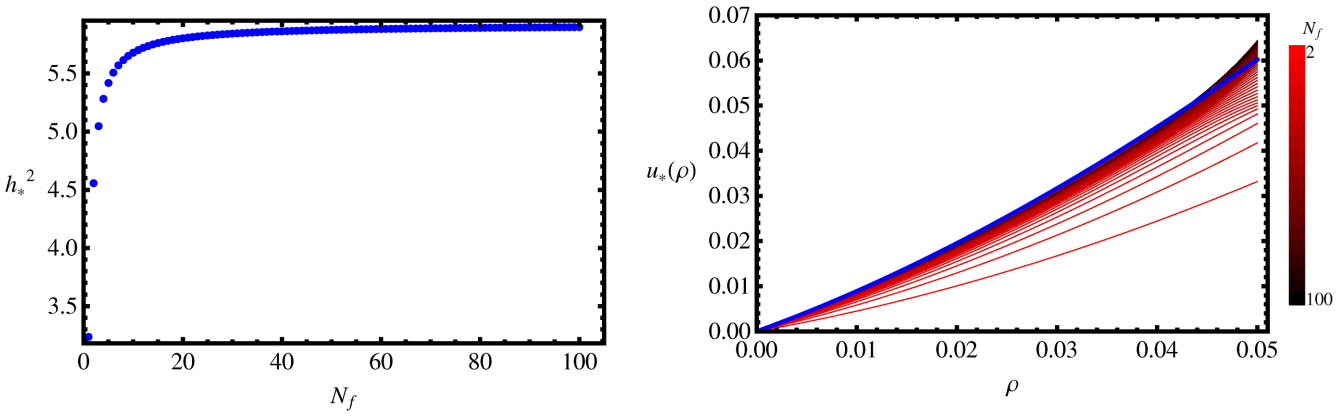

Figure 4.10: Left panel: Yukawa fixed-point values over $N_\mathrm{f} = 1, 2, 3, \ldots, 100$ in $d = 3$ from a 22nd-order approximation. Right panel: Fixed-point potentials $u_*(\rho)$ for $N_\mathrm{f} = 1, 2, 3, \ldots, 100$ in $d = 3$ also from a 22nd-order approximation. The large-N_f result is shown as a thick/blue line. Incidentally, for $N_\mathrm{f} = 0$ the potential approaches the Wilson-Fisher fixed-point potential with a nontrivial minimum near $\rho \simeq 0.3$ (not shown).

coupling in $d = 3$ are depicted in Fig. 4.10. For increasing N_f, the fixed point quickly approaches its large-N_f limit (4.68), whereas it tends to zero for small N_f leaving us with the Wilson-Fisher fixed point of a pure scalar model. As the latter is known to exhibit a fixed-point potential in the broken regime, i.e., with a nonvanishing expectation value of the scalar field σ, we expect such a fixed-point potential featuring a nontrivial minimum to occur for small N_f. For all integer values of $N_\mathrm{f} \geq 1$ Dirac (four-component) fermions, we still observe fixed-point potentials in the symmetric regime, in agreement with [80]. Nevertheless, the fixed point occurs in the broken regime for the model with one two-component fermion (corresponding to $N_\mathrm{f} = 1/2$ in our language) [80]. The fixed-point potential in $d = 3$ for various values of N_f is plotted in Fig. 4.10 in a 22nd-order approximation. Also the potential converges rapidly to the large-N_f result for increasing values of N_f. In Figs. 4.9, we compare our numerical results (from a 22nd-order approximation) to the anomalous dimensions obtained in a $1/N_\mathrm{f}$-expansion to order $1/N_\mathrm{f}^2$, cf. Eq. (4.19). We expect our results to improve upon the results Eq. (4.19), since the flow equations effectively perform a resummation to all orders in $1/N_\mathrm{f}$.

Let us now turn to the leading universal critical exponents $\Theta^{1,2}$. The convergence of the polynomial expansion of the potential is demonstrated in Tabs. 4.3 and 4.4, where the leading critical exponents for $N_\mathrm{f} = 2$ and $N_\mathrm{f} = 12$ are listed for increasing truncation order. In each case, the leading exponents converge to a stable value. We observe a more rapid convergence for larger values of N_f. The somewhat slower convergence for more scalar dominated models is familiar from pure O(N) models. The correlation length exponent and the subleading critical exponents are plotted as a function of N_f in Fig. 4.11. Table 4.5 lists the leading exponents for increasing number of N_f, illustrating the approach to the analytical large-N_f results.

$2n$	Θ^1	Θ^2	Θ^3	Θ^4	Θ^5	Θ^6
4	0.9928	−0.8687	−1.5743	–	–	–
6	0.9766	−0.8743	−1.0624	−5.4313	–	–
8	0.9831	−0.8721	−1.0790	−3.5622	−10.5959	–
10	0.9821	−0.8720	−1.0999	−3.4194	−6.8111	−17.4807
12	0.9819	−0.8723	−1.0897	−3.5628	−5.7949	−11.2156
14	0.9821	−0.8722	−1.0911	−3.5104	−6.0610	−8.6408
16	0.9820	−0.8722	−1.0920	−3.5062	−6.1190	−8.3598
18	0.9820	−0.8722	−1.0914	−3.5202	−5.9849	−8.9972
20	0.9821	−0.8722	−1.0915	−3.5132	−6.0516	−8.5869
22	0.9821	−0.8722	−1.0916	−3.5135	−6.0514	−8.5820

Table 4.3: Non-Gaußian critical exponents in $d = 3$ for increasing polynomial truncations for $N_\mathrm{f} = 2$. The results for the critical exponent Θ^1 agree within the error bars with the result from Monte-Carlo (MC) simulations [67], $1/\Theta^1_\mathrm{MC} = \nu_\mathrm{MC} \approx 1.00(4)$.

$2n$	Θ^1	Θ^2	Θ^3	Θ^4	Θ^5	Θ^6
4	0.9898	−0.9735	−1.0701	–	–	–
6	0.9903	−0.9735	−1.0489	−3.2583	–	–
8	0.9903	−0.9735	−1.0507	−3.1714	−5.5889	–
10	0.9903	−0.9735	−1.0505	−3.1821	−5.3368	−8.1011

Table 4.4: Non-Gaußian critical exponents in $d = 3$ for increasing polynomial truncations for $N_\mathrm{f} = 12$.

N_f	Θ^1	Θ^2	Θ^3	Θ^4	Θ^5	Θ^6
2	0.9821	−0.8722	−1.0916	−3.5135	−6.0514	−8.5820
4	0.9775	−0.9240	−1.1010	−3.3910	−5.7739	−8.2429
12	0.9903	−0.9735	−1.0506	−3.1810	−5.3665	−7.6004
50	0.9975	−0.9936	−1.0143	−3.0510	−5.1062	−7.1789
100	0.9987	−0.9968	−1.0073	−3.0263	−5.0550	−7.0934
∞	1	−1	−1	−3	−5	−7

Table 4.5: Non-Gaußian critical exponents for various flavor numbers N_f in $d = 3$ in the ρ^{11} truncation.

This approach is also visible in the anomalous dimension and the fixed-point values for the coupling, see Tab. 4.6. Whereas the fixed-point couplings are nonuniversal (holding for the linear regulator in this case), the anomalous dimensions are universal and illustrate the inequality (4.79).

We can compare our quantitative results for the leading critical exponent to other studies of the chiral quantum phase transition in the Gross-Neveu model aiming at the long-distance physics, noting that Θ^1 is related to the correlation length exponent ν by $\nu = 1/\Theta^1$. Together with the bosonic anomalous dimension and corresponding scaling and hyperscaling relations Eq. (4.18), the exponents δ, β, etc. of the phase transition are determined. Wherever comparable, our results agree quantitatively with the functional renormalization group study of [80] where both a polynomial expansion as well as a grid solution of the potential was used (note that our N_f counts four-component fermions, whereas [80] uses two-component Weyl fermions). Moreover, the agreement

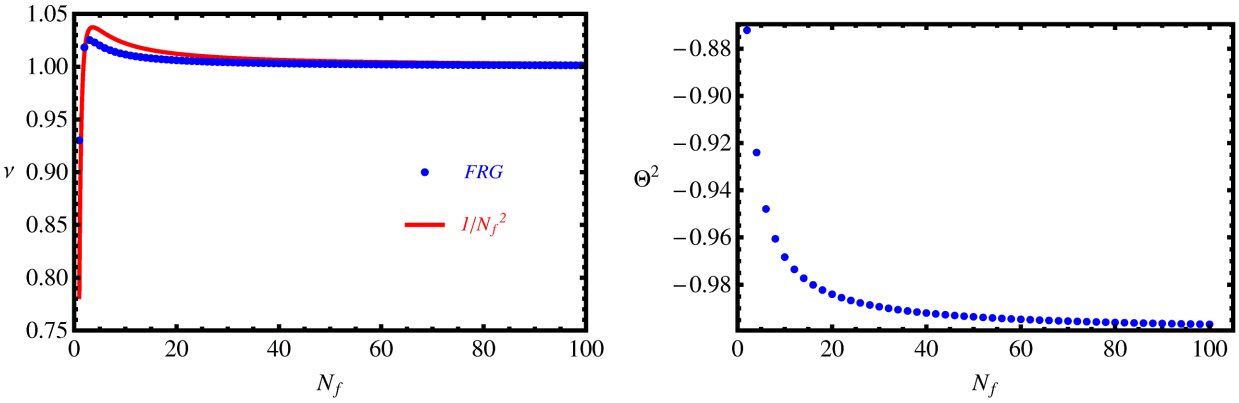

Figure 4.11: Left panel: Correlation length exponent ν (related to the relevant critical exponent Θ^1 by $\nu = 1/\Theta_1$) for $N_\mathrm{f} = 1, 2, 3, \ldots, 100$ in $d = 3$ from a 22nd-order approximation. The nonmonotonic behavior for small N_f is expected, since ν has to approach $\nu = 1/\Theta^1 \simeq 0.63$ for $N_\mathrm{f} = 0$ corresponding to a correlation length exponent of the $3d$ Ising universality class. However, the value for $N_\mathrm{f} = 1$ was taken from a σ^{18} truncation due to numerical difficulties in higher truncations. The red curves are the results to order $1/N_\mathrm{f}^2$, cf. Eq. (4.19). Right panel: First subleading irrelevant critical exponent Θ^2 for $N_\mathrm{f} = 1, 2, 3, \ldots, 100$ in $d = 3$ from a 22nd-order approximation.

with results from other methods such as $1/N_\mathrm{f}$-expansions [75] and Monte Carlo simulations [66, 67] is satisfactory, while we expect our results to improve upon those obtained in $1/N_\mathrm{f}$-expansions due to the resummation implicit in the flow equations. Discrepancies are mainly visible only in the anomalous dimensions for small N_f, a feature familiar from bosonic models. The polynomial expansion of the potential converges somewhat slower for the special case $N_\mathrm{f} = 1$, where our results for the leading exponents are compatible with those of [80], but subleading exponents seem to require a precise solution of the potential flow. It is worth mentioning, that for $N_\mathrm{f} = 1$ the fixed-point solutions seem more difficult to obtain. At first sight, additional relevant directions appear for fixed-point solution. These, however, could be proven to be unstable with deformations of the truncation, i.e., setting couplings not included in the truncation to arbitrary values different from zero.

To summarize, the nonperturbative features of the Gross-Neveu model near criticality can be well described by the functional renormalization group, as the model interpolates between two well-accessible limits: the large-N_f limit for $N_\mathrm{f} \to \infty$ and the Wilson-Fisher fixed point in the Ising universality class for $N_\mathrm{f} \to 0$. Our results suggest that the Gross-Neveu model has an interacting non-Gaußian fixed point for all $N_\mathrm{f} > 0$ and that the model depends on only a single parameter, even when we take into account corrections beyond the large-N_f limit. Equivalently, with respect to the construction of a continuum limit, the Gross-Neveu model in $d = 3$ is asymptotically safe for all $N_\mathrm{f} > 0$.

N_f	$\eta_{\sigma,*}$	$\eta_{\psi,*}$	h_*^2	$\lambda_{2,*}$
2	0.7596	0.0320	4.5565	0.3956
4	0.8870	0.0138	5.2820	0.5846
12	0.9644	0.0041	5.7206	0.7263
50	0.9917	0.0009	5.8746	0.7822
100	0.9958	0.0005	5.8983	0.7911
∞	1	0	5.9218	0.8

Table 4.6: Non-Gaußian fixed-point values of the universal anomalous dimensions for various flavor numbers N_f in $d = 3$. The (nonuniversal) fixed-point couplings hold for the linear regulator. In Monte-Carlo (MC) simulations [67] $\eta_{\sigma,*}^{\mathrm{MC}} = 0.754(8)$ has been found for $N_\mathrm{f} = 4$ two-component fermions (corresponding to $N_\mathrm{f} = 2$ in our language).

Discussion

We have used the functional renormalization group to describe the critical behavior of the Gross-Neveu model in $2 < d < 4$ dimensions. In agreement with many earlier results in the literature, the model features a 2nd order chiral quantum phase transition. The non-Gaußian fixed point controlling this transition at the same time facilitates nonperturbative renormalizability, providing a simple fermionic example of asymptotic safety in Weinberg's sense. The perturbative conclusion about nonrenormalizability is a mere artifact of naive power-counting which is only justified near the Gaußian fixed point.

Our work is amended by new results in the large-N_f limit, where the fixed-point potential as well as all critical exponents can be computed analytically. Moreover, we have also provided finite N_f results, demonstrating that the model interpolates between the large N_f limit and a purely bosonic model in the $3d$ Ising universality class.

Some final comments are in order: the simple fermionic Gross-Neveu action is minimalistic in the sense that it suffices to put the system into the right "Gross-Neveu universality class". Comparing the fermionic action with the fixed-point action in the partially bosonized version, we have to conclude that the fixed-point action in the fermionic language is far more complicated than the simple ansatz (4.22). In general, it will contain higher-order as well as nonlocal interaction terms. The deviations from the simple Gross-Neveu structure, however, are irrelevant operators which do not modify the predictive power of the Gross-Neveu model.

The simple Gross-Neveu action is also incomplete in the sense that it does not exhibit all possible four-fermi terms compatible with the defining symmetries of the model as listed in Chap. 3. A more complete renormalization group analysis thus has to include these terms possibly leading to the appearance of further fixed-points, as is known for the Thirring model [34]. If so, this implies the possible existence of a fermionic theory with a more interesting ground-state phase structure but with the same defining symmetries as the Gross-Neveu model and containing it as a special case.

Chapter 5

Chiral Restoration at Finite Temperature

As our preceding analysis of the fixed-point structure in Chap. 4 suggests, the Gross-Neveu model does not feature a nonanalyticity as a function of flavor number, which is in stark contrast to the behavior of the three-dimensional Thirring model [34] or QED_3 [116] or even many-flavor QCD [115]. Therefore, it remains to study the mutual influence of flavor number and temperature on the melting of the chiral condensate in a quantitative way. In this chapter we hence describe the construction of a many-flavor phase diagram. For this phase diagram we consider different flavor realizations of the Gross-Neveu model in thermal equilibrium with a heat bath characterized by a specific value of temperature. Temperature here also acts as a probe to study the stability of the condensate as a function of the number of flavor species. To achieve comparability between different microscopic realizations of the Gross-Neveu model with varying flavor number, we choose bare parameters such that the renormalized fermion masses in the symmetry broken $T = 0$ state of the theories are identical. Actually, as we will see already at the mean-field level, the finite temperature phase diagram is in a sense "universal", since the Gross-Neveu field theory microscopically depends only on a single scale/parameter.

As a byproduct, we can study the effects of finite temperature on the level of the flow equations. As pointed out in Chap. 1 and Chap. 4, one could have naively expected that the quantum critical point responsible for the zero temperature transition of the Gross-Neveu type with discrete chiral symmetry breaking could be described by an O(1)-model with fields defined over three-dimensional spacetime. This naive expectation related to the Hertz-Millis philosophy, however, is known to fail, as discussed in Chap. 4. Instead, the quantum corrections from the fermion sector induce scaling laws different from those obtained from a purely scalar model. Yet, as we increase temperature to study the melting of the chiral condensate – which, of course, also takes place in the large-N_f limit – the fermionic fluctuations become increasingly suppressed by acquiring an increasing thermal mass. The restoration of chiral symmetry by finite temperature is always continuous for vanishing chemical potential. Beyond the large-N_f limit, the collective bosonic fluctuations get suppressed

as well by the same mechanism, except for the Matsubara zero mode, which does not exist for fermionic degrees of freedom due to the antiperiodic boundary conditions in the (imaginary) time direction. Thus, for certain temperatures, the Matsubara zero mode is expected to dominate the IR physics of the model. In this respect, we can expect the finite temperature phase transition to be well described by an O(1)-model in *two* spacetime dimensions. This process of dimensional reduction can be studied in detail within the renormalization group framework.

As a starting point for the study of finite temperature effects in Sect. 5.1, we will analyze the mean-field solutions of the Gross-Neveu model in the presence of a heat bath. We consider the grand canonical quantum partition function, which as a further parameter includes a finite chemical potential controlling the number of charges in the system. Equipped with an upper bound on the critical temperature T_c from the limit $N_\mathrm{f} \to \infty$, in Sect. 5.2 we then move to finite flavor numbers and present our results for the many-flavor phase diagram. A critical discussion of the employed truncation is given. In Sec. 5.3, we finally show how the different flavor realizations of the Gross-Neveu model display regions of varying width where Ising-scaling in the proximity to the finite temperature transition is observable, i.e., the so-called *Ginzburg region*. To conclude, in Sect. 5.4 we briefly touch upon the difficulty of treating the full effective potential beyond LPA and the problem of including a finite chemical potential in a chirally symmetric theory in three spacetime dimensions within our renormalization group approach. Although in principle desirable from the point of view of QCD-inspired thermodynamics and condensed matter applications with doping away from the Dirac point, one obstacle to obtaining a consistent set of flow equations for Dirac fermions with finite chemical potential is the lack of a technically suitable regulator so far which can achieve a well defined and manageable set of threshold functions, incorporating the effects of a finite Fermi surface and its thermal excitations.

5.1 Mean-Field Phase Diagram

As discussed in Chap. 2, a field theory in thermal equilibrium can formally be described by compactifying the Euclidean time direction τ to a circle with a circumference identical to the inverse absolute temperature $\beta = 1/T$. Bosonic fields obey periodic, fermionic fields antiperiodic boundary conditions in the time direction. As already explained, this leads to summations over two different sets of discrete Matsubara frequencies for bosons ($\omega_n = 2\pi n/\beta$, $n \in \mathbb{Z}$) and fermions ($\nu_n = (2n+1)\pi/\beta$, $n \in \mathbb{Z}$). A quantum partition function coupled to a heat bath with constraints on some conserved charge describes the thermodynamics of a canonical ensemble. More convenient, however, is the description of the grand canonical ensemble, which allows for fluctuations of the conserved charges, i.e., they are only conserved on average.

Grand-Canonical Partition Function

The quantum partition function can be elegantly formulated as a functional integral without constraints. The grand canonical ensemble, we will consider in the following, takes into account a finite chemical potential $\mu \in \mathbb{R}$, which is conjugate to the number of conserved charges. These conserved charges are obtained as the integrated densities associated with the Noether current derived from invariance of the action under global U(1)-transformations. On a formal level, the chemical potential can be included in the Lagrangian of the system by the substitution

$$\gamma_0 \partial_0 \quad \rightarrow \quad \gamma_0(\partial_0 + \mu). \tag{5.1}$$

This leaves the chiral symmetries of the model intact. We thus define the quantum partition function as

$$\mathcal{Z}(\beta, \mu) = \int \prod_{j=1}^{N_\mathrm{f}} \mathcal{D}\bar{\psi}_j \mathcal{D}\psi_j \, \mathrm{e}^{-S[\{\bar{\psi}_j\},\{\psi_j\}]}, \tag{5.2}$$

with the finite temperature action

$$S[\{\bar{\psi}_j\},\{\psi_j\}] = \int_x \left\{ \sum_{j=1}^{N_\mathrm{f}} \bar{\psi}_j \left(\mathrm{i}\not{\partial} + \mathrm{i}\mu\gamma_0\right) \psi_j + \sum_{i,j=1}^{N_\mathrm{f}} \bar{\psi}_i \psi_i \frac{\bar{g}}{2N_\mathrm{f}} \bar{\psi}_j \psi_j \right\}, \tag{5.3}$$

where the shorthand $\int_x \equiv \int_0^\beta \mathrm{d}\tau \int \mathrm{d}^{d-1}\boldsymbol{x}$ for integration over $x = (\tau, \boldsymbol{x}) \in \mathbb{S}^1 \times \mathbb{R}^{d-1}$ was employed. The above mentioned global phase transformations do not mix different flavor species in the Gross-Neveu Lagrangian. So in principle we could generalize the partition function as $\mathcal{Z}(\beta, \mu) \rightarrow \mathcal{Z}(\beta, \mu_j)$, $j = 1, \ldots, N_\mathrm{f}$, with each flavor species having different average of its conserved U(1)-charge. Yet, this generalization would spoil the global U(N_f) symmetry, which allows us to obtain exact results in the limit $N_\mathrm{f} \rightarrow \infty$. So we shall deal with the degenerate case $\mu_i \equiv \mu_j$, $\forall i, j = 1, \ldots, N_\mathrm{f}$ only. In other words, we consider the grand canonical ensemble, where the *total* charge $Q \equiv \sum_{j=1}^{N_\mathrm{f}} Q_j$ is conserved on average.

The presence of the chemical potential in the bilinear part of the theory modifies the pole-structure of the fermionic propagator in the complex frequency plane. In frequency-momentum representation, it reads

$$G^+(p) \equiv G^+(\nu_n, \boldsymbol{p}) = -\frac{\gamma_0(\nu_n - \mathrm{i}\mu) + \boldsymbol{\gamma} \cdot \boldsymbol{p}}{(\nu_n - \mathrm{i}\mu)^2 + \boldsymbol{p}^2}, \tag{5.4}$$

where we have used the shorthand notation $p = (\nu_n, \boldsymbol{p})$. For[1] $\mu \neq 0$, the frequency-summation generates Fermi distributions, that cut off states beyond the so-called Fermi surface.[2]

The homogeneous mean-field solutions of the Gross-Neveu model have been studied extensively in the literature [85–93]. For our goal to obtain the finite temperature many-flavor phase structure, the mean-field solution provides a good starting point to familiarize with the finite temperature physics. To study the large-N_f contribution to the partition function, we again decouple the fermionic interaction by a Hubbard-Stratonovich transformation as in Sect. 4.1. Now, of course, the spacetime measure is adapted to finite temperature and the σ field as a composite object built from two fermionic fields fulfills periodic boundary conditions for bosonic statistics. We obtain the quantum partition function with the auxiliary σ field as

$$\mathcal{Z}(\beta,\mu) = \int \prod_{j=1}^{N_\mathrm{f}} \mathcal{D}\bar{\psi}_j \mathcal{D}\psi_j \mathcal{D}\sigma \, \mathrm{e}^{-S[\{\bar{\psi}_j\},\{\psi_j\},\sigma]} \tag{5.5}$$

with the boson-fermion action

$$S[\{\bar{\psi}_j\},\{\psi_j\},\sigma] = N_\mathrm{f} \int_x \frac{\bar{h}^2}{2\bar{g}}\sigma^2 + \int_x \sum_{j=1}^{N_\mathrm{f}} \bar{\psi}_j \left(\mathrm{i}\partial\!\!\!/ + \mathrm{i}\bar{h}\sigma + \mathrm{i}\mu\gamma_0\right)\psi_j. \tag{5.6}$$

As in Chap. 4, the quadratic fermionic piece can be integrated out and gives rise to a trace-log contribution $-N_\mathrm{f}\mathrm{Tr}\ln\left[\mathrm{i}\partial\!\!\!/ + \mathrm{i}\bar{h}\sigma + \mathrm{i}\mu\gamma_0\right]$ to the effective bosonic action $S[\sigma]$. In the limit $N_\mathrm{f} \to \infty$, only the stationary points in the exponent of Eq. (5.5) contribute.

Finite Temperature Mean-Field Solutions

For our presentation in this section, we mainly follow the seminal work [85] and expand upon the results obtained there, as far as representations of the effective potential and its analyticity properties are concerned. The homogeneous mean-field solutions are obtained from the stationarity condition

$$\frac{\delta}{\delta\sigma(x)} S[\sigma]|_{\sigma=\langle\sigma\rangle\equiv\mathrm{const.}} = N_\mathrm{f} \frac{\partial U(\beta,\mu;\sigma)}{\partial\sigma} \stackrel{!}{=} 0. \tag{5.7}$$

We have again identified the classical homogeneous field configuration with the expectation value of the quantum field, which is allowed at mean-field level as already explained in Sect. 4.1. $U(\beta,\mu;\sigma)$

[1] With respect to condensed matter applications discussed in Chap. 1, the case $\mu = 0$ refers to the particle-hole symmetric situation of a half-filled band.

[2] Strictly speaking, a Fermi surface is sharply defined only in the limit $T \to 0$. At finite temperature, the Fermi distribution function smears out the Fermi surface and controls the thermal occupation.

denotes the effective potential at finite temperature and chemical potential. Upon performing the Matsubara sum by contour integration we obtain [85, 86]

$$1 = d_\gamma\, \bar{g} \int_{\boldsymbol{p}} \frac{1}{\sqrt{\boldsymbol{p}^2 + \bar{h}^2\sigma^2}} \left\{ 1 - n_F\left(\sqrt{\boldsymbol{p}^2 + \bar{h}^2\sigma^2} + \mu\right) - n_F\left(\sqrt{\boldsymbol{p}^2 + \bar{h}^2\sigma^2} - \mu\right) \right\}, \tag{5.8}$$

where $\int_{\boldsymbol{p}} \equiv \int \frac{\mathrm{d}^{d-1}\boldsymbol{p}}{(2\pi)^{d-1}}$ and $n_F(z)$ denotes the Fermi distribution function at inverse temperature β,

$$n_F(z) = \frac{1}{\mathrm{e}^{\beta z} + 1}. \tag{5.9}$$

If we assume a broken ground state at $T = 0$, $\mu = 0$ with a finite mean-field value σ_0 for the σ field, we can perform also the spatial momentum integration and rearrange Eq. (5.8) into

$$\bar{m}_\mathrm{f} = \bar{m}_{\mathrm{f},0} - \frac{1}{\beta}\Big\{ \ln\left(1 + \mathrm{e}^{-\beta(\bar{m}_\mathrm{f} + \mu)}\right) + \ln\left(1 + \mathrm{e}^{-\beta(\bar{m}_\mathrm{f} - \mu)}\right) \Big\}. \tag{5.10}$$

Here, we have expressed the mean-field solutions σ and σ_0 by the respective fermion masses $\bar{m}_\mathrm{f} = \bar{h}\sigma$ and $\bar{m}_{\mathrm{f},0} = \bar{h}\sigma_0$ generated via mediation of the Yukawa coupling $\bar{h}$. The fact that a cutoff regularization is not necessary to integrate the finite temperature gap equation is explained by trading the formally divergent contribution to Eq. (5.8) for a finite fermion mass[3] $\bar{m}_{\mathrm{f},0}$. From Chap. 4 we know that in three spacetime dimensions the fermion mass $\bar{m}_{\mathrm{f},0}$ as a physical observable defines in a scheme-dependent way a pair $(\Lambda, \bar{g}(\Lambda))$. Then, for a bare coupling $\bar{g}(\Lambda)$ chosen with respect to a given UV cutoff Λ, the value of the dynamically generated fermion mass is independent of a particular microscopic realization of the model. So all the scheme dependence is "hidden" in $\bar{m}_{\mathrm{f},0}$. As expected, Eq. (5.10) shows that the nontrivial solutions for the order parameter will decrease with temperature. Solutions of the self-consistency equation Eq. (5.10) can be easily found numerically. The resulting phase diagram is depicted in Fig. 5.1. The dimensionful quantities were normalized with respect to the dynamically generated fermion mass $\bar{m}_{\mathrm{f},0}$ at both vanishing temperature and chemical potential. In the (T, μ)-plane, the chirally broken phase is separated from the chirally symmetric phase by a line of 2nd order phase transitions. Only at $T = 0$, $\mu/\bar{m}_{\mathrm{f},0} = 1$ a 1st order transition occurs in the μ-direction. We will address this issue in a moment. The phase boundary separating the ordered from the disordered phase can be obtained in closed form from Eq. (5.10) if we consider the limit $\bar{m}_\mathrm{f} \to 0$:

$$\mu_\mathrm{c}(\beta_\mathrm{c}) = \beta_\mathrm{c}^{-1} \mathrm{arcosh}\left[\frac{1}{2}\mathrm{e}^{\bar{m}_{\mathrm{f},0}\beta_\mathrm{c}} - 1\right], \tag{5.11}$$

[3] To see this, it is convenient to change the integration variable from spatial momentum $\boldsymbol{p}$ to $E \equiv \sqrt{\boldsymbol{p}^2 + \bar{h}^2\sigma^2}$. Assuming $\sigma_0 \neq 0$, we can write $\bar{h}\sigma - \bar{h}\sigma_0 = \int_{\bar{h}\sigma_0}^{\infty} \mathrm{d}E - \int_{\bar{h}\sigma}^{\infty} \mathrm{d}E$. Additionally using $\frac{1}{\bar{g}} = \frac{2}{\pi}\int_{\bar{h}\sigma_0}^{\Lambda} \mathrm{d}E$ and removed the cutoff. Performing the integration over E, one arrives at Eq. (5.10).

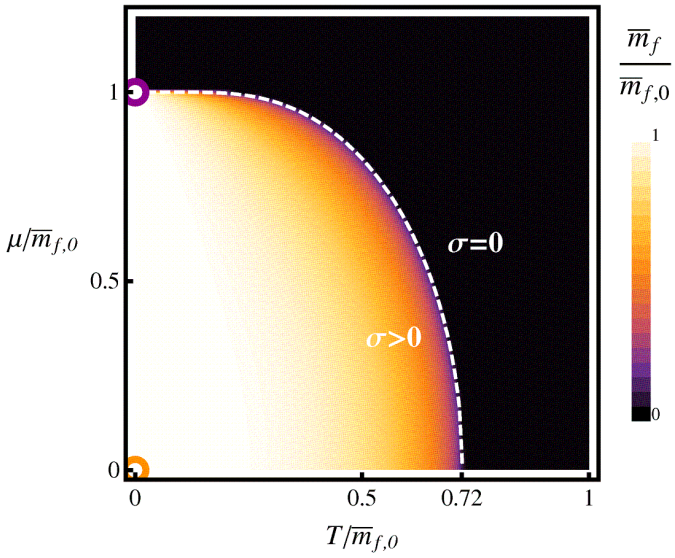

Figure 5.1: Mean-field phase diagram of the Gross-Neveu model for finite temperature T and chemical potential μ. All dimensionful quantities are normalized to the dynamically generated fermion mass $\bar{m}_{\mathrm{f},0}$ at $T = 0$, $\mu = 0$. The phase diagram was obtained by solving Eq. (5.10) numerically on a 100×100 grid in the (T, μ)-plane. The phase boundary (dashed white) can be obtained analytically, cf. Eq. (5.11). The orange open disk marks the $T = 0$, $\mu = 0$ state, whose tendency to form a chiral condensate for overcritical couplings was extensively discussed in Chap. 4. Along the phase boundary, the vanishing of the chiral condensate occurs continuously, except for the point $T = 0$, $\mu/\bar{m}_{\mathrm{f},0} = 1$ (marked by the violet open disk), where in the μ-direction, the phase transition is discontinuous.

where we display the critical chemical potential as a function of the critical (inverse) temperature. The mean-field result Eq. (5.11) explicitly reveals that the phase structure of the model is fixed in terms of a single scale, namely the dynamically generated fermion mass $\bar{m}_{\mathrm{f},0}$ at $T = 0$ and $\mu = 0$. Due to the fixed-point structure exposed in Chap. 4, we know that the value $\bar{m}_{\mathrm{f},0}$ and $\bar{g}$ are in a one to one correspondence, at least for $d = 3$. Since the feature of one relevant direction persists at finite N_{f}, we expect the many-flavor phase diagram to be constructed in the next section to be "universal".

The critical temperature at $\mu = 0$ can be read off from Eq. (5.11) to be given by

$$T_{\mathrm{c}}(\mu = 0) = \frac{\bar{m}_{\mathrm{f},0}}{2 \ln 2} \simeq 0.72\, \bar{m}_{\mathrm{f},0}. \tag{5.12}$$

At $T = 0$, the critical chemical potential turns out to be

$$\mu_{\mathrm{c}}(T = 0) = \bar{m}_{\mathrm{f},0}. \tag{5.13}$$

Note that the fermion mass at $T = 0$ remains constant as a function of the chemical potential until it reaches its critical value Eq. (5.13), where it jumps to zero discontinuously.

Effective Potential at Mean-Field Level

At this level of approximation, one can obtain the full thermodynamic effective potential simply by integrating the gap equation over the homogeneous field σ. Indeed [98, 117],

$$\begin{aligned} U(\beta,\mu;\sigma) &= \int_0^\sigma \mathrm{d}\sigma' \frac{\partial U(\beta,\mu;\sigma')}{\partial\sigma'} \\ &= \int_0^\sigma \mathrm{d}\sigma' \left[\frac{\bar{h}^2\sigma'}{\pi}\left(\bar{h}|\sigma'| - \bar{m}_{\mathrm{f},0}\right) + \frac{2\bar{h}\sigma'}{\beta}\left\{\ln\left(1+\mathrm{e}^{-\beta(\bar{h}|\sigma'|+\mu)}\right) + \ln\left(1+\mathrm{e}^{-\beta(\bar{h}|\sigma'|-\mu)}\right)\right\}\right] \\ &= \frac{1}{\pi}\left(\frac{1}{3}\bar{h}^3|\sigma|^3 - \frac{\bar{m}_{\mathrm{f},0}}{2}\bar{h}^2\sigma^2\right) + \left\{\frac{\bar{h}|\sigma|}{\pi\beta^2}\mathrm{Li}_2\left(-\mathrm{e}^{-\beta(\bar{h}|\sigma|+\mu)}\right) + \frac{1}{\pi\beta^3}\mathrm{Li}_3\left(-\mathrm{e}^{-\beta(\bar{h}|\sigma|+\mu)}\right)\right\} \\ &\quad + \left\{\mu \to -\mu\right\} + \text{const.}, \end{aligned} \tag{5.14}$$

where const. is chosen such that $U(\beta,\mu;\sigma=0)=0$. In Fig. 5.2 we plot the effective potential for different values of temperature and chemical potential. It is interesting to investigate the structure of the effective potential close to the 1st order transition. For $\mu \to \mu_{\mathrm{c}}(T=0)^-$ and $T=0$, there appear infinitely many degenerate solutions and the effective potential is flat[4] for $\sigma \in (-\bar{m}_{\mathrm{f},0}/\bar{h}, +\bar{m}_{\mathrm{f},0}/\bar{h})$. However, as temperature is switched on infinitesimally, the degeneracy is immediately lifted and the effective potential obtains two minima. Expanding Eq. (5.14) at $\mu = 0$ in powers of σ, we find

$$U(\beta,\mu=0;\sigma) = \text{const.} - \frac{3}{2\pi\beta^3}\zeta(3) + \frac{\bar{h}^2\ln 2}{\pi}\left(\frac{1}{\beta}-\frac{1}{\beta_{\mathrm{c}}}\right)\sigma^2 + \beta\frac{\bar{h}^4}{16\pi}\sigma^4 - \beta^6\frac{\bar{h}^6}{576\pi}\sigma^6 + \ldots \tag{5.15}$$

We can immediately deduce const. $= \frac{3}{2\pi\beta^3}\zeta(3)$, which is nothing but $-\mathrm{Tr}\ln \mathrm{i}\partial\!\!\!/$ in three spacetime dimensions with antiperiodic boundary conditions in the time direction, and $\zeta(x)$ denotes the Riemann zeta function[5]. At the mean-field level, the effective potential at finite temperature is thus analytic and stable in the order parameter σ around the origin in field space. Since only even powers of σ appear it immediately follows that the effective potential as a function of the $\mathbb{Z}_2$ invariant $\bar{\rho}$ is also analytic at finite temperature. This is in contrast to the $T=0$ solution, where we observe a $\bar{\rho}^{3/2}$ dependence, see Chap. 4.

[4] The *full* effective potential should be convex in any case. The mean-field effective potential we consider here, however, does not have to fulfill this condition. Once bosonic fluctuations are taken into account, convexity will be restored.

[5] $\zeta(3) = 1.202057\ldots$, cf. Ref. [107]

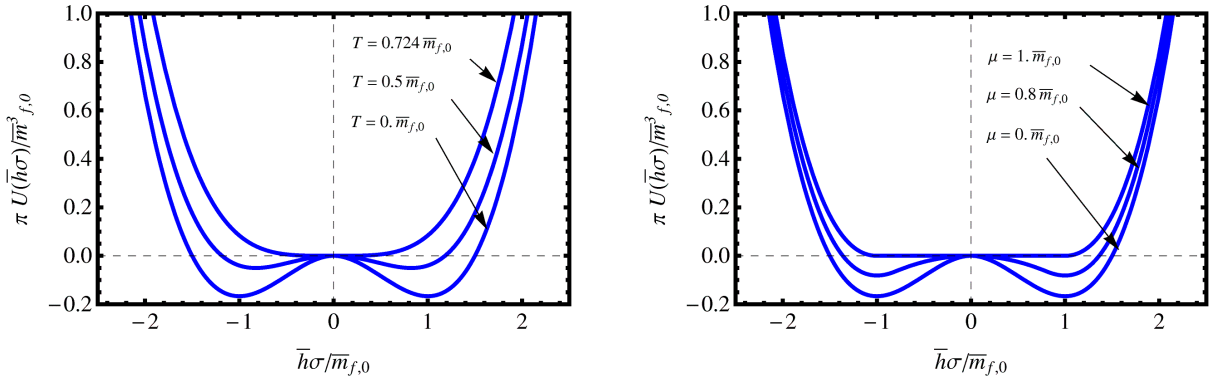

Figure 5.2: Left panel: plots of the bosonic effective potential Eq. (5.14) (as a function of $\bar{h}\sigma$) at mean-field level for $\mu = 0$ and different temperatures. Right panel: mean-field effective potential Eq. (5.14) at $T = 0$ for different values of the chemical potential. At $\mu = \bar{m}_{\mathrm{f},0}$ there appear infinitely many degenerate solutions in the interval $\sigma \in (-\bar{m}_{\mathrm{f},0}/\bar{h}, +\bar{m}_{\mathrm{f},0}/\bar{h})$. For any $T > 0$, this degeneracy is lifted. Increasing μ leads to a 1st order phase transition to the chirally symmetric phase.

Extracting Mean-Field Exponents

It is straightforward to extract the mean-field thermodynamic exponents[6] β and α from the gap equation Eq. (5.10) and the effective potential Eq. (5.14), Eq. (5.15). Adopting the usual conventions, the β-exponent measures the decay of the order parameter as the critical temperature is approached from $T < T_{\mathrm{c}}$, $\langle\sigma\rangle \propto |T_{\mathrm{c}} - T|^{\beta}$. The exponent α measures the corresponding singularity in the specific heat, $C \propto |T_{\mathrm{c}} - T|^{\alpha}$, where actually two exponents have to be defined for both sides of the transition, $T < T_{\mathrm{c}}$ or $T > T_{\mathrm{c}}$. The exponents defined to the left and right of T_{c} are indeed identical due to scaling relations. Expanding Eq. (5.10) close to $T_{\mathrm{c}}(\mu = 0)$ to second order in $\bar{m}_{\mathrm{f}}$, we obtain the relation [85]

$$\bar{m}_{\mathrm{f}} \simeq 2\sqrt{\bar{m}_{\mathrm{f},0}}\sqrt{T_c(\mu = 0) - T}, \tag{5.16}$$

from which we can read off $\beta = 1/2$. An analogous expansion for $\mu \neq 0$ suggests, that the thermodynamic exponents are not influenced by finite chemical potential. Plugging the above result into the formula for the effective potential $U(\beta, \mu = 0; \sigma)$, we arrive at the free energy $f(\beta, \mu = 0)$ per flavor species and unit area. Expanding the thermal contribution of $f(\beta, \mu = 0)$ to fourth order[7] in $\bar{m}_{\mathrm{f}}$ and differentiating twice with respect to temperature, the specific heat per unit area can be found as [85]

$$c = -T\frac{\partial^2}{\partial T^2} f(1/T, \mu = 0) \simeq \frac{8(\ln 2)^2}{\pi} T_{\mathrm{c}}^2(\mu = 0). \tag{5.17}$$

[6]Here, β should not be confused with the inverse absolute temperature. It should be clear from the context, whether the symbol β is referring to one or the other.

[7]Second and third order contributions in $\bar{m}_{\mathrm{f}}$ to the thermal part cancel against the vacuum part. First and fourth order both yield contributions $\propto (T_{\mathrm{c}}(\mu = 0) - T)^2$.

Since the free energy vanishes in the symmetric phase, this implies $\alpha = 0$, i.e., a jump in the specific heat across the transition.

The two correlation exponents ν and η_σ can be obtained from the bosonic propagator induced by the thermal fermion loop, cf. Chap. 4, Eq. (4.13)). Focusing on the ω_0-component for vanishing chemical potential, the inverse bosonic propagator in the broken phase ($T < T_\mathrm{c}$) reads [85]

$$\begin{aligned} & G_\sigma^{-1}(\omega_0, \boldsymbol{q})|_{T<T_\mathrm{c}} \\ &= \frac{d_\gamma}{16\pi}\bar{h}^2\left(\boldsymbol{q}^2 + 4\bar{m}_\mathrm{f}^2\right)\int_0^1 \mathrm{d}t \frac{1}{\sqrt{\boldsymbol{q}^2 t(1-t) + \bar{m}_\mathrm{f}^2}}\left[1 - 2n_F\left(\beta\sqrt{\boldsymbol{q}^2 t(1-t) + \bar{m}_\mathrm{f}^2}\right)\right] \\ &\simeq \frac{d_\gamma}{32\pi}\bar{h}^2\beta_\mathrm{c}\left(\boldsymbol{q}^2 + 4\bar{m}_\mathrm{f}^2\right) \end{aligned} \tag{5.18}$$

Where in the second step we approximated for $\beta\sqrt{\boldsymbol{q}^2 t(1-t) + \bar{m}_\mathrm{f}^2} \ll 1$. Identifying $\bar{m}_\sigma = 2\bar{m}_\mathrm{f} \propto \xi^{-1}$, where ξ is the correlation length, $\xi \propto |T_\mathrm{c} - T|^{-\nu}$, we can read off $\nu = \frac{1}{2}$. In the limit of chiral restoration $\bar{m}_\mathrm{f} \to 0$, we additionally find $\eta_\sigma = 0$. In the phase with restored chiral symmetry ($T > T_\mathrm{c}$), the propagator at ω_0 becomes [85]

$$\begin{aligned} G_\sigma^{-1}(\omega_0, \boldsymbol{q})|_{T>T_\mathrm{c}} &= 2\ln 2\left(\frac{1}{\beta} - \frac{1}{\beta_\mathrm{c}}\right) + G_\sigma^{-1}(\omega_0, \boldsymbol{q})|_{T<T_\mathrm{c}, \bar{m}_\mathrm{f}=0} \\ &\simeq 2\ln 2\,\bar{h}^2\left(\frac{1}{\beta} - \frac{1}{\beta_\mathrm{c}}\right) + \frac{d_\gamma}{32\pi}\bar{h}^2\beta_\mathrm{c}\,\boldsymbol{q}^2. \end{aligned} \tag{5.19}$$

Again we obtain $\nu = 1/2$. The anomalous dimension η_σ for the bosonic field vanishes, i.e., the IR region dominated by the Matsubara zero mode is described by a canonical, two-dimensional field. The exponents δ and γ, where δ describes the response of the order parameter to an external source and γ the divergence of the susceptibility with respect to the external source, were derived originally in [85] and also coincide with standard mean-field values. To conclude our review of the mean-field theory, we collect the Gross-Neveu mean-field exponents at finite temperature:

$$\alpha = 0,\ \beta = \frac{1}{2},\ \gamma = 1,\ \delta = 3,\ \nu = \frac{1}{2},\ \eta_\sigma = 0. \tag{5.20}$$

Note that these do *not* satisfy hyperscaling relations. We point out, that the above results fit our expectations. At finite temperature close to the phase transition, the fermionic theory is dimensionally reduced to a scalar O(1) model living in two space dimensions. Since bosonic fluctuations are completely suppressed by the infinite flavor number, mean-field exponents are observed for the finite-temperature melting of the chiral condensate. However, assuming continuity in N_f and invoking dimensional reduction and universality arguments, the finite temperature exponents should be independent of the number of fermion flavors. This in turn would suggest mean-field exponents Eq. (5.20) for all N_f. This clearly points us to an artifact of the $N_\mathrm{f} \to \infty$ limit. We will study this issue in Sec. 5.3, where we corroborate our view, that for finite flavor number at the finite temperature transition $2d$ Ising exponents should be observed.

5.2 Many-Flavor Phase Diagram

In the previous section we presented the mean-field phase diagram of the three-dimensional Gross-Neveu model at finite temperature and chemical potential. In the following, we will focus on finite temperature and a finite number of fermion flavors. Of course, this requires to go beyond the large-N_f approximation. Again, the functional renormalization group provides us with the means to study the phase diagram and the restoration of chiral symmetry for arbitrary flavor number. A detailed investigation at the full 1-loop level at finite temperature and chemical potential (in the presence of a source term) for $N_\mathrm{f} = 1$ can be found in [118–121]. A previous renormalization group study of the (T, μ)-phase diagram was obtained in [93]. However, the resolution in the (T, μ) plane was rather poor, possibly due to limited computational resources. Moreover, the employed proper-time flows do not follow from an exact equation. What appears to be missing in the already existing set of works on the Gross-Neveu phase diagram is a prediction for its many-flavor phase diagram, displaying critical temperatures as a function of the flavor number. Here we employ the functional renormalization group for the construction of a phase diagram in the (T, N_f)-plane. In order to compare theories with different flavor numbers, the bare parameters of each theory will be tuned, such that the dynamically generated fermion mass in the ground-state is equal for all N_f. At the end of this section, we will briefly comment on the full effective potential and the inclusion of a finite chemical potential into the flow equations presented here.

Finite Temperature Truncation

The starting point for our renormalization group calculation will be an ansatz for the effective average action of the form

$$\Gamma_k[\{\bar{\psi}_j\},\{\psi_j\},\sigma] \;=\; N_\mathrm{f}\int_x\left\{U_k(\sigma^2)+\frac{1}{2}Z_{\sigma,k}(\partial_\mu\sigma)^2\right\}+\int_x\sum_{j=1}^{N_\mathrm{f}}\left\{Z_{\psi,k}\bar{\psi}_j\mathrm{i}\partial\!\!\!/\psi_j+\mathrm{i}\bar{h}_k\bar{\psi}_j\sigma\psi_j\right\}, \tag{5.21}$$

and $\int_x \equiv \int_0^\beta \mathrm{d}\tau \int \mathrm{d}^{d-1}\boldsymbol{x}$ for finite temperature, as in the previous section. This truncation is of the same order in a derivative expansion as in Chap. 4 and thus a so-called LPA′-truncation, taking into account a running effective potential, anomalous dimensions and an nontrivially running Yukawa vertex.

Let us add a word of caution on the choice of the kinetic terms. In principle, due to the presence of a heat bath, the wave-function renormalizations should actually be split as $Z_{\sigma,k} \to (Z^{\parallel}_{\sigma,k}, Z^{\perp}_{\sigma,k})$ and $Z_{\psi,k} \to (Z^{\parallel}_{\psi,k}, Z^{\perp}_{\psi,k})$ multiplying the respective temporal ($\parallel$) and spatial ($\perp$) components. Such an analysis has been performed in [108], albeit with a dimensionally reduced regulator. Since a dimensionally reduced regulator breaks Lorentz symmetry already at high scales, the initial conditions have to be tuned carefully to restore Lorentz symmetry at $T = 0$ for $k \to k_\mathrm{IR}$. Here, we make

an isotropic approximation $Z_{\sigma,k} \equiv Z^{\parallel}_{\sigma,k} = Z^{\perp}_{\sigma,k}$ and $Z_{\psi,k} \equiv Z^{\parallel}_{\psi,k} = Z^{\perp}_{\psi,k}$, additionally employing a fully covariant regulator, not to spoil Lorentz invariance at the UV scale. The wave-function renormalizations $Z_{\sigma,k}$ and $Z_{\psi,k}$ are then obtained by projecting onto the spatial components, avoiding technicalities due to the discrete nature of Matsubara frequencies.

Since $\Gamma_k[\{\bar{\psi}_j\}, \{\psi_j\}, \sigma]$ captures finite-temperature effects, the vertex functions will of course also acquire a temperature dependence. To keep the notation clear, we do not write out the dependence on T explicitly. With the usual projection rules for the effective potential and the Yukawa vertex given in Appendix A.4, we can obtain the flow equations for the dimensionless renormalized quantities $u_k(\rho)$, h_k and the anomalous dimensions $\eta_{\sigma,k}$, $\eta_{\psi,k}$. Note, that in a consistent gradient expansion [108], both bosonic and fermionic propagators happen to be evaluated at the Matsubara frequencies of the opposite statistics in some regularized diagrams.

The diagrammatic representation of the beta functions is the same as displayed in Fig. 4.5. Since the prime interest here lies in the investigation of restoration of chiral symmetry, the flow needs to be continued into the broken regime. Formally, the flow equations are the same as in Eqs. (4.44)-(4.46) if we take into account the additional dependence of threshold functions on the dimensionless temperature parameter[8] $\tau = \frac{2\pi T}{k}$. The corresponding threshold functions for covariant regulators [48] can be found in Appendix A.6.

The covariant optimized regulators lead to flat propagators, i.e., momentum derivatives of a propagator function vanish. They also come with a further nice property: the finite temperature and vacuum parts factorize. By the presence of the additional scale set by temperature T, the evaluation of the corresponding 1-loop integrals is a bit more complicated than in the $T = 0$ case. We succeeded, however, in obtaining closed expressions for all but one threshold function. Dealing with this last threshold function requires an approximation in terms of a Bessel function expansion in the bosonic anomalous dimension. We have checked numerically, that the results for the dynamically generated fermion mass with the full threshold function and for our approximation yield a relative error of 10^{-5}. This gives us confidence in our approximation and drastically reduces computational time. For further technical details, we refer to Appendix A.6.

Numerical Results for the Many-Flavor Phase-Diagram

The evaluation of the flow equations is performed with a UV cutoff[9] $\Lambda = 100\,\text{a.u.}$ in a $\sigma^4 \propto \rho^2$ truncation. The stopping scale for the flow is as in Sect. 4.4 chosen as $t_{\text{IR}} = -10$. The initial Yukawa vertex is kept at $h_\Lambda = 18.0$, to ensure compositeness. The bosonic mass is then tuned to ensure a value $\bar{m}_{\text{f},0} \simeq 1\,\text{a.u.}$ for a specified flavor number. Further, we performed the same computations also for initial conditions $h_\Lambda = 6.0$ and a bare boson mass tuned to yield $\bar{m}_{\text{f},0} \simeq 5\,\text{a.u.}$. In all cases the initial conditions are close to the critical manifold.

[8] Not to be confused with the imaginary time variable.

[9] As mentioned in Chap. 4, we give numerical values of quantities with mass dimension 1 in "arbitrary units" (a.u.). To convert to "physical" units, we express dimensionful quantities with respect to the dynamically generated fermion mass at $T = 0$.

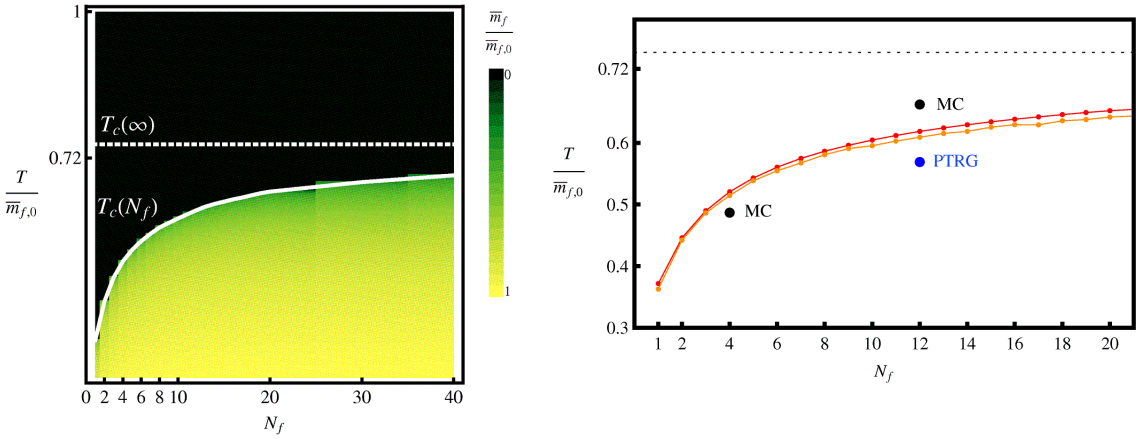

Figure 5.3: Left panel: the Gross-Neveu many-flavor phase diagram as obtained in a $\sigma^4 \propto \rho^2$ truncation. For each scan along the temperature axis in the range $T \in (0\,\text{a.u.}, 0.8\,\text{a.u.}]$ with 185 data points, we tuned the initial value of the dimensionless renormalized mass such that at $T = 0$ we obtain a fermion mass $\bar{m}_{\text{f},0} \simeq 1\,\text{a.u.}$. The Yukawa coupling is fixed to $h_\Lambda = 18.0$. From our numerical evaluation of the large-N_f flow equations at finite temperature, we obtain $T_\text{c}(\infty)/\bar{m}_{\text{f},0}(\infty) = 0.7439$ (dashed white). The color code gives the size of the normalized fermion mass. The phase boundary (white) is obtained by linear interpolation. We performed temperature scans for flavors $N_\text{f} = 1, 2, 3, \ldots, 19$ and $N_\text{f} = 20, 30, \ldots, 100$ (only results up to $N_\text{f} = 40$ are shown). Right panel: the phase boundary obtained from our flow equations (red corresponding to $\bar{m}_{\text{f},0} \simeq 1\,\text{a.u.}$ and $h_\Lambda = 18.0$ and orange to $\bar{m}_{\text{f},0} \simeq 5\,\text{a.u.}$ and $h_\Lambda = 6.0$) compared to available results from proper-time renormalization group (PTRG, $N_\text{f} = 12$) [93] and Monte Carlo simulations (MC, $N_\text{f} = 4$, 12) [122, 123] .

All dimensionful quantities are expressed with respect to the dynamically generated fermion mass $\bar{m}_{\text{f},0}$ at $T = 0$. This renders the different flavor realizations comparable with respect to their critical temperatures. Moreover, therein lingers the particular aspect of universality in the many-flavor phase diagram. As mentioned in the previous section, the Gross-Neveu field theory depends only on a single parameter. Though temperature defines a further scale, the critical temperature can only depend on the tuple $(N_\text{f}, \bar{m}_{\text{f},0}(N_\text{f}))$, where we made the flavor dependence explicit. As illustrated by the finite-temperature mean-field result, for dimensional reasons, $T_\text{c}(N_\text{f}, \bar{m}_{\text{f},0}(N_\text{f})) \propto \bar{m}_{\text{f},0}(N_\text{f})$, such that the ratio $T_\text{c}(N_\text{f}, \bar{m}_{\text{f},0}(N_\text{f}))/\bar{m}_{\text{f},0}(N_\text{f})$ actually is a function of N_f only. This argument can only be modified by irrelevant operators, allowing the cutoff scale Λ to "creep" back into the finite temperature solution. With our initial conditions tuned close to the critical manifold, however, we expect the Λ dependence to be negligible.

To obtain $T_c(N_f)$ for fixed N_f, we scan along the temperature axis with a resolution of 185 data points in the (unscaled) intervals $T \in (0\,\text{a.u.}, 0.8\,\text{a.u.}]$ and $T \in (0\,\text{a.u.}, 4.0\,\text{a.u.}]$ for the two sets of initial conditions. While the initial conditions are tuned to enter the broken regime at $T = 0$, for increasing temperature the value of the chiral condensate is diminished and eventually the flow will not enter the broken regime any longer. We identify the first flow where the system does not end in the broken regime with the critical temperature $T_c(N_f)$.

The numerical effort is rather small. We could easily increase the numerical precision of our results. However, since in the large-N_f limit we find $T_c(\infty)/\bar{m}_{f,0}(\infty) = 0.7439$ with the first set of initial conditions, with the exact result being $T_c(\infty)/\bar{m}_{f,0}(\infty) = 0.7213$, we obtain a relative deviation of $\sim 3\%$ within our truncation. Due to this error resulting from a combination of truncation and possibly small numerical errors a higher level of numerical precision seems less important at the current level of our truncation. We assume that this error check in the limit $N_f \to \infty$ is also indicative for the error size finite N_f.

Performing this procedure for $N_f = 1, 2, 3, \ldots, 19$ and $N_f = 20, 30, 40, \ldots, 100$, we obtain the many-flavor phase diagram displayed in Fig. 5.3. The phase boundary for $N_f = 20, \ldots, 100$ is well described by a simple fit in $1/N_f$ to the large-N_f tail,

$$T_c(N_f)/\bar{m}_{f,0}(N_f) \simeq 0.72686 - 1.55098/N_f. \tag{5.22}$$

By fitting the values for $N_f = 1, \ldots, 19$ the small N_f region with $N_f = 2, \ldots, 19$ can be described rather well by

$$T_c(N_f)/\bar{m}_{f,0}(N_f) \simeq 0.695994 - 1.11289/N_f + 2.18236/N_f^2 - 2.43492/N_f^3 + 1.04127/N_f^4. \tag{5.23}$$

The fits to our data are shown in Fig. 5.4.

The number of available results for $T_c(N_f)/\bar{m}_{f,0}(N_f)$ in the literature is rather small. In Tab. 5.1 and Fig. 5.3 (right panel), we compare our phase boundary (FRG results) to proper-time flows (PTRG) [93] (which do *not* follow from a formally exact flow equation) and predictions from Monte Carlo simulations (MC) [122, 123]. Obviously, there is still room for improvement, especially in view of comparing the predictions from different nonperturbative methods for the phase boundary. Our results differ from MC and PTRG results by $6\% - 8\%$, which is a quite sizable deviation. A systematic discussion of the deviation to the MC results with respect to finite size effects and other lattice artifacts seems not possible at the moment. We expect improvements on the FRG side by including higher bosonic self-interactions. Further, we did not perform a regulator study, probing the scheme dependence of our results. In extending our truncations, however, we meet an as yet unresolved technical obstruction to be discussed in the following.

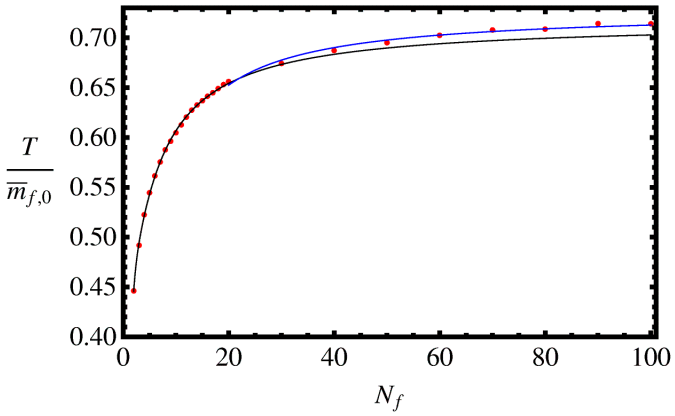

Figure 5.4: Plot of our data (red points) and the fits Eq. (5.23) (black curve) for $N_\mathrm{f} = 1, \ldots, 19$ and Eq. (5.22) (blue curve) for $N_\mathrm{f} = 20, 30, 40, \ldots, 100$. The large-$N_\mathrm{f}$ behavior can be well described by a $1/N_\mathrm{f}$ tail, while for small flavor numbers, sizeable corrections in powers of $1/N_\mathrm{f}$ appear.

	$N_\mathrm{f} = 4$ (MC) [123]	$N_\mathrm{f} = 4$ (FRG) [33]	$N_\mathrm{f} = 12$ (MC) [122]	$N_\mathrm{f} = 12$ (PTRG) [93]	$N_\mathrm{f} = 12$ (FRG) [33]
$\frac{T_\mathrm{c}(N_\mathrm{f})}{\bar{m}_{\mathrm{f},0}(N_\mathrm{f})}$	0.4868	0.5225	0.6622	0.5689	0.6204

Table 5.1: Comparison of our results (FRG) [33] for $T_\mathrm{c}(N_\mathrm{f})$ values to proper-time renormalization group flows (PTRG) [93] and Monte Carlo simulations (MC) [122, 123].

Failure of σ^6 and Higher Truncations and LPA

We have restricted our previously discussed analysis of the Gross-Neveu many-flavor phase diagram to a σ^4 truncation. For higher bosonic self-interactions included in the flow, we observe that at some temperature below $T_\mathrm{c}(N_\mathrm{f})$, the flow develops certain pathologies that finally keep us from integrating the flow in a sensible manner toward the IR. We scrutinized the different contributions to the flow – especially for the flow of the σ^6 vertex itself. It appears, that for a certain temperature contributions, which cancel each other almost exactly during the well behaved part of the flow, suddenly start deviating drastically from each other at a pathological scale. This leads to an uncontrolled increase in the σ^6 vertex which entails further artifacts, like quantizing η_σ dynamically to the value 4 which in turn leads to zeroes in threshold functions. We suspect, that only a *full* solution of the effective potential in an LPA′ truncation can resolve this issue and lead to a well behaved flow beyond σ^4 truncations. A higher order polynomial truncation is probably not capable of treating the change from $T = 0$ to $T > 0$ behavior in the effective potential. Similar observations were made for a model with global U($2N_\mathrm{f}$) symmetry [124] .

Moreover, the importance of going beyond LPA type truncations was already pointed out in Chap. 4. The main problem in three spacetime dimension arises from the fact that induced bosonic propagators do not behave canonically as long as the fermions circulating in the corresponding loop diagram are massless and thus strongly modify the IR behavior of the propagator. Since also the flow at finite temperature is initialized in the UV region of the model to ensure compositeness of the

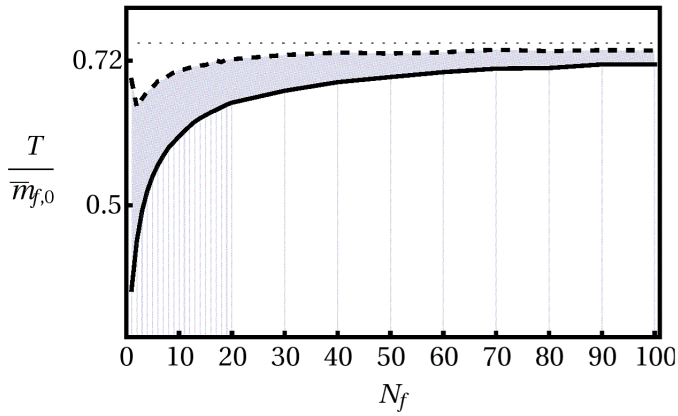

Figure 5.5: The shaded region corresponds to the temperature range $T_c(N_f) < T < T^*(N_f)$ where the flow enters the broken regime, but then flows out of it again. We interpret this region as short-ranged order. Interestingly, the $N_f = 1$ Gross-Neveu system shows an enlarged temperature range as compared to flavor realizations with $N_f > 1$.

bosonic field at high scales, the anomalous dimension $\eta_{\sigma,k}$ is a necessary ingredient to dynamically describe the "canonicalization" of the bosonic propagator, as the system evolves along a given renormalization group trajectory into the broken regime of the flow. A pure LPA level truncation would only be capable of describing a Gaußian fixed point – it thus contains more IR parameters than the Gross-Neveu universality class in three spacetime dimensions, cf. Chap. 4.

Short-Ranged Order for $T > T_c$

For a scan along the temperature axis, the first flow which does not end in the broken phase gives us a value for $T_c(N_f)$. But slightly increasing absolute temperature T, we observe that the flow again enters the broken regime, and only eventually re-enters the symmetric regime in the limit $k \to 0$. Further increasing the temperature above a certain value $T^*(N_f)$, the flow never enters the broken regime. As was done in [108] we identify this regime $T_c(N_f) < T < T^*(N_f)$ with short-ranged order in the system. We extract $T^*(N_f)$ from the flows, which makes it necessary to treat a flow starting in the symmetric, entering the broken and finally re-entering the symmetric regime. Our results for $T^*(N_f)$ are depicted in Fig. 5.5. $T^*(N_f)$ is bounded from above by the large-N_f result for the critical temperature. Interestingly, the $N_f = 1$ system shows an increase in the width of the region with short-ranged order as compared to the $N_f > 1$ systems. The flavor dependence of the region $T_c(N_f) < T < T^*(N_f)$ can be understood as coming from a competition between the (now only thermally gapped) fermionic fields and the massive bosonic fluctuations.

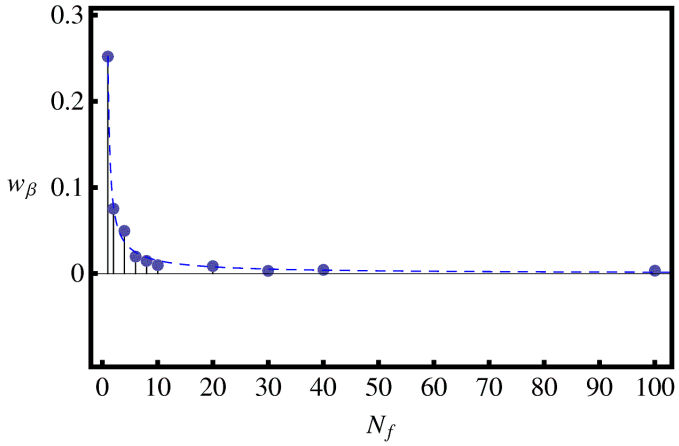

Figure 5.6: Plot of the width $w_\beta(N_\mathrm{f})$ of the Ginzburg region close to the finite temperature phase transition whereby chiral symmetry is restored as a function of flavor number N_f. Within the Ginzburg region, $2d$ Ising scaling can be observed. The Ginzburg region is suppressed as $\propto N_\mathrm{f}^{-1.4557}$ (dashed blue) with increasing number of fermion flavors.

5.3 Ising-Scaling and Ginzburg Region

In Sect. 5.1 we reproduced the Gross-Neveu phase diagram in three spacetime dimensions at finite temperature at mean-field level. The thermodynamic mean-field solution together with the induced large-N_f propagator of the bosonic fluctuations lead us to mean-field exponents for the finite temperature transition. We also argued, that invoking universality arguments and dimensional reduction in conjunction with analyticity of the Gross-Neveu model in flavor number N_f seems to suggest that mean-field exponents should also be observed at any finite N_f. This, however, turns out to be an artifact of the large-N_f limit. It is, per se, not a contradiction to the analyticity in N_f of the finite temperature critical exponents. Rather [126], the region where O(1), i.e., $2d$ Ising exponents can be observed – the so-called *Ginzburg region* – comes with a flavor dependence and is suppressed to zero in the large-N_f limit. As argued in [126], a crossover in scaling behavior from mean-field to Ising exponents should occur as $T_\mathrm{c}(N_\mathrm{f})$ is approached for fixed N_f.

With the flow equations used in Sect. 5.2 to study the many-flavor phase diagram, we now extract the β exponent, describing the decrease of the order parameter as the temperature tends to $T_\mathrm{c}(N_\mathrm{f})$ from below,

$$\langle\sigma\rangle \propto |T - T_\mathrm{c}|^\beta. \tag{5.24}$$

The flow equations describe the "evolution" of the Gross-Neveu model over a dynamically generated Yukawa theory with a noncanonical boson to a canonical Yukawa system, which is finally dimensionally reduced to an O(1) model by the presence of the heat bath. Since we are restricted to a

σ^4 truncation, we cannot expect to find exact $2d$ Ising exponents as following from Onsager's solution [127]. Rather, we extract critical exponents directly from a $2d$ O(1) theory in a σ^4 truncation. We find

$$\nu = 0.4007, \quad \eta_{\sigma,*} = 0.4648. \tag{5.25}$$

With hyperscaling relations – valid for the Ising model in two dimensions –, we obtain $\beta = 0.0931$. Next, we perform a two-parameter fit to our numerical data obtained from the full Gross-Neveu flow equations at finite temperature for fixed N_f over a selected temperature range of the form $A\,\mathrm{e}^{B\ln\langle\sigma\rangle}$. By varying the lower end of the temperature interval, we select the data range to be subsequently fitted by a one-parameter fit when $B \simeq \beta$. Using a one-parameter fit of the form $A\,\mathrm{e}^{\beta\ln\langle\sigma\rangle}$ in the preselected region with the O(1) value of β, we define the size of the Ginzburg region by requiring the relative deviation of the one-parameter fit from the numerical data to be less than 2%. The corresponding temperature is denoted by $T_\mathrm{G}(N_\mathrm{f})$. We thus obtain the width

$$w_\beta(N_\mathrm{f}) \equiv \left| \frac{T_\mathrm{G}(N_\mathrm{f}) - T_\mathrm{c}(N_\mathrm{f})}{T_\mathrm{c}(N_\mathrm{f})} \right| \tag{5.26}$$

of the Ginzburg region as defined by the scaling window where β can be observed. The results of our computations are displayed in Fig. 5.6. As already mentioned w_β decreases with increasing flavor number N_f. Fitting our data for w_β with $C\,\mathrm{e}^{-x\ln N_\mathrm{f}}$, we obtain $x = 1.4557$ and $C = 0.249$. This result agrees nicely with the findings[10] in [126], where both an analytic estimate ($x = 3/2$) and Monte Carlo simulations ($x = 1.51$) were used to quantitatively describe the suppression of the Ginzburg region with flavor number.

Ref. [126] further provides us with a definition of the so-called *classical regime*, which also sets the scale for dimensional reduction ($d \to d-1$) in the broken phase. It begins where the renormalized boson mass equals temperature, $\bar{m} = T^\mathrm{cl}$. In this region, only the bosonic Matsubara zero mode contributes significantly to the flow. We computed the width of the classical region below $T_\mathrm{c}(N_\mathrm{f})$, see Fig. 5.7. The width of the classical region (below $T_\mathrm{c}(N_\mathrm{f})$) can be seen to be roughly constant, although for small flavor numbers, the classical regime is reached already for lower temperatures.

5.4 Challenges and Open Questions

To conclude this chapter on the finite temperature phase diagram of the three-dimensional Gross-Neveu model, we comment on solutions for the full effective potential and the steps that would be necessary to extend these beyond LPA type truncations. Further we briefly list problems with

[10] It is important to note that the bosonic action in [126] is defined differently by a factor of N_f from ours. Taking this factor into account for the flavor dependence of $w_\beta(N_\mathrm{f})$, our results agree with those obtained in [126].

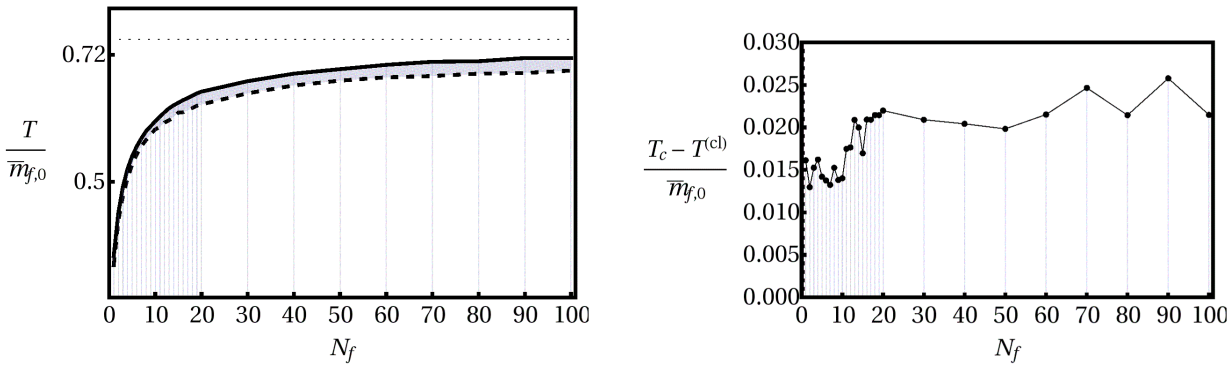

Figure 5.7: Left panel: plot of the classical regime (dashed black) below the phase boundary in the many-flavor phase diagram. The critical region begins where the renormalized thermal mass of the bosonic fluctuations equals temperature, $\bar{m} = T^{\mathrm{cl}}$. The physics in this region is dominated by the bosonic Matsubara zero mode. Right panel: size of the classical regime below the phase boundary as a function of flavor number. The classical regime is roughly constant. The small flavor region features slightly smaller classical regimes.

known regulators in handling a finite chemical potential for $d = 3$. At present, a regulator that can efficiently include a finite chemical potential for Gross-Neveu-type theories is not known.

Comments on the Full Effective Potential

A few comments are in order to briefly point out the difficulties arising from a treatment of the *full* effective potential Eq. (4.44). While this could in principle cure issues arising from possibly nonpolynomial effective potentials (in ρ), the emerging coupled system of a partial differential equation (PDE) in the renormalization group scale k and the invariant ρ for the function $u_k(\rho)$ and the ordinary differential equation (ODE) for the Yukawa coupling h_k augmented with the anomalous dimensions $\eta_{\sigma,k}$ and $\eta_{\psi,k}$ evaluated at the absolute minimum of the effective potential $u_k(\rho)$ is not amenable to standard solvers for differential equations[11]. While an iterative treatment seems possible with standard solvers, this procedure has turned out to be quite unstable and very sensitive to the numerical parameters used for solving the PDE. The basic idea is to first solve for the effective potential for fixed Yukawa coupling and anomalous dimensions, determine the trajectory of the minimum, and then solve the ODE in the background of the previously determined trajectory. These renormalization group flows are inserted back into the PDE and the iteration starts over again until observables converge to stable IR values. In this way, for flows at zero temperature, we could achieve up to three iterations. In the fourth iteration, the solver could not sensibly integrate the flow toward the IR. No signatures of convergence were seen after only three iterations and we thus did not employ this scheme for a full analysis of the phase diagram.

[11] For example, within Mathematica [35], this type of differential equation is of "delayed" type. However, up to the current version used for evaluating numerical problems, this type was not implemented and could thus not be dealt with easily.

Therefore a solution to this problem would have required to develop new numerical routines, which is beyond the scope of the present work. In principle, however, the task seems rather clear. It remains to formulate a PDE+ODE solver with suitable boundary conditions. Then, solutions for the full effective potential could be obtained in LPA′ truncations.

Nevertheless, with the present method it has still been possible to solve the PDE for $U_k(\bar{\rho})$ with fixed Yukawa coupling, $\bar{h}_k \equiv \bar{h}$ and $Z_{\psi,k} = Z_{\sigma,k} \equiv 1$ in a standard LPA truncation. This is done by evaluating the PDE with the Mathematica standard solver (see Appendix B.2 for details) on the domain $[0, \bar{\rho}_{\max}] \times [k_{\mathrm{IR}}, \Lambda]$, where $\bar{\rho}_{\max}$ is the largest value of the (dimensionful) invariant $\bar{\rho}$ that is kept in the solution. The flow is stopped at the infrared scale k_{IR}, where the dimensionful effective potential is "frozen out". Here, a dimensionally reduced Litim regulator has been used:

$$R_{B,k}(\boldsymbol{p}) = \boldsymbol{p}^2 \left(\frac{k^2}{\boldsymbol{p}^2} - 1\right) \Theta(k^2 - \boldsymbol{p}^2), \tag{5.27}$$

$$R^+_{F,k}(\boldsymbol{p}) = -\boldsymbol{\gamma}\cdot\boldsymbol{p} \left(\sqrt{\frac{k^2}{\boldsymbol{p}^2}} - 1\right) \Theta(k^2 - \boldsymbol{p}^2). \tag{5.28}$$

The resulting PDE reads

$$\partial_k U_k(\bar{\rho}) = \frac{k^3}{2\pi}\left(\frac{1}{2N_{\mathrm{f}}E_{B,k}}\left[n_B(E_{B,k}) + \frac{1}{2}\right] - \frac{1}{E_{F,k}}\left[1 - n_F(E_{F,k} - \mu) - n_F(E_{F,k} + \mu)\right]\right), \tag{5.29}$$

where $E_{B,k} = \sqrt{k^2 + U_k'(\bar{\rho}) + 2\bar{\rho}U_k''(\bar{\rho})}$, $E_{F,k} = \sqrt{k^2 + 2\bar{h}_k^2\bar{\rho}}$ and

$$n_B(z) = \frac{1}{\mathrm{e}^{\beta z} - 1} \tag{5.30}$$

is the Bose-Einstein distribution function. The initial condition at $k = \Lambda$ is provided by $U_{k=\Lambda}(\bar{\rho}) = \bar{m}^2_{k=\Lambda}\bar{\rho}$, and the boundary condition at $\bar{\rho} = \bar{\rho}_{\max}$ is given by the scale-dependent mean-field potential, which can be obtained in closed form by integrating Eq. (5.29) in the limit $N_{\mathrm{f}} \to \infty$:

$$\begin{aligned}\lim_{N_{\mathrm{f}}\to\infty} U_k\left(\bar{\rho} = \frac{1}{2}\sigma^2\right) = \frac{1}{2\pi}\Bigg[&\frac{E^2_{F,k'} - \bar{h}^2\sigma^2}{\beta}\left\{\mathrm{Li}_1\left(-\mathrm{e}^{-\beta(E_{F,k'}-\mu)}\right) + \mathrm{Li}_1\left(-\mathrm{e}^{-\beta(E_{F,k'}+\mu)}\right)\right\} \\ &+\frac{2E_{F,k'}}{\beta^2}\left\{\mathrm{Li}_2\left(-\mathrm{e}^{-\beta(E_{F,k'}-\mu)}\right) + \mathrm{Li}_2\left(-\mathrm{e}^{-\beta(E_{F,k'}+\mu)}\right)\right\} \\ &+\frac{2}{\beta^3}\left\{\mathrm{Li}_3\left(-\mathrm{e}^{-\beta(E_{F,k'}-\mu)}\right) + \mathrm{Li}_3\left(-\mathrm{e}^{-\beta(E_{F,k'}+\mu)}\right)\right\} \\ &-\left(\frac{1}{3}E^3_{F,k'} - \bar{h}^2\sigma^2 E_{F,k'}\right)\Bigg]\Bigg|^{k'=k}_{k'=\Lambda} + \frac{\bar{h}^2}{2\bar{g}}\sigma^2 + \text{const.}.\end{aligned} \tag{5.31}$$

This effective potential reproduces the phase diagram presented in Sec. 5.1 for suitably chosen parameters. Note that although $Z_{\sigma,k}$ receives contributions to leading order in $1/N_{\mathrm{f}}$, for the di-

mensionful potential as a function of the dimensionful unrenormalized variable $\bar{\rho}$, the flows for potential and wave-function renormalization decouple in the large-N_f limit. Unfortunately, the flow equation Eq. (5.29) is plagued by severe regularization artifacts. In fact, for generic initial conditions that will induce symmetry breaking during the flow, shortly below the critical scale the off-shell energies $E_{B,k} = \sqrt{k^2 + U_k'(\bar{\rho}) + 2\bar{\rho}U_k''(\bar{\rho})}$ cross zero and will eventually turn imaginary for $k^2 + U_k'(\bar{\rho}) + 2\bar{\rho}U_k''(\bar{\rho}) < 0$ with $\bar{\rho}$ taking values in a range which is typically close to, but below the position of the flowing minimum. Similar observations were reported in [125]. By tedious parameter scans, the scale where this pathology occurs can be suppressed further toward the infrared. Still, by tuning the bare boson mass, it could never be removed completely from the flow. In face of the failure of pure LPA truncations in describing Gross-Neveu universality in $d = 3$, we did not pursue this route any further.

Note on Inclusion of Finite Chemical Potentials

In writing Eq. (5.29), we made use of the fact that Matsubara sums can be performed exactly with a dimensionally reduced regulator of the form given in Eq. (5.27), which allows for the inclusion of a finite chemical potential μ. Unfortunately, this regulator yields a well-defined set of flow equations strictly at the LPA level only. Upon inclusion of the bosonic anomalous dimension $\eta_{\sigma,k}$ – as pointed out several times, an essential ingredient to capture Gross-Neveu universality – the flow equations are no longer well defined. The bosonic anomalous dimension behaves as $\frac{1}{d-3}$ [108], so in $d = 3$ the system directly sits on a pole. In a sense, the dimensionally reduced regulator shifts around upper and lower critical dimensions, defying an analysis of Gross-Neveu-like models in three spacetime dimensions with such a dimensionally reduced regulator. As an alternative one might consider a covariant regulator as used in the construction of the many-flavor phase diagram above. The chemical potential, however, enters into the threshold functions as an imaginary argument in a Heaviside step function, cf. Appendix A.6. These expressions are obviously ill-defined and yield divergent Matsubara sums after shifting integration variables. Since the Heaviside function does not have a unique extension to complex arguments, a formally imaginary chemical potential which is continued back to real chemical potential at a suitable step in the computation of the threshold functions cannot remedy the situation. This was checked for the large-N_f limit, where the mean-field phase diagram at finite chemical potential is known. In Ref. [41], a Callan-Symanzik-like regulator was employed to study the 4-dimensional quark-meson model. However, due to the presence of an additional parameter and the nonanalyticity of the Heaviside function we expect similar problems to occur in this approach. A strict Callan-Symanzik regulator at $\mu > 0$ leads to expressions containing square roots of complex arguments. This can, however, be removed by appropriately altering the shape function. The price to be paid is that an evaluation of the resulting mixed bosonic and fermionic 1-loop diagrams turns very tedious and propagator functions are no longer flat, making the evaluation of anomalous dimensions quite laborious. The completion of deriving Gross-Neveu flow equations at finite μ is left for future work.

Chapter 6

Magnetic Catalysis in the Gross-Neveu Model

Remarkably, when interacting planar Dirac fermions are subject to an external perpendicular magnetic field, symmetry breaking accompanied by the generation of a mass gap for the fermionic degrees of freedom occurs for all finite values of the interaction strength [128]. Indeed, this effect known by the name of *magnetic catalysis* is not particular to models defined in three spacetime dimensions, but has also been investigated in four dimensional quantum field theories [129, 130]. However, what is special about three spacetime dimensions is the fact that even in the absence of interactions a finite value of the chiral condensate is generated by applying an external magnetic field [128]. So also for a free system the (continuous) chiral symmetry is spontaneously broken. This phenomenon is sometimes referred to as a "quantum anomaly" [131], since it unexpectedly leads to the generation of a nonvanishing expectation value for a certain operator. For condensed matter model systems, possible applications of this effect have been studied for a variety of low-dimensional physical realizations, ranging from magnetic field induced insulating behavior in semi-metallic structures [132, 133] to anomalous Hall plateaus in graphene [131, 134–137] and transport properties in d-wave superconductors [138–140].

The interplay between strong magnetic fields and chiral symmetry breaking has also become of topical relevance in particle physics. For instance, noncentral heavy-ion collisions go along with extreme magnetic fields [144] that may even interfere with the topological structure of the QCD vacuum [145, 146] or simply take a parametric influence on the chiral phases of QCD [151–156]. Even though magnetic fields in strongly interacting fermionic systems generically support the formation of a chiral condensate at least in mean-field-type approximations, further interactions such as gluonic back-reactions may also lead to inverse effects [157].

There exist already a few works in the literature on the large-N_f results for the Gross-Neveu model [158–161]. Beyond leading-order results in a $1/N_\mathrm{f}$-expansion, magnetic catalysis has been studied both with truncated Dyson-Schwinger equations (in $d = 3$ [129, 162] and $d = 4$ [129, 163, 164]) and Wilson-style renormalization group equations (in $d = 4$ [150, 165, 166]) in the context

of fermionic models with short-ranged interactions and QED. However, a clear renormalization group picture in terms of a fixed-point analysis of the beta function appears to be still missing. Moreover, the inclusion of purely magnetically induced operators in the renormalization group flow and their effect on the running coupling has not been considered so far. In the following, we provide a clear renormalization mechanism for magnetic catalysis in the Gross-Neveu model by means of the functional renormalization group. Similar observations have been made in a renormalization group study of magnetic catalysis in a QCD low-energy model [167]. Moreover, we identify terms that are compatible with the symmetries of the Gross-Neveu action in the presence of an external magnetic field. In principle, all operators compatible with the symmetries of the initial action can be generated under renormalization group transformations. Therefore, our analysis addresses the question, whether the operator content of fermionic effective actions is modified in the IR by the very presence of such gauge backgrounds.

With Sect. 6.1 our analysis begins with the free chirally symmetric many-flavor Dirac Lagrangian in three spacetime dimensions in the presence of magnetic background. We briefly recapitulate the Landau level structure of the free mode solutions, and discuss the observed pattern of dimensional reduction by means of the full gauge-variant fermionic propagator. This will also allow us to directly access the "quantum anomaly" featured in this model. Building on the definition of the three dimensional, chirally symmetric Gross-Neveu model in an external magnetic field given in Sect. 3.1 and the results from Sect. 3.2 and Sect. 3.3, where we collected the transformation rules under both discrete symmetry and chiral transformations and studied the Gross-Neveu theory space, in Sect. 6.2 we present a derivation of the beta function for the four-fermi coupling in the pointlike limit. Importantly, it is shown that although a magnetic field spoils translation invariance, i.e., conservation of momentum, a consistent gradient expansion can nevertheless be formulated. We then discuss the effect of the magnetic field on the behavior of the beta function for the fermionic coupling in the pointlike approximation in a qualitative manner, while a quantitative discussion of the field dependence of the dynamically generated fermion mass inferred from the beta function is deferred to Sect. 6.3. We will show how a covariantly regularized propagator suitable for renormalization group studies can be obtained and take special care in defining vertex functions for a partially bosonized formulation in Appendix A.9, laying ground for the inclusion of collective neutral excitations.

6.1 Dirac Fermions in Abelian Gauge Background

We shall briefly review the most important properties and aspects of planar Dirac fermions propagating in the presence of a perpendicular magnetic field. This will provide us with the necessary ingredients for setting up a renormalization group equation in a language adapted to the problem at hand.

Landau Level Spectrum

The many-flavor Dirac Langragian without self-interactions is simply given by

$$\mathcal{L} = \sum_{j=1}^{N_\mathrm{f}} \bar{\psi}_j \mathrm{i}\not{D}[\mathcal{A}]\, \psi_j. \tag{6.1}$$

We chose the vector potential in the gauge

$$\mathcal{A}(x) = (0, 0, x_1 B)^T. \tag{6.2}$$

Within the three-dimensional formulation the magnetic field appears as a pseudo-scalar quantity. This corresponds to the fact that the magnetic flux associated to a magnetic field that is aligned perpendicularly to the (x_1, x_2)-plane can pierce this plane with two different orientations. As already pointed out in Sect. 3.2, this Lagrangian features a global $\mathrm{U}(2N_\mathrm{f})$ symmetry, stemming from both chiral and unitary flavor symmetry. The Landau level spectrum of Eq. (6.1) is easily obtained from the square of the operator $\mathrm{i}\not{D}[\mathcal{A}]$. With the conventions in Sect. 3.1, the squared Dirac operator can be written as

$$\begin{aligned} (\mathrm{i}\not{D}[\mathcal{A}])^2 &= -\left(D[\mathcal{A}]^2 \mathbb{1}_4 - \frac{q}{2}\sigma_{\mu\nu}\mathcal{F}_{\mu\nu}\right) \\ &= -\left(D[\mathcal{A}]^2\, \tau_0 \otimes \tau_0 + qB\, \tau_0 \otimes \tau_3\right), \end{aligned} \tag{6.3}$$

where $D[\mathcal{A}]^2$ is the covariant Laplacian. The spectrum of the squared Dirac operator in a perpendicular magnetic field is thus found to be given by the set

$$\left\{p_0^2 + \epsilon_n^2 + \tau q B \,|\, p_0 \in \mathbb{R}, n \in \mathbb{N}, \tau = \pm 1\right\}. \tag{6.4}$$

Here, $\epsilon_n^2 = qB(2n+1)$ (for notational convenience, in the following we will assume $qB > 0$) corresponds to Landau level energies and n is the associated Landau level index. The quantum number τ will be referred to as spin[1]. Analytic continuation onto the real frequency axis yields the corresponding poles of the resolvent operator or equivalently the eigenvalues of the Dirac Hamiltonian, which for $n > 0$ are then given by

$$E_{n,\tau}^{\pm} = \pm qB\sqrt{(2n+1) + \tau}. \tag{6.5}$$

[1]In condensed matter applications, the spinor structure *can*, but not necessarily has to be identical to physical spin. If we were to describe, e.g., a graphene system, the spinor structure encodes sublattice and valley quantum numbers and is referred to as a pseudospin. The physical spin degree of freedom would also couple through a Zeeman term to the external field. However, in so-called helical metals, where spin and momentum are locked into a spin texture in the first Brillouin zone, the spinor indeed describes the physical spin degree of freedom.

The massless and massive spectra are depicted schematically in Fig. 6.1. The lowest Landau level is specified by the quantum numbers $n = 0$, $\tau = -1$ with $E_{0,-1} = 0$. All further solutions with $n \geq 1$ for both negative and positive energy branches build up two degenerate towers of Landau levels for $\tau = +1$ and $\tau = -1$, respectively. Accounting for the density of states $\frac{qB}{2\pi}$ per spacetime volume for each Landau level, the trace operation can be decomposed as

$$\mathrm{Tr}(\,\cdot\,) = \Omega \sum_{n\in\mathbb{N}} \left(\frac{qB}{2\pi}\right) \int_{-\infty}^{\infty} \frac{\mathrm{d}p_0}{2\pi}\, \mathrm{tr}(\,\cdot\,), \tag{6.6}$$

where Ω denotes spacetime volume and $\mathrm{tr}(\,\cdot\,)$ is the trace over spinor indices (corresponding to $\tau = \pm 1$). It can be easily shown with, e.g., heat-kernel methods, that the number of zero modes per spacetime volume of the Hamiltonian corresponding to Eq. (6.1) equals $\frac{qB}{4\pi}$. So even though there is in principle room for $\frac{qB}{2\pi}$ states in a given volume Ω, only half of them are filled. This can be understood to be due to global charge conservation.

Dirac Propagator

The propagator for Dirac fermions in a magnetic field, that is the inverse of the Dirac operator, can be found to be given by [147, 148]

$$G^{+}(x, x') = \Phi(x, x')\tilde{G}^{+}(x - x'), \tag{6.7}$$

where we defined the gauge-dependent holonomy factor

$$\Phi(x, x') = \mathrm{e}^{\mathrm{i}q\int_x^{x'} \mathrm{d}\bar{x}\left(\mathcal{A}(\bar{x}) + \frac{1}{2}\mathcal{F}[\bar{x} - x']\right)} \tag{6.8}$$

with integration (e.g. along a linear path) connecting the spacetime points x and x' (see Appendix A.7 for brief sketch of a derivation). We furthermore defined the translation invariant function (in proper-time/Laplace representation)

$$\begin{aligned}\tilde{G}^{+}(x - x') \;=\; & \frac{\mathrm{i}}{(4\pi)^{d/2}} \int_0^{\infty} \mathrm{d}s\, \mathrm{e}^{-\bar{m}_{\mathrm{f}}^2 s} s^{-d/2} \left[-\frac{\gamma}{2}(\mathrm{i}q\mathcal{F})(\coth(\mathrm{i}q\mathcal{F}s) + 1)[x - x'] - \bar{m}_{\mathrm{f}}\right] \times \\ & \mathrm{e}^{-\frac{q}{2}\sigma\mathcal{F}s} \mathrm{e}^{-\frac{1}{2}\mathrm{tr}\ln\left\{(\mathrm{i}q\mathcal{F}s)^{-1}\sinh(\mathrm{i}q\mathcal{F}s)\right\}} \mathrm{e}^{-\frac{1}{4}[x-x'](\mathrm{i}q\mathcal{F}s)\coth(\mathrm{i}q\mathcal{F}s)[x-x']},\end{aligned} \tag{6.9}$$

and appropriate contractions of spacetime indices in Eq. (6.8) and Eq. (6.9) are implicit and for generality we also included a chirally nonsymmetric mass $\bar{m}_{\mathrm{f}}$. This decomposition will help us in the construction of a consistent gradient expansion, although translation invariance is strictly speaking lost. Thus $\tilde{G}^{+}(x - x')$ possesses a well defined Fourier transform, see Appendix A.8 for a direct

evaluation. In fact, the Fourier transform, denoted by $\tilde{G}^{+}(p)$ can be expanded over Landau levels, yielding the useful expression [130, 149]

$$\tilde{G}^{+}(p) = \sum_{n=0}^{\infty} \mathrm{e}^{-\frac{2\boldsymbol{p}^2}{qB}} (-1)^n \frac{D_n(p_0, \boldsymbol{p}; qB)}{p_0^2 + \bar{m}_{\mathrm{f}}^2 + 2qBn}, \tag{6.10}$$

where $L_n^{\alpha}(x)$ are generalized Laguerre polynomials [107] and the spin-resolved Landau level projector reads

$$\begin{aligned} D_n(p_0, \boldsymbol{p}; qB) &= L_n^0\left(\frac{2\boldsymbol{p}^2}{qB}\right) \left[-\gamma_0 p_0 - \mathrm{i}\bar{m}_{\mathrm{f}}\right] (\tau_0 \otimes \tau_0 + \tau_0 \otimes \tau_3) - \\ & L_{n-1}^0\left(\frac{2\boldsymbol{p}^2}{qB}\right) \left[-\gamma_0 p_0 - \mathrm{i}\bar{m}_{\mathrm{f}}\right] (\tau_0 \otimes \tau_0 - \tau_0 \otimes \tau_3) - \\ & 4L_{n-1}^1\left(\frac{2\boldsymbol{p}^2}{qB}\right) (\gamma_1 p_x + \gamma_2 p_y), \end{aligned} \tag{6.11}$$

where by definition $L_n^0(x) = 0$ for $n < 0$. We can read off from Eq. (6.10) some general features of Dirac fermions exposed to a homogeneous magnetic field. The $n = 0$ contribution is spin polarized due to the presence of the spin projector $\frac{1}{\sqrt{2}}(\tau_0 \otimes \tau_0 + \tau_0 \otimes \tau_3)$. All further Landau level modes with $n \geq 1$ are "massive", with mass $\propto \sqrt{qBn}$ and come in both polarizations. The expansion Eq. (6.10) makes obvious the decomposition of the 3-dimensional field theory into 1-dimensional dynamical systems. Only fluctuations in the time direction are possible, transverse fluctuations in the (x_1, x_2)-plane are exponentially suppressed with the characteristic scale $l = 1/\sqrt{qB}$, the so-called magnetic length.

Derivation of the Quantum Anomaly

Including a mass term $\bar{m}_{\mathrm{f}}$ in the Lagrangian Eq. (6.1), we can compute the expectation value $\sum_{j=1}^{N_{\mathrm{f}}} \langle \bar{\psi}_j \psi_j \rangle$ as [128, 148, 168, 169]

$$\begin{aligned} \sum_{j=1}^{N_{\mathrm{f}}} \langle \bar{\psi}_j \psi_j \rangle &= \lim_{\bar{m}_{\mathrm{f}} \to 0} \mathrm{i} \frac{\partial}{\partial \bar{m}_{\mathrm{f}}} \int \prod_{i=1}^{N_{\mathrm{f}}} \mathcal{D}\bar{\psi}_i \mathcal{D}\psi_i \, \mathrm{e}^{-\sum_{j=1}^{N_{\mathrm{f}}} \int_x \bar{\psi}_j \left(\mathrm{i}\not{D}[\mathcal{A}] + \mathrm{i}\bar{m}_{\mathrm{f}}\right) \psi_j} \\ &= -\lim_{\bar{m}_{\mathrm{f}} \to 0} \mathrm{i} \, \mathrm{tr} \int_p \tilde{G}^{+}(p) \\ &= -\mathrm{i} N_{\mathrm{f}} \frac{qB}{2\pi}, \end{aligned} \tag{6.12}$$

with $\tilde{G}^{+}(p)$ being the Fourier transform of $\tilde{G}^{+}(x)$ and a normal ordering prescription is implicit in the definition of the expectation value $\langle \bar{\psi}_j \psi_j \rangle$ (and the i is due to Wick rotation, taking into account that $\bar{\psi}_j \psi_j$ is "imaginary"). This demonstrates, that for a system of noninteracting Dirac fermions in three spacetime dimensions minimally coupled to a perpendicular magnetic field the continuous global $\mathrm{U}(2N_{\mathrm{f}})$ can *spontaneously* be broken down to $\mathrm{U}(N_{\mathrm{f}}) \times \mathrm{U}(N_{\mathrm{f}})$ for $B \neq 0$. Actually, a detailed

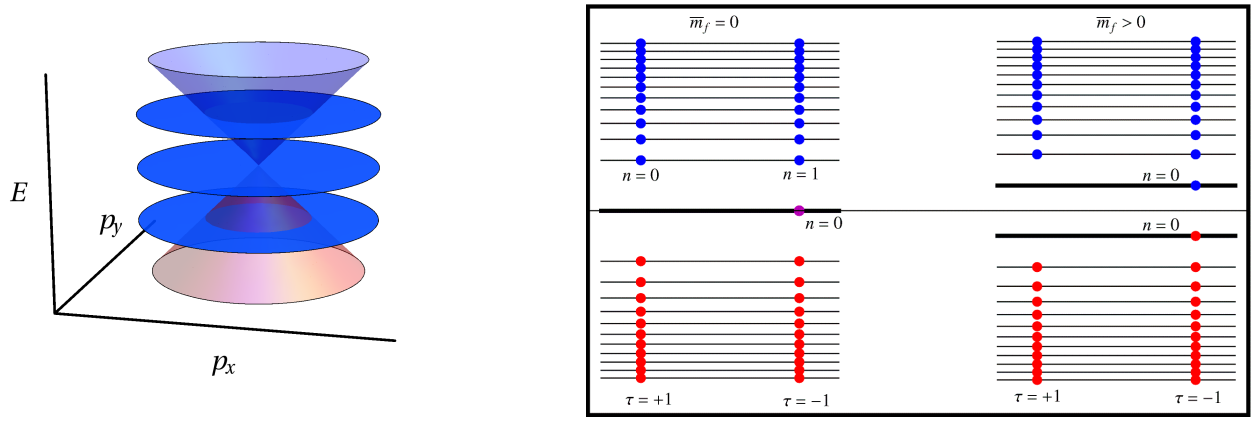

Figure 6.1: Left panel: In a perpendicular magnetic field, the linearly dispersing Dirac cone is replaced by relativistic Landau levels, i.e., momentum is no longer a good quantum number. Right panel: The τ-resolved Landau level spectrum for both massless ($\bar{m}_\mathrm{f} = 0$) and massive ($\bar{m}_\mathrm{f} \neq 0$) Dirac fermions. Blue blobs show positive, red blobs negative energy solutions. The magenta blob refers to the zero energy Landau level in the massless case. Obviously, the lowest Landau level is spin-polarized. *All* levels have a density of states $\frac{qB}{2\pi}$. In its ground-state, only half of the zero energy Landau level states are filled with fermions due to charge conservation [150].

discussion shows, that the value given in Eq. (6.12) is particular to a calculation with a finite mass and eventually sending the mass to zero. In [150], it is argued that by this prescription, only a particular ground-state out of a degenerate set of states containing both chirally symmetric and chirally nonsymmetric states is selected.

However, for vanishing interaction ($\bar{g} = 0$), this expectation value cannot couple back into the bilinear part of the theory. So although the chiral symmetry is broken and a finite chiral condensate is dynamically generated, it does not act as a mass term for the fermions and the spectrum of the theory remains unchanged.

6.2 Magnetic Beta Function

For giving a simple renormalization group picture of magnetic catalysis and also for avoiding technicalities, we stay within a pointlike, purely fermionic description. For finite flavor number we expect our arguments to be reliable until the onset of chiral symmetry breaking, where a proper description of the built up of a finite expectation value of the order parameter and the associated collective fluctuations need to be taken into account. For infinite flavor number, this approach is known be equivalent to a mean-field Dyson-Schwinger gap-equation approach [82].

To capture the effects of a magnetic field on the renormalization group flow, we make the following ansatz for the effective average action:

$$\Gamma_k[\bar{\psi}_j, \psi_j, \mathcal{A}] = \int_x \left\{ Z_{\psi,k} \sum_{j=1}^{N_\mathrm{f}} \bar{\psi}_j \mathrm{i}\not{D}[\mathcal{A}]\, \psi_j + \sum_{i,j=1}^{N_\mathrm{f}} \bar{\psi}_i \psi_i \frac{\bar{g}_k}{2N_\mathrm{f}} \bar{\psi}_j \psi_j \right\}, \tag{6.13}$$

where the coupling $\bar{g}_k$ is a function of the renormalization group scale k. Inserting this ansatz into the flow equation Eq. (2.27), we can project onto the flow of the dimensionless coupling g_k by collecting all appropriate terms quartic in the spinor fields. The presence of the magnetic field requires a slightly different approach in the derivation of the beta function, which is usually performed for the corresponding momentum-space quantities and fields. One problem is that the vector potential $\mathcal{A}(x)$ entering the quadratic part of the action renders the fermionic propagator a translationally noninvariant function of the spacetime coordinates. Taking gauge holonomy factors appropriately into account, cf. Eq. (6.7), it still becomes possible to study the ansatz in Eq. (6.13), which essentially constitutes the zeroth order in a derivative expansion. This implies that the derivative structure contained in the effective average action is the same as in the classical action. In the following, we demonstrate that Eq. (6.13) leads to a consistent flow equation within such a derivative expansion. We also argue that the scale dependence of a wave function renormalization entering the action in the form $Z_{\psi,k} \sum_{j=1}^{N_\mathrm{f}} \bar{\psi}_j \mathrm{i}\not{D}[\mathcal{A}]\, \psi_j$ in the present truncation is trivial, i.e., $Z_{\psi,k} \equiv 1$ like in standard flows for pointlike fermionic theories with chiral symmetry [34, 46].

Position-space Derivation of the Magnetic Beta Function

It is convenient to derive the flow equations in position space rather than momentum space due to the presence of the vector potential $\mathcal{A}(x)$. Strictly speaking, the propagator is in general no longer a translationally invariant function of spacetime coordinates. As shown above, it can, however, be decomposed into a holonomy factor $\Phi(x, x')$ times a translationally invariant factor [148], allowing in principle for a momentum-space formulation, if 1PI vertex functions are defined carefully. Still, a formulation in position space is more direct in the purely pointlike approximation. The flow equation Eq. (2.27) in Nambu representation can again be expanded as (here in contrast to Eq. (2.30), the bosonic sector is empty and we suppressed the dependence on the spinor fields)

$$\begin{aligned} \partial_t \Gamma_k &= \frac{1}{2} \mathrm{STr} \left\{ \left[\Gamma_k^{(2)} + R_{F,k} \right]^{-1} (\partial_t R_{F,k}) \right\} \\ &= -\frac{1}{2} \mathrm{Tr}\, \tilde{\partial}_t \ln G_k^{-1} - \frac{1}{2} \mathrm{Tr}\, \tilde{\partial}_t \sum_{l=1}^{\infty} \frac{(-1)^{l+1}}{l} (G_k \tilde{\Gamma}_k^{(2)})^l, \end{aligned} \tag{6.14}$$

where the $\tilde{\partial}_t$ derivative only acts on the regulator dependent part. As before (cf. Eq. (2.29)), we have decomposed the fluctuation kernel $\Gamma_k^{(2)} = \bar{\Gamma}_k^{(2)} + \tilde{\Gamma}_k^{(2)}$, where $\bar{\Gamma}_k^{(2)}$ is the field-independent part

and $\tilde{\Gamma}_k^{(2)}$ denotes the field-dependent vertex part. We also defined the scale-dependent regularized Nambu propagator

$$G_k \equiv \left[\bar{\Gamma}_k^{(2)} + R_{F,k}\right]^{-1}. \tag{6.15}$$

For the subsequent discussion, we choose a chirally invariant regulator

$$R_{F,k}^{+} = Z_{\psi,k}\left[\mathrm{i}\not{D}[\mathcal{A}] r_F\left(\frac{(\mathrm{i}\not{D}[\mathcal{A}])^2}{k^2}\right)\right], \tag{6.16}$$

with an as yet unspecified shape function $r_F(y)$. The fluctuation kernel in Nambu representation for the spinor fields (see e.g. [171]) becomes

$$G_k = \begin{pmatrix} 0 & G_k^{+} \\ G_k^{-} & 0 \end{pmatrix} \tag{6.17}$$

with $G_k^{+} = [Z_\psi(\mathrm{i}\not{D}[\mathcal{A}]) + R_{F,k}^{+}]^{-1}$, $G_k^{-} = [G_k^{+}]^T$ and

$$\tilde{\Gamma}_{k,ij}^{(2)} = \begin{pmatrix} \bar{H}_{ij,k} & -F_{ij,k}^T \\ F_{ij,k} & H_{ij,k} \end{pmatrix}. \tag{6.18}$$

While we have omitted flavor indices for the propagator part, which is diagonal in flavor space, the flavor structure of the vertex part is nontrivial. The matrix blocks are given by

$$\begin{aligned}
\bar{H}_{ij,k} &= -\frac{\bar{g}_k}{N_\mathrm{f}}\,\bar{\psi}_i^T\bar{\psi}_j, && (6.19)\\
-F_{ij,k}^T &= \frac{\bar{g}_k}{N_\mathrm{f}}\left\{\bar{\psi}_i^T\psi_j^T - \sum\nolimits_{l=1}^{N_\mathrm{f}}(\bar{\psi}_l\psi_l)\delta_{ij}\mathbb{1}_4\right\}, && (6.20)\\
F_{ij,k}^T &= \frac{\bar{g}_k}{N_\mathrm{f}}\left\{\psi_i\bar{\psi}_j + \sum\nolimits_{l=1}^{N_\mathrm{f}}(\bar{\psi}_l\psi_l)\delta_{ij}\mathbb{1}_4\right\}, && (6.21)\\
H_{ij,k} &= -\frac{\bar{g}_k}{N_\mathrm{f}}\,\psi_i\psi_j^T. && (6.22)
\end{aligned}$$

We define the position space representation of the operator $\mathrm{i}\not{D}[\mathcal{A}]$ as

$$\langle x|\mathrm{i}\not{D}[\mathcal{A}]|x'\rangle \equiv \mathrm{i}\not{D}[\mathcal{A}](x,x') = \gamma_\mu(\mathrm{i}\partial_\mu^x + \mathcal{A}_\mu(x))\delta(x-x'). \tag{6.23}$$

Accordingly, we proceed for the regulator part $R_{F,k}^{+}$ inserted into the Gaußian measure of the generating functional of Green's functions:

$$\langle x|R_{F,k}^{+}|x'\rangle \equiv R_{F,k}^{+}(x,x') = Z_{\psi,k}\left[\mathrm{i}\not{D}[\mathcal{A}] r_F\left(\frac{(\mathrm{i}\not{D}[\mathcal{A}])^2}{k^2}\right)\right](x,x'). \tag{6.24}$$

In this notation, the regularized propagator is given by

$$G_k^+(x,x') = Z_{\psi,k}^{-1}\left[\mathrm{i}\not{D}[\mathcal{A}]\left(1+r_F\left(\frac{(\mathrm{i}\not{D}[\mathcal{A}])^2}{k^2}\right)\right)\right]^{-1}(x,x'). \tag{6.25}$$

However, the wave function renormalization is $Z_{\psi,k} \equiv 1$ in this pointlike truncation. This can be seen from the tadpole diagram giving rise to self-energy corrections. The regularized tadpole diagram is proportional to

$$\int_x \tilde{\partial}_t \,\mathrm{tr}\, G_k^+(x,x). \tag{6.26}$$

Using the fact, that the covariantly regularized Dirac propagator can be decomposed into a holonomy times a translationally invariant part as in Eq. (6.7) (see Appendix A.9 for proof) and since the holonomy factor $\Phi(x,x')$ from Eq. (6.8) becomes trivial in the coincidence limit $x' \to x$, the remaining contribution to the trace comes from the translation invariant part and thus the tadpole carries no net momentum at all, like in the $B = 0$ case.

The vertex part of the fluctuation matrix becomes in position space representation

$$\begin{aligned}
\bar{H}_{ij,k}(x,x') &= -\frac{\bar{g}_k}{N_\mathrm{f}}\,\bar{\psi}_i^T(x)\bar{\psi}_j(x)\delta(x+x'), && (6.27)\\
-F_{ij,k}^T(x,x') &= \frac{\bar{g}_k}{N_\mathrm{f}}\left\{\bar{\psi}_i^T(x)\psi_j^T(x) - \sum\nolimits_{l=1}^{N_\mathrm{f}}(\bar{\psi}_l\psi_l)(x)\delta_{ij}\mathbb{1}_4\right\}\delta(x-x'), && (6.28)\\
F_{ij,k}^T(x,x') &= \frac{\bar{g}_k}{N_\mathrm{f}}\left\{\psi_i(x)\bar{\psi}_j(x) + \sum\nolimits_{l=1}^{N_\mathrm{f}}(\bar{\psi}_l\psi_l)(x)\delta_{ij}\mathbb{1}_4\right\}\delta(x-x'), && (6.29)\\
H_{ij,k}(x,x') &= -\frac{\bar{g}_k}{N_\mathrm{f}}\,\psi_i(x)\psi_j^T(x)\delta(x+x'). && (6.30)
\end{aligned}$$

The projection onto the beta function of the dimensionless coupling $g_k = k^{d-2}\bar{g}_k$ is facilitated by collecting all contributions on the r.h.s. of Eq. (6.14) which are quartic in the fermionic fields. We find two contributions, $\frac{1}{2}\mathrm{Tr}\,\tilde{\partial}_t\left\{G_k^+F_kG_k^+F_k\right\}$ and $\frac{1}{2}\mathrm{Tr}\,\tilde{\partial}_t\left\{G_k^+H_kG_k^-\bar{H}_k\right\}$. These will subsequently be evaluated for spatially constant spinor fields. Using the identity

$$\tilde{\partial}_t G_k^\pm = -G_k^\pm\partial_t R_{F,k}^+ G_k^\pm, \tag{6.31}$$

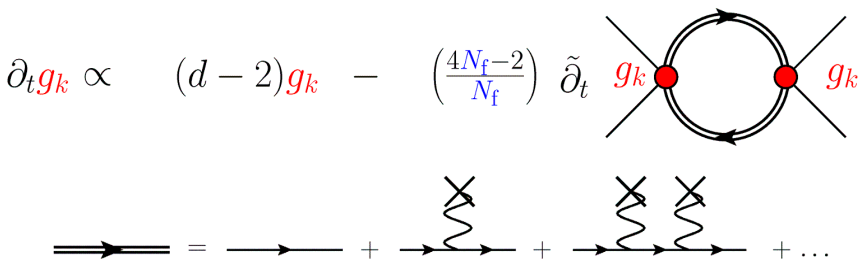

Figure 6.2: The upper part depicts a diagrammatic representation of the beta function for the dimensionless coupling g_k (red dot). The regularized fermionic loop contains the full B-dependence as given by the fermionic propagator coupling to the external gauge field $\mathcal{A}$ to all orders as shown in the lower part. The coupling to $\mathcal{A}$ is indicated by a cross. The $\tilde{\partial}_t$ derivative acts on the regulator dependent part of the propagators and generates diagrams with regulator insertions, see Eq. (6.31).

and after some algebra we arrive at

$$\begin{aligned}
&\frac{N_\mathrm{f}}{2}\mathrm{Tr}\,\tilde{\partial}_t\left\{G_k^+F_kG_k^+F_k+G_k^+H_kG_k^-\bar{H}_k\right\} \qquad (6.32)\\
&\quad=\frac{2}{N_\mathrm{f}}\bar{g}_k^2\sum_{i,j=1}^{N_\mathrm{f}}\int_x\bar{\psi}_i\left(\left[\mathrm{i}\not{D}[\mathcal{A}]\left(1+r_F\left(\frac{(\mathrm{i}\not{D}[\mathcal{A}])^2}{k^2}\right)\right)\right]^{-3}\partial_t R_{F,k}^+\right)(x,x)\,\psi_i(\bar{\psi}_j\psi_j)\\
&\quad-\bar{g}_k^2\,\mathrm{tr}\int_x\underbrace{\left(\left[\mathrm{i}\not{D}[\mathcal{A}]\left(1+r_F\left(\frac{(\mathrm{i}\not{D}[\mathcal{A}])^2}{k^2}\right)\right)\right]^{-3}\partial_t R_{F,k}^+\right)(x,x)}_{\propto f\left(\frac{\mathrm{i}\not{D}[\mathcal{A}])^2}{k^2}\right)\text{ see Eq. (6.34)}}\sum_{i,j=1}^{N_\mathrm{f}}(\bar{\psi}_i\psi_i)(\bar{\psi}_j\psi_j),
\end{aligned}$$

where $\mathrm{tr}(\,\cdot\,)$ denotes the trace over spinor indices. The first term on the r.h.s. in the first line of Eq. (6.32) contains not only a contribution to the flow of g_k, but also a term $\sim\frac{1}{N_\mathrm{f}}(\bar{\psi}_i\sigma_{\mu\nu}\mathcal{F}_{\mu\nu}\psi_i)(\bar{\psi}_j\psi_j)$ is generated in an infinitesimal renormalization group step. Nevertheless, in the large-N_f limit, this contribution drops out from the fermionic loop. It is also important to note that the spinors $\bar{\psi}_i$ and ψ_i are to be contracted with the term in round brackets. It is interesting to note, that within the chirally broken phase, such a term corresponds to an anomalous magnetic moment of the fermionic fields, with the strength of this moment being directly related to the value of the chiral condensate. Similar observations have also been made in [141–143].

From Eq. (6.32) we can read off that the pointlike limit as the lowest order in a derivative expansion is well defined. Holonomy factors $\Phi(x,x')$ from the fermionic propagators fulfill the composition law $\Phi(x,x')\Phi(x',x'')=\Phi(x,x'')$ and are once again rendered trivial by the coincidence limit. In principle, the trace could be performed in momentum space, using Eq. (6.9). However, having arrived at Eq. (6.32), it is rather easy to perform traces over the Landau level spectrum diagonalizing the spatial part of the Dirac operator.

To expose the magnetically induced operator more clearly, it is suitable to employ a Laplace transformation,

$$f(y) = \int_0^\infty \mathrm{d}s \tilde{f}(s)\, \mathrm{e}^{-ys}, \tag{6.33}$$

where here (see Eq. (6.32))

$$f(y) = \left(\frac{1}{1+r_F(y)}\right)^3 r_F'(y), \tag{6.34}$$

with $y = (\mathrm{i}\not{D}[\mathcal{A}])^2/k^2$, in order to handle the appearing traces. Since the spectrum of $(\mathrm{i}\not{D}[\mathcal{A}])^2$ is known (cf. Eq. (6.4)), we perform the functional trace with help of Eq. (6.6) and obtain

$$\mathrm{Tr}'\mathrm{e}^{-(\mathrm{i}\not{D}[\mathcal{A}])^2/k^2 s} = \Omega\left(\frac{qB}{2\pi}\right)\left[\frac{k}{4\sqrt{\pi s}\sinh\left(\frac{qBs}{k^2}\right)}\right]\left[\cosh\left(\frac{qBs}{k^2}\right)\tau_0\otimes\tau_0 + \sinh\left(\frac{qBs}{k^2}\right)\tau_0\otimes\tau_3\right], \tag{6.35}$$

where the prime indicates that the trace over spinor indices is not included. The last term in Eq. (6.35) makes the generation of a magnetically induced operator explicit. However, neglecting this contribution and only keeping terms $\sim \tau_0\otimes\tau_0 = \mathbb{1}_4$, the flow equation for g_k can be derived in closed form by specifying the shape function $r_F(y)$ as

$$r_F(y) = \sqrt{\frac{y+1}{y}} - 1, \tag{6.36}$$

i.e., by using the Callan-Symanzik regulator giving rise to scale dependent mass $\propto k^2$. The Laplace transform is known in this case and reads

$$\tilde{f}(s) = -\frac{1}{2}\mathrm{e}^{-s}s. \tag{6.37}$$

Upon performing the Laplace integral, we finally arrive at the rather simple result

$$\beta_{g_k} \equiv \partial_t g_k = (d-2)g_k - \frac{1}{16\pi}\left(\frac{N_\mathrm{f}\, d_\gamma - 2}{N_\mathrm{f}}\right) g_k^2\left[\sqrt{\frac{2}{b}}\zeta\left(\frac{3}{2},\frac{1}{2b}\right) - 2b\right], \tag{6.38}$$

where $b \equiv \frac{qB}{k^2}$ denotes the dimensionless external field and $\zeta(u,v)$ is the Hurwitz zeta function. It obeys

$$\lim_{b\to 0}\left[\sqrt{\frac{2}{b}}\zeta\left(\frac{3}{2},\frac{1}{2b}\right) - 2b\right] = 4, \tag{6.39}$$

giving us back the beta function for vanishing gauge background in the limit $b \to 0$, cf. Chap. 4. We can immediately read off the nontrivial "dynamical" fixed point $g_*(b)$,

$$g_*(b) = 16\pi(d-2)\left(\frac{N_\mathrm{f}\, d_\gamma - 2}{N_\mathrm{f}}\right)^{-1}\left[\sqrt{\frac{2}{b}}\zeta\left(\frac{3}{2},\frac{1}{2b}\right) - 2b\right]^{-1}, \tag{6.40}$$

which still depends on the renormalization group scale via the presence of the magnetic field. Formally, for $d > 2$ and $b \to \infty$ (corresponding to the IR limit $k \to 0$), $g_*(b)$ tends to 0^+. From this we obtain the b independent critical exponent

$$\Theta = -\left.\frac{\partial \beta_g}{\partial g}\right|_{g=g_*(b)} = d - 2 \overset{d=3}{=} 1. \tag{6.41}$$

For quantitative statements, we actually have to determine the full renormalization group trajectory. We will discuss the implicatios of our findings in greater detail in the following sections.

Qualitative Modifications of the Flow by a Magnetic Field

In the following, we will elaborate on how the phenomenon of magnetic catalysis manifests itself in the IR behavior of the beta function Eq. (6.38) for the coupling $\bar{g}_k$.

As already discussed in Sect. 4.2, this beta function has also a non-Gaußian, i.e., strong-coupling fixed point besides the Gaußian fixed point of a noninteracting theory. At this non-Gaußian fixed point the scaling dimension is altered from $\Theta_{\text{Gauß}} < 0$ at the Gaußian one to $\Theta_{\text{non-Gauß}} > 0$, cf. [31] and Chap. 4. So in contrast to a naive scaling analysis, the coupling actually corresponds to a relevant direction in theory space at this nontrivial zero of the beta function. The nontrivial fixed point acts as a separatrix for different regimes of the flow. These two different regimes translate into different phases realized in the respective ground states of the quantum field theory [39, 81]. For values $g_k < g_*$, the flow is toward a noninteracting theory, while for $g_k > g_*$ the coupling diverges at some finite IR scale k_c, indicating that the discrete chiral symmetry is spontaneously broken. Thus, g_* can be interpreted as the (nonuniversal) critical value of g_k corresponding to a chiral quantum phase transition, as discussed in Chap. 4. With the magnetic field, a new scale enters the scene, the so-called magnetic length $l = 1/\sqrt{qB}$. The inverse magnetic length thus describes the typical energy and momentum scales associated with fermions moving in a magnetic field. For strong magnetic fields, the fermionic fluctuations that experience Landau level quantization are primarily driven by the lowest Landau level ($n = 0$, $\tau = -1$, cf. Sect. 6.1). A Landau level can roughly be attributed an extent of l in all spatial directions orthogonal to the magnetic field. The present quantum field theory in $d = 3$ is thus dimensionally reduced via the external field to essentially a quantum mechanical problem ($d \to d - 2 = 1$), as was already discussed in Sect. 6.1 by means of the full propagator for $\bar{g} = 0$.

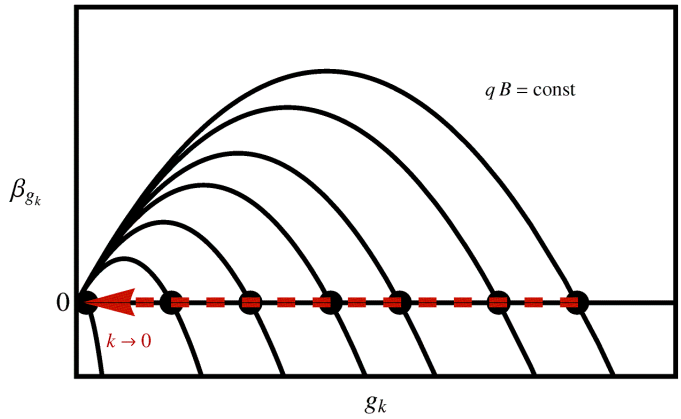

Figure 6.3: Plot of the beta function β_g (cf. Eq. (6.38)) of the coupling g in the presence of an external magnetic field B in arbitrary units. As the RG scale k tends to zero for fixed B, the quadratic part of the beta function dominates over the linear part due to dimensional flow. The strong-coupling fixed point (black dots) is pushed toward the Gaußian fixed-point as the scale moves from the high UV to the IR regime (indicated by dashed red arrow). This leads to a divergence in g at a finite scale associated with chiral symmetry breaking, for arbitrary values of the initial coupling at the UV scale Λ. From right to left b takes the values 0.1, 1, 2, 3, 5, 10, 100, 1000.

In the regime $l^{-1} \ll k$, the high-momentum quantum fluctuations on the scale k are not affected by the long-wavelength physics associated with the low-momentum scale l^{-1}. From the initial UV scale $k = \Lambda$ down to the magnetic scale $k = l^{-1}$, we expect the beta function to be very similar to its zero field counterpart. However, as we evolve the system toward the IR by sending the renormalization group scale k to zero, the IR fluctuations in the regime $l^{-1} \gg k$ are dominated by magnetic-field effects.

This behavior is depicted in Fig. 6.3. At high scales ($b \ll 1$), the beta function shows the typical competition between a positive linear and negative quadratic contribution, cf. Eq. (4.27). Its shape is unaffected by the presence of an external magnetic field. Upon lowering k, the non-Gaußian fixed point starts moving toward the Gaußian fixed point. In the deep IR limit, the non-Gaußian fixed point asymptotically merges with the Gaußian one. However, only the negative branch of the beta function survives in this limit, rendering g_k a relevant perturbation, completely oblivious of the initial UV value of the coupling. In this way, the divergence of g_k at a finite scale is catalyzed by the external field for arbitrary finite values of g_k.

6.3 Dynamical Mass Generation by External Fields

The phenomenon of spontaneous chiral symmetry breaking is accompanied by the dynamical generation of a mass $\bar{m}_{\rm f}$ for the fermionic degrees of freedom which drive the symmetry breaking. In a partially bosonized formulation, that we described earlier in Chap. 4 for vanishing magnetic field,

Regime	$g_0^{(\mathrm{RG})}$	$\Lambda^{(\mathrm{RG})}$	$g_0^{(\mathrm{DS})}$	$\Lambda^{(\mathrm{DS})}$
(A) $g_0 \ll g_*$	0.20	100 a.u.	0.206	100 a.u.
(B) $g_0 \lesssim g_*$	2.00	100 a.u.	2.76	100 a.u.
(C) $g_0 \gtrsim g_*$	6.50	100 a.u.	65.00	100 a.u.

Table 6.1: Initial or bare value of the interaction g_0 and cutoff scale Λ in the large-N_f renormalization group (RG) and Dyson-Schwinger (DS) gap equation. The scheme dependent critical values are $g_*^{(\mathrm{RG})} = \pi$ and $g_*^{(\mathrm{DS})} \simeq 5.39$.

the condensation of an order parameter field σ introduces a mass term into the free part of the Dirac Lagrangian. The onset of symmetry breaking driven by quantum fluctuations typically occurs at some critical scale k_c. We expect that $\bar{m}_\mathrm{f} \sim k_\mathrm{c}$. The collective fluctuations of the fermionic system encoded in fluctuations of the σ field about its expectation value will typically diminish this value.

Quantitative Results

The beta function Eq. (6.38) can now be used to analyze the field dependence of the dynamically induced fermion mass. For this, we use the identification $\bar{m}_\mathrm{f} = k_\mathrm{c}$, ignoring possible $\mathcal{O}(1)$ factors arising from fluctuations in the symmetry-broken regime. The critical scale k_c can be identified with the scale where the flow of g_k diverges. Therefore it is convenient to reformulate the beta function for g_k as a beta function for the inverse coupling $1/g_k$. From β_{1/g_k} we can move to the actual trajectory $1/g_k$ by solving the flow equation with a given initial condition $g_{k=\Lambda} = g_0$ and record whenever $1/g_{k=k_\mathrm{c}} = 0$.

The result of this analysis is shown in Fig. 6.4. The initial or bare value g_0 was chosen from three different regimes. The flow equation was evaluated for flavor numbers ranging from $N_\mathrm{f} = 1$ to $N_\mathrm{f} = 100$, which at this level of the truncation is indiscernible from the large-N_f limit. For clarity, only the curves for $N_\mathrm{f} = 1$ and $N_\mathrm{f} = 100$ are shown. The curves for $1 < N_\mathrm{f} < 100$ fall into the shaded regions and do not cross in the B-interval we scanned. The precise values for g_0 and Λ are listed in Table 6.1. In the weak coupling regime $g_0 \ll g_*$ we find $\bar{m}_\mathrm{f} \propto B$. For intermediate, but sub-critical values of the initial coupling $g_0 \lesssim g_*$ deviations from the linear behavior show up. In a sense, in this regime the generation of a fermion mass is due to the interplay of the "quantum anomaly" of the free system for $B \neq 0$ mentioned in Sect. 6.2 and the four-point vertex $\bar{g}$ (in the pointlike approximation). While the anomaly generates a finite chiral condensate, the four-point vertex allows for coupling this condensate back into the single particle spectrum, such that a mass gap opens up. In the strong coupling regime $g_0 \gtrsim g_*$ the fermion mass is generated already for $B = 0$ in the usual chiral quantum phase transition from a massless phase to a phase with massive Dirac fermions controlled by the beta function for vanishing field.

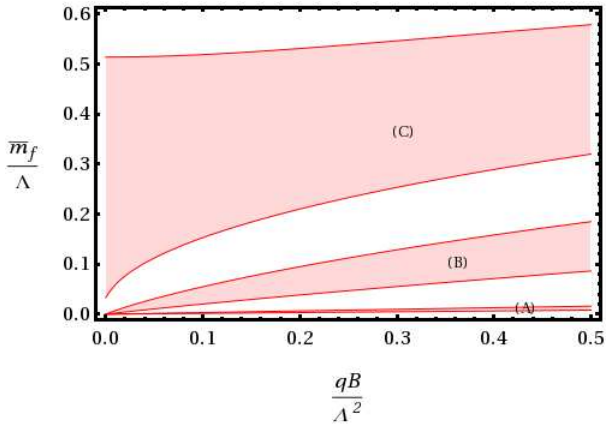

Figure 6.4: B dependence of the dynamically generated fermion mass $\bar{m}_\mathrm{f}$ as determined from the critical scale k_c. The lowest boundary of each band corresponds to $N_\mathrm{f} = 1$ and the upper boundary to $N_\mathrm{f} = 100$. The curves for intermediate N_f can be computed as easily, but are not shown for clarity. Band (A) is the weak coupling $g_0 \ll g_*$, band (B) the intermediate but sub-critical coupling $g_0 \lesssim g_*$, and (C) the strong coupling regime, $g_0 \gtrsim g_*$.

Comparing with Mean-Field Theory

To assess the validity of the pointlike approximation of the four point vertex and the naive identification of the dynamically generated fermion mass $\bar{m}_\mathrm{f}$ with the critical scale k_c we use in this work, we compared the large-N_f limit of our flow equation with the large-N_f Dyson-Schwinger gap equation. This equation was derived in e.g. [128] and can be written as

$$1 = \frac{\bar{g}}{2\pi^{\frac{3}{2}}} \int_{1/\Lambda^2}^{\infty} \frac{\mathrm{d}t}{t^{\frac{3}{2}}} \mathrm{e}^{-\bar{m}_\mathrm{f}^2 t} (qBt) \coth(qBt) \,. \tag{6.42}$$

The integral is regularized in the proper-time formulation and can be performed by analytic continuation, such that a closed but cutoff-dependent expression is obtained (see [128]). The results are shown in Fig. 6.5. The values of the cutoff scale Λ and the bare interaction g_0 used in the two different schemes (renormalization group and Dyson-Schwinger gap equation) are given in Table 6.1. In order to compare these two approaches, the values of Λ and g_0 were chosen, such that the dynamically generated fermion mass $\bar{m}_\mathrm{f}$ obtained from the RG flow and the self-consistent solution to Eq. (6.42) coincide for $qB/\Lambda^2 = 0.1$. Since the Gross-Neveu model (or its corresponding universality class) only has a single parameter (which remains true beyond the pointlike approximation), this fixing prescription is sufficient. We find excellent agreement over a wide range of qB. Small deviations occur due to cutoff effects when $qB/\Lambda^2 \sim 0.35$, as expected for scheme dependencies. Unfortunately, this quantitative check cannot be carried over to finite N_f in a fully controlled manner. Especially the identification $\bar{m}_\mathrm{f} = k_\mathrm{c}$ cannot be expected to hold any longer, since collective excitations – which are completely damped in the large-N_f limit – will modify the value of $\bar{m}_\mathrm{f}$ beyond the critical scale k_c that for finite flavor numbers signals only the onset of chiral symmetry breaking.

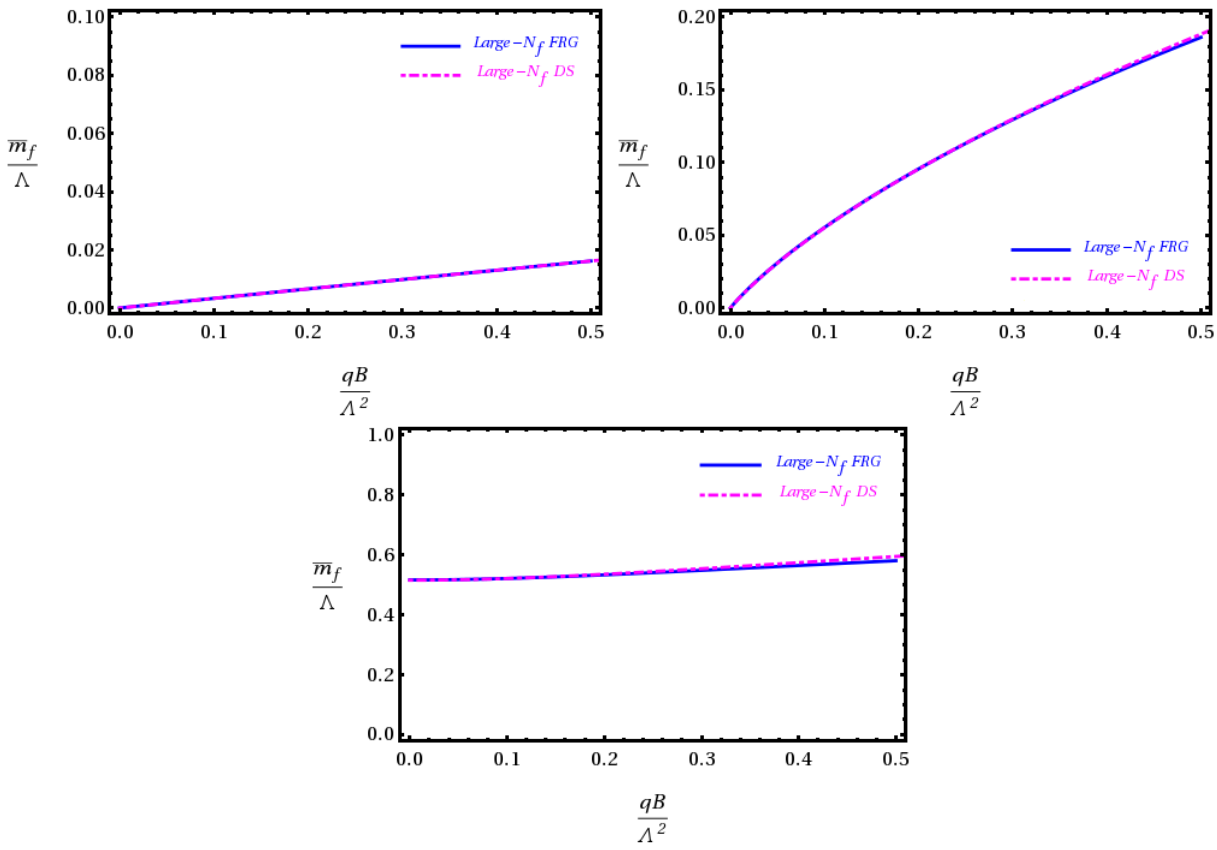

Figure 6.5: Quantitative comparison of the B dependence of the dynamically generated fermion mass $\bar{m}_{\mathrm{f}}$ from the large-N_{f} flow equation (solid blue) and the large-N_{f} gap equation in the weak- (top left), intermediate- (top right) and strong-coupling regime (bottom). For cutoff Λ and bare value of g_0, see Table 6.1.

Discussion

We have studied the phenomenon of magnetic catalysis within the three dimensional Gross-Neveu model. Minimally coupling the Dirac fermions to an external magnetic field catalyzes chiral symmetry breaking for arbitrary bare values of the fermionic interaction. Even in the free system, chiral symmetry breaking occurs and can be attributed to a form of "quantum anomaly". However, only in the interacting case does the symmetry breaking lead to a mass generation for the fermionic degrees of freedom. Using the functional renormalization group flow equation for the generating functional of 1PI irreducible vertices, we have obtained the beta function for the coupling parameterizing the fermionic interaction in a pointlike approximation. An analysis of the IR behavior of the beta function yielded a clear picture of magnetic catalysis in the language of the renormalization group. The strong-coupling fixed point is pushed toward the Gaußian fixed point. But in the deep IR limit, we find that only the negative branch of the beta function remains, and subsequently the coupling always flows into the strong coupling regime and eventually signals the breakdown of chiral symmetry in a divergence at a finite critical scale.

This fixed-point picture of the approach to criticality in fact occurs in many fermionic systems [46]. For instance, also a gauge-field background giving rise to a nonvanishing Polyakov loop pushes the strong-coupling fixed point towards the Gaußian fixed point [170]. The unique feature of a magnetic background is the occurrence and subsequent IR dominance of the lowest Landau level acting as a symmetry-breaking catalyzer [128, 129].

Additionally, magnetically induced operators might affect chiral symmetry breaking in external fields. We find that a fermionic tensor-scalar contribution is generated for finite flavor number, when starting from the naive Gross-Neveu action with only scalar-scalar interactions. The occurrence of these magnetically-induced operators is not particular to the Gross-Neveu model but certainly a generic feature of any fermionic system. In fact, this is yet another example for the proliferation of operators in the presence of further Lorentz tensors as is familiar from the classification of operators, e.g., at finite temperature [46, 108]. It should be emphasized that mean-field studies typically ignore contribution of such terms.

Within our truncation, there is no critical magnetic field, i.e., symmetry breaking occurs for all B. In principle there might be the possibility to compensate the "driving force" from the scalar-scalar channel, such that for certain regimes, a critical field B_c might be necessary to enter the broken phase. This is indeed the case at finite temperature. Here it is interesting to consider the dimensional reduction $d \to d-2$ by the external magnetic field, followed by $d \to d-1$ in the high-temperature regime [158–161], literally boiling down the relevant and universal mode content to a 0-dimensional theory, which should correspond to a simple (Grassmann) integral. In a partially bosonized description, we would obtain a 0-dimensional (gapped) fermionic mode coupled to 2-dimensional (gapless) bosonic fluctuations.

Also, we neglected the back-reaction of collective neutral excitations onto the fermionic system. For small flavor numbers, we expect sizable quantitative modifications from the fluctuations of the order-parameter field. For infinite flavor numbers, we recover the exact results of the large-N_f theory.

Chapter 7

Conclusions and Outlook

In this thesis, we established the Gross-Neveu model in three-dimensional spacetime as a simple, yet nonperturbative, benchmark system for a derivative expansion at the LPA′ level at zero (Chap. 4) and finite temperature (Chap. 5) within the functional renormalization group as formulated by Wetterich. We laid ground for an extension of our analysis by identifying the Gross-Neveu theory space in Chap. 3 at the four-fermi level. The derivation of the Gross-Neveu beta function in the presence of a magnetic field in Chap. 6 allowed us to gain an intuitive picture for the phenomenon of magnetic catalysis. In the following, we would like to briefly go through several open questions and interesting extensions of the topics touched upon in this thesis.

Gross-Neveu Phase Diagram at Finite Chemical Potential

Since the Gross-Neveu model in three spacetime dimensions can be treated with Monte Carlo simulations even at finite chemical potential, it is desirable to compare results from different nonperturbative approaches, especially to demonstrate the validity and power of the functional renormalization group. As we explained in Sect. 5.2, a convenient regulator which can handle finite chemical potentials in low-dimensional fermionic theories with chiral symmetry is currently unknown. To construct a suitable regulator and to extend the phase diagram along the μ axis is an attractive goal for the Gross-Neveu theory. To understand the difficulties arising from polynomial truncations of the effective potential and possibly to move to the full effective potential beyond LPA in low-dimensional models would complete this line of research.

Magnetic Catalysis with Collective Neutral Excitations

The treatment of magnetic catalysis in Chap. 6 was restricted to the four-fermi level, yielding estimates for the dynamically generated fermion mass. These values will be reduced, once the back-action of collective fluctuations of the order parameter are considered in the truncation. The inclusion of collective excitations at the LPA′ level requires a sensible ansatz for the flowing vertices, taking into account gauge-dependent holonomy factors. We have derived a consistent set of flow

equations which forms the starting point for a fixed-point analysis analogous to Chap. 4 in the presence of finite magnetic flux. To access the UV structure of the Gross-Neveu model within this formalism, a resummation over all Landau level contributions is necessary. For any finite truncation, the UV fixed-point is "lost". The LPA′ level truncation lends itself to an improved resolution of the field dependence of the magnetically induced chiral condensate.

Thirring Model with Magnetic Flux

In contrast to the Gross-Neveu model, the three-dimensional Thirring model features nonanalytic behavior with respect to flavor number [34]. The Thirring theory space features a rich fixed-point structure. In the Gross-Neveu model, the presence of a magnetic field generates a dynamical fixed point, running toward the Gaußian fixed point with the renormalization group evolution, simultaneously catalyzing dynamical symmetry breaking. It appears interesting to study the interaction of the more complicated Thirring fixed-point structure with external magnetic flux.

Magnetic "Quantum Anomaly" in Topological Insulators

The low-energy properties of surface states of topological insulators can be described by Dirac Hamiltonians. Due to the increasing interest in the transport properties of topological insulators, it seems worthwhile to investigate the possible effects of the magnetic "quantum anomaly" featured by Dirac systems in the presence of a perpendicular magnetic field and Coulomb repulsion. Accurate knowledge of the field dependence of the gap in the fermionic single-particle spectrum could provide a quantitative bridge to the understanding of transport experiments on topological insulators.

Bibliography

[1] K. Sibold, "Theory of the elementary particles," Stuttgart, Germany: Teubner (2001) 197 p.

[2] W. N. Cottingham and D. A. Greenwood, "An introduction to the standard model of particle physics," Cambridge, UK: Univ. Pr. (2007) 272 p.

[3] P. A. M. Dirac, "The Quantum Theory of the Electron," Proc. R. Soc. Lond. A **117** 610 (1928).

[4] E. Noether, "Invariant Variation Problems," Gott. Nachr. **1918**, 235 (1918) [Transp. Theory Statist. Phys. **1**, 186 (1971)].

[5] N. Goldenfeld, "Lectures on phase transitions and the renormalization group," Reading, USA: Addison-Wesley (1992) 394 p. (Frontiers in physics, 85)

[6] S. Weinberg, "Critical Phenomena for Field Theorists," HUTP-76-160.

[7] S. Weinberg, "What is quantum field theory, and what did we think it is?," In *Boston 1996, Conceptual foundations of quantum field theory* 241-251.

[8] S. Weinberg, "Living with Infinities," arXiv:0903.0568 [hep-th].

[9] J. A. Hertz, "Quantum critical phenomena," Phys. Rev. B **14** 1165 (1976).

[10] A. J. Millis, "Effect of a nonzero temperature on quantum critical points in itinerant fermion systems," Phys. Rev. B **48** 7183 (1993).

[11] H. v. Lohneysen, A. Rosch, M. Vojta and P. Wolfle, "Fermi-liquid instabilities at magnetic quantum phase transitions," Rev. Mod. Phys. **79**, 1015 (2007).

[12] D. J. Gross and A. Neveu, "Dynamical Symmetry Breaking in Asymptotically Free Field Theories," Phys. Rev. D **10**, 3235 (1974).

[13] K. S. Novoselov, A. K. Geim, S. V. Morozov, D. Jiang, M. I. Katsnelson, I. V. Grigorieva, S. V. Dubonos and A. A. Firsov, "Two-dimensional gas of massless Dirac fermions in graphene," Nature **438**, 197 (2005).

[14] A. J. Leggett "What DO we know about high Tc?," Nat. Phys. **2**, 134 (2006).

[15] J. Zaanen, S. Chakravarty, T. Senthil, P. Anderson, P. Lee, J. Schmalian, M. Imada, D. Pines, M. Randeria, C. Varma, M. Vojta, M. Rice, "Towards a complete theory of high Tc," Nat. Phys. **2**, 138 (2006).

[16] F. Liang, C. L. Kane and E. J. Mele, "Topological Insulators in Three Dimensions," Phys. Rev. Lett. **98**, 106803 (2007).

[17] M. Z. Hasan and C. L. Kane, "Topological Insulators," Rev. Mod. Phys. **82**, 3045 (2010).

[18] X.-L. Qi and S.-C. Zhang, "Topological insulators and superconductors," Rev. Mod. Phys. **83** 1057 (2011).

[19] S. Raghu, X. L. Qi, C. Honerkamp, S.-C. Zhang "Topological Mott Insulators," Phys. Rev. Lett. **100**, 156401 (2008).

[20] I. F. Herbut, V. Juricic and B. Roy, "Theory of interacting electrons on the honeycomb lattice," Phys. Rev. B **79**, 085116 (2009).

[21] V. P. Gusynin, S. G. Sharapov and J. P. Carbotte, "AC conductivity of graphene: from tight-binding model to 2+1-dimensional quantum electrodynamics," Int. J. Mod. Phys. B **21**, 4611 (2007).

[22] M. Vojta, Y. Zhang and S. Sachdev, "Quantum Phase Transitions in d-Wave Superconductors," Phys. Rev. Lett. **85**, 4940 (2000).

[23] D. V. Khveshchenko and J. Paaske, "Incipient nodal pairing in planar d-wave superconductors," Phys. Rev. Lett. **86**, 4672 (2001).

[24] E. H. Fradkin, "Field theories of condensed matter systems," Redwood City, USA: Addison-Wesley (1991) 350 p. (Frontiers in physics, 82)

[25] X. G. Wen, "Quantum field theory of many-body systems: From the origin of sound to an origin of light and electrons," Oxford, UK: Univ. Pr. (2004) 505 p.

[26] F. D. M. Haldane, "Model for a Quantum Hall Effect without Landau Levels: Condensed-Matter Realization of the 'Parity Anomaly'," Phys. Rev. Lett. **61**, 2015 (1988).

[27] K. L. Lee, B. Grémaud, R. Han, B.-G. Englert and C. Miniatura, "Ultracold fermions in a graphene-type optical lattice," Phys. Rev. A **80** 043411 (2009).

[28] L. K. Lim, A. Hemmerich, and C. M. Smith, "Artificial staggered magnetic field for ultracold atoms in optical lattices," Phys. Rev. A **81** 023404 (2010).

[29] D. V. Khveshchenko, "Ghost Excitonic Insulator Transition in Layered Graphite," Phys. Rev. Lett. **87**, 246802 (2001).

[30] I. F. Herbut, "Interactions and phase transitions on graphene's honeycomb lattice," Phys. Rev. Lett. **97**, 146401 (2006).

[31] J. Braun, H. Gies and D. D. Scherer, "Asymptotic safety: a simple example," Phys. Rev. D **83**, 085012 (2011).

[32] D. D. Scherer and H. Gies, "Renormalization Group Study of Magnetic Catalysis in the 3d Gross-Neveu Model," Phys. Rev. B **85**, 195417 (2012).

[33] D. D. Scherer, J. Braun and H. Gies, in preparation.

[34] H. Gies and L. Janssen, "UV fixed-point structure of the three-dimensional Thirring model," Phys. Rev. D **82**, 085018 (2010).

[35] Wolfram Research, Inc., Mathematica, Version 7.0, Champaign, IL (2008).

[36] C. S. Fischer, "Infrared properties of QCD from Dyson-Schwinger equations," J. Phys. G G **32**, R253 (2006)

[37] E. S. Swanson, "A Primer on Functional Methods and the Schwinger-Dyson Equations," AIP Conf. Proc. **1296**, 75 (2010)

[38] T. Matsubara, "A New approach to quantum statistical mechanics," Prog. Theor. Phys. **14**, 351 (1955).

[39] C. Wetterich, "Exact evolution equation for the effective potential," Phys. Lett. B **301**, 90 (1993).

[40] H. Gies, "Running coupling in Yang-Mills theory: A flow equation study," Phys. Rev. D **66**, 025006 (2002).

[41] J. Berges, N. Tetradis and C. Wetterich, "Nonperturbative renormalization flow in quantum field theory and statistical physics," Phys. Rept. **363**, 223 (2002).

[42] J. M. Pawlowski, "Aspects of the functional renormalisation group," Annals Phys. **322**, 2831 (2007).

[43] H. Gies, "Introduction to the functional RG and applications to gauge theories," hep-ph/0611146.

[44] P. Kopietz, L. Bartosch and F. Schutz, "Introduction to the functional renormalization group," Lect. Notes Phys. **798**, 1 (2010).

[45] W. Metzner, M. Salmhofer, C. Honerkamp, V. Meden and K. Schonhammer, "Functional renormalization group approach to correlated fermion systems," arXiv:1105.5289 [cond-mat.str-el].

[46] J. Braun, "Fermion Interactions and Universal Behavior in Strongly Interacting Theories," arXiv:1108.4449 [hep-ph].

[47] D. F. Litim, "Optimization of the exact renormalization group," Phys. Lett. B **486**, 92 (2000).

[48] D. F. Litim, "Optimized renormalization group flows," Phys. Rev. D **64**, 105007 (2001).

[49] D. F. Litim, "Mind the gap," Int. J. Mod. Phys. A **16**, 2081 (2001).

[50] H. Gies and M. M. Scherer, "Asymptotic safety of simple Yukawa systems," Eur. Phys. J. C **66**, 387 (2010).

[51] C. Wetterich, "Spinors in euclidean field theory, complex structures and discrete symmetries," Nucl. Phys. B **852**, 174 (2011)

[52] K. Gawedzki and A. Kupiainen, "Renormalization Of A Nonrenormalizable Quantum Field Theory," Nucl. Phys. B **262**, 33 (1985).

[53] M. Gomes, R. S. Mendes, R. F. Ribeiro and A. J. da Silva, "Gauge structure, anomalies and mass generation in a three-dimensional Thirring model," Phys. Rev. D **43**, 3516 (1991).

[54] L. L.D., in Niels Bohr and the Development of Physics edited by W. Pauli (Pergamon Press, London) (1955).

[55] M. Gell-Mann and F. E. Low, "Quantum electrodynamics at small distances," Phys. Rev. **95**, 1300 (1954).

[56] M. Gockeler, R. Horsley, V. Linke, P. E. L. Rakow, G. Schierholz and H. Stuben, "Is there a Landau pole problem in QED?," Phys. Rev. Lett. **80**, 4119 (1998).

[57] H. Gies and J. Jaeckel, "Renormalization flow of QED," Phys. Rev. Lett. **93**, 110405 (2004).

[58] E. Brezin, J. C. Le Guillou and J. Zinn-Justin, "Field Theoretical Approach to Critical Phenomena," In *Phase Transitions and Critical Phenomena, Vol.6*, London 1976, 125-247.

[59] M. Luscher and P. Weisz, "Scaling Laws and Triviality Bounds in the Lattice phi**4 Theory. 1. One Component Model in the Symmetric Phase," Nucl. Phys. B **290**, 25 (1987).

[60] U. Wolff, "Precision check on triviality of phi**4 theory by a new simulation method," Phys. Rev. D **79**, 105002 (2009).

[61] B. Rosenstein, B. J. Warr and S. H. Park, "The Four Fermi Theory Is Renormalizable in (2+1)-Dimensions," Phys. Rev. Lett. **62**, 1433 (1989).

[62] K. Gawedzki and A. Kupiainen, "Renormalizing The Nonrenormalizable," Phys. Rev. Lett. **55**, 363 (1985).

[63] C. de Calan, P. A. Faria da Veiga, J. Magnen and R. Seneor, "Constructing the three-dimensional Gross-Neveu model with a large number of flavor components," Phys. Rev. Lett. **66**, 3233 (1991).

[64] J. Zinn-Justin, "Four fermion interaction near four-dimensions," Nucl. Phys. B **367**, 105 (1991).

[65] A. Hasenfratz, P. Hasenfratz, K. Jansen, J. Kuti and Y. Shen, "The Equivalence of the top quark condensate and the elementary Higgs field," Nucl. Phys. B **365**, 79 (1991).

[66] S. Hands, A. Kocic and J. B. Kogut, "Four Fermi theories in fewer than four-dimensions," Annals Phys. **224**, 29 (1993).

[67] L. Karkkainen, R. Lacaze, P. Lacock and B. Petersson, "Critical behavior of the 3-d Gross-Neveu and Higgs-Yukawa models," Nucl. Phys. B **415**, 781 (1994) [Erratum-ibid. B **438**, 650 (1995)].

[68] M. Niedermaier and M. Reuter, "The Asymptotic Safety Scenario in Quantum Gravity," Living Rev. Rel. **9**, 5 (2006).

[69] R. Percacci, "Asymptotic Safety," In *Oriti, D. (ed.): Approaches to quantum gravity* 111-128.

[70] O. J. Rosten, "Fundamentals of the Exact Renormalization Group," Phys. Rept. **511**, 177 (2012).

[71] H. Gies, J. Jaeckel and C. Wetterich, "Towards a renormalizable standard model without fundamental Higgs scalar," Phys. Rev. D **69**, 105008 (2004).

[72] H. Gies, C. Gneiting, unpublished.

[73] H. Gies, S. Rechenberger and M. M. Scherer, "Towards an Asymptotic-Safety Scenario for Chiral Yukawa Systems," Eur. Phys. J. C **66**, 403 (2010).

[74] G. Gat, A. Kovner and B. Rosenstein, "Chiral phase transitions in d = 3 and renormalizability of four Fermi interactions," Nucl. Phys. B **385**, 76 (1992).

[75] J. A. Gracey, "Computation of critical exponent eta at O(1/N**3) in the four Fermi model in arbitrary dimensions," Int. J. Mod. Phys. A **9**, 727 (1994).

[76] A. N. Vasiliev, S. E. Derkachov, N. A. Kivel and A. S. Stepanenko, "The 1/n expansion in the Gross-Neveu model: Conformal bootstrap calculation of the index eta in order 1/n**3," Theor. Math. Phys. **94**, 127 (1993) [Teor. Mat. Fiz. **94**, 179 (1993)].

[77] E. Focht, J. Jersak and J. Paul, "Interplay of universality classes in a three-dimensional Yukawa model," Phys. Rev. D **53**, 4616 (1996).

[78] T. Reisz, "The Gross-Neveu model and QCDs chiral phase transition," In *Wuppertal 1997, Field theoretical tools for polymer and particle physics* 192-230.

[79] E. Babaev, "Mass generation without symmetry breakdown in the chiral Gross-Neveu model at finite temperature and finite N in (2+1)-dimensions," Phys. Lett. B **497**, 323 (2001).

[80] F. Hofling, C. Nowak and C. Wetterich, "Phase transition and critical behavior of the D = 3 Gross-Neveu model," Phys. Rev. B **66**, 205111 (2002).

[81] L. Rosa, P. Vitale and C. Wetterich, "Critical exponents of the Gross-Neveu model from the effective average action," Phys. Rev. Lett. **86**, 958 (2001).

[82] J. Jaeckel and C. Wetterich, "Flow equations without mean field ambiguity," Phys. Rev. D **68**, 025020 (2003).

[83] J. Jaeckel, "Effective actions for strongly interacting fermionic systems," hep-ph/0309090.

[84] H. Gies, L. Janssen, S. Rechenberger and M. M. Scherer, "Phase transition and critical behavior of d=3 chiral fermion models with left/right asymmetry," Phys. Rev. D **81**, 025009 (2010).

[85] B. Rosenstein, B. J. Warr and S. H. Park, "Thermodynamics Of (2+1)-dimensional Four Fermi Models," Phys. Rev. D **39**, 3088 (1989).

[86] S. Hands, A. Kocic and J. B. Kogut, "The Four Fermi model in three-dimensions at nonzero density and temperature," Nucl. Phys. B **390**, 355 (1993)

[87] S. Hands, S. Kim and J. B. Kogut, "The U(1) Gross-Neveu model at nonzero chemical potential," Nucl. Phys. B **442**, 364 (1995).

[88] V. Schon and M. Thies, "Emergence of Skyrme crystal in Gross-Neveu and 't Hooft models at finite density," Phys. Rev. D **62**, 096002 (2000).

[89] M. Thies and K. Urlichs, "Revised phase diagram of the Gross-Neveu model," Phys. Rev. D **67**, 125015 (2003).

[90] M. Thies, "Analytical solution of the Gross-Neveu model at finite density," Phys. Rev. D **69**, 067703 (2004).

[91] G. Basar and G. V. Dunne, "Self-consistent crystalline condensate in chiral Gross-Neveu and Bogoliubov-de Gennes systems," Phys. Rev. Lett. **100**, 200404 (2008).

[92] G. Basar and G. V. Dunne, "A Twisted Kink Crystal in the Chiral Gross-Neveu model," Phys. Rev. D **78**, 065022 (2008).

[93] P. Castorina, M. Mazza and D. Zappala, "Renormalization group analysis of the three-dimensional Gross-Neveu model at finite temperature and density," Phys. Lett. B **567**, 31 (2003).

[94] R. Stratonovich, "A method for calculating quantum distribution functions," Dokl. Akad. Nauk. **115**, 1097 (1957).

[95] J. Hubbard, "Calculation of partition functions," Phys. Rev. Lett. **3**, 77 (1959).

[96] D. Nickel, "Inhomogeneous phases in the Nambu-Jona-Lasino and quark-meson model," Phys. Rev. D **80**, 074025 (2009).

[97] T. Kojo, Y. Hidaka, L. McLerran and R. D. Pisarski, "Quarkyonic Chiral Spirals," Nucl. Phys. A **843**, 37 (2010).

[98] F. Cooper and V. M. Savage, "Dynamics of the chiral phase transition in the (2+1)-dimensional Gross-Neveu model," Phys. Lett. B **545**, 307 (2002).

[99] J. Zinn-Justin, "Quantum field theory and critical phenomena," Int. Ser. Monogr. Phys. **113**, 1 (2002).

[100] S. Hands, A. Kocic and J. B. Kogut, "Compositeness, anomalous dimensions and renormalizability in four Fermi theories," Phys. Lett. B **273**, 111 (1991).

[101] J. A. Gracey, "Calculation of exponent eta to O(1/N**2) in the O(N) Gross-Neveu model," Int. J. Mod. Phys. A **6**, 395 (1991), [Erratum-ibid. A **6**, 2755 (1991)].

[102] J. A. Gracey, "Computation of Beta-prime (g(c)) at O(1/N**2) in the O(N) Gross-Neveu model in arbitrary dimensions," Int. J. Mod. Phys. A **9**, 567 (1994).

[103] J. A. Gracey, "The Beta function of the chiral Gross-Neveu model at O(1 / N**2)," Phys. Rev. D **50**, 2840 (1994), [Erratum-ibid. D **59**, 109904 (1999)].

[104] N. Tetradis and D. F. Litim, "Analytical solutions of exact renormalization group equations," Nucl. Phys. B **464**, 492 (1996).

[105] S. Diehl, H. Gies, J. M. Pawlowski and C. Wetterich, "Flow equations for the BCS-BEC crossover," Phys. Rev. A **76**, 021602 (2007).

[106] S. Diehl, H. Gies, J. M. Pawlowski and C. Wetterich, "Renormalisation flow and universality for ultracold fermionic atoms," Phys. Rev. A **76**, 053627 (2007).

[107] I. S. Gradshteyn and I. M. Ryzhik, Table of integrals, series, and products (Jeffrey, Alan (ed.), Academic Press, 2000).

[108] J. Braun, "Thermodynamics of QCD low-energy models and the derivative expansion of the effective action," Phys. Rev. D **81**, 016008 (2010).

[109] N. Tetradis and C. Wetterich, "Critical exponents from effective average action," Nucl. Phys. B **422**, 541 (1994).

[110] D. F. Litim and J. M. Pawlowski, "Predictive power of renormalization group flows: A Comparison," Phys. Lett. B **516**, 197 (2001).

[111] D. F. Litim, "Critical exponents from optimized renormalization group flows," Nucl. Phys. B **631**, 128 (2002).

[112] C. Bervillier, A. Juttner and D. F. Litim, "High-accuracy scaling exponents in the local potential approximation," Nucl. Phys. B **783**, 213 (2007).

[113] F. Benitez, J. -P. Blaizot, H. Chate, B. Delamotte, R. Mendez-Galain and N. Wschebor, "Solutions of renormalization group flow equations with full momentum dependence," Phys. Rev. E **80**, 030103 (2009).

[114] D. F. Litim and D. Zappala, "Ising exponents from the functional renormalisation group," Phys. Rev. D **83**, 085009 (2011).

[115] J. Braun, C. S. Fischer and H. Gies, "Beyond Miransky Scaling," Phys. Rev. D **84**, 034045 (2011)

[116] C. Strouthos and J. B. Kogut, "The Phases of Non-Compact QED(3)," PoS LAT **2007**, 278 (2007)

[117] H. Caldas and R. O. Ramos, "Magnetization of planar four-fermion systems," Phys. Rev. B **80**, 115428 (2009).

[118] A. Barducci, R. Casalbuoni, M. Modugno, G. Pettini and R. Gatto, "Thermodynamics of the massive Gross-Neveu model," Phys. Rev. D **51**, 3042 (1995)

[119] A. Barducci, M. Modugno and G. Pettini, "The massive Gross-Neveu model at finite temperature and density," Nucl. Phys. Proc. Suppl. **39BC**, 459 (1995).

[120] A. Barducci, R. Casalbuoni, M. Modugno, G. Pettini and R. Gatto, "Low temperature dominance of pion - like excitations in the massive Gross-Neveu model at order 1/N," Phys. Rev. D **55**, 2247 (1997)

[121] A. Barducci, R. Casalbuoni, M. Modugno, G. Pettini and R. Gatto, "1/N(c) expansion for the partition function in four fermion models," Mod. Phys. Lett. A **11**, 1579 (1996)

[122] S. Hands, "Four fermion models at nonzero density," Nucl. Phys. A **642**, 228 (1998)

[123] J. B. Kogut and C. G. Strouthos, "Chiral symmetry restoration in the three-dimensional four fermion model at nonzero temperature and density," Phys. Rev. D **63**, 054502 (2001)

[124] D. Mesterhazy, private communication.

[125] B. -J. Schaefer and J. Wambach, "The Phase diagram of the quark meson model," Nucl. Phys. A **757**, 479 (2005)

[126] J. B. Kogut, M. A. Stephanov and C. G. Strouthos, "Critical region of the finite temperature chiral transition," Phys. Rev. D **58**, 096001 (1998)

[127] L. Onsager, "Crystal statistics. 1. A Two-dimensional model with an order disorder transition," Phys. Rev. **65**, 117 (1944).

[128] V. P. Gusynin, V. A. Miransky and I. A. Shovkovy, "Dynamical flavor symmetry breaking by a magnetic field in (2+1)-dimensions," Phys. Rev. D **52**, 4718 (1995).

[129] V. P. Gusynin, V. A. Miransky and I. A. Shovkovy, "Dimensional reduction and dynamical chiral symmetry breaking by a magnetic field in (3+1)-dimensions," Phys. Lett. B **349**, 477 (1995).

[130] V. P. Gusynin, V. A. Miransky and I. A. Shovkovy, "Dimensional reduction and catalysis of dynamical symmetry breaking by a magnetic field," Nucl. Phys. B **462**, 249 (1996).

[131] V. P. Gusynin and S. G. Sharapov, "Unconventional integer quantum Hall effect in graphene," Phys. Rev. Lett. **95**, 146801 (2005).

[132] D. V. Khveshchenko, "Magnetic-Field-Induced Insulating Behavior in Highly Oriented Pyrolitic Graphite," Phys. Rev. Lett. **87**, 206401 (2001).

[133] H. Leal and D. V. Khveshchenko, "Excitonic instability in two-dimensional degenerate semimetals," Nucl. Phys. B **687**, 323 (2004).

[134] I. F. Herbut, "Theory of integer quantum Hall effect in graphene," Phys. Rev. B **75**, 165411 (2007).

[135] V. P. Gusynin, V. A. Miransky, S. G. Sharapov and I. A. Shovkovy, "Excitonic gap, phase transition, and quantum Hall effect in graphene," Phys. Rev. B **74**, 195429 (2006).

[136] V. P. Gusynin and S. G. Sharapov, "Transport of Dirac quasiparticles in graphene: Hall and optical conductivities," Phys. Rev. B **73**, 245411 (2006).

[137] V. P. Gusynin, S. G. Sharapov and J. P. Carbotte, "Unusual microwave response of Dirac quasiparticles in graphene," Phys. Rev. Lett. **96**, 256802 (2006).

[138] G. W. Semenoff, I. A. Shovkovy and L. C. R. Wijewardhana, "Phase transition induced by a magnetic field," Mod. Phys. Lett. A **13**, 1143 (1998).

[139] K. Krishana, N. P. Ong, Y. Zhang, et al. 1999, "Quasiparticle thermal Hall angle and magnetoconductance in $YBa_2Cu_3O_x$," Phys. Rev. Lett. **82**, 5108 (1999).

[140] D. V. Khveshchenko, W. F. Shively, "Excitonic pairing between nodal fermions," Phys. Rev. B **73**, 115104 (2006).

[141] E. J. Ferrer and V. de la Incera, "Dynamically Induced Zeeman Effect in Massless QED," Phys. Rev. Lett. **102**, 050402 (2009).

[142] E. J. Ferrer and V. de la Incera, "Dynamically Generated Anomalous Magnetic Moment in Massless QED," Nucl. Phys. B **824**, 217 (2010).

[143] E. J. Ferrer, V. de la Incera and A. Sanchez, "Paraelectricity in Magnetized Massless QED," Phys. Rev. Lett. **107**, 041602 (2011).

[144] V. Skokov, A. Y. Illarionov and V. Toneev, "Estimate of the magnetic field strength in heavy-ion collisions," Int. J. Mod. Phys. A **24**, 5925 (2009).

[145] D. E. Kharzeev, L. D. McLerran and H. J. Warringa, "The Effects of topological charge change in heavy ion collisions: 'Event by event P and CP violation'," Nucl. Phys. A **803**, 227 (2008).

[146] K. Fukushima, D. E. Kharzeev and H. J. Warringa, "The Chiral Magnetic Effect," Phys. Rev. D **78**, 074033 (2008).

[147] J. S. Schwinger, "On gauge invariance and vacuum polarization," Phys. Rev. **82**, 664 (1951).

[148] W. Dittrich and H. Gies, "Probing the quantum vacuum. Perturbative effective action approach in quantum electrodynamics and its application," Springer Tracts Mod. Phys. **166**, 1 (2000).

[149] A. V. Kuznetsov and A. A. Okrugin, "The Exact Electron Propagator in a Magnetic Field as the Sum over Landau Levels on a Basis of the Dirac Equation Exact Solutions," Int. J. Mod. Phys. A **26**, 2725 (2011)

[150] G. W. Semenoff, I. A. Shovkovy and L. C. R. Wijewardhana, "Universality and the magnetic catalysis of chiral symmetry breaking," Phys. Rev. D **60**, 105024 (1999).

[151] I. A. Shushpanov and A. V. Smilga, "Quark condensate in a magnetic field," Phys. Lett. B **402**, 351 (1997).

[152] T. D. Cohen, D. A. McGady and E. S. Werbos, "The Chiral condensate in a constant electromagnetic field," Phys. Rev. C **76**, 055201 (2007).

[153] A. V. Zayakin, "QCD Vacuum Properties in a Magnetic Field from AdS/CFT: Chiral Condensate and Goldstone Mass," JHEP **0807**, 116 (2008).

[154] A. J. Mizher, M. N. Chernodub and E. S. Fraga, "Phase diagram of hot QCD in an external magnetic field: possible splitting of deconfinement and chiral transitions," Phys. Rev. D **82**, 105016 (2010).

[155] R. Gatto and M. Ruggieri, "Dressed Polyakov loop and phase diagram of hot quark matter under magnetic field," Phys. Rev. D **82**, 054027 (2010).

[156] J. K. Boomsma and D. Boer, "The Influence of strong magnetic fields and instantons on the phase structure of the two-flavor NJL model," Phys. Rev. D **81**, 074005 (2010).

[157] G. S. Bali, F. Bruckmann, G. Endrodi, Z. Fodor, S. D. Katz, S. Krieg, A. Schafer and K. K. Szabo, "The QCD phase diagram for external magnetic fields," arXiv:1111.4956 [hep-lat].

[158] K. G. Klimenko, "Three-dimensional Gross-Neveu model in an external magnetic field," Theor. Math. Phys. **89**, 1161 (1992) [Teor. Mat. Fiz. **89**, 211 (1991)].

[159] K. G. Klimenko, "Three-dimensional Gross-Neveu model at nonzero temperature and in an external magnetic field," Z. Phys. C **54**, 323 (1992).

[160] I. V. Krive and S. A. Naftulin, "Dynamical symmetry breaking and phase transitions in a three-dimensional Gross-Neveu model in a strong magnetic field," Phys. Rev. D **46**, 2737 (1992).

[161] S. Kanemura, H. -T. Sato and H. Tochimura, "Thermodynamic Gross-Neveu model under constant electromagnetic field," Nucl. Phys. B **517**, 567 (1998).

[162] J. Alexandre, K. Farakos and G. Koutsoumbas, "Magnetic catalysis in QED(3) at finite temperature: Beyond the constant mass approximation," Phys. Rev. D **63**, 065015 (2001).

[163] C. N. Leung, Y. J. Ng and A. W. Ackley, "Schwinger-Dyson equation approach to chiral symmetry breaking in an external magnetic field," Phys. Rev. D **54**, 4181 (1996).

[164] V. P. Gusynin, V. A. Miransky and I. A. Shovkovy, "Theory of the magnetic catalysis of chiral symmetry breaking in QED," Nucl. Phys. B **563**, 361 (1999).

[165] D. K. Hong, Y. Kim and S. -J. Sin, "RG analysis of magnetic catalysis in dynamical symmetry breaking," Phys. Rev. D **54**, 7879 (1996).

[166] D. K. Hong, "Magnetic catalysis in quantum electrodynamics," Phys. Rev. D **57**, 3759 (1998).

[167] K. Fukushima and J. M. Pawlowski, in preparation (2011).

[168] R. R. Parwani, "On chiral symmetry breaking by external magnetic fields in QED in three-dimensions," Phys. Lett. B **358**, 101 (1995).

[169] G. V. Dunne and T. Hall, "Inhomogeneous condensates in planar QED," Phys. Rev. D **53**, 2220 (1996).

[170] J. Braun and A. Janot, "Dynamical Locking of the Chiral and the Deconfinement Phase Transition in QCD," arXiv:1102.4841 [hep-ph].

[171] H. Gies and C. Wetterich, "Renormalization flow of bound states," Phys. Rev. D **65**, 065001 (2002).

[172] J. Braun, "The QCD Phase Boundary from Quark-Gluon Dynamics," Eur. Phys. J. C **64**, 459 (2009).

[173] F. Synatschke, J. Braun and A. Wipf, "N=1 Wess Zumino Model in d=3 at zero and finite temperature," Phys. Rev. D **81**, 125001 (2010).

Appendix A

Technical Details

A.1 Wick Rotation

In this thesis we consider fermionic quantum field theories in Euclidean spacetime with metric $\delta_{\mu\nu} = \mathrm{diag}(+1, +1, +1)$. The starting point for relativistic theories is a given action in Minkowski spacetime with metric $\eta_{\mu\nu} = \mathrm{diag}(+1, -1, -1)$. The free, Minkowskian action for massless Dirac fermions reads

$$S_M = \int_x \bar{\psi}_M \mathrm{i} \not{\partial}_M \psi_M, \tag{A.1}$$

with $\not{\partial}_M = \gamma_M^\mu \partial_\mu$ and the gamma matrices fulfill

$$\{\gamma_M^\mu, \gamma_M^\nu\} = 2\eta^{\mu\nu} \mathbb{1}_4. \tag{A.2}$$

The so-called Wick rotation corresponds to the substitution $t \to -\mathrm{i}\tau$ in Eq. (A.1), where τ is the imaginary time variable. We perform the following substitutions in the kinetic term (the spacetime measure is of course also sensitive to this substitution and picks up a factor $-\mathrm{i}$):

$$\begin{aligned} t &\to -\mathrm{i}\tau, \\ \partial_t &\to \mathrm{i}\partial_\tau, \\ \psi_M &\to \psi, \\ \bar{\psi}_M &\to \mathrm{i}\bar{\psi}, \\ \gamma_M^0 &\to -\gamma_0, \\ \gamma_M^i &\to -\mathrm{i}\gamma_i, \end{aligned} \tag{A.3}$$

This yields the Euclidean expression

$$-\mathrm{i}S_M = S = \int_x \bar{\psi}\mathrm{i}\not{\partial}\psi, \tag{A.4}$$

with Euclidean gamma matrices satisfying

$$\{\gamma_\mu, \gamma_\nu\} = 2\delta_{\mu\nu}\mathbb{1}_4. \tag{A.5}$$

Further bilinears and operators with higher mass dimension need to be Euclidean invariants. Together with an appropriate definition of complex conjugation for Dirac spinor fields, a complete list of invariant bilinears was given in [51]. As to the mass term, since $\bar{\psi}\psi$ is purely imaginary, for it to be real it enters the action as

$$\int_x \mathrm{i}\bar{m}_\mathrm{f}\bar{\psi}\psi., \tag{A.6}$$

which can be confirmed by the substitution rules Eq. (A.3)

A.2 Fourier Conventions

We formulate the Fourier conventions used in this thesis for a superfield $\Phi_a(x)$ (see A.3 for a definition and conventions). We define

$$\Phi_a(x) = \int_p \mathrm{e}^{\mathrm{i}px}\,\Phi_a(p), \tag{A.7}$$

where $\int_p = \int \frac{d^dp}{(2\pi)^d}$ is the Euclidean integration in momentum space at zero temperature, $T = 0$, and $px \equiv \delta_{\mu\nu}p_\mu x_\nu$. The inverse Fourier transform is then given by

$$\Phi_a(p) = \int_x \mathrm{e}^{-\mathrm{i}px}\,\Phi_a(x), \tag{A.8}$$

with $\int_x = \int d^dx$ for the integration over Euclidean spacetime. The delta functions obtained by functional field derivatives are thus normalized as

$$\frac{\delta\Phi_a(x)}{\delta\Phi_b(x')} = \delta_{ab}\,\delta(x - x') \tag{A.9}$$

in real space, and

$$\frac{\delta\Phi_a(p)}{\delta\Phi_b(p')} = (2\pi)^d\delta_{ab}\,\delta(p - p') \tag{A.10}$$

for the corresponding momentum space Fourier amplitudes. As usual, the delta functions expressed as the Fourier transform of 1 is thus given by

$$\delta(x-x') = \int_p \mathrm{e}^{\mathrm{i}(x-x')p} \tag{A.11}$$

and

$$(2\pi)^d \delta(p-p') = \int_x \mathrm{e}^{-\mathrm{i}(p-p')x}, \tag{A.12}$$

which for $p = p'$ yields $\delta(0) = \Omega$, with Ω denoting spacetime volume. At finite temperature, $T > 0$, in real space we need the substitution

$$\int_x = \int d^d x \qquad \to \qquad \int_x = \int_0^\beta \mathrm{d}\tau \int \mathrm{d}^{d-1}\boldsymbol{x}, \tag{A.13}$$

while in momentum space the corresponding changes are

$$p_0 \to p_0 = \begin{cases} \omega_n = 2\pi n/\beta, & \text{bosonic} \\ \nu_n = (2n+1)\pi/\beta, & \text{fermionic} \end{cases} \quad \text{for } n \in \mathbb{Z}, \tag{A.14}$$

and

$$\int_p = \int \frac{d^d p}{(2\pi)^d} \qquad \to \qquad \beta^{-1} \sum_{n\in\mathbb{Z}} \int_{\boldsymbol{p}} = \beta^{-1} \sum_{n\in\mathbb{Z}} \int \frac{\mathrm{d}^{d-1}\boldsymbol{p}}{(2\pi)^{d-1}}. \tag{A.15}$$

A.3 Superfield Formalism

In this appendix, we give the definition of the conventional superfield formulation of the Wetterich flow equation adapted to the (partially bosonized) Gross-Neveu model, treating fermionic and bosonic degrees of freedom on an equal footing. Here, we focus on the momentum space representation of fields, which is usually employed in the derivation of flow equations. We first combine the Fourier transformed Dirac spinors $\bar{\psi}_j(p)$, $\psi_j(p)$ into Nambu spinors defined as

$$\Psi_j(p) \equiv \begin{pmatrix} \psi_j(p) \\ \bar{\psi}_j^T(-p) \end{pmatrix}, \quad \Psi_j^T(-p) \equiv \left(\psi_j^T(-p), \bar{\psi}_j(p)\right), \tag{A.16}$$

and rearrange fermionic bilinears according to

$$\int_{p,p'} \bar{\psi}_j(p) M^+(p,p') \psi_j(p') \equiv \tfrac{1}{2} \int_{p,p'} \Psi_j^T(-p) M(p,p') \Psi_j(p'). \tag{A.17}$$

The matrix M is defined in Nambu space as

$$M \equiv \begin{pmatrix} 0 & M^- \\ M^+ & 0 \end{pmatrix}, \tag{A.18}$$

with momentum space components $M^+(p,p')$ and $M^-(p,p') \equiv -M^T(-p',-p)$. We now further collect the bosonic and all N_f fermionic degrees of freedom into a single, $(N_\mathrm{f}+1)$-component *superfield* Φ with components Φ_a, $a = 1,\ldots,N_\mathrm{f}+1$, which in Fourier representation reads

$$\Phi(p) \equiv \begin{pmatrix} \sigma(p) \\ \Psi_1(p) \\ \vdots \\ \Psi_{N_\mathrm{f}}(p) \end{pmatrix}, \qquad \Phi^T(-p) \equiv \left(\sigma(-p), \Psi_1^T(-p), A\ldots, \Psi_{N_\mathrm{f}}^T(-p)\right). \tag{A.19}$$

At this stage we also introduce left- and right-functional derivatives with respect to a superfield Φ by:

$$\frac{\overrightarrow{\delta}}{\delta\Phi^T(-p)} \equiv \begin{pmatrix} \frac{\overrightarrow{\delta}}{\delta\sigma(-p)} \\ \frac{\overrightarrow{\delta}}{\delta\Psi_1^T(-p)} \\ \vdots \\ \frac{\overrightarrow{\delta}}{\delta\Psi_{N_\mathrm{f}}^T(-p)} \end{pmatrix}, \qquad \frac{\overleftarrow{\delta}}{\delta\Phi(p)} \equiv \left(\frac{\overleftarrow{\delta}}{\delta\sigma(p)}, \frac{\overleftarrow{\delta}}{\delta\Psi_1(p)}, \cdots, \frac{\overleftarrow{\delta}}{\delta\Psi_{N_\mathrm{f}}(p)}\right), \tag{A.20}$$

where

$$\frac{\overrightarrow{\delta}}{\delta\Psi^T(-p)} \equiv \begin{pmatrix} \frac{\overrightarrow{\delta}}{\delta\psi^T(-p)} \\ \frac{\overrightarrow{\delta}}{\delta\bar{\psi}(p)} \end{pmatrix}, \qquad \frac{\overleftarrow{\delta}}{\delta\Psi(p)} \equiv \left(\frac{\overleftarrow{\delta}}{\delta\psi(p)}, \frac{\overleftarrow{\delta}}{\delta\bar{\psi}^T(-p)}\cdot\right), \tag{A.21}$$

The product $(\cdot,\cdot)$ of two fields Φ, Ξ is defined in momentum space as

$$(\Phi,\Xi) \equiv \sum_a \int_p \Phi_a^T(-p)\Xi_a(p), \tag{A.22}$$

and similarly for a general superfield bilinear

$$(\Phi, M\,\Phi) \equiv \sum_{a,a'} \int_{p,p'} \Phi_a^T(-p) M_{a,a'}(p,p')\Phi_{a'}(p'), \tag{A.23}$$

with M acting in superfield space. The mixed boson-fermion action for the partially bosonized Gross-Neveu model can be compactly represented as

$$S[\Phi] = \frac{1}{2}(\Phi, G^{-1}\Phi), \tag{A.24}$$

where the inverse superfield propagator G^{-1} is specified by

$$G^{-1} = \begin{pmatrix} G_\sigma^{-1} & 0 \\ 0 & \mathbb{1}_{N_\mathrm{f}} \otimes G_\Psi^{-1} \end{pmatrix}. \tag{A.25}$$

The bare inverse propagator describing the bosonic sector of the Gross-Neveu model is simply given by

$$G_\sigma^{-1}(p,p') = (2\pi)^d \bar{m}^2 \delta(p-p'). \tag{A.26}$$

The Nambu propagator G_Ψ is related to the Dirac propagator G^+ by Eq. (A.17) and its inverse reads

$$G_\Psi^{-1} \equiv \begin{pmatrix} 0 & [G^-]^{-1} \\ [G^+]^{-1} & 0 \end{pmatrix}. \tag{A.27}$$

Here we exploited the trivial identity $[G^\pm]^{-1} = [G^{-1}]^\pm$. In momentum space the Dirac components of the bare inverse propagator G (in the partially bosonized description) reads

$$\begin{aligned} (G^+)^{-1}(p,p') &= -(2\pi)^d \not{p}\, \delta(p-p') + \mathrm{i}\bar{h}\sigma(p-p')\mathbb{1}_4, \\ (G^-)^{-1}(p,p') &= -(2\pi)^d \not{p}^T \delta(p-p') - \mathrm{i}\bar{h}\sigma(p-p')\mathbb{1}_4. \end{aligned} \tag{A.28}$$

A.4 Projection Rules for LPA′ Truncations

Here we collect the projection rules, from which one can obtain the flows of the effective potential $U_k(\rho)$, the Yukawa vertex $\bar{h}_k$ in the pointlike approximation, and the wave-function renormalizations $Z_{\sigma,k}$, $Z_{\psi,k}$ giving rise to anomalous dimensions $\eta_{\sigma,k}$, $\eta_{\psi,k}$. The flow equations for dimensionless renormalized quantities as displayed in Chap. 4 can then be obtained easily.

The fluctuation kernel $\Gamma_k^{(2)}[\Phi] = \bar{\Gamma}_k^{(2)} + \tilde{\Gamma}_k^{(2)}[\Phi]$ is split into a field-independent propagator part $\bar{\Gamma}_k^{(2)}$ (still containing background/reference configurations) and a field-dependent vertex part $\tilde{\Gamma}_k^{(2)}[\Phi]$. Anticipating condensation of the σ-field, we shift $\sigma(x) \to \sigma + \frac{1}{\sqrt{N_\mathrm{f}}}\chi(x)$, where $\chi(x)$ is the fluctuating part, and σ captures a homogeneous chiral condensate, to be determined from the flow. We keep only the fluctuating part $\chi(x)$ in the definition of the fluctuating superfield $\Phi(x)$. From Eq. (4.38) we obtain for the vertex part (keeping only a single flavor species for clarity)

$$\tilde{\Gamma}_k^{(2)}[\Phi] = \left(\begin{array}{c|ccc} \tilde{\Gamma}_{\chi\chi} & \tilde{\Gamma}_{\chi\psi} & \tilde{\Gamma}_{\chi\bar{\psi}^T} & \cdots \\ \hline \tilde{\Gamma}_{\psi^T\chi} & \tilde{\Gamma}_{\psi^T\psi} & \tilde{\Gamma}_{\psi^T\bar{\psi}^T} & \cdots \\ \tilde{\Gamma}_{\bar{\psi}\chi} & \tilde{\Gamma}_{\bar{\psi}\psi} & \tilde{\Gamma}_{\bar{\psi}\bar{\psi}^T} & \cdots \\ \vdots & \vdots & \vdots & \ddots \end{array}\right), \tag{A.29}$$

and the ellipses indicate further flavor contributions. Computing the functional derivatives in momentum space representation, one arrives at

$$\begin{aligned}
\tilde{\Gamma}_{\chi\chi}(p,p') &= +\frac{1}{\sqrt{N_\mathrm{f}}}\frac{\partial^3}{\partial\sigma^3}U_k|_{\sigma=\sigma_0}\chi(p-p'),\\
\tilde{\Gamma}_{\chi\psi}(p,p') &= +\frac{1}{\sqrt{N_\mathrm{f}}}\mathrm{i}\bar{h}_k\bar{\psi}(p'-p),\\
\tilde{\Gamma}_{\chi\bar{\psi}^T}(p,p') &= -\frac{1}{\sqrt{N_\mathrm{f}}}\mathrm{i}\bar{h}_k\psi^T(p-p'),\\
\tilde{\Gamma}_{\psi^T\chi}(p,p') &= -\frac{1}{\sqrt{N_\mathrm{f}}}\mathrm{i}\bar{h}_k\bar{\psi}^T(p'-p),\\
\tilde{\Gamma}_{\bar{\psi}\chi}(p,p') &= +\frac{1}{\sqrt{N_\mathrm{f}}}\mathrm{i}\bar{h}_k\psi(p-p'),\\
\tilde{\Gamma}_{\psi^T\psi}(p,p') &= 0\\
\tilde{\Gamma}_{\psi^T\bar{\psi}^T}(p,p') &= -\frac{1}{\sqrt{N_\mathrm{f}}}\mathrm{i}\bar{h}_k\chi(p-p'),\\
\tilde{\Gamma}_{\bar{\psi}\psi}(p,p') &= +\frac{1}{\sqrt{N_\mathrm{f}}}\mathrm{i}\bar{h}_k\chi(p-p'),\\
\tilde{\Gamma}_{\bar{\psi}\bar{\psi}^T}(p,p') &= 0.
\end{aligned}$$

Since σ is a flavor singlet, within our truncation $\tilde{\Gamma}_k^{(2)}[\Phi]$ does not couple different flavors. The flow equation for the effective potential $U_k(\sigma)$ is obtained by evaluating Eq. (2.27) for $\chi = 0$, $\bar{\psi}_j = \psi_j = 0$, $\forall j$:

$$(2\pi)^d\delta(0)\partial_t U_k(\sigma) = \partial_t\Gamma_k[\Phi]|_{\Phi=0}. \tag{A.30}$$

The projection onto the Yukawa vertex in the pointlike approximation reads (again, we omit flavor indices due to the singlet structure of the Yukawa vertex)

$$(2\pi)^d\delta(0)\mathrm{i}\partial_t\bar{h}_k = \frac{1}{d_\gamma}\mathrm{tr}\,\frac{\overrightarrow{\delta}}{\delta\chi(q)}\frac{\overrightarrow{\delta}}{\delta\bar{\psi}(-p)}\partial_t\Gamma_k[\Phi]\frac{\overleftarrow{\delta}}{\delta\psi(p')}\bigg|_{\substack{\Phi=0\\q,p,p'=0}}. \tag{A.31}$$

The bosonic wave-function renormalization is extracted from

$$(2\pi)^d\delta(0)\partial_t Z_{\sigma,k} = \frac{1}{d}\,\Delta_p\left(\frac{\overrightarrow{\delta}}{\delta\chi(-p)}\partial_t\Gamma_k[\Phi]\frac{\overleftarrow{\delta}}{\delta\chi(p')}\right)\bigg|_{\substack{\Phi=0\\p,p'=0}}, \tag{A.32}$$

and similarly the fermionic wave-function renormalization

$$(2\pi)^d\delta(0)\partial_t Z_{\psi,k} = \frac{1}{d_\gamma d}\,\mathrm{tr}\left(\not{p}_p\frac{\overrightarrow{\delta}}{\delta\bar{\psi}(-p)}\partial_t\Gamma_k[\Phi]\frac{\overleftarrow{\delta}}{\delta\psi(p')}\right)\bigg|_{\substack{\Phi=0\\p,p'=0}}. \tag{A.33}$$

Here, we defined the momentum space differential operators $\Delta_p \equiv \frac{\partial^2}{\partial p_0^2} + \frac{\partial^2}{\partial p_1^2} + \cdots + \frac{\partial^2}{\partial p_{d-1}^2}$ and $\not{\partial}_p \equiv \gamma_0 \partial_{p_0} + \cdots + \gamma_{d-1}\partial_{p_{d-1}}$. Applying these functional derivatives to Eq. (2.30), we obtain the corresponding flow equations. The appearing regularized 1-loop integrals give rise to so-called threshold functions, which capture the scale behavior of the renormalization due to quantum fluctuations. We give the threshold functions for zero temperature in Appendix A.5 and threshold functions for finite temperature can be found in Appendix A.6.

A.5 Threshold Functions at Zero Temperature

In this appendix, we give the general expressions for threshold functions at zero temperature (cf. Chap. 4), suitable for the covariantly regularized partially bosonized system. Let us define the propagator functions[1] $\mathcal{G}_\psi(y;\omega_F) \equiv \frac{1}{(1+r_F)^2 y+\omega_F}$ and $\mathcal{G}_\sigma(y;\omega_B) \equiv \frac{1}{(1+r_B)y+\omega_B}$.

$$
\begin{aligned}
l_n^d(\omega_B;\eta_\sigma) &= \frac{\delta_{n,0}+n}{2}\int_0^\infty \mathrm{d}y\, y^{\frac{d}{2}} \left(\mathcal{G}_\sigma(y;\omega_B)\right)^{n+1} \frac{\partial_t(Z_{\sigma,k}\, r_B)}{Z_{\sigma,k}},\\
l_n^{(F)d}(\omega_F;\eta_\psi) &= (\delta_{n,0}+n)\int_0^\infty \mathrm{d}y\, y^{\frac{d}{2}} \left(\mathcal{G}_\psi(y;\omega_F)\right)^{n+1} \frac{(1+r_F)\partial_t(Z_{\sigma,k}\, r_F)}{Z_{\psi,k}},\\
l_{n,m}^{(FB)d}(\omega_F,\omega_B;\eta_\psi,\eta_\sigma) &= -\frac{1}{2}\int_0^\infty \mathrm{d}y\, y^{\frac{d-2}{2}} \tilde{\partial}_t \left\{(\mathcal{G}_\psi(y;\omega_F))^n (\mathcal{G}_\sigma(y;\omega_B))^m\right\},\\
m_2^{(F)d}(\omega_F;\eta_\psi) &= -\frac{1}{2}\int_0^\infty \mathrm{d}y\, y^{\frac{d}{2}} \tilde{\partial}_t \left(\frac{\partial}{\partial y}\mathcal{G}_\psi(y;\omega_F)\right)^2,\\
m_4^{(F)d}(\omega_F;\eta_\psi) &= -\frac{1}{2}\int_0^\infty \mathrm{d}y\, y^{\frac{d+2}{2}} \tilde{\partial}_t \left(\frac{\partial}{\partial y}[(1+r_F)\mathcal{G}_\psi(y;\omega_F)]\right)^2,\\
m_{n,m}^{d}(\omega_{B,1},\omega_{B,2};\eta_\sigma) &= -\frac{1}{2}\int_0^\infty \mathrm{d}y\, y^{\frac{d}{2}} \tilde{\partial}_t \left\{\left(\frac{\partial}{\partial y}\mathcal{G}_\sigma(y;\omega_{B,1})\right)^{n/2} \left(\frac{\partial}{\partial y}\mathcal{G}_\sigma(y;\omega_{B,2})\right)^{m/2}\right\},\\
m_{n,m}^{(FB)d}(\omega_F,\omega_B;\eta_\psi,\eta_\sigma) &= -\frac{1}{2}\int_0^\infty \mathrm{d}y\, y^{\frac{d}{2}} \tilde{\partial}_t \left\{(1+r_F)(\mathcal{G}_\psi(y;\omega_F))^n \left(\frac{\partial}{\partial y}\mathcal{G}_\sigma(y;\omega_B)\right)^{m/2}\right\}.
\end{aligned}
$$

The $\tilde{\partial}_t$-derivative acts on the regulator dependence as

$$
\tilde{\partial}_t|_\sigma = \left(-2y\frac{\partial}{\partial y} r_B - \eta_\sigma r_B\right)\frac{\partial}{\partial r_B}, \tag{A.34}
$$

$$
\tilde{\partial}_t|_\psi = \left(-2y\frac{\partial}{\partial y} r_F - \eta_\psi r_F\right)\frac{\partial}{\partial r_F}, \tag{A.35}
$$

[1] Here and in the following, we will suppress the y-dependence of $r_F(y)$ and $r_B(y)$, respectively, to keep the equations readable.

whenever it hits a bosonic or fermionic shape function, respectively. For covariant and optimized Litim shape functions [47–49] as used in Chap. 4,

$$r_B(y) = \left(\frac{1}{y} - 1\right)\Theta(1-y), \qquad r_F(y) = \left(\sqrt{\frac{1}{y}} - 1\right)\Theta(1-y), \tag{A.36}$$

the threshold functions can be evaluated in closed form and are given by

$$\begin{aligned}
l_n^d(\omega_B;\eta_\sigma) &= \frac{2}{d}\left(1-\frac{\eta_\sigma}{d+2}\right)\left(\frac{1}{1+\omega_B}\right)^n,\\
l_n^{(F)d}(\omega_F;\eta_\psi) &= \frac{2}{d}\left(1-\frac{\eta_\psi}{d+1}\right)\left(\frac{1}{1+\omega_F}\right)^n,\\
l_{n,m}^{(FB)d}(\omega_F,\omega_B;\eta_\psi,\eta_\sigma) &= \frac{2}{d}\left(\frac{1}{1+\omega_F}\right)^n\left(\frac{1}{1+\omega_B}\right)^m\left[\frac{1}{1+\omega_F}\left(1-\frac{\eta_\psi}{d+1}\right)+\frac{1}{1+\omega_B}\left(1-\frac{\eta_\sigma}{d+2}\right)\right],\\
m_2^{(F)d}(\omega_F;\eta_\psi) &= \left(\frac{1}{1+\omega_F}\right)^4,\\
m_4^{(F)d}(\omega_F;\eta_\psi) &= \left(\frac{1}{1+\omega_F}\right)^4+\frac{1-\eta_\psi}{d-2}\left(\frac{1}{1+\omega_F}\right)^3-\left(\frac{1-\eta_\psi}{2d-4}+\frac{1}{4}\right)\left(\frac{1}{1+\omega_F}\right)^2,\\
m_{n,m}^d(\omega_{B,1},\omega_{B,2};\eta_\sigma) &= \left(\frac{1}{1+\omega_{B,1}}\right)^n\left(\frac{1}{1+\omega_{B,2}}\right)^m,\\
m_{n,m}^{(FB)d}(\omega_F,\omega_B;\eta_\psi,\eta_\sigma) &= \left(1-\frac{\eta_\sigma}{d+1}\right)\left(\frac{1}{1+\omega_F}\right)^n\left(\frac{1}{1+\omega_B}\right)^{m/2}.
\end{aligned}$$

A.6 Threshold Functions at Finite Temperature

At finite temperature (as discussed in Chap. 5), we have to perform the substitutions Eq. (A.14), Eq. (A.15) to evaluate the regularized 1-loop diagrams. As for $T = 0$, we assume "covariant" regulators, i.e., we regularize both frequency sums and momentum integrations, and in the limit $T \to 0$, we obtain fully covariant regulators. The propagator functions are now defined as $\mathcal{G}_\psi(\tau c_n, y; \omega_F) \equiv \frac{1}{(1+r_F)^2[(\tau c_n)^2+y]+\omega_F}$ and $\mathcal{G}_\sigma(\tau c_n, y; \omega_B) \equiv \frac{1}{(1+r_B)[(\tau c_n)^2+y]+\omega_B}$, with dimensionless temperature parameter[2] $\tau = \frac{2\pi T}{k}$ and $c_n|_\psi = c_{F,n} = n + \frac{1}{2}$ or $c_n|_\sigma = c_{B,n} = n$ for $n \in \mathbb{Z}$. Whether a propagator function is evaluated for bosonic or fermionic Matsubara frequencies severely depends on the structure of the diagram at hand within a consistent gradient expansion, as thoroughly discussed in [172]. Arguments of shape functions are obtained by making the replacement $y \to (\tau c_n)^2 + y$. With the same

[2]Not to be confused with the imaginary time variable τ. It should be clear from the context, whether we refer to one or the other.

techniques and definitions as for $T = 0$ and with $v_d^{-1} = 2^{d+1}\pi^{d/2}\Gamma(d/2)$ accounting for Euclidean volume factors, we obtain

$$\begin{aligned}
l_n^d(\tau,\omega_B;\eta_\sigma) &= \frac{\delta_{n,0}+n}{2}\frac{v_{d-1}}{v_d}\frac{\tau}{2\pi}\sum_{n\in\mathbb{Z}}\int_0^\infty \mathrm{d}y\, y^{\frac{d-3}{2}}\times \\
&\quad ((\tau c_{B,n})^2+y)\left(\mathcal{G}_\sigma(\tau c_{B,n},y;\omega_B)\right)^{n+1}\frac{\partial_t(Z_{\sigma,k}\, r_B)}{Z_{\sigma,k}}, \\
l_n^{(F)d}(\tau,\omega_F;\eta_\psi) &= (\delta_{n,0}+n)\frac{v_{d-1}}{v_d}\frac{\tau}{2\pi}\sum_{n\in\mathbb{Z}}\int_0^\infty \mathrm{d}y\, y^{\frac{d-3}{2}}\times \\
&\quad ((\tau c_{F,n})^2+y)\left(\mathcal{G}_\psi(\tau c_{F,n},y;\omega_F)\right)^{n+1}\frac{(1+r_F)\partial_t(Z_{\sigma,k}\, r_F)}{Z_{\psi,k}}, \\
l_{n,m}^{(FB)}(\tau,\omega_F,\omega_B;\eta_\psi,\eta_\sigma) &= -\frac{1}{2}\frac{v_{d-1}}{v_d}\frac{\tau}{2\pi}\sum_{n\in\mathbb{Z}}\int_0^\infty \mathrm{d}y\, y^{\frac{d-3}{2}}\tilde\partial_t\left\{(\mathcal{G}_\psi(\tau c_{F,n},y;\omega_F))^n(\mathcal{G}_\sigma(\tau c_{F,n},y;\omega_B))^m\right\}, \\
m_2^{(F)d}(\tau,\omega_F;\eta_\psi) &= -\frac{1}{2}\frac{v_{d-1}}{v_d}\frac{d}{d-1}\frac{\tau}{2\pi}\sum_{n\in\mathbb{Z}}\int_0^\infty \mathrm{d}y\, y^{\frac{d-1}{2}}\tilde\partial_t\left(\frac{\partial}{\partial y}\mathcal{G}_\psi(\tau c_{F,n},y;\omega_F)\right)^2, \\
m_4^{(F)d}(\tau,\omega_F;\eta_\psi) &= -\frac{1}{2}\frac{v_{d-1}}{v_d}\frac{d}{d-1}\frac{\tau}{2\pi}\sum_{n\in\mathbb{Z}}\int_0^\infty \mathrm{d}y\, y^{\frac{d-1}{2}}\times \\
&\quad ((\tau c_{F,n})^2+y)\tilde\partial_t\left(\frac{\partial}{\partial y}\left[(1+r_F)\mathcal{G}_\psi(\tau c_{F,n},y;\omega_F)\right]\right)^2, \\
m_{n,m}^d(\tau,\omega_{B,1},\omega_{B,2};\eta_\sigma) &= -\frac{1}{2}\frac{v_{d-1}}{v_d}\frac{d}{d-1}\frac{\tau}{2\pi}\sum_{n\in\mathbb{Z}}\int_0^\infty \mathrm{d}y\, y^{\frac{d-1}{2}}\times \\
&\quad \tilde\partial_t\left\{\left(\frac{\partial}{\partial y}\mathcal{G}_\sigma(\tau c_{B,n},y;\omega_{B,1})\right)^{n/2}\left(\frac{\partial}{\partial y}\mathcal{G}_\sigma(\tau c_{B,n},y;\omega_{B,2})\right)^{m/2}\right\}, \\
m_{1,2}^{(FB)d}(\tau,\omega_F,\omega_B;\eta_\psi,\eta_\sigma) &= -\frac{1}{2}\frac{v_{d-1}}{v_d}\frac{d}{d-1}\frac{\tau}{2\pi}\sum_{n\in\mathbb{Z}}\int_0^\infty \mathrm{d}y\, y^{\frac{d-1}{2}}\times \\
&\quad \tilde\partial_t\left\{(1+r_F)(\mathcal{G}_\psi(y;\omega_F))\left(\frac{\partial}{\partial y}\mathcal{G}_\sigma(y;\omega_B)\right)\right\}.
\end{aligned}$$

"Covariant", optimized shape functions now read

$$r_B((\tau c_n)^2+y) = \left(\frac{1}{[(\tau c_n)^2+y]}-1\right)\Theta(1-[(\tau c_n)^2+y]), \tag{A.37}$$

$$r_F((\tau c_n)^2+y) = \left(\sqrt{\frac{1}{[(\tau c_n)^2+y]}}-1\right)\Theta(1-[(\tau c_n)^2+y]). \tag{A.38}$$

The $\tilde\partial_t$-derivative acts as before, with the replacement $y \to (\tau c_n)^2 + y$. The optimized covariant regulators lead to factorization of thermal and vacuum contributions to threshold functions. In the

following, full thermal threshold functions and their vacuum counterparts are distinguished by the dependence on the temperature parameter τ. We find

$$
\begin{aligned}
l_n^d(\tau,\omega_B;\eta_\sigma) &= \left(s_0^d(\tau)-\eta_\sigma \hat{s}_0^d(\tau)\right) l_n^d(\omega_B;0),\\
l_n^{(F)d}(\tau,\omega_F;\eta_\psi) &= \left(s_0^{(F)d}(\tau)-\eta_\sigma \hat{s}_0^{(F)d}(\tau)\right) l_n^{(F)d}(\omega_F;0),\\
l_{n,m}^{(FB)}(\tau,\omega_F,\omega_B;\eta_\psi,\eta_\sigma) &= \left(\frac{1}{1+\omega_F}\right)^n \left(\frac{1}{1+\omega_B}\right)^m \times\\
&\quad \left\{ n\left(s_0^{(F)d}(\tau)-\eta_\psi \hat{s}_0^{(F)d}(\tau)\right) l_0^{(F)d}(\omega_F;0) + m\left(s^d(\tau)-\eta_\psi \hat{s}^d(\tau)\right) l_0^d(\omega_B;0), \right\}\\
m_2^{(F)d}(\tau,\omega_F;\eta_\psi) &= s_0^{(F)d}(\tau) m_2^{(F)d}(\omega_F;0),\\
m_4^{(F)d}(\tau,\omega_F;\eta_\psi) &= s_0^{(F)d}(\tau)\left(\frac{1}{1+\omega_F}\right)^4 + \frac{1-\eta_\psi}{2} t_4(\tau)\left(\frac{1}{1+\omega_F}\right)^3 -\\
&\quad \left(\frac{1-\eta_\psi}{4} t_4(\tau) + \frac{1}{4} s_0^{(F)d}(\tau)\right)\left(\frac{1}{1+\omega_F}\right)^2,\\
m_{n,m}^d(\tau,\omega_{B,1},\omega_{B,2};\eta_\sigma) &= s_0^d(\tau) m_{n,m}^d(\omega_{B,1},\omega_{B,2};0),\\
m_{1,2}^{(FB)d}(\tau,\omega_F,\omega_B;\eta_\psi,\eta_\sigma) &= \left(s^d(\tau)-\eta_\sigma \hat{t}^{(FB)d}(\tau)\right) m_{1,2}^{(FB)d}(\omega_F,\omega_B;0,0).
\end{aligned}
$$

The thermal threshold factors are themselves given by the following Matsubara sums

$$
\begin{aligned}
s_0^d(\tau) &= \frac{v_{d-1}}{v_d}\frac{d}{d-1}\frac{\tau}{2\pi}\sum_{n\in\mathbb{Z}} \Theta(1-c_{B,n}^2\tau^2)\left(1-c_{B,n}^2\tau^2\right)^{\frac{d-1}{2}},\\
\hat{s}_0^d(\tau) &= \frac{v_{d-1}}{v_d}\frac{d}{d-1}\frac{\tau}{2\pi}\sum_{n\in\mathbb{Z}} \Theta(1-c_{B,n}^2\tau^2)\left(1-c_{B,n}^2\tau^2\right)^{\frac{d+1}{2}},\\
s_0^{(F)d}(\tau) &= \frac{v_{d-1}}{v_d}\frac{d}{d-1}\frac{\tau}{2\pi}\sum_{n\in\mathbb{Z}} \Theta(1-c_{F,n}^2\tau^2)\left(1-c_{F,n}^2\tau^2\right)^{\frac{d-1}{2}},\\
\hat{s}_0^{(F)d}(\tau) &= \frac{v_{d-1}}{v_d}\frac{d}{d-1}\frac{\tau}{2\pi}\sum_{n\in\mathbb{Z}} \Theta(1-c_{F,n}^2\tau^2)\left(1-c_{F,n}^2\tau^2\right)^{\frac{d-1}{2}} \times\\
&\quad \left\{1-|c_{F,n}\tau|\,{}_2F_1\left(-1/2,\frac{d-1}{2};\frac{d+1}{2};\frac{c_{F,n}^2\tau^2-1}{c_{F,n}^2\tau^2}\right)\right\}\\
s^d(\tau) &= \frac{v_{d-1}}{v_d}\frac{d}{d-1}\frac{\tau}{2\pi}\sum_{n\in\mathbb{Z}} \Theta(1-c_{F,n}^2\tau^2)\left(1-c_{F,n}^2\tau^2\right)^{\frac{d-1}{2}},\\
\hat{s}^d(\tau) &= \frac{v_{d-1}}{v_d}\frac{d}{d-1}\frac{\tau}{2\pi}\sum_{n\in\mathbb{Z}} \Theta(1-c_{F,n}^2\tau^2)\left(1-c_{F,n}^2\tau^2\right)^{\frac{d+1}{2}},\\
\hat{t}^{(FB)d}(\tau) &= \frac{v_{d-1}}{v_d}\frac{d}{d-1}\frac{\tau}{2\pi}\sum_{n\in\mathbb{Z}} \Theta(1-c_{F,n}^2\tau^2)\left(1-c_{F,n}^2\tau^2\right)^{\frac{d+1}{2}} \times\\
&\quad |c_{F,n}\tau|^{-1}\,{}_2F_1\left(1/2,\frac{d+1}{2};\frac{d+3}{2};\frac{c_{F,n}^2\tau^2-1}{c_{F,n}^2\tau^2}\right),\\
t_4(\tau) &= \frac{v_{d-1}}{v_d}\frac{d}{d-1}\frac{\tau}{2\pi}\sum_{n\in\mathbb{Z}} \Theta(1-c_{F,n}^2\tau^2)\left\{c_{F,n}^2\tau^2-1-2\ln(c_{F,n}\tau)\right\},
\end{aligned}
$$

with the hypergeometric function ${}_2F_1(a,b;c;z)$ [107]. In the following, we will give closed expressions for the thermal threshold factors, specifically for three spacetime dimensions ($d=3$), which can be obtained by applying the Poisson resummation formula

$$\sum_{n\in\mathbb{Z}} f(n) = \sum_{l\in\mathbb{Z}} \int_{\mathbb{R}} \mathrm{d}q\, f(q)\, \mathrm{e}^{-2\pi \mathrm{i} q l}, \tag{A.39}$$

and the identity

$$\mathrm{Li}_n(-z) - (-1)^{n-1}\mathrm{Li}_n(-1/z) = -\frac{(2\pi\mathrm{i})^n}{n!} B_n\left(\frac{\ln z}{2\pi\mathrm{i}} + \frac{1}{2}\right),\ z \notin (0,1) \tag{A.40}$$

where $B_n(z)$ are Bernoulli polynomials and $\mathrm{Li}_n(z)$ denotes the nth Polylogarithm. With $\ln\left(\mathrm{e}^{-2\pi\mathrm{i}/\tau}\right) = -2\pi\mathrm{i} + 2\pi\mathrm{i} s_F(\tau)$, $\ln\left(-\mathrm{e}^{-2\pi\mathrm{i}/\tau}\right) = \mathrm{i}\pi - \frac{2\pi\mathrm{i}}{\tau} + 2\pi\mathrm{i} s_B(\tau)$ and the definitions of the fermionic and bosonic floor functions [173] $s_F(\tau) = \left\lfloor \frac{1}{\tau} + \frac{1}{2} \right\rfloor$, $s_B(\tau) = \left\lfloor \frac{1}{\tau} \right\rfloor$, we arrive at

$$\begin{aligned}
s_0^d(\tau) &= \frac{d}{d-1}\frac{v_{d-1}}{v_d}\frac{1}{2\pi}\frac{1}{3}\left(-(\tau + 2\tau s_B(\tau))\left(-3 + \tau^2 s_B(\tau) + \tau^2 s_B(\tau)^2\right)\right), \\
\hat{s}_0^d(\tau) &= \frac{d}{d^2-1}\frac{v_{d-1}}{v_d}\frac{1}{2\pi}\frac{1}{15}\tau(1+2s_B(\tau))\Big(15 - \tau^2\left(10+\tau^2\right)s_B(\tau) + \\
&\quad 2\tau^2\left(-5+\tau^2\right)s_B(\tau)^2 + 6\tau^4 s_B(\tau)^3 + 3\tau^4 s_B(\tau)^4\Big), \\
s_0^{(F)d}(\tau) &= \frac{d}{d-1}\frac{v_{d-1}}{v_d}\frac{1}{2\pi}\frac{1}{6}\tau s_F(\tau)\left(12 + (1+12)\tau^2 - 4\tau^2 s_F(\tau)^2\right), \\
\hat{s}_0^{(F)d}(\tau) &= \frac{d}{d-1}\frac{v_{d-1}}{v_d}\frac{1}{2\pi}\frac{1}{12}\Big(4s_F(\tau) + \left(4+\tau^2\right)s_F(\tau) - \tau^3 s_F(\tau)^2 - 4\tau^2 s_F(\tau)^3 + \\
&\quad 2\tau^3 s_F(\tau)^4 + \tau^2\left(s_F(\tau) - \tau s_F(\tau)^2 - 4s_F(\tau)^3 + 2\tau s_F(\tau)^4\right)\Big), \\
s^d(\tau) &= \frac{d}{d-1}\frac{v_{d-1}}{v_d}\frac{1}{2\pi}\frac{1}{6}\tau s_F(\tau)\left(12 + \tau^2 - 4\tau^2 s_F(\tau)^2\right), \\
\hat{s}^d(\tau) &= \frac{d}{d^2-1}\frac{v_{d-1}}{v_d}\frac{1}{2\pi}\frac{1}{120}\left(\tau s_F(\tau)(240 + 40\tau^2 + 7\tau^4 - 40\tau^2(4+\tau^2)s_F\tau^2 + 48\tau^4 s_F\tau^4)\right), \\
\hat{t}^{(FB)d}(\tau) &= \frac{d}{d^2-1}\frac{v_{d-1}}{v_d}\frac{1}{2\pi}\frac{2}{3}\tau s_F(\tau)\left(4 + \tau^2 + \tau^2 s_F(\tau)(-\tau + 2s_F(\tau)(-2 + \tau s_F(\tau)))\right), \\
t_4(\tau) &= \frac{d}{d-1}\frac{v_{d-1}}{v_d}\frac{1}{2\pi}\Big(\frac{1}{6}\tau s_F(\tau)(-12 - \tau^2 + 4\tau^2 s_F(\tau)^2) + \frac{1}{3}\tau(32 s_F(\tau) + 2\tau(-12-\tau^2)s_F(\tau)^2 + \\
&\quad 4\tau^3 s_F(\tau)^4 - \frac{1}{20}\tau(-32 s_F(\tau) + 2\tau(40 + 20\tau^2 + 7\tau^4)s_F(\tau)^2 + \\
&\quad 40\tau^3(-2-\tau^2)s_F(\tau)^4 + 32\tau^5 s_F(\tau)^6)) + \ldots\Big).
\end{aligned}$$

The expression for $t_4(\tau)$ is only approximate. The Poisson resummation could not be performed analytically. However, after performing the Poisson integration, the resulting expression contains a sine integral, which can be expanded in terms of Bessel functions, $\mathrm{Si}(z) = \pi\sum_{k=0}^{\infty}\left(J_{k+1/2}\left(\frac{z}{2}\right)\right)^2$.

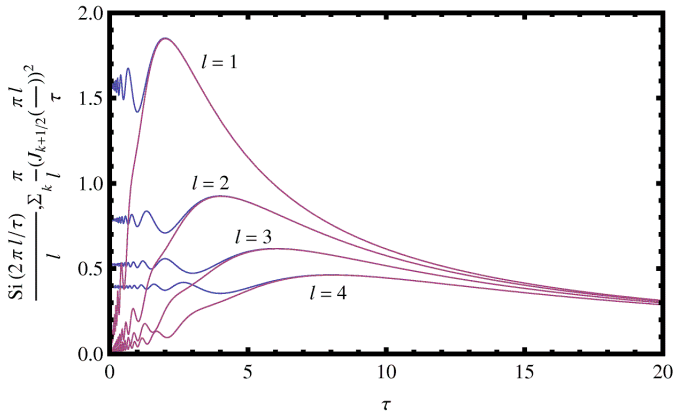

Figure A.1: Comparing $\frac{1}{l}\mathrm{Si}\left(\frac{2\pi l}{\tau}\right)$ (blue) and the approximant $\sum_{k=0}^{2}\frac{\pi}{l}\left(J_{k+1/2}\left(\frac{\pi l}{\tau}\right)\right)^2$ (magenta) as a function of τ for the Poisson indices $l=1,2,3,4$. The Poisson resummation over l can be done in closed form for the approximant. The deviation for $\tau\to 0$ is immaterial since the sine integral enters the thermal threshold factor with a prefactor τ. This ensures that the limit $\tau\to 0$, corresponding to $k\to\Lambda\to\infty$ is reproduced exactly within our approximation.

For the approximant, the Poisson resummation can be done in closed form. Above, we expanded to $k=2$ and cross-checked with numerical evaluation of $t_4(\tau)$, see also Fig. A.1. The agreement is satisfactory and only leads to spurious artifacts, which, however, do not affect our results.

A.7 Sketch of Derivation for the Dirac Propagator $G^+(x,x')$ in a Gauge Background

In this appendix, we briefly sketch the derivation of the Dirac propagator in a fixed gauge background as given in Eq. (6.7) following [147]. We rewrite

$$\begin{aligned} G^+(x,x') &= \langle x|\frac{1}{\mathrm{i}\not{D}[\mathcal{A}]+\mathrm{i}\bar{m}_\mathrm{f}}|x'\rangle \\ &= \langle x|\frac{1}{(\mathrm{i}\not{D}[\mathcal{A}])^2+\bar{m}_\mathrm{f}^2}[\mathrm{i}\not{D}[\mathcal{A}]+\mathrm{i}\bar{m}_\mathrm{f}]|x'\rangle \\ &= \langle x|\int_0^\infty \mathrm{d}s\,\mathrm{e}^{-[(\mathrm{i}\not{D}[\mathcal{A}])^2+\bar{m}_\mathrm{f}^2]s}[\mathrm{i}\not{D}[\mathcal{A}]+\mathrm{i}\bar{m}_\mathrm{f}]|x'\rangle, \end{aligned} \tag{A.41}$$

where in the last step we afforded a proper-time/Laplace representation of the denominator. Inserting a resolution of identity in position space, we obtain the proper-time transition amplitude (in Euclidean representation) of an auxiliary quantum mechanical particle

$$\langle x,s|x',0\rangle \equiv \langle x|\underbrace{\mathrm{e}^{-(\mathrm{i}\not{D}[\mathcal{A}])^2 s}}_{\equiv\mathrm{e}^{-Hs}}|x'\rangle, \tag{A.42}$$

with Hamiltonian H. Solving the (Euclidean) Heisenberg equations of motion for the canonically conjugate operators $x(s)$ and $\mathrm{i}\not{D}[\mathcal{A}](s)$, we can obtain a solution to the Schrödinger equation for $\langle x, s|x', 0\rangle$, which is given by

$$\langle x, s|x', 0\rangle = C(x, x')s^{-\frac{d}{2}}\mathrm{e}^{-\frac{q}{2}\sigma\mathcal{F}s}\mathrm{e}^{-\frac{1}{2}\mathrm{tr}\ln\left\{(\mathrm{i}q\mathcal{F}s)^{-1}\sinh(\mathrm{i}q\mathcal{F}s)\right\}}\mathrm{e}^{-\frac{1}{4}[x-x'](\mathrm{i}q\mathcal{F}s)\coth(\mathrm{i}q\mathcal{F}s)[x-x']}. \tag{A.43}$$

The normalization can be found to be

$$C(x, x') = \frac{1}{(4\pi)^{\frac{d}{2}}}\Phi(x, x'), \tag{A.44}$$

with the holonomy factor $\Phi(x, x')$, cf. Eq. (6.8). Putting things back together and once again invoking the equation of motion for $\mathrm{i}\not{D}[\mathcal{A}]$, we arrive at Eq. (6.7).

A.8 $\tilde{G}^+(p)$-Factor of the Dirac Propagator in a Gauge Background

In Sect. 6.1, we gave the proper-time (Laplace) form of the Dirac propagator in an external gauge background $\mathcal{F}_{\mu\nu}$, cf. Eqs. 6.7-6.9. Its homogeneous part, $\tilde{G}^+(x-x')$, can be Fourier transformed to momentum space. For arbitrary backgrounds, we obtain after performing a d-dimensional Gaußian integral

$$\begin{aligned}\tilde{G}^+(p) &= \int_x \mathrm{e}^{-\mathrm{i}px}\tilde{G}^+(x)\\ &= \mathrm{i}\int_0^\infty \mathrm{d}s\,\mathrm{e}^{-\bar{m}_\mathrm{f}^2 s}\left[\mathrm{i}\gamma(1+\tanh(\mathrm{i}q\mathcal{F}s))p - \bar{m}_\mathrm{f}\right]\times\\ &\quad \mathrm{e}^{-\frac{q}{2}\sigma\mathcal{F}s}\mathrm{e}^{-\frac{1}{2}\mathrm{tr}\ln\cosh(\mathrm{i}q\mathcal{F}s)}\mathrm{e}^{-p(\mathrm{i}q\mathcal{F})^{-1}\tanh(\mathrm{i}q\mathcal{F}s)p},\end{aligned} \tag{A.45}$$

where contractions of spacetime indices are again implicit. For a magnetic configuration (in $d = 3$)

$$\mathcal{F} = \begin{pmatrix} 0 & 0 & 0\\ 0 & 0 & B\\ 0 & -B & 0\end{pmatrix}, \tag{A.46}$$

we obtain the simplifications (the inversion of $\mathcal{F}$ poses no problem, since it can always be inverted in the appropriate subspace which yields contributions to the following expressions)

$$\mathrm{e}^{-\frac{q}{2}\sigma\mathcal{F}} = \cosh(qBs)\tau_0\otimes\tau_0 + \sinh(qBs)\tau_0\otimes\tau_3, \tag{A.47}$$

$$p(\mathrm{i}q\mathcal{F})^{-1}\tanh(\mathrm{i}q\mathcal{F}s)p = \left[p_0^2 + \boldsymbol{p}^2\frac{\tanh(qBs)}{qBs}\right]s, \tag{A.48}$$

$$\gamma\tanh(\mathrm{i}q\mathcal{F}s)p = \mathrm{i}\left(\gamma_1 p_y - \gamma_2 p_x\right)\tanh(qBs). \tag{A.49}$$

Putting everything back together gives

$$\begin{aligned}&\tilde{G}^{+}(p) \qquad\qquad (A.50)\\ &= \mathrm{i}\int_0^\infty \mathrm{d}s\, \mathrm{e}^{-\left[p_0^2+\boldsymbol{p}^2+\bar{m}_\mathrm{f}^2\right]s}\left[\mathrm{i}\not{p}-\bar{m}_\mathrm{f}-(\gamma_1 p_y-\gamma_2 p_x)\tanh(qBs)\right](\tau_0\otimes\tau_0+\tanh(qBs)\tau_0\otimes\tau_3)\,.\end{aligned}$$

Using the generating function for generalized Laguerre polynomials $L_n^\alpha(x)$,

$$(1-z)^{-(\alpha+1)}\mathrm{e}^{x\frac{z}{z-1}}=\sum_{n=0}^{\infty}L_n^\alpha(x)z^n, \qquad (A.51)$$

with $x=\frac{2\boldsymbol{p}^2}{qB}$, $z=-\mathrm{e}^{-2qBs}$, the Laplace integral can be performed, and we finally obtain the Landau level decomposition Eq. (6.10)

$$\tilde{G}^{+}(p)=\sum_{n=0}^{\infty}\mathrm{e}^{-\frac{2\boldsymbol{p}^2}{qB}}(-1)^n\frac{D_n(p_0,\boldsymbol{p};qB)}{p_0^2+\bar{m}_\mathrm{f}^2+2qBn}, \qquad (A.52)$$

with the spin-resolved Landau level projector

$$\begin{aligned}D_n(p_0,\boldsymbol{p};qB) \;=\;& L_n^0\left(\frac{2\boldsymbol{p}^2}{qB}\right)\left[-\gamma_0 p_0-\mathrm{i}\bar{m}_\mathrm{f}\right](\tau_0\otimes\tau_0+\tau_0\otimes\tau_3)-\\ & L_{n-1}^0\left(\frac{2\boldsymbol{p}^2}{qB}\right)\left[-\gamma_0 p_0-\mathrm{i}\bar{m}_\mathrm{f}\right](\tau_0\otimes\tau_0-\tau_0\otimes\tau_3)-\\ & 4L_{n-1}^1\left(\frac{2\boldsymbol{p}^2}{qB}\right)(\gamma_1 p_x+\gamma_2 p_y)\,. \qquad (A.53)\end{aligned}$$

A.9 Covariantly Regularized Dirac Propagator in a Gauge Background

Here we will show, that the propagator $G^+(x,x')$ can be regularized in a covariant way, maintaining the factorization property $G^+(x,x') = \Phi(x,x')\tilde{G}^+(x-x')$. The regularized propagator Eq. (6.25) for $Z_{\psi,k} \equiv 1$ reads

$$G_k^+(x,x') = \left[\mathrm{i}\not{D}[\mathcal{A}] \left(1 + r_F\left(\frac{(\mathrm{i}\not{D}[\mathcal{A}])^2}{k^2} \right) \right) \right]^{-1}(x,x'). \tag{A.54}$$

We can again employ a Laplace representation to obtain

$$\begin{aligned} G_k^+(x,x') &= \langle x| \int_0^\infty \mathrm{d}s \, \left\{ \mathrm{i}\not{D}[\mathcal{A}]\, \tilde{\alpha}(s) - \mathrm{i}\bar{m}_\mathrm{f}\, \tilde{\beta}(s) \right\} \mathrm{e}^{-(\mathrm{i}\not{D}[\mathcal{A}])^2 s} |x'\rangle \\ &= \int_0^\infty \mathrm{d}s \, \langle x,s| \left\{ \mathrm{i}\not{D}[\mathcal{A}](0)\, \tilde{\alpha}(s) - \mathrm{i}\bar{m}_\mathrm{f}\, \tilde{\beta}(s) \right\} |x',0\rangle \\ &= \int_0^\infty \mathrm{d}s \left\{ \langle x,s|\mathrm{i}\not{D}[\mathcal{A}](0)|x',0\rangle\, \tilde{\alpha}(s) - \mathrm{i}\bar{m}_\mathrm{f} \langle x,s|x',0\rangle\, \tilde{\beta}(s) \right\}, \end{aligned} \tag{A.55}$$

with $\langle x,s|x',0\rangle$ obeying the same time evolution as in the unregularized case. We furthermore defined the functions

$$\alpha(y) = \frac{1}{k^2} \frac{1 + r_F(y)}{(1+r_F(y))^2 y + \omega_F}, \quad \beta(y) = \frac{1}{k^2} \frac{1}{(1+r_F(y))^2 y + \omega_F}, \tag{A.56}$$

where $\tilde{\alpha}(s)$ and $\tilde{\beta}(s)$ denote the respective Laplace transforms,

$$\alpha(y) = \int_0^\infty \mathrm{d}s \tilde{\alpha}(s) \mathrm{e}^{-ys}, \quad \beta(y) = \int_0^\infty \mathrm{d}s \tilde{\beta}(s) \mathrm{e}^{-ys}. \tag{A.57}$$

By also making use of the equations of motion for $\mathrm{i}\not{D}[\mathcal{A}](s)$ and plugging in the result for $\langle x,s|x',0\rangle$, we obtain a proper-time representation of the covariantly regularized propagator, which then factorizes into a holonomy times a translation invariant function as before.

With the same techniques the regulator function $R_{F,k}^+(x,x')$ can be shown to factorize in the same way as

$$R_{F,k}^+(x,x') = \Phi(x,x')\tilde{R}_{F,k}^+(x-x'). \tag{A.58}$$

Appendix B

Description of Numerical Code

In this appendix be briefly describe how the numerical integration of flow equations was performed within Mathematica [35] to obtain the results presented in this thesis.

B.1 Solving ODEs for Polynomial Effective Potentials

In Chap. 4 and Chap. 5, we integrated LPA′ truncations numerically using Mathematica's NDSolve [35] routine. Threshold functions were defined as functions in a Mathematica notebook to facilitate a modular structure. The beta functions were then themselves defined as functions of mass parameters (and temperature). The algebraic system for the anomalous dimensions $\eta_{\sigma,k}$ and $\eta_{\psi,k}$ was solved by Solve[...] for both the symmetric and the broken regime. The parameter dependent ODE solver in the symmetric regime was then set up as

$$\begin{aligned}&\mathsf{solSYM}[\alpha_{1\_}, \alpha_{2\_}, d_{\_}, \tau_{\_}, N_{\mathrm{f}\_}, \eta_{\sigma\_}, \eta_{\psi\_}, t_{\mathrm{UV}\_}, t_{\mathrm{IR}\_}] \;:= \\ &\quad \mathsf{NDSolve}[\mathsf{FlowEquationSYM}[\alpha_1, \alpha_2, d, \tau, N_{\mathrm{f}}, \eta_\sigma, \eta_\psi, t_{\mathrm{UV}}], \{\dots\}, \{t, t_{\mathrm{UV}}, t_{\mathrm{IR}}\}, \mathsf{MaxSteps} \to \infty].\end{aligned} \tag{B.1}$$

The parameter choices $\alpha_1 = 0$, $\alpha_2 = 1$ and $\alpha_1 = 1$, $\alpha_2 = 1$ correspond to large-N_{f} and finite N_{f} truncations, respectively. By d one can specify the spacetime dimension (at least for $T = 0$; for $T \neq 0$, the representation of the threshold functions is limited to $d = 3$) and τ denotes the dimensionless temperature parameter (not present in $T = 0$ computations). Aside from initial conditions, FlowEquationSYM[...] contains the flow equations valid in the symmetric regime with the beta functions defining the right-hand side. The parameters t_{UV} and t_{IR} specify the logarithmic starting and stopping scale for the integration. In $\{\dots\}$, the list of functions to integrate is given, here containing the Yukawa coupling and the (finite set of) Taylor coefficients of the effective potential expressed as a function of the $\mathbb{Z}_2$ invariant ρ. The solver solSSB[...] for the broken regime is set up analogously.

In practice, the flow starts in the broken regime. We therefore use solSYM[...] until the linear coefficient of the effective potential crosses zero. Here, η_σ and η_ψ are given by the solutions to the

respective algebraic equations in the symmetric regime. The symmetry breaking scale and the values of all couplings at the symmetry breaking scale are then fed into solSSB[...] as initial conditions. The flow is then integrated to t_{IR} with the appropriate solutions for η_σ and η_ψ.

Often, the evaluation of flows is performed with surrounding For[...] structures. To automatize the detection of symmetry breaking, it is advisable to employ the EventLocator routine together with a Catch[...] enclosing the solver function. In essentially the same way EventLocator can be used to handle the case of a flow that first enters, and subsequently leaves the broken regime to fully integrate the flow to t_{IR}.

The output corresponds to a renormalization group trajectory of dimensionless renormalized couplings as a function of the logarithmic renormalization group scale t.

B.2 Solving the PDE for the Full Effective Potential

The finite N_{f} flow equation for the full effective potential Eq. (5.29) with dimensionally reduced regulators (cf. Eq. (5.27)) was integrated using NDSolve [35] with suitable specifications for partial differential equations. The parameter (β: inverse temperature, μ: chemical potential) dependent solver on the domain $[0, \bar{\rho}_{\max}] \times [k_{\mathrm{IR}}, \Lambda]$ is set up as

$$\begin{aligned} &\mathsf{sol}[\beta\_, \mu\_, \alpha\_] \;:= \\ &\quad \mathsf{NDSolve}[\mathsf{PDE}[\beta, \mu, \alpha], f, \{k, \Lambda, k_{\mathrm{IR}}\}, \{\bar{\rho}, 0, \bar{\rho}_{\max}\}, \mathsf{MaxSteps} \to \infty, \mathsf{Method} \to \{\dots\}] \end{aligned} \tag{B.2}$$

with

$$\begin{aligned} \{\dots\} = \{&\text{"MethodOfLines"}, \\ &\text{"SpatialDiscretization"} \to \\ &\{\text{"TensorProductGrid"}, \text{"DifferenceOrder"} \to \mathsf{DO}, \text{"MinPoints"} \to \mathsf{GridRes}\}, \\ &\text{"TemporalVariable"} \to k, \text{"DifferentiateBoundaryConditions"} \to \mathsf{False}\}. \end{aligned} \tag{B.3}$$

PDE[...] contains the flow equation for f, which represents the first derivative of $U_k(\bar{\rho})$, and further specifies the boundary conditions. We chose a flow equation for f, since it removes the vacuum contribution and stabilizes the numerics. DO specifies the difference order used to approximate derivatives and GridRes gives the minimal number of points to be used for the discretization.

The boundary conditions are given as

$$\begin{aligned} \mathsf{BoundaryConditions}[\beta\_, \mu\_] \;:=\; &\{f[k, \bar{\rho}_{\max}] == \mathsf{BoundaryRho1}[k, \beta, \mu], \\ &\mathsf{Derivative}[0, 1][f][k, \bar{\rho}_{\max}] == \mathsf{BoundaryRho2}[k, \beta, \mu], \\ &f[\Lambda, \bar{\rho}] == \mathsf{BoundaryLambda}[\bar{\rho}, \beta, \mu]. \end{aligned} \tag{B.4}$$

BoundaryRho1[...] is given by the $\bar{\rho}$ derivative of Eq. (5.31), BoundaryRho2[...] accordingly the second $\bar{\rho}$ derivative of Eq. (5.31). BoundaryLambda[...] is just given by $\bar{m}^2_{k=\Lambda}\bar{\rho}$.

Since for practically all initial conditions, we observe a region where $k^2 + U_k'(\bar{\rho}) + 2\bar{\rho}U_k''(\bar{\rho}) < 0$, we have employed the replacement $k^2 + U_k'(\bar{\rho}) + 2\bar{\rho}U_k''(\bar{\rho}) \to g_\alpha(k^2 + U_k'(\bar{\rho}) + 2\bar{\rho}U_k''(\bar{\rho}))$ with

$$g_\alpha(x) = \begin{cases} \alpha & \text{for } x \leq 0, \\ \frac{\alpha}{1-\mathrm{e}^{-\alpha/x}} & \text{for } x > 0. \end{cases} \tag{B.5}$$

With $\alpha \ll 1$ this has allowed us to integrate the flow in the first place. Subsequently, we have analyzed how the pathological scale could be further reduced toward t_{IR} und variation of the initial conditions.

Danksagung

Für die Möglichkeit mich in Jena quantenfeldtheoretischen Fragestellungen zu widmen und in einer angenehmen Atmosphäre zu forschen möchte ich mich bei Holger Gies und Andreas Wipf bedanken. Dank gilt insbesondere Holger Gies für seine jederzeit kompetente Betreuung und die Chance, eigene Ideen zu verfolgen und zu entwickeln.

Zu Forschungs- und Institutsatmosphäre wesentlich beigetragen haben sowohl gute Zusammenarbeit als auch Diskussionsfreude vieler Kollegen. Für viele lehrreiche und unterhaltsame Gespräche möchte ich mich insbesondere bei Jens Braun bedanken. Dank gilt hier auch den Kollegen Michael M. Scherer, Lukas Janssen, Raphael Flore, Babette Döbrich, Astrid Eichhorn und Felix Karbstein.

Für technische Unterstützung Dank an Christian Wozar, Daniel Körner, Axel Maas und Martin Weiss.

Für die Möglichkeit Konferenzen, Sommer- und Winterschulen zu besuchen nochmals Dank an Andreas Wipf und Holger Gies. Dank auch an Carsten Honerkamp für das Ermöglichen eines dreimonatigen Forschungsaufenthaltes in seiner Arbeitsgruppe an der RWTH Aachen und die Zusammenarbeit mit den Kollegen vor Ort.

Für finanzielle Unterstützung meiner Doktorarbeit bin ich auch der Deutschen Forschungsgemeinschaft und im Besonderen dem Graduiertenkolleg 1523/1 sowie der DFG Forschergruppe 723 zu großem Dank verpflichtet.

Ehrenwörtliche Erklärung

Ich erkläre hiermit ehrenwörtlich, daß ich die vorliegende Arbeit selbständig, ohne unzulässige Hilfe Dritter und ohne Benutzung anderer als der angegebenen Hilfsmittel und Literatur angefertigt habe. Die aus anderen Quellen direkt oder indirekt übernommenen Daten und Konzepte sind unter Angabe der Quelle gekennzeichnet. Auch die Ergebnisse, die in Zusammenarbeit mit den Mitgliedern des Lehrstuhles für Quantenfeldtheorie in Jena und anderen Kooperationen entstanden sind, sind in der Arbeit entsprechend benannt.

Weitere Personen waren an der inhaltlich-materiellen Erstellung der vorliegenden Arbeit nicht beteiligt. Insbesondere habe ich hierfür nicht die entgeltliche Hilfe von Vermittlungs- bzw. Beratungsdiensten (Promotionsberater oder andere Personen) in Anspruch genommen. Niemand hat von mir unmittelbar oder mittelbar geldwerte Leistungen für Arbeiten erhalten, die im Zusammenhang mit dem Inhalt der vorgelegten Dissertation stehen. Die Arbeit wurde bisher weder im In- noch im Ausland in gleicher oder ähnlicher Form einer anderen Prüfungsbehörde vorgelegt.

Die geltende Promotionsordnung der Physikalisch-Astronomischen Fakultät ist mir bekannt.

Ich versichere ehrenwörtlich, dass ich nach bestem Wissen die reine Wahrheit gesagt und nichts verschwiegen habe.

Jena, 15.05.2012

Daniel David Scherer

Curriculum Vitae

Personal Information

Name	Daniel David Scherer
Born	December 19, 1982 in Nürnberg, Germany

Education and University Studies

04/2009 – 09/2012	PhD at the Friedrich-Schiller-University Jena.
01/2008 – 12/2008	Diploma at the Institute for Theoretical Physics, University of Bayreuth, Supervisor: Prof. Dr. M. Kastner.
08/2005 – 12/2008	Graduate Studies in Physics at the University of Bayreuth.
10/2003 – 08/2005	Undergraduate Studies in Physics at the University of Bayreuth.
07/2002 – 03/2003	Military Service, Walldürn/Ulm/München.
07/2002	Graduation from High School, Abitur at the Wolfgang-Borchert-Gymnasium Langenzenn.

Teaching and Seminar Organization

04/2009 – 04/2012	Co-organization of Graduate Seminar at the Institute for Theoretical Physics, Friedrich-Schiller-University Jena.
04/2011 – 07/2010	Tutoring a Basic Quantum Mechanics Course, Summer Term '11, Friedrich-Schiller-University Jena.
04/2010 – 07/2010	Tutoring and Organization of an Advanced Seminar for Physics in Strong Electromagnetic Fields, Friedrich-Schiller-University Jena.
10/2008 – 02/2009	Tutoring an Advanced Quantum Mechanics Course, Winter Term 08/09, University Bayreuth.

Talks (to be found at `http://www.tpi.uni-jena.de/qfphysics/homepage/daniel/talks.html`)

1	Low-Dimensional Chiral Physics: Magnetic Catalysis. FOR 723 Reisensburg Workshop, 2011;
2,3,4	Low-Dimensional Chiral Physics: Gross-Neveu Universality & Magnetic Catalysis. Group Seminar, RWTH Aachen, 2011; Group Seminar, University Leipzig, 2011; Group Seminar, TU Dresden, 2012;

5,6	Low-Dimensional Chiral Physics: Gross-Neveu Universality & Magnetic Catalysis. Cold Quantum Coffee, Heidelberg, 2011; Strong Interaction Days Jena-Graz, Jena, 2011;
7,8	Asymptotic Safety in the 3d Gross-Neveu Model. Theory seminar, University Mainz, 2011; Schladming Winter School 2011, Schladming, 2011;
9	Asymptotic Safety by Quantum Criticality. Oppurg Workshop: Research Training Group Quantum and Gravitational Fields, Oppurg, 2010;
10	Geometric Characterization of Phase Transitions in the Lipkin-Meshkov-Glick Model. DPG Spring Meeting, Condensed Matter Section, Dresden, 2009;
11	Geometric Characterization of Phase Transitions in the Fully Connected XY Model. Theory seminar, University Bayreuth, 2008;

Jena, 15.05.2012

List of Publications

1. Renormalization Group Study of Magnetic Catalysis in the 3d Gross-Neveu Model.
   D. D. Scherer, Holger Gies,
   Phys. Rev. B 85, 195417 (2012)
   [arXiv:1201.3746]

2. Asymptotic Safety: A Simple Example.
   J. Braun, H. Gies, D. D. Scherer,
   Phys. Rev. D 83, 085012 (2011),
   [arXiv:1011.1456]

3. Finite-Temperature Fidelity-Metric Approach to the Lipkin-Meshkov-Glick Model.
   D. D. Scherer, C. A. Müller, M. Kastner,
   J. Phys. A: Math. Theor. 42 (2009) 465304, selected for IoP Select,
   [arXiv:0907.3367]